Aus dem Institut für Klinische Neuroimmunologie

Klinikum der Ludwig-Maximilians-Universität München

Vorstand: Prof. Dr. Martin Kerschensteiner

Discovery and Validation of Essential Modules of T cell Migration into the Central Nervous System in a Genome-wide CRISPR/Cas9 Screening in Experimental Autoimmune Encephalomyelitis

Dissertation

zum Erwerb des Doktorgrades der Naturwissenschaften

an der Medizinischen Fakultät der

Ludwig-Maximilians-Universität zu München

vorgelegt von

Katrin Franziska Lämmle

aus

Erlangen

Jahr

2023

Mit Genehmigung der Medizinischen Fakultät

der Universität München

Betreuer:	PD Dr. Naoto Kawakami
Zweitgutachter:	Prof. Dr. Jörg Renkawitz
Dekan:	Prof. Dr. med. Thomas Gudermann
Tag der mündlichen Prüfung:	15. Dezember 2023

Table Of Contents

ABSTRACT

Multiple sclerosis (MS) is an autoimmune, neuroinflammatory disease where peripheral immune cells infiltrate the central nervous system (CNS), causing inflammation and subsequent demyelination that ultimately leads to neuronal degeneration. The pathogenesis of MS is thought to be primarily driven by autoreactive T cells, which are the first immune cells to migrate into the CNS. Although efforts to restrict T cell migration into the CNS have yielded some success in treating MS, the need for additional treatment options remains. With this in mind, this study aimed to identify crucial genes necessary for T cell migration in the CNS in experimental autoimmune encephalomyelitis (EAE), an animal model for MS.

In this work we used an adoptive T-cell transfer EAE model in Lewis rats to conduct an *in vivo* genome-wide loss-of-function CRISPR/Cas9 screening in encephalitogenic T cells. Through a subsequent validation screening, a diverse set of molecules essential for T cell migration during the initial phase of EAE pathogenesis was identified. To gain comprehensive insights into the functional role of these identified candidates in regulating T cell migration, we performed validation experiments involving the generation of single knockout T_{MBP} cells and elucidated their underlying mechanisms. This systematic approach facilitated the clustering of these genes into functionally coherent modules with significant implications for understanding T cell migration regulation.

The adhesion module comprises of the α4-integrin, its binding partner β1-integrin and the integrin chaperone Hsp90b1. Loss of those genes leads to impaired attachment of T cells to vascular endothelial cells, consequently hindering the process of transmigration into the CNS. The second chemotaxis module involves the Chemokine receptor Cxcr3, its intracellular binding partner Gnai2, and its transcription factor Tbx21. Perturbation of this module alters the overall chemoattractive response of T cells. The third module, centered around the kinase Grk2, influences T cell egress. *In vivo* microscopy experiments revealed that Grk2-deficient T cells are capable of adhering to vascular endothelial cells but fail to complete the diapedesis process. Mechanistically, this impairment arises from defective S1PR1 internalization mediated by Grk2 phosphorylation. Moreover, we identified two interacting proteins, Arih1 and Ube2l3, both involved in the ubiquitination process to affect T cell migration. Lastly, we discovered that Ets1 acts as an inhibitor of T cell migration, as evidenced by the accumulation of Ets1-deficient T cells within the CNS.

Collectively, our study offers valuable insights into the regulatory mechanisms underlying T cell migration in the context of EAE, thereby holding promising implications for the development of innovative therapeutic strategies.

ZUSAMMENFASSUNG

Multiple Sklerose (MS) ist eine autoimmune, neuroinflammatorische Erkrankung, die durch die Infiltration von Immunzellen in das zentrale Nervensystem (ZNS) gekennzeichnet ist und zu Entzündungen und anschließender Entmarkung führt, was letztendlich in der Degeneration von Neuronen endet. Die Pathogenese von MS wird hauptsächlich durch autoreaktive T-Zellen getrieben, die als erste Immunzellen in das ZNS migrieren. Obwohl Bemühungen, die Migration von T-Zellen in das ZNS zu begrenzen, teilweise erfolgreich waren, besteht weiterhin Bedarf an zusätzlichen Behandlungsoptionen. Vor diesem Hintergrund zielte diese Arbeit darauf ab, essentielle Gene zu identifizieren, die für die T-Zell-Migration in das ZNS während der experimentellen autoimmunen Enzephalomyelitis (EAE), einem Tiermodel für MS, erforderlich sind.

In dieser Arbeit verwendeten wir ein EAE Modell des adoptiven T-Zell-Transfers in Lewis Ratten, um ein *in vivo* genomweites CRISPR/Cas9-Screening in enzephalitogenen T-Zellen durchzuführen. Durch ein anschließendes Validierungsscreening konnten wir eine Gruppe von Molekülen identifizieren, die während der initialen Phase der EAE-Pathogenese für die Migration von T-Zellen essentiell sind. Um weitere Erkenntnisse über die funktionelle Rolle dieser identifizierten Kandidaten bei der Regulation der T-Zell-Migration zu gewinnen, führten wir Validierungsexperimente mit individuellem Gen-Knockout in T-Zellen durch. Dieser Ansatz ermöglichte die Gruppierung dieser Gene in funktional kohärente Module die entscheidend zur Regulation der T-Zell-Migration beitragen.

Das Adhäsionsmodul besteht aus α4-Integrin, seinem Bindungspartner β1-Integrin und dem Integrin-Chaperon Hsp90b1. Der Verlust dieser Gene führt zu einer beeinträchtigten Anheftung von T-Zellen an die endothelialen Zellen der Blutgefäße, was die Transmigration in das ZNS behindert. Das zweite Chemotaxis-Modul umfasst den Chemokinrezeptor Cxcr3, seinen intrazellulären Bindungspartner Gnai2 und seinen Transkriptionsfaktor Tbx21. Die Beeinträchtigung dieses Moduls hat Auswirkungen auf die Reaktion von T-Zellen auf chemotaktische Signale. Das dritte Modul, das sich um die Kinase Grk2 zentriert, beeinflusst den Austritt von T-Zellen. *In vivo* Mikroskopie-Experimente zeigten, dass Grk2-defiziente T-Zellen in der Lage sind, an endotheliale Zellen zu binden, jedoch den Prozess der Diapedese nicht vollständig abschließen können. Mechanistisch gesehen entsteht diese Beeinträchtigung durch eine fehlerhafte Internalisierung von S1PR1, welcher von Grk2 phosphoryliert wird. Darüber hinaus identifizierten wir zwei interagierende Proteine, Arih1 und Ube2l3, die beide am Prozess der Ubiquitinierung beteiligt sind und die T-Zell-Migration beeinflussen. Schließlich

entdeckten wir, dass Ets1 eine inhibitorische Rolle bei der T-Zell-Migration spielt, was sich durch die Ansammlung von Ets1-defizienten T-Zellen im ZNS zeigte.

Zusammenfassend liefert unsere Studie wertvolle Erkenntnisse über die regulatorischen Mechanismen, die der T-Zell-Migration im Kontext von EAE zugrunde liegen, und hat somit vielversprechende Implikationen für die Entwicklung innovativer therapeutischer Strategien.

List of Figures

LIST OF TABLES

List of Abbreviations

Arih1	ariadne-1 homolog
aT-EAE	adoptive transfer EAE
APC	antigen-presenting cell
BBB	blood-brain barrier
BCR	B cell receptor
BFP	blue fluorescent protein
BLIMP-1	B lymphocyte-induced maturation protein-1
Cas9	CRISPR-associated protein 9
Cbfb	core-binding factor subunit beta
CD	cluster of differentiation
CFA	complete Freund's adjuvant
CIS	clinically isolated syndrome
CNS	central nervous system
CRISPR	clustered regularly interspaced short palindromic repeats
crRNA	CRISPR-RNA
CSF	cerebrospinal fluid
DICAM	dual immunoglobulin domain containing cell adhesion molecule
DNA	deoxyribonucleic acid
DSB	double-stranded breaks
EAE	experimental autoimmune encephalomyelitis
EBV	Epstein-Barr virus
EGFP	enhanced green fluorescent protein
FBS	fetal bovine serum
Foxo1	forkhead box protein O1
FoxP3	forkhead box protein P3
FPR3	formyl peptide receptor 3
G	guanine
gDNA	genomic DNA
GM-CSF	granulocyte macrophage colony-stimulating factor
Gnai2	guanine nucleotide-binding protein G(i) subunit alpha-2
GO	gene ontology
GPCR	G protein coupled receptor
Grk2	G protein coupled kinas2
gRNA	guide RNA
HHARI	human homolog of drosophila ariadne
HLA	human leukocyte antigen
HR	homologous recombination
Hsp90b1	heat shock protein 90 beta family member 1
IFNγ	interferon gamma
IL	interleukin

indel	nucleotide insertions or deletions
Iono	ionomycin
i.p.	intraperitoneally
i.v.	intravenously
Jak3	janus kinase 3
JCV	John Cunningham virus
Klf2	krüpple-like factor 2
KO	knockout
LFA-1	lymphocyte function-associated antigen 1
LN	lymph node
MBP	myelin basic protein
MCAM	melanoma cell adhesion molecule
MFI	mean fluorescent intensity
MHC	major histocompatibility complex
MOG	myelin oligodendrocyte glycoprotein
MS	multiple sclerosis
NF-κB	nuclear transcription factor-kappa B
NHEJ	non-homologous end joining
NT	non-targeted
OSE	opticospinal EAE
PAM	protospacer-adjacent motif
PB	intracellular staining perm wash buffer
PFA	paraformaldehyde
PLP	proteolipid protein
PMA	phorbol 12-myristat 13-acetat
PML	progressive multifocal leukoencephalopathy
PPMS	primary-progressive multiple sclerosis
Prdm1	PR domain zinc finger protein 1
PSGL-1	P-selectin glycoprotein ligand 1
pt	parathymic
PTX	pertussis toxin
RM	restimulation medium
RNA	ribonucleic acid
RNP	ribonucleoprotein
RR	relapsing-remitting
RRMS	relapsing-remitting multiple sclerosis
RT	room temperature
sgRNA	single guide RNA
SpCas9	streptococcus pyogenes Cas9
SPMS	secondary-progressive multiple sclerosis
S1P	sphingosine-1-phosphate
S1PR1	sphingosine-1-phosphate receptor 1

TAE	Tris-Acetat-EDTA
TCGF	T cell growth factor medium
TCM	T cell medium
TCR	T cell receptor
TGF-β	transforming growth factor-β
Tln1	talin-1
T_{MBP} cell	MBP-specific T cell
TNF-α	tumor necrosis factor α
tracr-RNA	trans-activating CRISPR RNA
Treg cell	regulatory T cell
Ube2l3	ubiquitin-conjugating enzyme E2 L3
VCAM-1	vascular cell adhesion molecule 1
VLA-4	very late antigen 4
ZFP407	zinc finger protein 407

1 INTRODUCTION

1.1 Multiple Sclerosis

Multiple sclerosis (MS) is an autoimmune, inflammatory, demyelinating disease of the central nervous system (CNS) afflicting around 2.8 million people worldwide (Walton et al., 2020, Baecher-Allan et al., 2018). Among young adults it is the most common neurological disease and the leading cause of non-traumatic disability (Attfield et al., 2022). MS patients display a heterogeneous disease course with a wide spectrum of neurological dysfunction and varying clinical presentation, which makes clinical characterization challenging. Depending on the lesion side symptoms can range from an inflammation of the optic nerve with complete or partial loss of vision in one or both eyes to inflammation in the spinal cord or brain leading to muscle weakness, spasticity, sensory disturbances, and bladder or bowel dysfunction. If the lesion side is located in the brainstem, symptoms can also consist of dizziness or vertigo, nausea, fatigue, double vision and pain (Garg and Smith, 2015, Miller et al., 2005, Sastre-Garriga et al., 2010). In most cases the disease onset occurs between the age of 20 and 40 with a clinically isolated syndrome (CIS) that consists of a single episode of neurological impairment for at least 24 hours (Attfield et al., 2022). Although not necessary, the CIS often progresses into a relapsing-remitting MS (RRMS) where patients experience reversible episodes of neurological dysfunction that can last for some days up to several weeks (Miller et al., 2005). The RRMS is characterized by clearly defined relapses of new or increasing neurological symptoms followed by periods of remission with partial or complete recovery (Figure 1). With time, the recovery after each episode becomes incomplete and irreversible neurological deficits persist, however there is no progression of disease during the periods of remission. This changes if patients transition into a secondary-progressive MS (SPMS) where symptoms do not revolve but progress further outside of attacks (Miller and Leary, 2007). However, an SPMS patient can still have relapses and time periods without progression. While 85 % of MS patients develop RRMS and about half of them progress into SPMS, a minority of around 15 % of the patients develops a primary-progressive MS (PPMS) (Ruiz et al., 2019). The PPMS is characterized by the progressive development of irreversible clinical and cognitive deficits from the beginning without relapses (Figure 1). In all forms of the disease, the pathological hallmark is the formation of focal inflammatory demyelinating lesions in the CNS that disseminate in time and space. The lesions are caused by the infiltration of autoreactive immune cells into the parenchyma where they induce inflammation and attack the myelin sheath. This results in demyelination, oligodendrocyte loss, reactive gliosis, and axonal degeneration ultimately causing neurological deficits (Baecher-Allan et al., 2018).

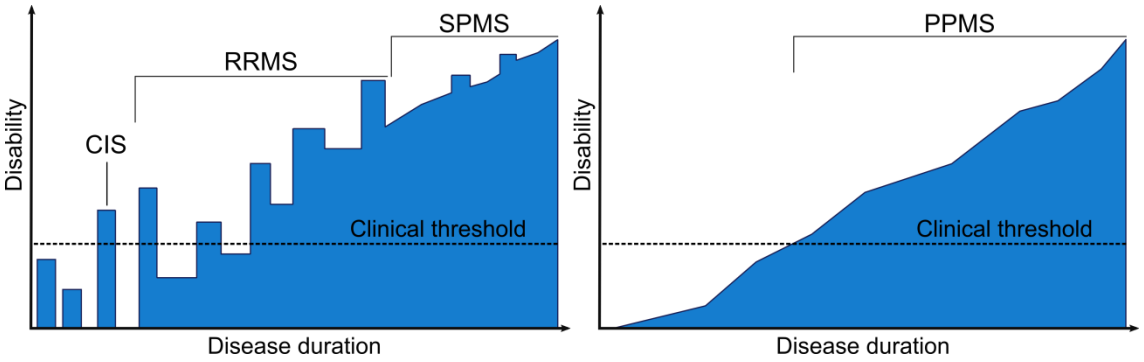

Figure 1 Types and progression of multiple sclerosis

Before onset of the first CIS, preclinical disease activity without clinical symptoms can already occur. In RRMS relapses are followed by partial or complete clinical recovery, while disease progresses in between relapses once transitioned into SPMS. In PPMS, there is a constant progression from disease onset on without relapses. Own graphic, based on (Baecher-Allan et al., 2018).

The cause of MS is unknown but it is considered to be multifactorial by a combination of genetic and environmental influences. The observation of increased heritability within families and studies with twin and sibling pairs as well as adoptees provide evidence that there is a genetic component in the development of MS (Sawcer et al., 2014). While the general population carries a risk of developing MS around 0.1 %, this increases to 2-4 % for first-degree family members (Compston and Coles, 2008, Reich et al., 2018). Genome-wide association studies identified over 200 risk alleles that are associated with a higher susceptibility to MS (Thompson et al., 2018). Most of them have a direct link to the immune system, for example the regions of the interleukin (IL) 7 receptor, IL-2 receptor, or tumor necrosis factor receptor superfamily member 1A, lymphocyte function-associated antigen 3 or tyrosine kinase 2 (Sawcer et al., 2014, Hafler et al., 2007). The strongest association was found with the human leukocyte antigen (HLA) region of chromosome 6, where the most prominent gene variant is the major histocompatibility complex (MHC) allele HLA DRB1*15:01, which increases the risk of developing MS threefold (Lill, 2014). However, genetic factors can only account for 30 % of the explainable risk of MS (Dendrou et al., 2015). Indeed, a monozygotic twin of an MS patient has only a 25 % risk of developing the disease themselves and no singular genetic, epigenetic or transcriptomic mechanism explaining the disease discordance of monozygotic twins was detected yet (Baranzini et al., 2010). This indicates that common risk alleles, each exerting only modest effects, affect the susceptibility to MS but additional environmental factors play an essential role in the development of MS (Hafler et al., 2007). MS exhibits a latitudinal gradient in its global distribution, with the prevalence of the disease increasing as one moves further north or south of the equator in areas where individuals of European descent live (Simpson et al., 2011). The discrepancies in prevalence can be attributed to differences in sunlight exposure, reflected in changes in ultraviolet radiation and vitamin D levels. Elevated levels of both are associated with a protective effect on the MS risk (Lucas et al., 2015). In addition,

according to the hygiene hypothesis, exposure to multiple pathogens especially in early life, as is often the case in subtropical and tropical regions, suppress allergic and autoimmune disorders (Bach, 2002). Also an increased numbers of younger siblings reduces the risk of developing MS, as well likely due to a higher exposure to infections (Olsson et al., 2017). In contrast, the infection with the Epstein-Barr virus (EBV) has long been implicated with the development of MS. Over 95 % of the population becomes infected in their adult life and while infection during children often remains symptom free, an infection later in life often leads to infectious mononucleosis, therefore the time point of EBV infection in life seems to be important for determining the severity of the disease (Kuri et al., 2020). A recent study in a cohort of more than 10 million people showed that the risk of developing MS increased 32-fold after infection with EBV but not after infection with similarly transmitted viruses. In the same study, the onset of MS was nearly always only after EBV seroconversion (Bjornevik et al., 2022). Although the data suggest that EBV might be essential for the development of MS, the exact mechanism still remains elusive. Like in most autoimmune disorders, females are more often affected by MS than males. Over the past 30 years, the female to male sex ratio has increased markedly due to increased incidence of MS in women (Koch-Henriksen and Sørensen, 2010). This is likely to be explained by environmental factors and changes in lifestyle, such as increased smoking and adolescent obesity, which are well-established risk factors for MS (Olsson et al., 2017). In addition, changes in female reproductive behaviour might play a role since pregnancies exert a beneficial effect on autoimmune diseases like MS (Ponsonby et al., 2012). Recently, the gut microbiome has come into the focus of science as it participates in immunoregulatory pathways. Studies showed that composition of the microbiota differed between MS patients and healthy controls (Jangi et al., 2016). In addition, when transferred into mice the MS patient derived gut microbiota induced autoimmunity at a significantly higher incidence than the control-derived microbiota (Berer et al., 2017). Although causality has not been established yet, it is likely that the microbiome plays an important role in MS. In order to provide comprehensive medical care for people at risk, further research and analysis of risk factors is crucial. As far as known, no single factor but rather the combination of genetic and environmental factors that interact with each other causes the development of MS.

1.2 Experimental Autoimmune Encephalomyelitis

To gain insight into the complex pathogenesis of MS, which involves various interactions between cells of the immune system and the CNS, research has relied extensively on animal models. However, in a complex disease like MS with profound heterogeneity in clinical

symptoms and immunological phenotypes, there is no single animal model that reflects the entire pathology (Wekerle et al., 1994, Wekerle et al., 2012). Hence, multiple animal models have been developed to study different aspects of the disease. Frequently used animal models are the toxin-induced demyelination model and the Theiler's murine encephalomyelitis virus infection, which is based on virally-induced chronic demyelination. Those models are suitable to study the de- and re-myelination processes as well as axonal injury and repair (Procaccini et al., 2015). Nonetheless, to study the autoimmune pathology of MS the best characterized and most common used animal model is the experimental autoimmune encephalomyelitis (EAE). It was first described in 1925, when Koritschoner and Schweinburg discovered that inoculation of rabbits with human spinal cord emulsion inflicts inflammation of the spinal cord and paralysis in the animals (Koritschoner and Schweinburg, 1925). This observation was later reproduced by repeated injections of rabbit brain extracts into monkeys, which developed clinical signs of a CNS disease with immune cell infiltration and demyelinating lesions (Rivers et al., 1933). A major breakthrough was the discovery of the mineral oil-based Freund's adjuvant, a potent immunostimulant that can be supplemented with heat-inactivated mycobacteria tuberculosis (complete Freund's adjuvant, CFA) to further potentiate the immune response (Freund and McDermott, 1942). When the brain extract was emulsified in CFA, only one injection is sufficient to elicit EAE in the animal, whereas earlier approaches required multiple injections (Kabat et al., 1951). In the following years, EAE experiments have been performed in multiple animal species like monkey (Kabat et al., 1947, Morgan 1947), guinea pig (Freund et al., 1947), mouse (Olitsky and Yager, 1949) and rat (Lipton and Freund, 1952, Procaccini et al., 2015). Until the 1980s, rats and guinea pigs were the model of choice to study EAE due to high reproducibility and consistent disease course (Croxford et al., 2011, Gold et al., 2006). This changed when more susceptible mouse strains were identified, and pertussis toxin (PTX) was introduced to enhance the EAE incidence. Subsequently, with the ease of genetic manipulation leading to new transgenic and gene knockout (KO) mouse strains and the availability of antibodies for mouse immune markers, mice became the most regularly used EAE model species.

EAE can be broadly categorized into three sub forms: active EAE, adoptive-transfer EAE and transgenic spontaneous EAE models. In the above described active EAE, disease is induced by immunization with either brain homogenate, brain-specific antigens such as myelin oligodendrocyte protein (MOG), proteolipid protein (PLP) and, myelin basic protein (MBP) or peptides with encephalitogenic epitopes of those proteins in an emulsion with CFA (Robinson et al., 2014). The initial immunization can be followed by single or multiple injections of PTX to open the blood-brain barrier (BBB) or a second round of immunization a week after the initial

dose (Stromnes and Goverman, 2006). The susceptibility as well as the disease phenotype of EAE varies between different mouse strains depending on the used encephalitogen and the protocol of immunization. While for example immunization of SJL/J mice with $PLP_{139–151}$ leads to a relapsing-remitting EAE course, C57BL/6J mice immunized with MOG_{35-55} display a chronic EAE progress (Procaccini et al., 2015).

However, the ability of encephalitogenic T cells to induce disease is not restricted to the immunized animal itself. In 1960, Paterson described that the transfer of lymph node cells from an immunized rat to a naïve rat can also mediate EAE (Paterson 1960). Subsequently, in the 1980s, Ben-Nun demonstrated that MBP-specific T cells that were isolated from an immunized rat and *in vitro* stimulated can induce EAE when injected into naïve rats and thereby established the basis for the so-called adoptive transfer EAE (aT-EAE) (Ben-Nun et al., 1981). Building on this accomplishment, the model was subsequently expanded to include mice (Mokhtarian et al., 1984). Over time, the aT-EAE mice model underwent continual refinement and modification, facilitating the exploration of diverse T cell subpopulations and their corresponding impacts (Jäger et al., 2009, Kroenke et al., 2008). While active EAE relies on strong adjuvants, which can confound the study, the aT-EAE is solely mediated by transfer of encephalitogenic T cells that initiate the recruitment of other immune cells (Robinson et al., 2014). The T cells are isolated from a brain-specific antigen-primed donor animal and stimulated with their corresponding peptide *in vitro* before they are either injected intravenously (i.v.) or intraperitoneally (i.p.) into a recipient animal. This method allows the generation of a homogenous population of antigen-specific T cells, which can be *in vitro* manipulated, e.g. by fluorescent labelling, genetic editing or specific polarization (Robinson et al., 2014).

With the advances of technology and genetic engineering, transgenic mice strains that do not rely on an exogenous stimulus but spontaneously develop EAE have become available. Most mediate disease via a transgenic T cell receptor (TCR) and/or a transgenic B cell receptor (BCR) with reactivity towards specific CNS antigens. One of those models is the SJL/J relapsing-remitting (RR) mouse that carries a transgenic TCR reactive to $MOG_{92–106}$. In around 80 % of the animals transgenic T cells manage to recruit autoreactive B cells from the endogenous pool ensuing disease, which is characterised by spontaneous onset followed by episodes of remission (Pöllinger et al., 2009). A second model of spontaneous EAE is the double transgenic opticospinal EAE (OSE) mouse with a C57BL/6 background (Krishnamoorthy et al., 2006). It combines the TH mouse line, which expresses a BCR derived from a rearranged immunoglobulin h chain of a MOG-specific monoclonal antibody (Litzenburger et al., 1998) with the 2D2 mouse line that expresses a MOG-specific T-cell receptor (Bettelli et al., 2003).

While only a minor percentage of 2D2 and none of the TH mice spontaneously develop symptoms of EAE, around 50 % of OSE mice develop lesions that are restricted to the spinal cord and optic nerve (Krishnamoorthy et al., 2006).

Although initiation and manifestation of EAE differ in the individual animal models, e.g. chronic-progressive, monophasic, or relapsing-remitting EAE, the clinical symptoms are usually similar and are assessed by a 5-point scale (Stromnes and Goverman, 2006). The first symptom is body weight loss, often already paired with a weakness in the tail, followed by a paralysis with increasing intensity. The paralysis progresses from caudal to rostral, first affecting the tail and progressing into hindlimb and finally forelimb paralysis (Batoulis et al., 2011). These clinical signs of disease manifestation are due to inflammation predominantly localized in the spinal cord. Depending on the used EAE model, the disease course could be potentially lethal, but often the animals recover completely or develop a chronic or fluctuating disease course.

1.2.1 Adoptive transfer EAE in the Lewis rat

Since its initial report in the 1980s, the adoptive-transfer model in Lewis rats has become a valuable laboratory animal model to study autoimmune-mediated inflammation in the CNS (Ben-Nun et al., 1981). Until today, aT-EAE is usually induced by intravenous transfer of cluster of differentiation (CD) 4^+ effector T cells reactive against MBP (T_{MBP}). The major benefit of the aT-EAE rat model is the high incidence of EAE with a stable, reproducible clinical course that follows a steady time kinetic. Following the transfer of activated T cells, the cells do not immediately enter the CNS, but rather enter a preclinical phase lasting two to three days during which the cells stay in the lung or secondary lymphatic organs (Kawakami et al., 2012, Odoardi et al., 2012, Flügel et al., 2001). The onset of clinical symptoms in Lewis rats typically coincides with a massive infiltration of T cells into the CNS, and includes weight loss and tail paralysis observed on day three. In the following two to three days the disease intensity reaches its maximum and the rats display first hind limb and with increasing severity also front limb paralysis. The symptoms decline in the following week and the rats reach complete clinical remission latest two weeks after T cell transfer (Figure 2).

Another major advantage of the Lewis rat aT-EAE model is the possibility to culture and stimulate the T_{MBP} cells with their respective antigen *in vitro* for long periods of time, up to 13 cycles of restimulation. This allows for genetic modification or treatment of the T cells prior to injection. Labelling of T_{MBP} cells with a fluorescent protein allowed exploring the migratory pathway of the cells from injection to infiltration into the CNS (Flügel et al., 1999). Interestingly, activated T_{MBP} cells do not infiltrate the CNS immediately, but migrate first through peripheral organs over a latency period of three days. Immediately after injection the

T_{MBP} cells accumulate in the lung, where they actively migrate within the airways (Odoardi et al., 2012). One to two days after transfer, the T_{MBP} cells migrate into the parathymic lymph nodes and from there further into the spleen on day three (Flügel et al., 2001). During their journey, the T_{MBP} cells maturate and acquire a migratory phenotype, which is characterized by a profound reprogramming of their expression profile and upregulation of chemokine receptors and membrane receptors (Odoardi et al., 2012, Flügel et al., 2001). This maturation process is essential for the T_{MBP} cell's ability to cross the blood-brain barrier and infiltrate the CNS. When T_{MBP} cells isolated on day three from the spleen are directly injected into a naïve rat, they are able to induce EAE much faster than their *in vitro* activated counterpart. After the preclinical phase the T cells migrate into the CNS via the leptomeninges. Notably, it was shown that over 90 % of the infiltrating T cells are transferred autoantigen specific T cells (Flügel et al., 2001).

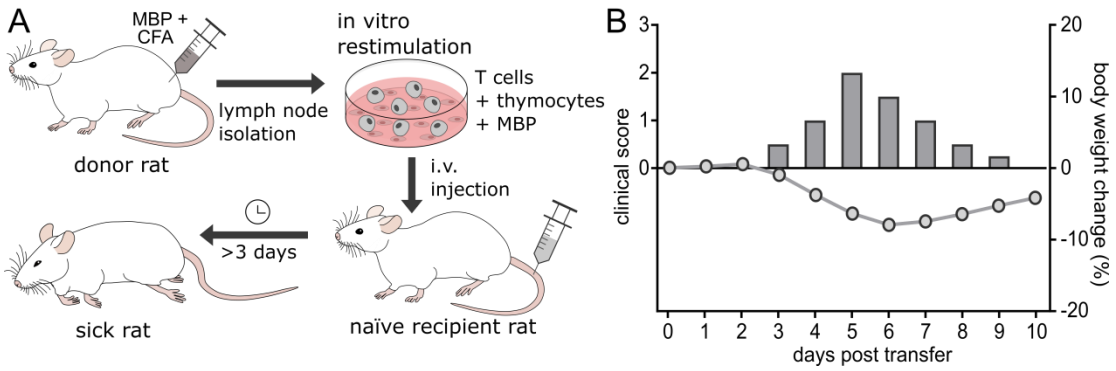

Figure 2 Lewis rat adoptive transfer EAE model

A) Experimental design. A donor Lewis rat was injected with MBP + CFA followed by isolation of MBP-specific T cells from draining lymph nodes. The T_{MBP} cells were *in vitro* restimulated by thymocytes presenting the MBP antigen. After 48 h the T_{MBP} cells were i.v. injected into a naïve recipient rat to induce EAE. On day three, the animal starts to show first clinical symptoms and develop full EAE the following days. **B)** Example of a typical clinical course of aT-EAE induced by T_{MBP} cells measured by percentage of body weight change (lines) and EAE scores (bars) of injected animals.

In the MBP-based aT-EAE model the T_{MBP} cells rather infiltrate into the spinal cord than into the brain. Lesions occur predominantly in the spinal cord and the medulla oblongata and are characterized by inflammatory infiltrates concentrated in meningeal and perivascular areas. They are mainly composed of effector T cells and recruited monocytes and macrophages (Kawakami et al., 2004). With ongoing disease, T cells leave the perivascular space and migrate deeply into the parenchyma, where they trigger clinical EAE (Ben-Nun et al., 2014). Although the transfer of T cells inflicts a pronounced inflammation in the CNS, no considerable demyelination occurs at the lesion site, unless anti-MOG antibodies are injected in addition (Lassmann et al., 1988). Remission of the lesions is associated with increased apoptosis of T cells at the inflammation site (Schmied et al., 1993). In contrast to human MS, the monophasic disease course is rather driven by inflammation than demyelination of the CNS,

which is a critical limitation in the EAE model (Gold et al., 2006). Nevertheless, the early phase of MS is considered to be directed by T cells and the similarities in the pathological picture suggest that the Lewis rat aT-EAE is a suitable model to study the earliest phase of the inflammatory events in MS (Flügel et al., 2007). Especially the predictable time course of the disease allows investigation of the behaviour of autoreactive T cells that just breached the BBB and are about to infiltrate the CNS.

1.3 Pathogenesis of MS and EAE

1.3.1 Role of T lymphocytes in CNS autoimmunity

Currently, the exact pathogenesis of MS is still unknown, but it is believed that $CD4^+$ T cells are the main driver of the disease. This hypothesis is supported by the strong association of the MHC class II locus with MS susceptibility, the central role of T cells in the immune response and the fact that encephalitogenic T cells alone can induce EAE in animal models (Barcellos et al., 2003). A repertoire of naïve myelin-reactive T cells can be found in healthy individuals as well as in MS patients (Burns et al., 1983, Kaskow and Baecher-Allan, 2018). However, the ones in MS patients display a higher activation state indicating a presuming activation (Lovett-Racke et al., 1998, Scholz et al., 1998), where reduced suppressive capacity of regulatory T cells (Treg) possibly plays a role (Venken et al., 2008). While the initial triggering mechanism remains to be determined, the peripheral activation of autoreactive T cells is considered to be the initiator of the disease. The activated T cells cross the BBB and infiltrate the CNS. Here the $CD4^+$ T cells are reactivated by local antigen-presenting cells (APC) and recruit further T cells, B cells, neutrophils and monocytes to establish the inflammatory lesion.

$CD4^+$ T cells are usually found deep in acute lesions while $CD8^+$ T cells are predominantly found on the lesion margin, often in chronic lesions (Traugott et al., 1983, Raine, 1994). For the different subpopulations of $CD4^+$ and $CD8^+$ T cells mainly proinflammatory but also anti-inflammatory properties as well as contrasting results between EAE and MS studies have been described (Kaskow and Baecher-Allan, 2018). This is suggesting a high plasticity and complexity of these populations, likely driven by local signals of the CNS microenvironment (Attfield et al., 2022). Nevertheless, $CD4^+$ T cells are believed to be pathogenic initiators of MS. After encountering their antigen, presented by APC via MHC class II molecules the activated $CD4^+$ T cells polarize into effector subtypes triggered by the present cytokines in the surrounding micromilieu. In turn, their produced cytokines affect and recruit further immune cells. The major proinflammatory $CD4^+$ T cell populations are interferon gamma (IFNγ) producing Th1 cells, driven by their lineage-specific transcription factor Tbx21/T-bet and Th17 cells that are characterized by the unique expression of RORC2 and secrete IL-17, IL-21, and IL-22 (Yang et

al., 2008, Qu et al., 2013). Both are found with increased frequency in the cerebrospinal fluid (CSF) of MS patients (Giunti et al., 2003, Brucklacher-Waldert et al., 2009). Although the Th17 population is the smaller proportion, their frequency increases during relapses and in later stages of disease while Th1 cells that are the larger proportion and remain stable before and during CNS inflammation (Brucklacher-Waldert et al., 2009). However it should be noted that also a population with an intermediate phenotype, simultaneously expressing IFNγ and IL-17, can be found in MS patients and EAE mice, which preferentially cross the human BBB and accumulate in the murine CNS (Kebir et al., 2009).

It was long believed, that IFNγ-producing Th1 cells induced by IL-12 are the driving force during EAE, since knockout of the IL-12 p40 subdomain protects mice from EAE (Becher et al., 2002). However, mice lacking IFNγ develop even more severe EAE and injection of neutralizing antibodies to IFNγ exacerbates the disease (Billiau et al., 1988). Together with the fact that administration of recombinant IFNγ has a protective effect, it was concluded that IFNγ is beneficial in the mouse model (Segal et al., 1998, Voorthuis et al., 1990). Also in humans IFNγ levels are higher in MS patients and correlate with disability, and IFNγ production in T cells of patients increases before a relapse (Dettke et al., 1997, Petereit et al., 2000). Intriguingly, transfer of this theory showed that administration of IFNγ into MS patients actually exacerbated the disease (Panitch et al., 1987). With the discovery that the p40 domain is not only a component of IL-12 but also of IL-23, the focus shifted onto Th17 cells, whose phenotype is stabilized by IL-23 (Aggarwal et al., 2003). In parallel to IFNγ, while mice are protected from EAE, a human trial with the IL-12/23 p40 neutralising antibody Ustekinumab showed no clinical effect in MS patients (Segal et al., 2008). However, in a trial with the anti-IL-17A antibody Secukinumab, patients showed reduced lesions (Havrdová et al., 2016). While IFNγ, IL-23 and IL-17 and their corresponding T cells appear to play a role in EAE and human MS, further studies are needed to resolve the paradoxical outcome of IL-23 and IL-17 blocking. Likely, the different T cell subsets and their cytokines play distinct roles during initiation and disease progression.

In MS patients the majority of CNS-resident T cells are $CD8^+$ T cells, so it is not surprising that they play a significant role in the disease. $CD8^+$ T cells recognize peptides of endogenous intracellular proteins presented by the MHC class I molecules and kill their target cells via cell contact-dependent mechanisms or the release of granzymes and perforin (Baecher-Allan et al., 2018). A correlation between the extent of axon damage and the numbers of cytotoxic $CD8^+$ T cells and macrophages/microglia was shown (Kuhlmann et al., 2002). MHC Class I expression is increased on astrocytes, oligodendrocytes, and neurons during disease and can be recognized and lysed by $CD8^+$ T cells (Höftberger et al., 2004, Denic et al., 2013). In addition to

their cytotoxic function, some $CD8^+$ T cells can also produce IL-17 and IFNγ and hereby contribute to the pathogenesis (Tzartos et al., 2008, Zang et al., 2004, Huber et al., 2013). Both cytokines activate local microglia and APCs, which encourages them to upregulate MHC class I and II molecules (Kaskow and Baecher-Allan, 2018). Those in turn can activate microglia to become phagocytic, present antigens and secrete pro-inflammatory mediators, like cytokines, reactive oxygen intermediates, proteinases, and complement proteins (Baecher-Allan et al., 2018). In addition, IL-17 promotes the expression of proinflammatory cytokine IL-6, granulocyte macrophage colony-stimulating factor (GM-CSF), and tumor necrosis factor α (TNF-α) (Kaskow and Baecher-Allan, 2018). Nevertheless, with the increased understanding of the different T effector subsets and the array of cytokines they produce, it become obvious that no single pathogenic T cell phenotype is responsible for initiation of CNS autoimmunity. After the initiation of inflammation by T cells, they, along with CNS resident cells such as microglia or astrocytes, and infiltrating cells including monocytes, macrophages, dendritic cells, neutrophils, and B cells collectively mediate oligodendrocyte destruction, loss of myelin and axonal damage, eventually leading to neurological dysfunction.

In MS a relapse is usually followed by at least partial remyelination, which is due to the fact that most cell types have immune-modulatory subtypes that display anti-inflammatory properties, thereby limiting the immune response and initiating repair. Similar to effector T cells, there are multiple regulatory $CD4^+$ T cell subsets with a variety of suppressive mechanisms that play a role in MS. In general, the population of Treg cells is characterized by the expression of the lineage-determining transcription factor Forkhead box protein P3 (FoxP3). They can limit the immune response by an array of mechanisms; one is the secretion of anti-inflammatory molecules like cytokines IL-10, IL-35 and transforming growth factor-β (TGF-β) or adenosine (Sakaguchi et al., 2020). Further, Tregs can secrete Granzyme B to kill effector cells (Gondek et al., 2005) or directly suppress effector T cells or dendritic cells by cell-cell interaction (Wardell et al., 2021). In addition, Tregs can take up IL-2, which is essential for T cell survival and thereby deprive effector T cells of it resulting in their apoptosis (Pandiyan et al., 2007). Also regulatory subsets of $CD8^+$ T cells, B cells and natural killer cells have been described (Baecher-Allan et al., 2018).

1.3.2 Infiltration of T cells into the CNS

The migration of T cells is considered to be one of the hallmarks of MS and EAE pathogenesis, since they are the first immune cells to invade the CNS, where they can initiate the inflammatory cascade and subsequently potential relapses. There are three potential routes to enter the CNS, the T cell can either egress from the blood to the CSF across the choroid plexus,

to subarachnoid space or to the parenchymal perivascular space (Ransohoff et al., 2003). With the exception of the choroid plexus, the capillary endothelium of the cerebral vasculature forms the BBB with its unique feature of interendothelial tight junctions that prohibit circulating cells as well as serum macromolecules from entering into the CNS. Resting lymphocytes do not breach the BBB (Piccio et al., 2002), so in order to cross this barrier, T cells have to be first activated in the periphery to acquire a migratory phenotype. This phenotype is characterized by upregulation of migration-related genes and increased expression of adhesion molecules and chemokine receptors thus enabling the T cells to reach and attach to the BBB (Kuchroo et al., 1993, Flügel et al., 2001). The process leading to T cell extravasation is a finely regulated sequence of steps influenced by the lymphocyte subtype, the anatomical site of egress and the physiological or pathological situations in the CNS, which are influencing the expression and accessibility of adhesion molecules and activating factors. Nevertheless, a typical T cell extravasation involves the following steps (Figure 3).

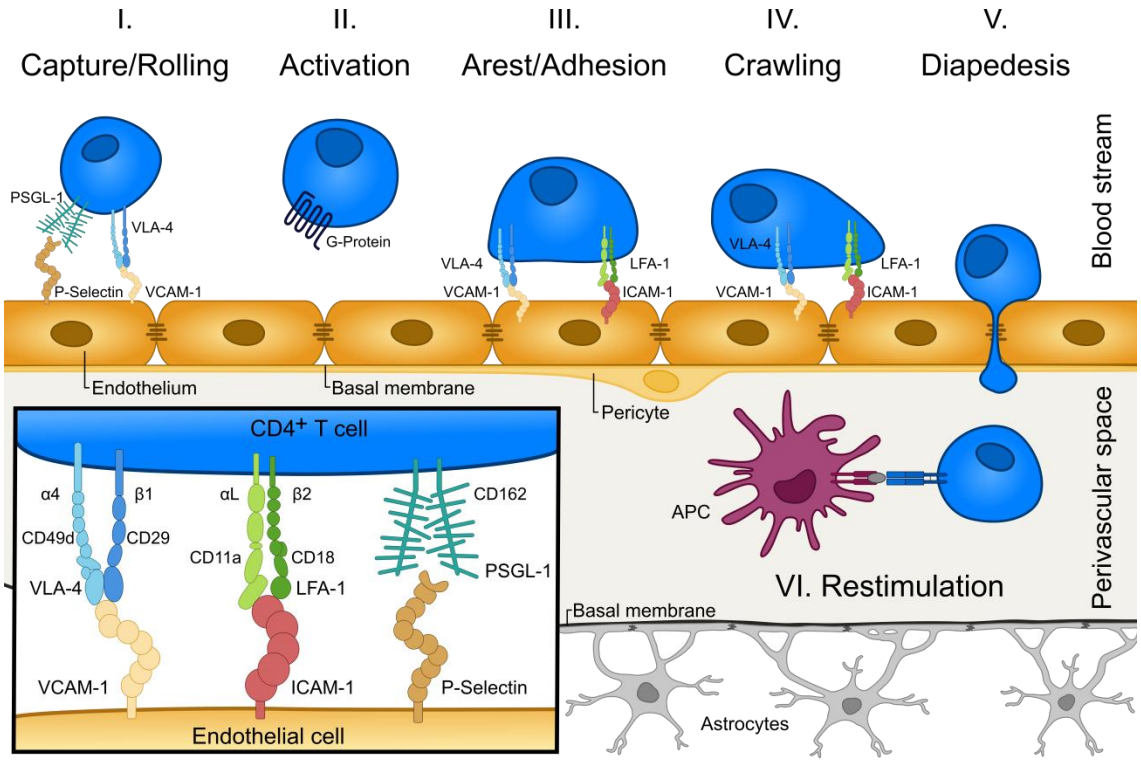

ICAM-1 = intercellular adhesion molecule 1, LFA-1 = lymphocyte function-associated antigen 1, PSGL-1 = P-selectin glycoprotein ligand 1, VCAM-1 = vascular cell adhesion module 1, VLA-4 = very late antigen 4

Figure 3 Molecular mechanisms involved in T cell migration across the BBB

The endothelial cells of post-capillary venules express P-selectin, that allows T cell in the blood stream to tether via its ligand PSGL-1 and thus reduce their velocity. Activation by chemokines via their respective receptors is followed by firm T cells adhesion mediated by VLA-4 and LFA-1 and their respective ligands VCAM-1 and ICAM-1. After intraluminal crawling the T cells cross the BBB and enter the perivascular space between the endothelial basement membrane and the glial limitans, consisting of astrocyte feet. T cells get activated by presentation of autoantigens by local APCs and initiate the inflammation cascade and further immune cell recruitment. Own graphic, based on (Mapunda et al., 2022, Engelhardt and Ransohoff, 2012).

Initially, the circulating T cell builds transient contact with the vascular endothelium to induce rolling on the vessel wall and reduce velocity. This can be mediated by selectins, like endothelial E-selectin or P-selectin interacting with its ligand P-selectin glycoprotein ligand 1 (PSGL-1). Further integrins participate in the rolling process. The leucocyte surface ligand very late antigen 4 (VLA-4), a heterodimer of α4- and β1-integrins can engage with its endothelial counterpart of the immunoglobulin superfamily, vascular cell adhesion molecule (VCAM)-1 to mediate adhesion (Engelhardt and Ransohoff, 2012). Once the lymphocytes tether and slowly roll along the vascular wall, they can then sense chemokines on the luminal surface of the endothelium via G protein coupled receptors (GPCRs). Those rapidly increase affinity and induce conformational change of integrins and thus mediate the shear resistant arrest of the leucocyte to the vessel wall (Constantin et al., 2000). Most relevant to the firm leukocyte arrest are the integrins belonging to the β1-integrin and β2-integrin subfamilies, especially VLA-4 (α4β1-integrin) and lymphocyte function-associated antigen 1 (LFA-1), consisting of αL-integrin and β2-integrin and there endothelial ligands VCAM-1 and intercellular adhesion molecule (ICAM)-1 (Ley et al., 2007). Before extravasation, T cells crawl along the intraluminal side of the blood vessel, preferentially against the direction of the blood stream potentially looking for a preferred site of transmigration (Bartholomäus et al., 2009). Diapedesis of leucocytes can occur either via the paracellular route through endothelial junctions by opening their endothelial contacts or via the transcellular route where the leukocyte migrates through the endothelial body by inducing the formation of pore-like structures (Engelhardt and Ransohoff, 2012). After the leucocytes have penetrated the endothelium, their basement membrane and the surrounding pericytes, they enter the perivascular or subarachnoid space. Here, they encounter MHC class II-expressing APCs like perivascular macrophages or dendritic cells that effectively present local autoantigens and thus activate T cells (Kivisäkk et al., 2009).

Upon activation, T cells produce proinflammatory trafficking mediators that recruit additional immune cells from the bloodstream and cross the glia limitans to migrate deep into the CNS parenchyma (Kawakami et al., 2004, Bartholomäus et al., 2009). Further, the secreted IL-17 and IL-22 disrupt BBB tight junctions thereby inducing a breach in the BBB and promoting the recruitment of additional $CD4^+$ T cells (Kebir et al., 2007). Also the BBB endothelium undergoes changes during neuroinflammation and increases the expression of adhesion molecules, proinflammatory cytokines and chemokines on the luminal surface (Marchetti and Engelhardt, 2020). Under physiological conditions, endothelial cells of the brain do not express the adhesion molecules necessary for T cell adhesion. Therefore, lymphocytes for immune-surveillance are assumed to enter via the blood-CSF barrier, where adhesion molecules are constitutively expressed, and migrate into the subarachnoid space (Goverman, 2009). Indeed,

in aT-EAE, pioneer T_{MBP}-GFP cells arrive first on the spinal cord leptomeninges within 3 h after transfer and are restricted to subarachnoidal areas, while the majority of the cells does not infiltrate until day three and only then induce inflammation (Bartholomäus et al., 2009).

The surface expression of the α4β1-integrin (VLA-4 receptor) is essential for this process. In an *in vitro* adhesion assay tested against various adhesion molecules only the blockage of α4β1-integrin inhibited binding (Yednock et al., 1992). In addition, *in vivo* infusion of anti-α4β1-integrin antibodies diminished intraluminal crawling and diapedesis of T cells and prevented the development of EAE (Yednock et al., 1992, Bartholomäus et al., 2009). Likewise, the administration of Natalizumab, a humanized anti-α4 integrin monoclonal antibody that blocks the binding of α4β1-integrin and α4β7-integrin to their respective receptors, into RRMS patients efficiently attenuated the rate of clinical relapses (Polman et al., 2006). While the effective inhibition of T cell migration with Natalizumab is beneficial in MS, it can have disastrous adverse effects in patients that contracted the John Cunningham virus (JCV), a human polyoma virus. JCV is usually harmless and asymptomatic in immunocompetent humans, but can cause progressive multifocal leukoencephalopathy (PML) in immuno-compromised people. PML is characterized by inflammatory demyelination of the white matter at multiple locations that often ends fatal, since no specific treatment is available (Cortese et al., 2021). Therefore, blocking the migration of only autoreactive T cells is essential in the treatment of MS but solely targeting those remains still a challenge.

1.4 CRISPR/CAS9 mediated gene editing

1.4.1 Genome editing with CRISPR/Cas9

The clustered regularly interspaced short palindromic repeats (CRISPR)/CRISPR-associated protein 9 (Cas9) system is a naturally occurring defence mechanism used by bacteria and archaea against bacteriophage infection and plasmid transfer (Barrangou et al., 2007). Its main feature – the ability to cleave site-specific double-stranded breaks (DSB) into DNA sequences – has been adapted in the last years to serve as a genome editing tool in mammalian cells (Jinek et al., 2012, Mali et al., 2013, Cong et al., 2013). So far around 93 Cas genes have been identified in different organisms (Butiuc-Keul et al., 2022), but the best known in genetic engineering is the Cas9 enzyme that originates from the bacteria Streptococcus pyogenes (SpCas9) (Haeussler and Concordet, 2016). In general, the CRISPR/Cas9 technique utilises a ribonucleoprotein (RNP) that consists of the RNA-guided endonuclease Cas9 and a noncoding guide RNA (gRNA) to localise the target sequence on the DNA. The guide RNA is originally a unique dual-RNA hybrid structure consisting of a CRISPR-RNA (crRNA) that encodes at its 5' end a so called "spacer" of 20 - 30 nucleotide long complementary sequence to the target DNA

and on its 3’ end a repeat sequence that allows binding to a second RNA; the trans-activating CRISPR RNA (tracrRNA). The tracrRNA binds the repeat sequence of the crRNA at its 5’ end and has a complex secondary structure on its 3’ end that enables the binding of the RNA complex to the Cas9 enzyme (Deltcheva et al., 2011). Both structures can be combined in a synthetic single guide RNA (sgRNA) that features the user-defined nucleotide sequence and the scaffold for the endonuclease (Jiang and Doudna, 2017). To successfully target a gene of interest, two factors are required. First, the gRNA and the target DNA need to have extensive complementarity with a sequence that is unique compared to the rest of the genome to avoid off-target cut sites. Secondly, the target sequence needs to be flanked by a protospacer-adjacent motif (PAM) of 2 - 6 nucleotides that serves a binding signal for the Cas9. The sequence of the PAM is specific to the Cas protein, when using the SpCas9, it is 5'-NGG-3' with N being any nucleobase followed by two guanine (G) nucleobases (Ran et al., 2013). If both conditions are met, the gRNA guides the RNP to the complementary nucleic-acid sequence in the target gene which the Cas9 endonuclease enzymatically cleaves. The resulting DSB is then repaired by one of the cell’s DNA repair mechanisms. The two major pathways are the efficient but error-prone, template-independent non-homologous end joining (NHEJ) and the less efficient but high-fidelity, template-dependent homology-directed repair (HDR) (Xue and Greene, 2021). Unlike HDR, NHEJ is active throughout the entire cell cycle making it the most active repair mechanism with only minimal DNA end processing. NHEJ relies on the binding of the Ku70/Ku80 protein heterodimer onto the broken DNA ends, which prevents further DNA-end resection and provides high affinity for the binding of the DNA-dependent protein kinase catalytic subunit. This in turn recruits further NHEJ polymerase, nuclease and ligase complexes. Depending on the base pairing between the ends, the complex can resect and/or add nucleotides in order to achieve compatible DNA ends and ligate those, thus repairing the DSB (Chang et al., 2017). Although NHEJ is capable of joining two DNA ends without nucleotide loss or addition from either DNA end, it often causes small (1-10 bp) nucleotide insertions or deletions (indels) at the DSB site (Figure 4). Those mutations can be extremely hetero-geneous, if the length of an indel is a multiple of three, there is either in an addition, exchange or loss of one or multiple amino acids in the coding regions of the genome. Any other indel size will introduces a frameshift mutation that leads to premature stop codons within the open reading frame of the targeted gene during mRNA synthesis. Depending on the position of the stop codon, the resulting faulty mRNA can be either degraded by nonsense mediated mRNA decay or transcribed into a truncated, likely malfunctioning version of the protein (Tuladhar et al., 2019). Apart from disruptions in the coding sequence also the binding sites of trans-acting factors in promoters or enhancers can be affected. In contrast, during HDR a desired sequence

can be inserted into the target locus by recombination with either an exogenous double-stranded or single-stranded DNA donor template that contains a homologous sequence surrounding the target locus. The precise sequence modifications make it a versatile tool for genomic engineering, especially for the generation of knockin or knockout animal models if germline competent cells are used. However, since recombination events occurs rarely and infrequent, the low efficiency presents an enormous challenge for certain experimental setups (Hsu et al., 2015). Further limitations are off-target edits due to sequence similarity with the target DNA, while rare, they may have severe consequences. In addition, delivery of CRISPR/Cas9 to a large number of cells can be challenging. Therefore, delivery by viral vectors is often the method of choice, which raises further issues. First, constant expression of the RNAs and the Cas9 enzyme may increase the chance of off-targets effects, secondly the presence of exogenous DNA can activate cellular receptors (e.g. Toll-like receptor 9), which in turn can induce an immune response (Xue and Greene, 2021). While only transient delivery of the CRISPR/Cas9 RNP can overcome some of these problems, it may result in decreased editing efficiency. Nevertheless, the simple two-component CRISPR/Cas9 allows easy, precise and efficient modification of the DNA, providing a cost-effective genome editing method to achieve a targeted KO of specific genes.

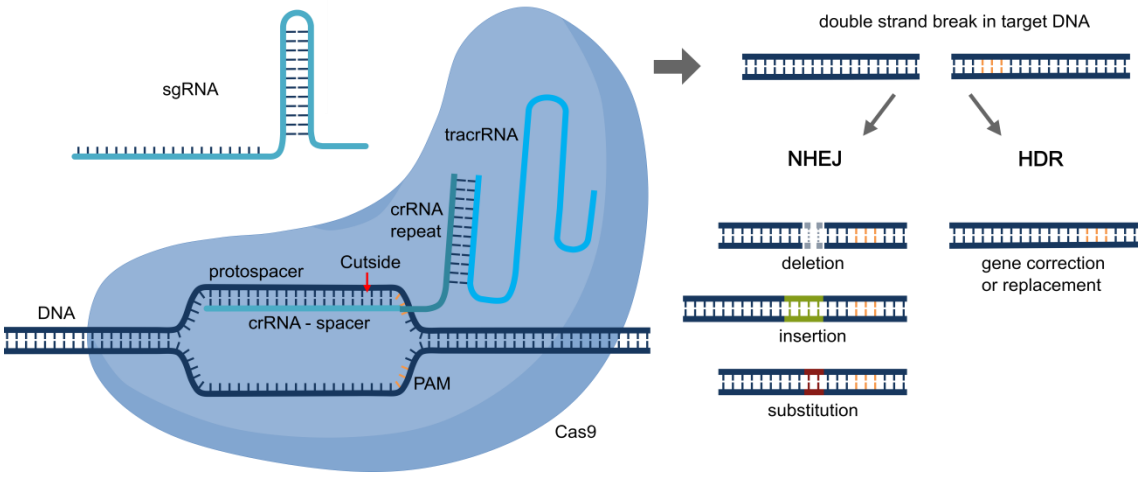

Figure 4 CRISPR/Cas9 mediated DNA editing

The CRISPR/Cas9 system comprises two components: A guide RNA and the Cas9 Nuclease. The guide RNA can either be a crRNA, that consists of a spacer that recognizes the target-sequence and a repeat sequence, that allows binding to the tracrRNA. The tracrRNA is a scaffold that in turn binds the Cas9 protein. Both can be combined in a single guide RNA that directs the Cas9 to the genomic DNA target side to introduce a site-specific DSB. This can be repaired by either HDR leading to gene correction or replacement with a given template or NHEJ that often results in indels resulting in a compromised gene. Own graphic, based on (Jiang and Doudna, 2017).

1.4.2 CRISPR/Cas9 library screening

An interesting application of the CRISPR/Cas9 system is its use in genetic screening studies of a specific phenotype or biological process to identify previously unknown genes, pathways and molecular mechanisms. For the purpose of discovery usually a pooled CRISPR/Cas9 screening is conducted in a model system, which can range from *in vitro* cell lines or primary cells to organoids and *in vivo* transplanted cells or even direct editing in an organism. Depending on the chosen model, the gRNAs and the Cas9 protein can be either stably expressed via lentiviral transduction or genome engineering or transiently introduced as a plasmid, mRNA or protein in the target cells (Chan et al., 2022). A stable expression is often favoured, since it allows preselection of clones with high expression levels. The design of the gRNA library is crucial for the screening. While a genome-wide screenings allows for an unbiased approach that does not depend on existing knowledge it requires a high number of cells to reach appropriate coverage making it unfeasible for certain cell types. In contrast, a library with a smaller selection of genes allows for a higher number of cells per gRNA, but due to the preselection some unexpected mechanisms might be missed in the screening. CRISPR/Cas9 screens usually target the protein-coding region of genes, but also non-coding DNA, regulatory regions or miRNAs can be targeted. Independent of the chosen library each gene should be targeted with at least four gRNAs (Hart et al., 2017). In a typical screen, the library of gRNAs is delivered to a pool of cells by viral transduction with a low multiplicity of infection to ensure that a majority of cells receive only one gRNA at once. The integration of the gRNA into the DNA serves as a distinct barcode that allows to determine the induced mutation and to count the number of cells carrying the gRNA sequence (Wang et al., 2014). The bulk gene-editing creates a pool of cells, where each has a unique loss-of-function mutation. Those are usually challenged with a selection pressure that forces them to compete with each other for representation in the final pool of the phenotypic read-out. The challenge can range from simple survival or proliferation studies to more complex drug treatment, environmental toxins, viral infection or functional biological assays *in vitro* or *in vivo* (Bock et al., 2022). Succeeding the phenotypic screen, the genomic DNA is extracted, the gRNA amplified and then identified and counted by high-throughput sequencing (Joung et al., 2017). In a pooled screening the raw sequencing reads are mapped to reference, processed and converted into a count matrix. In the resulting data, the abundance of the gRNAs are compared between treatments and controls and ranked according to their effect on the phenotype (Li et al., 2014). Depletion of multiple gRNAs, targeting the same gene in the final pool indicate that the disruption of this gene makes the cell more prone to the selective pressure, in contrast enriched gRNAs identify genes whose disruption gives cells an advantage in the challenge. The gene ranking can further be analysed

to identify enriched or depleted pathways or gene sets in the screening (Bock et al., 2022). Since the first descriptions of CRISPR/Cas9 screens in mammalian cells in 2014 (Wang et al., 2014, Shalem et al., 2014, Zhou et al., 2014, Koike-Yusa et al., 2014), they have been used in a wide range of applications. Among those are fundamental biological processes such as regulation of transcription (Grevet et al., 2018), cell signaling (Breslow et al., 2018) and differentiation (Li et al., 2019), but also general immunological processes including T cell activation (Chen et al., 2021), proliferation (Shifrut et al., 2018) and fate determination (Sutra Del Galy et al., 2021). CRISPR/Cas9 screens were also intensely used to study cancer-specific processes, including oncogenic transcriptional regulation (Lopes et al., 2021), immune evasion (Sheffer et al., 2021) and drug targets (Shi et al., 2015).

2 OBJECTIVES

MS and EAE share a similar pathogenesis, where the infiltration of encephalitogenic T cells over the BBB into the CNS is a critical event. Once in the CNS, these T cells become reactivated and trigger an inflammatory cascade, leading to damage and disability. Therefore, limiting T cell migration into the CNS has been a primary target for MS treatment. Despite significant progress in understanding MS/EAE and its treatment, research efforts have mainly focused on the roles of molecules involved in T cell trafficking. While these studies have provided valuable insights into the mechanisms of T cell entry into the CNS, there remain critical areas of knowledge that require further investigation. Specifically, we still lack a comprehensive understanding of the essential molecular cues and signaling pathways that enable or limit T cell entry into the CNS. Identifying these pathways could lead to the discovery of alternative targets for therapy, which may provide new treatment options for MS patients.

The first aim of this work was to conduct an unbiased *in vivo* genome-wide CRISPR/Cas9 KO screening in activated encephalitogenic $CD4^+$ T_{MBP} cells in an adoptive-transfer EAE model in Lewis rats to identify essential regulators of T cell that enhance or inhibit T cell transmigration across the BBB into the CNS.

The second objective of this study aimed to validate the potential candidates that were identified by the CRISPR/Cas9 KO screening in single KO T_{MBP} cells. The validation procedure encompassed both *in vitro* and *in vivo* experiments to elucidate the mechanism of action of the identified candidates and to gain a deeper understanding of their role in the regulation of T cell migration.

3 MATERIAL AND METHODS

3.1 Material

3.1.1 Plasmids

Table 1 Plasmids

Name	Provider
pCL-Eco	Mues et al. (2013)
pMSCV-neo	Clontech
MSCV-pU6-(BbsI)-CcdB-(BbsI)-Pgk-Puro-T2A-BFP	Addgene

3.1.2 Antigens

The MBP was prepared from frozen guinea pig brain homogenates as previously described (Campbell et al., 1973).

3.1.3 Media, Reagents and Buffers

Table 2 Media, reagents and buffers

Medium	Amount	Constituent	Company
ACK buffer	8.024 mg/l	NH_4Cl	Merck KGaA
	1.001 mg/l	$KHCO_3$	Merck KGaA
	3.722 mg/l	$EDTA.Na_2{\cdot}2H_2O$	Merck KGaA
EH	97.5 % Vol.	DMEM	Sigma-Aldrich
	2.5 % Vol.	HEPES solution, 1 M	Sigma-Aldrich
Flow cytometry buffer	99 % Vol.	PBS	-
	1 % Vol.	Rat serum	-
	0.05 % Vol.	NaN_3	Carl Roth GmbH
Freezing medium	50 % Vol.	Horse serum	Gibco
	40 % Vol.	EH	-
	10 % Vol.	Dimethylsulfoxide (DMSO)	Sigma-Aldrich
Isotonic Percoll	90 % Vol.	Percoll	Cytiva
	10 % Vol.	10x PBS	-
Lysis Buffer	100 µl/ml	Tris, 1M, pH=8.0	Sigma-Aldrich
	10 µl/ml	EDTA, 0.5 M, pH=8.0	Merck KGaA
	40 µl/ml	NaCl, 3 M	Carl Roth GmbH
	5 µl/ml	Tween 20	Sigma-Aldrich
Nycoprep	141 g/l	Nycodenz	Serumwerk
	3 g/l	NaCl	VWR Chemicals
	50 ml/l	Tricine, 100mM	Sigma-Aldrich
PBS, adjusted to pH 7.4 [10x]	100 mM	Na_2HPO_4	Carl Roth GmbH
	18 mM	KH_2PO_4	Merck KGaA
	1.4 M	NaCl	Carl Roth GmbH
	27 mM	KCl	Merck KGaA
	90 % Vol.	MilliQ water	-
Restimulation medium (RM)	99 % Vol.	TCM	-
	1 % Vol.	Rat serum	-
Sorting buffer	99 % Vol.	PBS	-
	1 % Vol.	Rat serum	-

	2mM	EDTA	Merck KGaA
Tris-Acetat-EDTA (TAE) [10x]	48.9 g/l	Trizma base	Sigma-Aldrich
	11.1 ml/l	Glacial acetic acid	Sigma-Aldrich
	3.7 g/l	EDTA	Merck KGaA
T cell medium (TCM)	Ad 1 l	DMEM	Sigma-Aldrich
	2 mM	L-Glutamine	Sigma-Aldrich
	100 µg/ml	Penicillin/Streptomycin	Sigma-Aldrich
	36 mg/l	Asparagine	Sigma-Aldrich
	1 mM	Sodium-Pyruvate	Sigma-Aldrich
	10 ml/l	Non-essential amino acids	Sigma-Aldrich
	4 µl/l	β-Mercaptoethanol	Merck KGaA
TCM + Fetal Bovine Serum (FBS)	90 % Vol.	TCM	-
	10 %	FBS	Merck KGaA
T cell growth factor medium (TCGF)	88 % Vol.	TCM	-
	10 % Vol.	Horse serum	Gibco
	2 % Vol.	Supernatant of ConA stimulated EL4.Il-2 cells	-
Underlay Percoll	65 % Vol.	Isotonic Percoll	-
	35 % Vol.	PBS	-

3.1.4 Antibodies

Table 3 Antibodies

Primary antibodies

Specificity Clone	**Host and conjugation**	**Provider**	**Catalogue #**
IgG1 Isotype control MOPC31c	mouse unconjugated	Sigma	M-1398
IgG2 Isotype control Ha4/8	armenian hamster unconjugated	BD Pharmingen	553961
IgG1 Isotype control R3-34	rat PE conjugated	BD Pharmingen	554685
CD4 OX38	mouse unconjugated	BD Pharmingen	554841
CD11a Wt.1	mouse unconjugated	Biolegend	201902
CD18 Wt.3	mouse unconjugated	ThermoFischer	MA1817
CD25 OX39	mouse unconjugated	ThermoFischer	MA517490
CD49d TA2	mouse unconjugated	ThermoFischer	MA49D7
CD134 OX40	mouse unconjugated	Serotec	MCA730XZ
IFNy DB1	mouse unconjugated	eBioscience	14-7310-85
TCR R73	mouse unconjugated	Serotec	MAC453G

CD29 HMβ1-1	armenian hamster unconjugated	Biolegend	102202
CD49b Hma2	armenian hamster unconjugated	ThermoFischer	16-0491-85
IL-17A TC11-18H10	rat PE conjugated	BD Pharmingen	559502

Secondary antibodies

Specificity	**Host and conjugation**	**Provider**	**Catalogue #**
Armenian hamster IgG (H+L)	Goat APC conjugated	Jackson ImmunoResearch	127-136-160
Mouse IgG (H+L)	Donkey APC conjugated	Jackson ImmunoResearch	715-136-151
Mouse IgG (H+L)	Goat AF647 conjugated	SouthernBiotech	1038-31

3.1.5 Oligonucleotides

Table 4 Primers TIDE Sequencing

Target gene	**gRNA sequence**	**Forward & reverse primer sequence**
Non-Targeting	GCTGCATGGGGCGCGAATCA	-
CCR5	ATAATGTGCAAATTATTCAC	TTATAGTATGTCAGCACCCTGC
		ACACGATCAGGATTGACTTGC
Cxcr3	TCTGCGTGTACTGCAGCTAG	AACATCAACTTCTACGCAGG
		TCTTCCTCTTCTCACACAGG
Ets1	TGCTGCTCGGAGTTAACAGT	GTGGAAACCCCCTTCAGTTT
		GTAACCAGCTCTTCGGTCTG
Gnai2	TGGGTGGTCAGCGATCTGAG	TACTAATAGCTTCTCCCGCCT
		CTCGTCATACTTGTTGGCCC
Grk2	GATTTGTCAGAACCTCCGAG	TGGCTGTGACTGAAAATGCT
		CTGAACCATCTGGAAGAGGC
Hsp90b1	GTCTCACGGGAAACATTGAG	ATCTAGACGGTGACTCTGTTCT
		TGGCAAAAGGGCTTATTGAAAG
Itga4	GATGCTGTTGCTGTACTTCG	TGCTGCACTTCATCTCTTGG
		GCGTGGCGTTAAAGTTGAAA
Itgb1	TCCCAACATTCCTACCAATG	CAAGAGGGCTGAAGACTACCC
		GAAGGTTACACACTACACCACA
S1PR1	GCGGCTTCGAGTCCTCACCA	TCTGTCTGCCTCAGTCTTCA
		AGACCTGATCTCCACCCTTC
Tbx21	GACGTATAAGCGGTTCCCTG	ATGATGAGACCTACCGCCTA
		TGGGATATCGGGACCATCA
Ube2l3	GCTTGAAGGGATACTCTGCT	CATCTTGGCTGGGAATCCTG
		ATCCCCTAGGACTTGACTGG

Methods

3.1.6 Cell culture

HEK293T culture

HEK293 T cells were cultured in 10 cm culture dishes with 10 ml TCM + 10 % FBS in an incubator with culture conditions of 37 °C with 10 % CO_2. Once the cells reached around 90 % confluency they were passaged. Cells were frozen in cryotubes at a concentration of 1 x 10^6/ml in freezing medium first at -80°C and kept in liquid nitrogen for long term storage. Prior to culturing, cells were thawed in a 37 °C water bath and once washed with 10 ml EH to remove DMSO.

Retrovirus production

24 h prior to transfection 1.2x10^6 HEK293 T cells were plated in a 10 cm culture dishes with 10 ml TCM + 10 % FBS. For transfection 3.5 µg pCL-Eco packaging vector and 6 µg pMSCV retroviral plasmid were first incubated 5 min in 500 µl TCM. After addition of in 20 µl 2 mg/ml PEI Max (Polysciences) in 500 µl DMEM, vortexing and 20 min incubation at room temperature (RT) the mixture was added dropwise onto cells. HEK293 T cells were cultured 24 h at 37 °C with 5 % CO_2. Successful transfection was confirmed by expression of fluorescent proteins under fluorescent microscope and medium was exchanged to 8 ml TCM + 10 % FBS. At 48 h and 72 h after transfection the virus containing cell supernatant was collected, centrifuged at 2000 g for 10 min and stored at 4°C. Prior to virus concentration the supernatant was warmed up to RT and filtered with a 0.45 µm sterile filter (Merck Millipore). To concentrate the virus the cell supernatant was centrifuged at 4000 g for 20 min at RT in an Amicon Ultra-15 (100K) Centrifugal Filter Unit (Merck KGaA). The viral concentrate was directly used for retroviral transduction of T_{MBP} cells.

T_{MBP} cell culture

A stock of T_{MBP} cells has been previously generated in our lab by immunizing Lewis rats with MBP by PD Dr. Naoto Kawakami as described before (Kawakami et al., 2004) and was stored in liquid nitrogen until use. Prior to restimulation the T cell were thawed in a 37 °C water bath and once washed with 10 ml EH to remove DMSO. For restimulation 3.5x10^6 T_{MBP} cells were mixed with 70-100x10^6 irradiated (50 Gy) syngeneic thymic cells in 5 ml RM supplemented with 1 mg/ml MBP. Cells were cultured in a 6 cm cell culture dishes (BD) in a humidified incubator at 37 °C with 10 % CO_2. After 48 h the T_{MBP} cells reached their maximum activation capacity and were either used in experiments or expanded by transfer into a 10 cm cell culture dish and addition of 5 ml TCGF. T_{MBP} cells were cultured under the same conditions as before for additional 96 h and splitted when needed. Then T_{MBP} cells were either restimulated again or

20-50x10^6 cells were resuspended in 1 ml FM and stored at -80°C. For long-term storage the cells were transferred into liquid nitrogen.

Isolation of T_{MBP} cells with nycoprep gradient

Restimulated T cells were isolated from culture usually 48 h after restimulation by a nycoprep gradient. For *in vitro* cytokine stainings, isolation was performed at 24 h after restimulation. Cells were resuspended in 5 ml EH and carefully overlaid onto 3 ml nycoprep solution. After centrifugation at 675 g, RT for 10 min with mild acceleration and brake, the lymphocytes were collected from the interface and once washed with PBS.

Retroviral transduction of T_{MBP} cells

Stable Cas9-EGFP expressing T_{MBP} cells were prior generated by PD Dr. Naoto Kawakami and Dr. Arek Kendirli by transducing T_{MBP} cells with a pMSCV-Cas9-EGFP-neo vector and expansion under Neomycin selection followed by cell sorting (Kendirli et al., 2023). The T_{MBP} Cas9-EGFP cells were transduced at a maximum multiplicity of infection of 0.3 to prevent multiple integrations. In addition T cell numbers were kept high (90 x 10^6 cells for the genome-wide screen, and 12 x 10^6 cells for the validation screen) during the process to ensure a minimum of 1000 T cells having the same sgRNA (1000x coverage). For transduction, 48 h restimulated T_{MBP} cells were isolated by nycoprep gradient and resuspended in TCGF with 8 µg/ml polybrene (Sigma) at a concentration of 4x10^6/ml. After plating 500 µl/well of the cell suspension in non-tissue culture treated 12-well plates concentrated virus solution was added at 50 µl/well and plates were centrifuged at 2000 g, RT for 90 min. 1 ml TCGF was added per well and T_{MBP} cells were further cultured in 10 % CO_2 at 37°C. The addition of 0.5 µg/ml Puromycin 24 h later selected for transduced T_{MBP} cells. Those were further cultured and restimulated as described above, before injection into recipient animals.

Nucleofection of T_{MBP} cells

For the generation of single KO T_{MBP} cells DNA modifications were introduced by RNP electroporation into previously blue fluorescent protein (BFP) or enhanced green fluorescent protein (EGFP) transduced T_{MBP} cells. The sgRNAs were designed with the GPP sgRNA designer and synthesized by Integrated DNA Technologies. The Cas9 protein and the respective sgRNA were electroporated into T_{MBP} cells by using Amaxa 4D-Nucleofector System and P4 Primary Cell 4D-Nucleofector® X Kit S (Lonza) according to manufacturer's instructions. Briefly, for the gRNA 0.75 µl of Alt-R CRISPR-Cas9 tracrRNA (200 pmol/µl; IDT) and 0.75 µl of target-specific Alt-R CRISPR-Cas9 crRNA (200 pmol/µl; IDT) were mixed. Those were first incubated at 95°C for 5 min, then with decreasing temperature to 70°C at the rate of 0.5°C/sec, at 70°C for 1 min, then cooled to 22°C. Next 7.5 µg Alt-R S.p. HiFi Cas9 Nuclease V3 (IDT) was added and

incubated at RT for 20 min. T_{MBP} cells, 48 h after restimulated were isolated by nycoprep gradient, washed with PBS and resuspended in 21 µl of a master mix consisting of 18 µl of P4 primary solution, 4 µl of supplement 1 and 1 µl of electroporation enhancer (stock: 100 µM; IDT). After addition of the RNP solution, the mixture was transferred into a nucleofection cuvette and electroporated with the pulse code CM137. The electroporated T_{MBP} cells were transferred into 3 ml pre-warmed TCGF in a 6-well plate and further cultured at 37°C with 10 % CO_2.

3.1.7 DNA techniques

sgRNA library construction

A list of gene- and miRNA-targeting sgRNAs of the rat genome was kindly provided by the Functional Genomics Consortium of The Broad Institute, Massachusetts, USA. In the genome-wide library, four sgRNA per gene or miRNA were selected wherever possible, in some cases e.g. for miRNAs only fewer unique sgRNAs were available. To increase the confidence of the hits from the initial screening, six sgRNAs per gene were used in the validation library. For the genome-wide library a total of 87,690 oligonucleotides and for the validation library 12,000 oligonucleotides were purchased from Twist Bioscience, each as a 79-mer with a sequence of 5'-GCAGATGGCTCTTTGTCCTAGACATCGAAGACAACACCGN_{20}GTTTTAGTCTTCTCGTCGCC-3', with N_{20} indicating the sgRNA sequence. The library cloning was performed by Dr. Arek Kendirli as previously described (Koike-Yusa et al., 2014) with minor modifications. The correct insertion was confirmed with Sanger sequencing (sequencing service, LMU Biozentrum).

Plasmid isolation from Escherichia coli

Transformed Escherichia coli bacteria from glycerol stock were first incubated in a shaker overnight in 3 ml LB medium at 37°C with 180 rpm. The culture was expanded by adding 400 ml LB medium and cultured under the same conditions overnight. The plasmid DNA was isolated from the bacteria using the NucleoBond Xtra Midi EF kits (Macherey-Nagel) according to the manufacturer's instructions. To establish an Escherichia coli glycerol stock 800 µl bacteria solution was mixed in a ratio of 1:1 with 50 % glycerol (Sigma) and stored at -80 °C.

Tide assay

The KO efficiency of T_{MBP} single KO cells was validated on the DNA level prior to experiments. To isolate genomic DNA (gDNA) nycoprep isolated T cells were incubated with 500 µl lysis buffer that was prior supplemented with 50 µl/ml Proteinase K first at 56°C for 15 min and then 10 min at 95°C followed by cooling on ice. Next 350 µl isopropanol were added and the mixture was incubated for 10 min at RT and centrifuged at 16000 g for 10 min at 4°C. After washing of the pellet by addition of 1 ml of 70 % ethanol and 5 min centrifugation at 16000 g

at 4°C, the supernatant was discharged and the pellet was first dried for 10 min at 56°C to remove residual ethanol and then resuspended in 50 µl water. For each KO cell line a DNA sequence ranging from around 200 bp before to approximately 700 bp after the expected cut side was amplified by PCR using 10 µl 2x Optima PCR HotStart Polymerase (FastGene), 1 µl respective primer mix (10 µM) for each target gene and 9 µl DNA solution. After running the PCR products on a 1 % agarose gel in TAE buffer, they were purified using the Wizard SV Gel and PCR Clean-Up System (Promega) and resuspended in 50 µl water. The DNA fragments were submitted to Sanger Sequencing (sequencing service, LMU Biozentrum) and their INDELs and KO efficiency were assessed by the ICE (Inference of CRISPR Edits) v2 software tool (Conant et al., 2022).

NGS sgRNA library preparation

The NGS sgRNA library preparation was performed by Dr. Arek Kendirli as previously described (Kendirli et al., 2023). The gDNA from lymphocytes or sorted T_{MBP} cells was isolated with the DNeasy Blood and Tissue Kit (Qiagen) and a one-step PCR amplification was performed for a total of 24 cycles using Q5 High Fidelity DNA Polymerase with 2.5 µg of gDNA per reaction, Fwd-Lib (8 staggered primers) and Rev-Lib (8 bp of unique barcode) primers. Illumina adapters were introduced together with the amplification primers. The amplified DNA amplicons were purified with SPRIselect (Beckman Coulter, B23317) with a ratio of 1:0.8 (DNA to beads) and eluted in nuclease-free water. The presence of ~250 bp DNA amplicons was confirmed and the concentration was measured with Agilent Bioanalyzer on DNA 1000 Chips (5067-1504). All samples were sent to “The Laboratory for Functional Genome Analysis” (LAFUGA) at the Gene Center Munich for sequencing single-end 50 bp on a HiSeq 1500.

3.1.8 Flow Cytometry

Surface staining

In vitro T_{MBP} cells were purified by nycoprep, 48 h after restimulation and transferred into V-shaped 96-well plates. The cells were incubated 15 min with 150 µl flow cytometry buffer on ice, followed by centrifugation at 500 g for 3 min at 4°C. Next the cells were incubated with 100 µl 1:100 diluted primary antibodies in flow cytometry buffer for 30 min on ice. Afterwards the samples were washed three times with flow cytometry buffer with each washing step following a centrifugation step of 500 g for 3 min at 4°C. The secondary antibodies were added in a dilution of 1:1000 in flow cytometry buffer and incubated 30 min on ice, protected from light. After washing once with flow cytometry buffer and once with PBS, the cells were resuspended in PBS and analyzed by flow cytometry on a CytoFlex S (Beckman Coulter).

Intracellular staining

In vitro T_{MBP} cells were purified by nycoprep, 24 h after restimulation and transferred into V-shaped 96-well plates. Cells of the non-stimulated group were resuspended in 100 µl RM supplemented with 5 µM Brefeldin A (Sigma Aldrich) and cultured in the incubator at 37°C with 10 % CO_2 for 5 hrs. The other part of the cells was first stimulated with 100 ng/ml phorbol 12-myristat 13-acetat (PMA) and 100 nM Ionomycin in 100 µl RM for 2 h in the incubator at 37°C with 10 % CO_2. Then brefeldin A was added to a final concentration of 5 µM and cells were cultured for another 3 h. After centrifugation at 500 g for 3 min at 4°C cells were resuspended in 150 µl 2 % paraformaldehyde (PFA) and incubated for 15 min on ice. Following fixation and centrifugation at 500 g for 3 min at 4°C, the samples were resuspended in 150 µl PBS and stored at 4°C until further use. For staining the cells were permeabilized 15 min with 150 µl 1x Intracellular Staining Perm Wash Buffer (PB) (Biolegend) on ice, followed by centrifugation at 500 g for 3 min at 4°C. Next the cells were incubated with 100 µl 1:100 diluted conjugated or unconjugated primary antibodies in PB buffer for 30 min on ice, protected from light. Afterwards the samples were washed three times with PB with each washing step following a centrifugation step of 500 g for 3 min at 4°C. The secondary antibodies were added in a dilution of 1:1000 in PB and incubated 30 min on ice, protected from light. After washing once with PB and once with PBS, the cells were resuspended in PBS and analysed by flow cytometry on a CytoFlex S (Beckman Coulter).

Cell sorting

For the *ex vivo* sorting of the CRISPR screens BFP^+ T_{MBP} cells were sorted either only from the spleen in the genome-wide screening or from spleen, blood, meninges and parenchyma for the validation screening by Dr. Arek Kendirli. *In vitro* T_{MBP} Itgb1-KO cells were sorted on day four after restimulation, following surface staining of β1-integrin. All samples were sorted using a FACS Aria III (BD) or FACS Fusion (BD) at the Flow Cytometry Core Facility of the Biomedical Centre, LMU.

Data analysis

The flow cytometry data was analysed using FlowJo (Tree Star Inc).

3.1.9 Chemotactic assay

In vitro T_{MBP} cells were purified by nycoprep, 48 h after restimulation and resuspended in RM. NT-BFP^+ and KO-$EGFP^+$ T_{MBP} cells were counted and mixed at a ratio of 1:1 that was adjusted and confirmed by flow cytometry analysis. The chemotaxis assays were performed using a 96-well transwell chamber with 5 µm pore size (Corning). While each upper insert received 0.2×10^6 T cells in 75 µl RM, 235 µl RM with or without chemotactic stimulus of 30 ng/ml

recombinant CXCL10 (PeproTech, 400-33) or recombinant CCL5 (PeproTech, 400-13) was added to the lower compartment. After centrifugation at 400 g for 1 min the cells were incubated at 37°C with 10 % CO_2 for 5 h and the migrated cells in the lower chamber were subsequently analyzed by flow cytometry using LSRFortessa (BD) or CytoFlex S (Beckman Coulter).

3.1.10 Rat routine

Licence

Lewis rats were purchased from Charles River or Janvier and bred in the Core Facility Animal Models of the Biomedical Center, LMU. All animal experiments and their care were carried out in accordance with the regulations of the applicable animal welfare acts and protocols were approved by the responsible regulatory authority (Regierung von Oberbayern). All animals had free access to food and water. Animals were kept at room temperature 22 +/- 2°C, humidity 55 +/- 10 % with a Light/Dark cycle, 12h/12h (6:30-18:30). Male and female Lewis rats between 5-20 weeks old were used for the experiments.

Adoptive transfer EAE

AT-EAE was induced by intravenous injection of *in vitro* activated T_{MBP} cells into the tail vein of rats. The number of transferred T_{MBP} cells ranged from $1x10^6$ T_{MBP} cells for the assessment of the clinical course, a mix of $3.5x10^6$ NT and $3.5x10^6$ KO T_{MBP} cells for the evaluation of migration into the CNS to $10x10^6$ T_{MBP} cells for the CRISPR screenings. After the T_{MBP} cell transfer, the body weight and the clinical score of the rats were monitored daily. The EAE score was evaluated as follows:

0, no clinical signs; 0.5, partial tail weakness; 1, tail paralysis; 1.5, gait instability or impaired righting ability; 2, hind limb paresis; 2.5, hind limb paresis with dragging of one foot; 3, total hind limb paralysis.

Isolation of T_{MBP} cells

For the CRISPR screening and the *in vivo* migration analysis the rats were sacrificed three days after T_{MBP} cell transfer. First blood was drawn by heart puncture into a heparinized syringe and subsequently diluted with PBS in a 1:1 ratio. After a nycoprep gradient with centrifuge settings at 800 g, 30 min, RT the lymphocytes were collected from the interface, once washed with PBS and incubated for 2 min with 2 ml ACK buffer to remove remaining erythrocytes, followed by another washing step. The spleen, parathymic lymph nodes, leptomeninges and parenchyma of the spinal cord were dissected and homogenized by passing through a metal strainer using a syringe plunger. Plate and strainer were washed with EH and cells were centrifuged at 400 g

for 5 min at 4°C. The splenic samples were treated with 5 ml ACK buffer for 2 min, followed by a washing step with PBS. The cells were resuspended in 13 ml TCM + 10 % FBS, transferred into a 10 cm culture dish and incubated for 1 h at 37°C with 10 % CO_2 to allow macrophages to attach. After gentle swirling of the plate the suspension cells were collected and passed through a 40 µm cell strainers (Greiner Bio-One GmbH). For sorting during the CRISPR screens the $CD4^+$ T cells were further enriched by using the EasySep™ Rat $CD4^+$ T cell Isolation Kit (StemCell technologies) according to manufactures' instructions. The lymphocytes from the spinal cord parenchyma were isolated using a Percoll gradient. For this 25 ml cell suspension in EH were mixed with 10.8 ml isotonic Percoll and 10 ml underlay percoll were underlayed. After centrifugation at 1200 g for 30 min at RT with mild acceleration and brake the lymphocytes were collected from the interface and washed with PBS. For the CRISPR screening experiments the cells from a minimum of eight animals for a single genome-wide replicate and of six animals per validation screening replicate were pooled. Depending on the experiment the isolated T cells were either subjected to sorting, DNA isolation or flow cytometry analysis with and without surface or intracellular staining as described above.

3.1.11 Intravital two-photon microscopy

Imaging setup

Intravital imaging of the spinal cord leptomeninges was performed on a Leica SP8 microscope two or three days after intravenous co-transfer of $1x10^6$ NT-BFP^+ and $1x10^6$ Grk2-KO-$EGFP^+$ T cells as previously described by our lab (Bartholomäus et al., 2009) with Dr. Isabel Bauer. First the animal was anesthetized by intramuscular injection of MMF (2 mg/kg Midazolam, 150 µg/kg Medetomidine and 5 µg/kg Fentanyl) and a tracheotomy was performed to allow mechanical ventilation with 1.5-2.0 % isoflurane in air. In addition, a catheter was inserted into the tail vein, which later allows the intravenous injection of 100 µg Texas-Red conjugated 70 kDa dextran (Invitrogen/ThermoFisher) in order to visualize the blood plasma during imaging. During the whole procedure the rats body temperature was maintained by a heat-pad placed underneath. For the laminectomy the skin was opened with a midline incision of 3 cm at the dorsal part of Th12/13 and the paravertebral musculature was removed. For stable imaging and reduction of artifacts such as breathing three spines were fixed using a custom-made stage and the animal was slightly lifted. After removal of the dorsal part of the central spine disc with a dental drill (Foredom) the open spine was surrounded by a ring of low-melting agarose. This was filled with PBS to keep the tissue hydrated and to allow the use of a water-immersion 25x objective lens (N.A.: 1.00, WD: 2.6 mm). Last the dura was removed. A pulsed-laser from an InSight DS+ Single (Spectra Physics) was adjusted to 840 nm for the

excitation of BFP and EGFP. The fluorescence signals were first separated with a beam splitter BS560, then the signals of shorter wavelength were again split by BS505 and detected after the band pass filters HC405/150 (BFP) and ET525/50 (EGFP). The signals of a longer wavelength were again separated by beam splitter RSR620 and detected after the band pass filter BP585/40 (Texas Red). All images were acquired from a field of approximately 440 µm x 440 µm with a resolution of 512x512 pixels and an approximate 100 µm z-stack, with an interval of 2-3 µm.

Image processing and analysis

Time-lapse images were acquired with the LAS X software (Leica) and processed and analysed using ImageJ (NIH). A Gaussian Blur filter with a cut off of 1 pixel was used before maximum Z-projection of the stacks. When necessary, bleed-through liner subtraction was applied. The signal intensity was adjusted by linearly adjusting contrast and brightness. The locations of T cells were analysed by the Cell Counter Plugin of ImageJ. Moving T cells were tracked using the manual tracking plugin of ImageJ. The obtained coordinates in combination with information on pixel resolution and time were used to calculate the cells speed and track length in Excel.

3.1.12 Bioinformatic analysis

All bioinformatical analysis and resulting graphs in the figures (Figure 5, Figure 6 and Supplementary Figure 1) were conducted and described by Clara de la Rosa del Val as followed (Kendirli et al., 2023):

CRISPR screening analysis

The genome-wide CRISPR screening and the validation screening both consisted of three replicates each. However, one of the blood replicates in the genome-wide screening was excluded due to technical issues. Data analysis was performed using the Galaxy platform (Afgan et al., 2018). De-multiplexing of the raw fastq files was done with Je-Demultiplex-Illu, followed by Cutadapt and Trimmomatic to obtain the 20 bp sgRNA sequence. MAGeCK was used for counting (Li et al., 2014) (version 0.5.7.1+) and normalization across samples was conducted in R (version 4.0.0+) (R Core Team, 2021) using the geometric mean per sgRNA after applying a 50 raw count threshold. SgRNAs with fewer than 50 counts in more than two replicates of the same tissue were discarded. The MAGeCK test was run without normalization or zero removal and with default parameters on Galaxy, where the information of non-targeting sgRNAs was used for noise correction. Further data processing was performed in R.

Genome-wide screening analysis and validation screening design

To model the behaviour of a wild-type gene based on individual sgRNAs, four random control sgRNAs were selected with replacement from the control sgRNA pool, and their log2(Fold Change) was averaged for plotting the control values in the genome-wide analysis results. This process was repeated 800 times for a total of 800 combinations of control "genes," each consisting of four different NT sgRNAs. The validation screening candidates were selected based on MAGeCK results from the genome-wide screen. Genes with an absolute "neg|1fc" or "pos|1fc" > 0.5 in meninges vs blood and parenchyma vs blood comparisons were included. For other comparisons such as meninges or parenchyma vs spleen and spleen vs blood, genes were included when the absolute “neg|lfc” or “pos|lfc” > 1 and the number of “neg|goodsgrna” for negative “neg|lfc” candidates or of “pos|goodsgrna” for positive “pos|lfc” candidates ≥ 2, or the absolute “neg|lfc” or “pos|lfc” > 0.6 and the number of “neg|goodsgrna” or “pos|goodsgrna” > 2.

The validation library was restricted to genes expressed in T cells, as detailed in (Schläger et al., 2016), with the exception of genes from the meninges or parenchyma vs. blood comparisons, which were included if their absolute “neg|1fc” or “pos|1fc” was greater than 0.85. We further included genes that are associated with the following Gene Ontology (GO) terms for the purpose of validating their functions: GO:0004896 (Cytokine receptor activity), GO:0050840 (Extracellular matrix binding), GO:0004930 (G protein-coupled receptor activity), GO:0005178 (Integrin binding) and GO:0033627 (Cell adhesion mediated by integrin). Further, top gene sets were chosen by running GSEA(Broad) with default parameters and the exception of metric ranking genes = log2_Ratio_of_Classes, using the GSEA molecular signature databases v7.0, and with exclusion of gene sets with maximum and minimum sizes of 20000 and 5, respectively. The selected gene sets were GO:0043112 (receptor metabolic process), GO:0072583 (clathrin-dependent endocytosis), GO:0097384 (cellular lipid biosynthetic process), GO:0042092 (type 2 immune response), GO:0051955 (regulation of amino acid transport), GO:0098661 (inorganic anion transmembrane transport), GO:0015698 (inorganic anion transport), GO:0035655 (interleukin-18-mediated signaling pathway), GO:0071277 (cellular response to calcium ion), GO:0016574 (histone ubiquitination), GO:0043968 (histone H2A acetylation), GO:0006089 (lactate metabolic process), GO:0070670 (response to interleukin-4), GO:0032606 (type I interferon production) and GO:0002755 (MyD88-dependent toll-like receptor signaling pathway). In certain GO terms, only genes with a negative log2(Fold Change) were included when the GO term was negatively enriched, while genes with a positive log2(Fold Change) were included when the GO term was positively enriched. This led to the

inclusion of 1374 genes based on log2(Fold Change) and significance cut-offs in different comparisons, and 587 genes based on GO terms.

Identification of essential regulators of migration

The validation screening candidates were considered essential regulators of T cell migration to the CNS if they fulfilled the following conditions, based on the MAGeCK analysis results: “neg|lfc” < -3 x standard deviation of control (non-targeting) “neg|lfc” and “pos|lfc” in the sample, the number of “neg|goodsgrna” ≥ 3, and the “neg|p-value” < 0.05; or “pos|lfc” > 3 x standard deviation of control “neg|lfc” and “pos|lfc” in the sample, the number of “pos|goodsgrna” ≥ 3, and the “pos|p-value” < 0.05.

3.1.13 Statistical analysis

Flow cytometry data was analysed using FlowJo (version 10+). Statistical analyses and plotting were performed using GraphPad Prism version 7+ (GraphPad Software) and R (version 4.0.0+) (Wickham et al., 2019, R Core Team, 2021). Total cell numbers were calculated using R and Excel (Microsoft Office). Figures were prepared using Inkscape. The Gaussian distribution of the data was determined using the Shapiro-Wilk normality test. Parametric tests were used for data with Gaussian distributions, and non-parametric tests were used for non-Gaussian data, except for grouped data analysed by two-way ANOVA, such as integrin and activation marker surface stainings, and intracellular cytokine stainings, where non-parametric tests were not applicable. If multiple comparisons were run in parallel, the test statistics were corrected for multiple testing using the two-stage linear step-up procedure of Benjamini, Krieger, and Yekutieli. The control values for *in vitro* surface staining experiments and *in vitro* and *in vivo* intracellular cytokine stainings are reused and thus remain identical across all figure panels. In the flow cytometry evaluation of T_{MBP} KO cell migration validation experiments, animals with less than 100 cells detected in any organs were excluded from the analysis. The KO/control phenotype datasets were statistically evaluated using one-sample t-tests (parametric) or Wilcoxon signed-rank tests (non-parametric). The Grk2-KO values for the Grk2-KO/S1RR1-KO and double KO experiment are the same as previously depicted for the Grk2-KO migration phenotype data. An ordinary one-way ANOVA with Tukey's multiple comparison tests (parametric) and Kruskal-Wallis test with Dunn's multiple comparison test (non-parametric) were conducted for the KO/NT phenotypes across the different KOs in the Grk2/S1PR1-KO experiment. In disease course experiments, control animals were chosen based on the same date of cell transfer as the KO-transferred animals. As a result, some control animals were utilized for more than one KO. To evaluate the disease induction and weight changes phenotypes of the KO cell transfer, a repeated measures two-way ANOVA was conducted for

time and genotype variations (days zero to eight after T_{MBP} cell transfer for disease score and days zero to eight for weight changes), followed by Sidak's multiple comparison test. All measurements were biological replicates and not duplicated, except for clinical course experiments where the same animal was monitored over multiple days. KO/NT comparisons were expressed as a ratio of KO phenotype/control NT phenotype, unless otherwise stated. Relevant information, including sample sizes, was included in the figure legends. The data are presented as mean ± SD (standard deviation) and the significance was indicated by p-value as follows: * = $p<0.05$, ** = $p<0.01$, *** = $p<0.001$, **** = $p\leq0.0001$

4 RESULTS

4.1 CRISPR/Cas9 screening in EAE

4.1.1 Unbiased whole-genome screening of T_{MBP} cell trafficking *in vivo*

To study the mechanisms essential to the migration of T cells into the CNS we used the Lewis rat aT-EAE model, since its stable clinical course allows specifically observing T cells involved in the initial phase of EAE. To conduct a genome-wide CRISPR/Cas9 screening first autoreactive T_{MBP} cells, that stably express Cas9 together with EGFP (T_{MBP} Cas9) were generated and validated by PD Dr. Naoto Kawakami and Dr. Arek Kendirli (Kendirli et al., 2023). Once the gene editing capabilities were confirmed the T_{MBP} Cas9 cells were transduced with a genome-wide sgRNA library that contained 87,690 sgRNAs targeting 21,410 genes and 396 miRNAs (4 sgRNA/gene), as well as 800 non-targeted (NT) control sgRNAs together with BFP for labelling. The ratio of virus to cells was calculated so that statistically each T cell would receive only one sgRNA. Following restimulation the T_{MBP} cells were injected i.v. into the rats and the animals were sacrificed on day three, which coincided with the onset of disease that is mainly characterised by body weight loss and in some cases first clinical symptoms. The T_{MBP} cells were isolated from the "peripheral compartment" represented by blood and spleen as well as the "CNS compartment" consisting of spinal cord meninges and parenchyma (Figure 5 A). The presence of T_{MBP} cells in each organ was confirmed by BFP expression in flow cytometry. To achieve a high yield of T cells for a valid library representation eight to ten animals were pooled per replicate and the splenic samples were sorted for BFP^+ cells. The extracted genomic DNA was submitted to NGS and the resulting sgRNA count numbers were analysed by Clara de la Rosa del Val using the MAGeCK software, which was developed to identify hits from CRISPR/Cas9 screenings (Li et al., 2014, Kendirli et al., 2023). With this bioinformatic analysis the sgRNA distribution of each gene could be compared between the peripheral compartment and the CNS compartment, allowing us to identify genes whose deletion leads to impaired or enhanced migration of the T_{MBP} cells into the CNS (Figure 5 B). Hereby, the gene *Itgα4* functioned as a positive control. It encodes for the α4-integrin, which is part of the VLA-4 heterodimer that has a well-established role in T cell migration into the CNS. Indeed, the count of the *Itgα4* sgRNA was lower in both the meninges and the parenchyma compared to the sgRNA counts in the blood and spleen. Consequently, *Itgα4* ranked among the top most-depleted genes in all comparisons of peripheral compartments versus CNS compartments and thereby confirming the ability of this genome-wide CRISPR/Cas9 screening to identify genes relevant for migration of T_{MBP} cells across the BBB. Interestingly, there is a strong correlation of

significantly differentially regulated genes between the comparisons of the two CNS compartments to blood and spleen, indicating that during aT-EAE the same set of genes regulate the entry of T cells to both the meninges and the parenchyma (Figure 5 C).

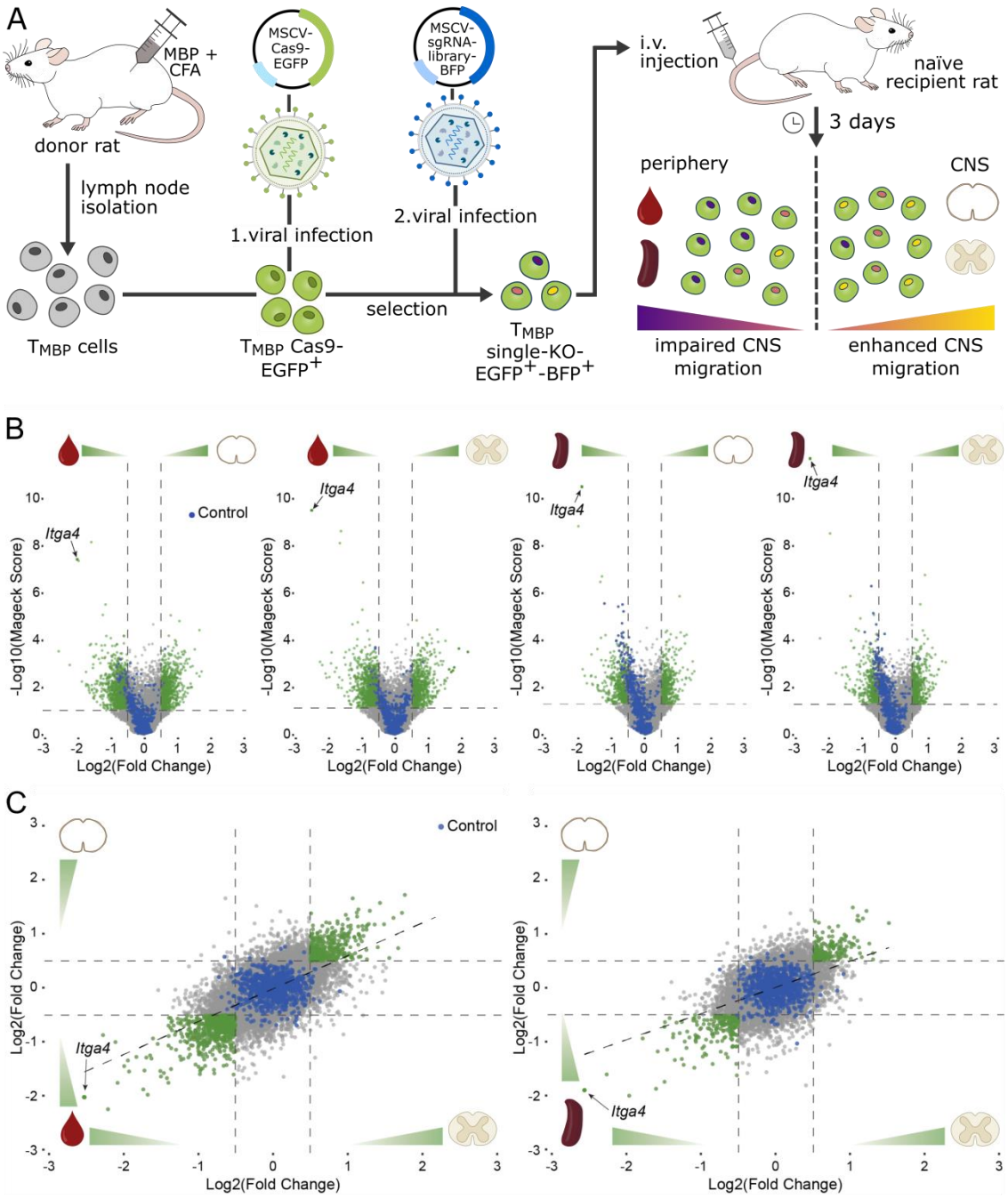

Figure 5 Genome-wide CRISPR/Cas9 screening of T cell migration in aT-EAE

A) Experimental design. T_{MBP} cells were first virally transduced with the Cas9 nuclease and EGFP and then with the genome-wide CRISPR library and BFP. After selection and *in vitro* restimulation the cells were i.v. injected into rats. After three days the rats were sacrificed and T_{MBP} cells were isolated from blood, spleen, and spinal cord meninges and parenchyma for further analysis. **B)** Volcano plots depicting the results of the genome-wide CRISPR/Cas9 screening per gene across the four tissue comparisons.

Green dots represent genes whose KO showed a sizeable change in the ability of T_{MBP} cells trafficking into the CNS. Blue dots represent the NT control. Threshold lines indicate p-value = 0.05 and log2(Fold change) = ±0.5. **C)** Correlations of the log2(Fold Change) left for meninges vs. blood compared to parenchyma vs. blood (Pearson correlation index 0.62) and right meninges vs. spleen compared to parenchyma vs. spleen (0.48). Green dots represent genes whose KO showed a sizeable change in the ability of T_{MBP} cells trafficking into the CNS. Blue dots represent the NT control. Modified from (Kendirli et al., 2023).

4.1.2 A second validation screening increases confidence in the top hits

Since a large sgRNA library used in the genome-wide screening can result in an impaired signal to noise ratio, we aimed to increase the confidence in the primary hits by performing a validation screening. The results of the genome-wide screening were subjected to a set of selection criteria based on effect size and statistical significance and resulted in a list of 1,950 candidate genes, which was used to generate a validation sgRNA library with 12,000 sgRNAs (6 sgRNAs/gene). The same adoptive transfer experiment as for the whole genome library was performed, but this time T cells from all organs were sorted to increase their purity and more stringent selection criteria were used during data analysis (Figure 6 A). Considering the sgRNA distribution in the different compartments and their relative fold change, we could identify a list of ranked genes that either enhance or inhibit T cell trafficking into the CNS (Figure 6 B). Since the aim in the treatment of MS is to decrease the number of autoreactive T cells in the brain we first focussed on genes that are required for T cell trafficking into the CNS. These genes act as positive regulators of T cell migration and their knockout reduced the ability of T_{MBP} cells to transmigrate into the CNS. This subset was characterized by increased counts of sgRNAs in the peripheral organs and decreased numbers in the CNS compartments. Apart from our absolute gene ranking we also checked in which gene ontology (GO) our top hits fell, among those were the clusters “adhesion modules”, “chemokine receptors”, “transcription factors” and “G protein-coupled receptor (GPCR)” (Figure 6 C-F).

Among our top hit the first two, *Itgα4* and *Fermt3*, were part of the “adhesion molecule” GO term (Figure 6 C). As described above *Itgα4*, which encodes for the α4-integrin and forms part of the heterodimer VLA-4, is a well-established molecule in T cell trafficking that functioned as a positive control in the screening. Therefore, it is not surprising but rather a confirmation of our approach to see it also as the top hit in our validation screening. However, to our surprise the *Itgb1* gene that encodes for β1-integrin, which is the other subunit of the VLA-4 receptor only exhibited a milder fold change. This suggests that other integrins might compensate for its loss.

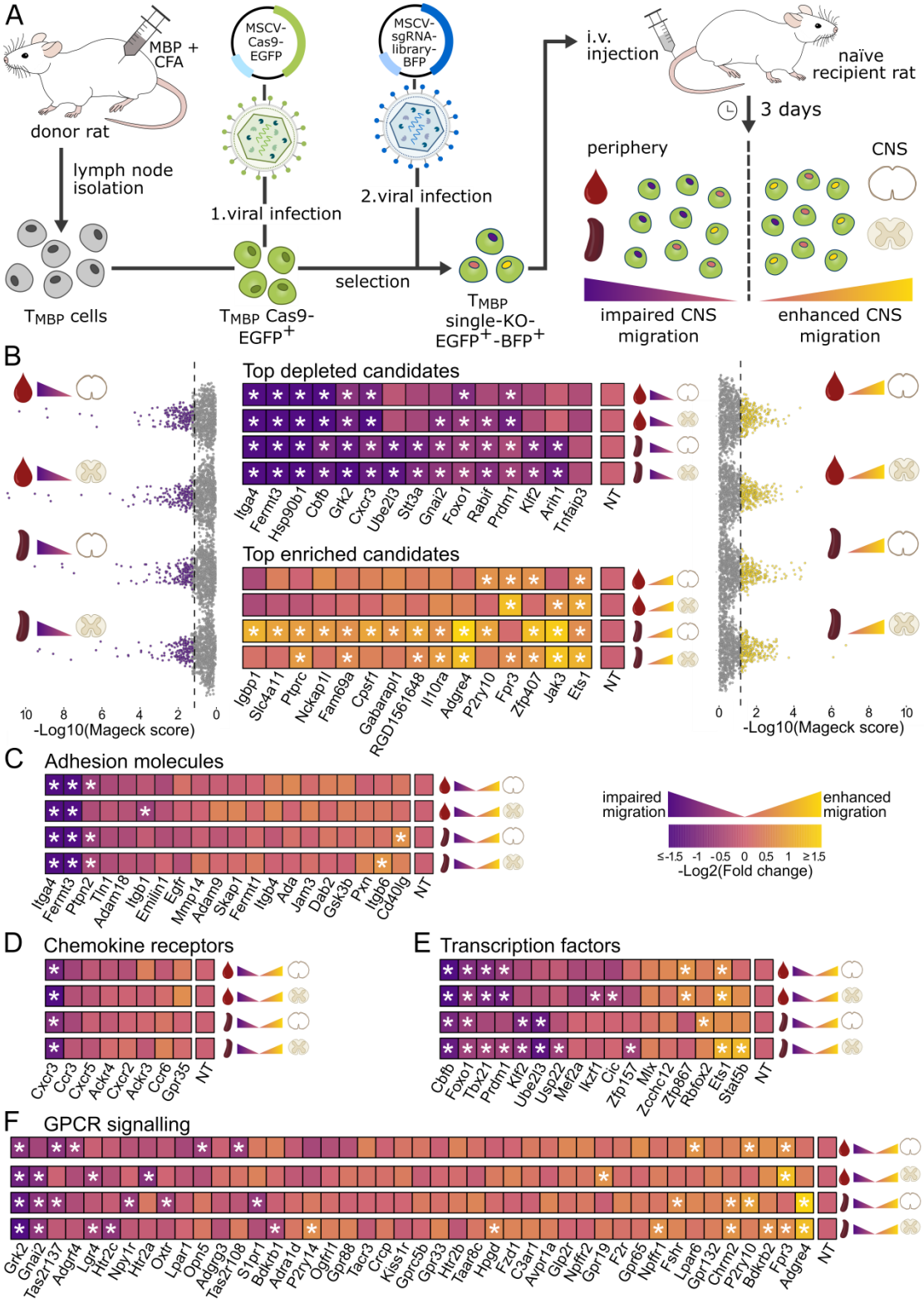

Figure 6 Validation CRISPR/Cas9 screening of T_{MBP} cell migration into the CNS

A) Experimental design. T_{MBP} cells were first virally transduced with the Cas9 nuclease and EGFP and then with the validation CRISPR library and BFP. After selection and *in vitro* restimulation the cells were i.v. injected into rats. After three days the rats were sacrificed and T_{MBP} cells were isolated from blood, spleen, and spinal cord meninges and parenchyma for further analysis. **B)** Validation screening results depicting the top-ranking genes whose KO showed impaired (left) or enhanced (right) migration into the

CNS, across comparisons, displayed as volcano plots. In the middle log2(Fold Change) heatmaps showing on the top panel positive regulators of T_{MBP} cell entry into the CNS (KO impairs migration, purple) and the lower panel negative regulators of CNS migration (KO enhances migration, yellow). Essential candidates were defined as detailed in the methods section. **C-F)** Log2(Fold Change) heatmaps illustrating the T_{MBP} cells migratory phenotype of gene KOs based on the validation screening results for adhesion related genes (**C**) (GO terms GO.0050901, GO.0033631 and GO.0005178), chemokine receptors (**D**) (GO.0004950), transcription factors (**E**) (GO.0003700, GO.0003713 and GO.0003714) and GPCRs (**F**) (GO.0004930, GO.0004703, GO.0001664 and guanine nucleotide binding genes of GO.0001664, excluding genes present in GO.0004950 or GO.0004896). Only genes of the GO term with a p-value<0.05 (**C, D**) or p< .01 (**E**, **F**) and ≥3 "neg/pos|goodsgrna" as per the validation screening results are shown. Stars indicate, for all heatmaps, p-value<0.05, absolute log2(Fold Change) > 3 standard deviations of the log2(Fold Changes) of the controls and ≥3 "neg/pos|goodsgrna". Modified from (Kendirli et al., 2023).

The second hit *Fermt3* encodes for Kindlin-3 an intercellular protein that is involved in integrin activation by allosteric modification of their affinity state. Our results confirmed a study in which observed that VLA-4 and LFA-1 mediated T cell arrest and adhesion are regulated by Kindlin-3 and that Kindlin-3-deficient T cells fail to induce adoptive transfer EAE (Moretti et al., 2013). In close relation to the kindlin family also proteins of the talin family are involved in integrin activation (Moser et al., 2009). In our screening talin-1 (*Tln1*) was among the candidates with a milder fold change, indicating only a moderate effect on T cell migration compared to *Fermt3* (Figure 6 C). Another one of the top regulated candidates was the heat shock protein 90 beta family member 1 (*Hsp90b1*) (Figure 6 B). Although it does not belong to the class of adhesion molecule itself it implicated in the correct surface expression of various integrins, as it functions as a chaperone (Staron et al., 2010).

Remarkably, among the cluster of chemokine receptors only *Cxcr3*, which transduces the signals of its ligands CXCL9, CXCL10 and CXCL11 (Groom and Luster, 2011), was a top hit in our screening (Figure 6 D). Although a previous study in the same aT-EAE model reported that Cxcr3 as well as CCR5 are essential for T cell trafficking into the CNS (Schläger et al., 2016), we could only confirm the imperative nature of *Cxcr3* while *CCR5* was dispensable for the migration of autoreactive T cells in our screening.

In the GO cluster of "transcription factors" the core-binding factor subunit beta (*Cbfb*) was the gene with the highest fold change (Figure 6 E). It forms a heterodimer with one of three alpha subunits (RUNX proteins) and so far has been reported to play a critical role in different stages of T cell development (Zhao et al., 2007). Another transcription factor that reached significance in all four comparisons was the forkhead box protein O1 (*Foxo1*). *Foxo1* is a prominent regulator of T cell homeostasis (Newton et al., 2018). Two studies also pointed to its role in naïve T cell homing by regulating the expression of L-selectin and Krupple-like factor

2 (*Klf2*) (Fabre et al., 2008, Kerdiles et al., 2009). Interestingly, *Klf2* also was among hits, although it shows only significant changes in the comparisons to spleen and only milder ones in the blood comparisons. Similar to Foxo1, Klf2 expression is assumed to regulate the migration of naïve T cells (Sebzda et al., 2008), however our CRISPR/Cas9 screening also suggests an implication in differentiated and activated $CD4^+$ T_{MBP} cells. Another essential transcriptional regulator was the T-box transcription factor *Tbx21*, also known as *T-bet*. It regulates T-helper cell commitment to a Th1 phenotype and controls the expression of the hallmark Th1 cytokine, IFNγ (Miller and Weinmann, 2010). Similarly, the *Prdm1* (PR domain zinc finger protein 1) gene, encoding the BLIMP-1 transcription factor, has the ability to function as both an activator and a repressor, which can ultimately decide the fate of multiple T-cell lineages. Furthermore, it plays a critical role in the modulation of peripheral T cell activation and proliferation (Fu et al., 2017). Particularly interesting was the observation that some genes only had a strong effect size in one of the two comparisons of the CNS compartment with the peripheral organs. Two genes, namely *Arih1* and *Ube2l3*, demonstrated a substantial fold change in the comparisons between the spleen and the two CNS compartments, yet their impact was only minimally reduced in the comparisons with the blood (Figure 6 B). The ubiquitin-conjugating enzyme E2 L3 (*Ube2l3*), also known as *UBCH7*, was described to regulate cytokine-driven nuclear transcription factor-kappa B (NF-κB) activation (Fu et al., 2014) (Figure 6 B, E). Notably, the second essential gene that showed this particular profile was the ariadne-1 homolog (*Arih1*) an E3 ubiquitin-protein ligase, which was shown to interact with Ube2l3 (Ardley et al., 2001).

In the group of GPCR the G protein coupled kinase 2 (*Grk2*) and the Guanine nucleotide-binding protein G(i) subunit alpha-2 (*Gnai2*) were the top hits with the highest fold change and significant results in a least three comparisons (Figure 6 F). Grk2 phosphorylates activated GPCR, which promotes the binding of an arrestin proteins that in turn block their cellular signaling and resulting in receptor desensitization and internalization. In addition, it can also establish functional or scaffolding interactions with an extensive number of non-GPCR proteins making it versatile signaling-hub (Penela et al., 2019). Gnai2 is required to activate downstream effectors to transduce the signals of the GPCR. The majority of chemoattractants and chemokines signal through GPCRs, so it is not surprising that Gnai2-deficient T cells have profound defects in in chemokine receptor signaling and chemoattractant induced cell mobility (Hwang et al., 2007).

In addition to the genes that limit the entry of autoreactive T_{MBP} cells into the CNS, our CRISPR/Cas9 screening also identified negative regulator hits, whose loss resulted in enhanced

T cell migration to the spinal cord meninges and parenchyma (Figure 6 B). Among those genes, *Ets1* was the only top hit with a high fold change that was robust across all comparisons. It encodes for a transcription factor that was shown to regulate differentiation, survival and proliferation of lymphoid cells and has been identified as a susceptibility locus for several autoimmune diseases (Testoni et al., 2015, He et al., 2022) (Figure 6 E). Other regulators that were only significantly regulated in some of the tissue comparisons were the tyrosin kinase Janus kinase 3 (*Jak3*), the *Adgre4* gene, which is the gene locus of the GPCR *EMR4*, *ZFP407* encoding for Zinc finger protein 407, and formyl peptide receptor 3 (*FPR3*) (Figure 6 B, F). None of them was shown to increase T cell migration before.

4.2 Validation of candidate genes in single knockout T_{MBP} cells

While the two rounds of CRISPR/Cas9 screening identified several candidate genes that appear to facilitate or restrict the entry of T_{MBP} cells into the CNS during aT-EAE there remains the possibility of a false positive hit. In order to validate the results of the screening and to investigate the role of the individual genes further single KO clones had to be established. To reduce the cell disturbance by the double viral transduction as well as the possibility of off-target effects by continuous Cas9 and sgRNA expression, both were only transiently delivered as a RNP to T_{MBP} cells by the nucleofection method. Prior to gene editing the T_{MBP} cells were transduced with fluorescent proteins; BFP was used to label NT control cells while EGFP marked the individual KO cells. The DNA perturbation of each target gene was confirmed by TIDE sequencing (Supplementary Table 5) and if possible, also by antibody staining followed by analysis with flow cytometry. For each KO the T_{MBP} cells were first tested *in vitro* for any phenotypical changes of activation markers, adhesion molecules or the production of certain cytokines. In the next step we analysed how the KO affects the migration behaviour of T_{MBP} cells *in vivo* and whether those cells still have the ability to induce EAE.

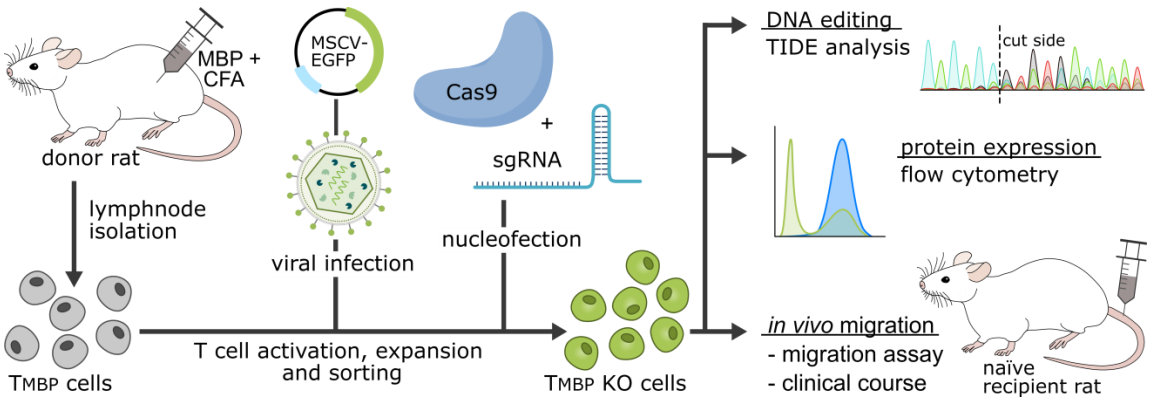

Figure 7 Generation of single KO T_{MBP} cells and their validation strategy

After isolation of MBP-specific T cells from the donor rat, T_{MBP} cells were first transduced with a virus either containing EGFP or BFP (not shown here) to label the T cells. Following sorting and expansion the labelled T_{MBP} cells were nucleofected with their specific sgRNA and Cas9. The DNA editing was confirmed by TIDE analysis and if possible by flow cytometry. The effect of the KO on T cell trafficking was then tested *in vitro* and *in vivo*.

4.3 Validation of the adhesion module

4.3.1 Deletion of α4-integrin in T_{MBP} cells blocks EAE development

As the *Itga4* gene is among our strongest candidate hits and essential to T cell adhesion, we confirmed our validation strategy by testing the KO of α4-integrin as positive control first. To ensure that the gene KO specifically abrogates the CNS migration and does not affect general T cell functions, the edited T cells were first characterized *in vitro* (Figure 8 A). Restimulated T cells were checked for their production of the cytokines IL-17A and IFNy first under normal cell culture conditions. In addition, to test whether the T cells have the capability to produce cytokines following stimulation the same experiment was performed after addition of PMA and Ionomycin. While PMA activates the protein kinase C, Ionomycin increases intracellular calcium ion concentrations. Both compounds bypass the T cell membrane receptor complex leading to T cell activation and production of a variety of cytokines (Ai et al., 2013). In both conditions, the proportion of cells exhibiting different cytokine production profiles was assessed, including those that did not produce IL-17A or IFNy (negative phenotype), only produced IL-17A (Th17 phenotype), only produced IFNy (Th1 phenotype), or produced both IL-17A and IFNy (Th1+Th17 phenotype). Without stimulation T_{MBP} Itga4-KO cells and control T_{MBP} NT cells both show no polarization to a specific phenotype but display a similar distribution of produced cytokines. However, upon stimulation, the majority of T_{MBP} Itga4-KO cells and T_{MBP} NT cells produced IL-17A and IFNy in parallel, thereby exhibiting a Th1+Th17 phenotype in a similar manner (Figure 8 B, C). To further address the activation status of the T cells and the expression of integrins important for T cell migration a surface staining followed by flow cytometry analysis was performed on the day of maximal activation. For the activation status we checked for the surface expression of the T cell receptor (TCR) and its co-receptor CD4, the IL-2 receptor alpha chain (CD25) and the OX40 receptor, also known as tumor necrosis factor receptor superfamily member 4 (CD134). There was no difference in the activation of T_{MBP} Itga4-KO cells in comparison to control T_{MBP} NT cells (Figure 8 D, E). Further we analysed the surface expression of the α4-integrin (CD49d) and the β1-integrin (CD29) that together form the heterodimer VLA-4. Further the components of LFA-1, αL-integrin (CD11a) and β2-integrin (CD18) were stained as well as the α2-integrin (CD49b). There was no

difference in the expression of αL-integrin (CD11a), β2-integrin (CD18) and α2-integrin (CD49b) between T_{MBP} Itga4-KO cells and T_{MBP} NT cells. Expectedly, α4-integrin (CD49d) is strongly downregulated, which additionally confirms the successful KO of Itga4 in the T cells. However, also its binding partner β1-integrin (CD29) appears to be downregulated in the T_{MBP} Itga4-KO cells although not significantly and not as strong as α4-integrin (CD49d) (Figure 8 D, E). This is probably due its ability to form further complexes with a variety of different α-integrins (Takada et al., 2007). Overall, the T_{MBP} Itga4-KO cells appear to have normal T cell function regarding their activation state and cytokine production and only the KO gene and its associated binding partner seem to be affected.

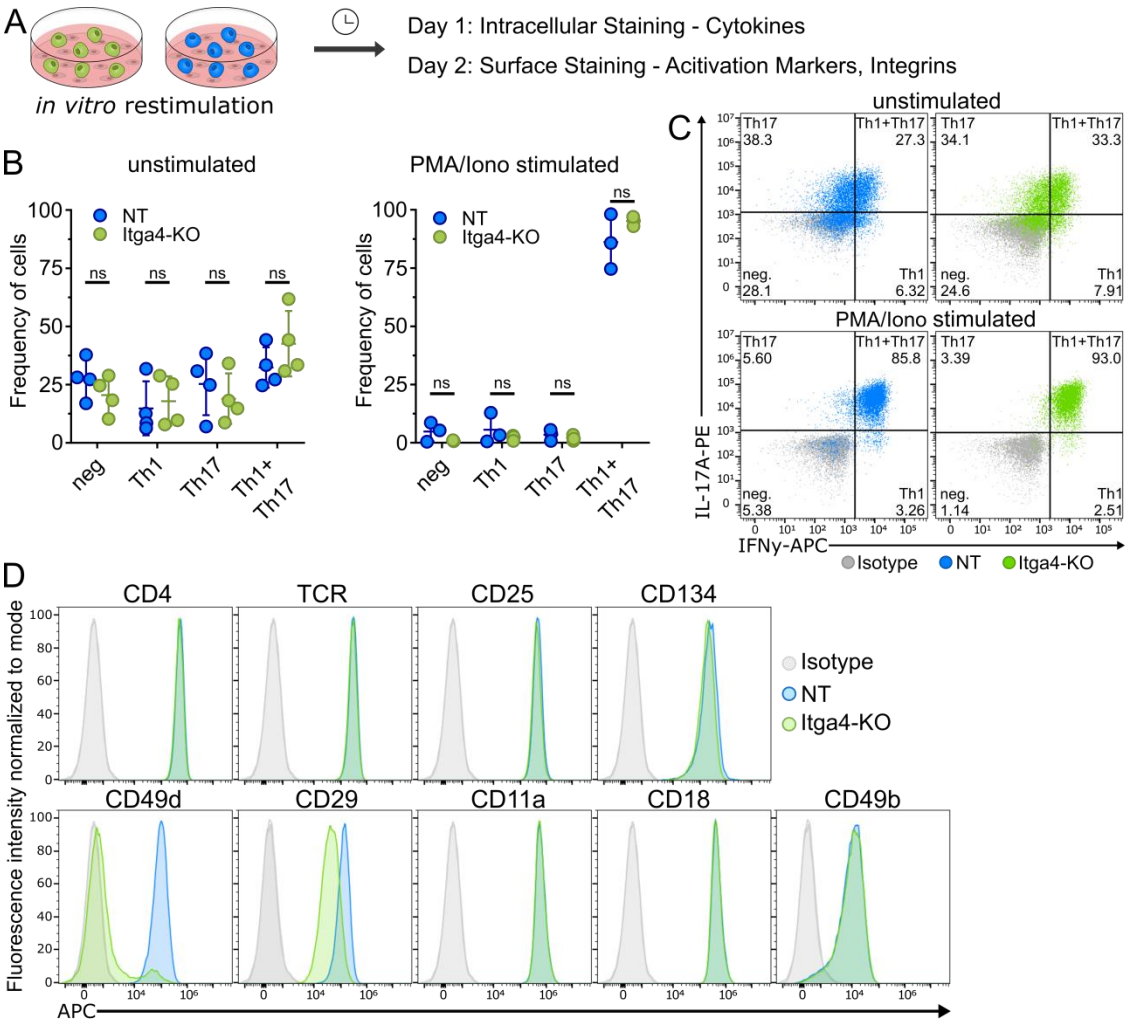

Figure continues on next page

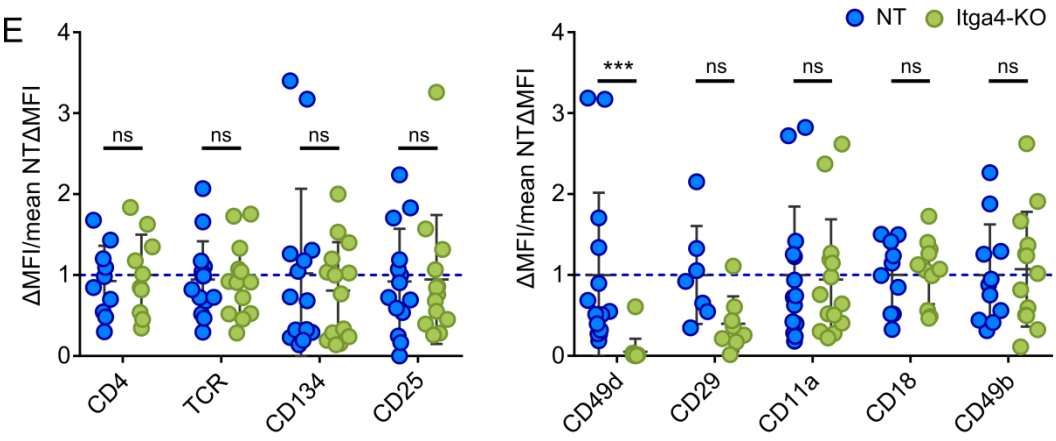

Figure 8 *In vitro* analysis of T_{MBP} Itga4-KO cells

A) Experimental design. T_{MBP} Itga4-KO and T_{MBP} NT cells were *in vitro* restimulated. After 24 h cells were stained for their produced cytokines and after 48 h activation markers or integrins were stained on the cell surface. **B)** Quantification of T cell subpopulation based on cytokine profile in flow cytometry analysis. Two-way ANOVA with multiple comparisons with the two-stage linear step-up procedure of Benjamini, Krieger and Yekuteli. Unstimulated: F < 0.0001, P = ns, n = 4; stimulated: F < 0.0001, P = ns, n = 3. Mean ± SD. **C)** Representative flow cytometry plots showing intracellular staining of IL-17A or IFNy with or without stimulation and their classification into $IFNy^+$ Th1 cells, $IL\text{-}17A^+$ Th17 and $IFNy^+$ and $IL\text{-}17A^+$ Th1+Th17 cells. Cells were gated on lymphocytes > single cells > BFP^+ or GFP^+ > APC and PE values. **D)** Representative flow cytometry plots showing surface expression of various activation markers and integrins. Cells were gated on lymphocytes > single cells > BFP^+ or GFP^+. **E)** Quantification of the ΔMFI (MFI-MFI isotype control) of the surface staining normalized to the mean ΔMFI of NT cells. MFI, two-way ANOVA with multiple comparisons with the two-stage linear step-up procedure of Benjamini, Krieger and Yekuteli. Activation markers: F = 0.04989, P = ns, CD4: n = 10, TCR/CD25: n = 14, CD134 n = 14 (NT)/n = 13 (Itga4-KO); integrins: F = 5.589, P = 0.0199, CD49d/CD11a: n = 14, CD29: n = 7 (NT)/n = 8 (Itga4-KO), CD18: n = 10 (NT)/ n = 11 (Itga4-KO). CD49b n = 11 (NT)/ n = 13 (Itga4-KO). Mean ± SD.

To validate the effect of the Itga4 KO on T cell migration we co-transferred stimulated T_{MBP} Itga4-KO cells in a 1:1 ratio with T_{MBP} NT cells i.v. into rats. With the onset of disease after three days, the rats were sacrificed and cells from blood, spleen and parathymic lymph nodes (pT LN) as well as spinal cord meninges, parenchyma and CSF were collected (Figure 9 A). Flow cytometry analysis allowed us to determine the ratio of EGFP expressing T_{MBP} Itga4-KO cells and BFP expressing T_{MBP} NT cells in each organ (Figure 9 B). To correct for disturbances in the injection mix as well as for differences in survival and proliferation the ratios were normalized to the cell ratio in the blood (Figure 9 C). The significantly reduced ratio in meninges, parenchyma and CSF confirmed that the deletion of Itga4 significantly reduced the T_{MBP} cell migration into the CNS. In addition, T_{MBP} Itga4-KO cells migrate less into the parathymic lymph node (pt LN), but appear to leave the blood stream and accumulate in the spleen. To further characterize the behaviour of T_{MBP} Itga4-KO cells *in vivo* cells of the spleen were stained for activation markers, albeit they are downregulated during the acquisition of the migratory

phenotype (Flügel et al., 2001). In addition the surface expression of the integrins of VLA-4 and LFA-1 was assessed. In line with the *in vitro* data there was no difference in the expression of CD25, CD134 as well as of αL-integrin (CD11a) or β2-integrin (CD18), while α4-integrin (CD49d) as well as β1-integrin (CD29) are strongly downregulated (Figure 9 D, E). Additional staining of cells in the spleen for the cytokines IL-17A and IFNy showed that they were neither produced by T_{MBP} Itga4-KO cells nor T_{MBP} NT cells (Figure 9 F, G). Likely, the lack of VLA-4, which is essential for the attachment of T cells on the blood vessels and the subsequent trafficking of T cells, prevents T_{MBP} Itga4-KO cells to migrate into the CNS during EAE.

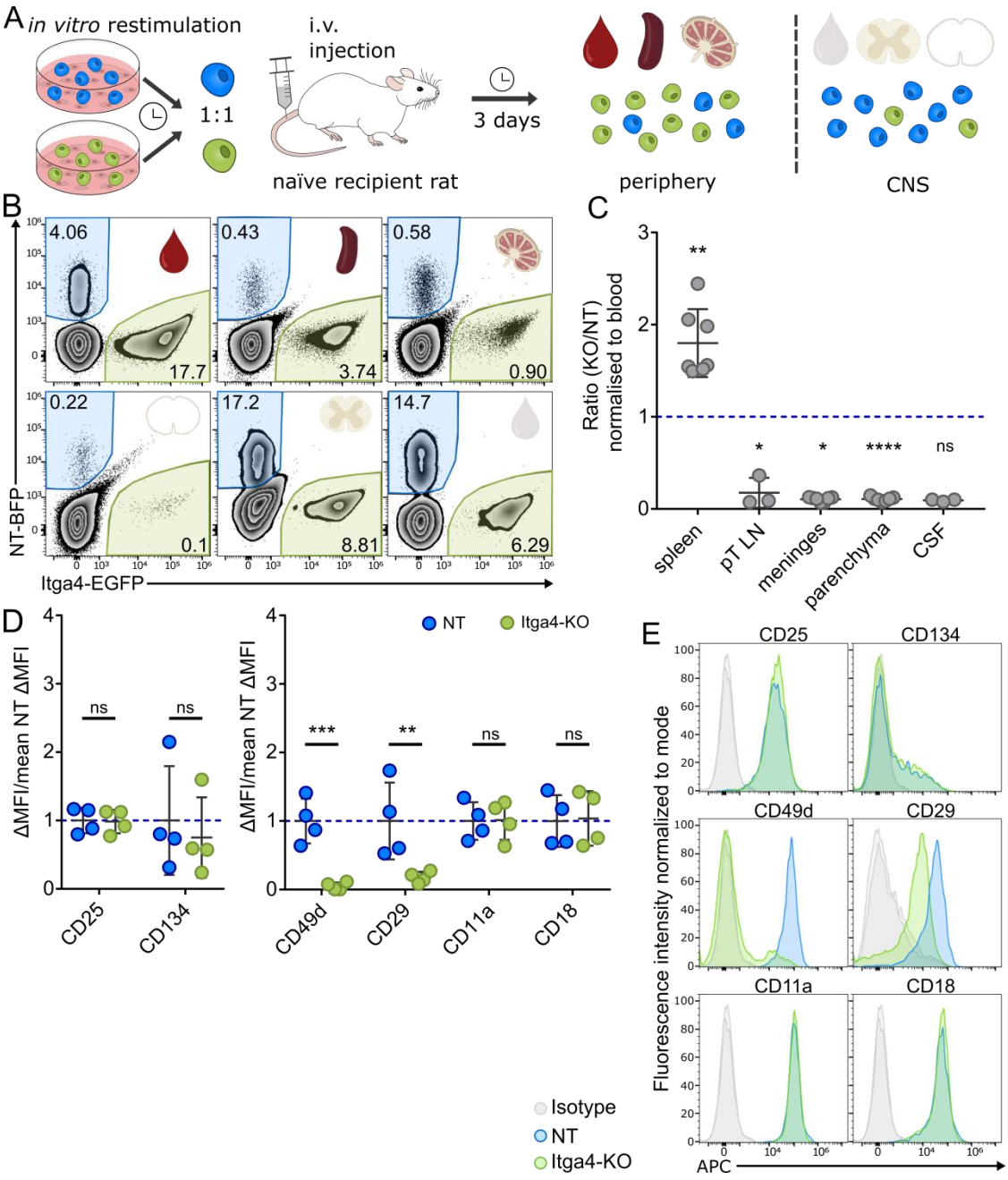

Figure continues on next page

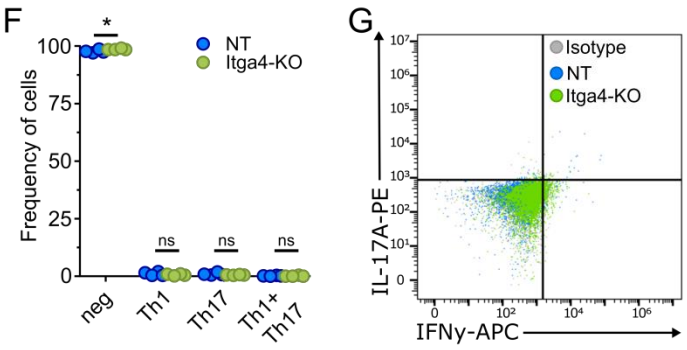

Figure 9 *In vivo* migration analysis following co-transfer of T_{MBP} Itga4-KO cells

A) Experimental design. T_{MBP} Itga4-KO and T_{MBP} NT cells were *in vitro* restimulated. After 48 h the fully restimulated T_{MBP} cells were mixed in a 1:1 ratio and injected into rats. With onset of disease on day three, rats were sacrificed and cells from peripheral organs (blood, spleen and pt LN) as well as CNS compartments (CSF, parenchyma, meninges) were collected. **B)** Representative flow cytometry plot with the distribution of T_{MBP} cells in different organs following co-transfer. BFP^+ T_{MBP} NT cells are highlighted in blue, $EGFP^+$ T_{MBP} Itga4-KO in green. Gated on lymphocytes > single cells > BFP^+ or GFP^+. **C)** Migratory phenotype of T_{MBP} Itga4-KO cells compared to T_{MBP} NT cells in different organs, shown as the ratio of KO cell number/ NT cell number divided by the KO/NT ratio in blood. A ratio of 1 indicates the migration behaviour of control T_{MBP} cells, a ratio below 1 indicates impaired migration and a ratio above 1 enhanced migration towards an organ. One sample t-test against hypothetical mean = 1. n = 7 (spleen, meninges parenchyma), n = 3 (pT LN, CSF). Mean ± SD. **D)** Quantification of the ΔMFI (MFI-MFI Isotype control) of the surface staining normalized to the mean ΔMFI of T_{MBP} NT cells. MFI, two-way ANOVA with multiple comparisons with the two-stage linear step-up procedure of Benjamini, Krieger and Yekuteli. Activation markers: F = 0.2656, P = ns, all stainings: n = 4; integrins: F = 13.37, P = 0.0013, all stainings: n = 4. Mean ± SD. **E)** Representative flow cytometry plots showing surface expression of activation markers and integrins of ex vivo splenic cells. Cells were gated on lymphocytes > single cells > BFP^+ or GFP^+. **F)** Quantification of T_{MBP} cell subpopulation based on the intracellular flow cytometry staining. Two-way ANOVA with multiple comparisons with the two-stage linear step-up procedure of Benjamini, Krieger and Yekuteli. F = 0.000867, P = ns, n = 4. Mean ± SD. **G)** Representative flow cytometry plots showing intracellular staining of IL-17A and IFNγ of *ex vivo* splenic T_{MBP} Itga4-KO and T_{MBP} NT cells. Cells were gated on lymphocytes > single cells > BFP^+ or GFP^+ > APC and PE values.

We further tested whether and to which extent the T_{MBP} Itga4-KO cells were able to induce clinical EAE, therefore they were injected i.v. into rats and the subsequent clinical course was monitored (Figure 10 A). In accordance to the previous results, rats that received T_{MBP} Itga4-KO cells did not develop disease symptoms and also did not lose body weight, while the rats that were injected with T_{MBP} NT cells developed the classical EAE disease course (Figure 10 B, C). Since Itga4's role in T cell migration is already well-established, these findings served to validate two important aspects. Firstly, they confirmed the accuracy of the CRISPR/Cas9 screening results, which indicated diminished migration of Itga4-deficient T_{MBP} cells into the CNS relative to peripheral organs. Secondly, these results demonstrate the effectiveness of our single KO and validation strategy, establishing its suitability for testing additional candidate genes.

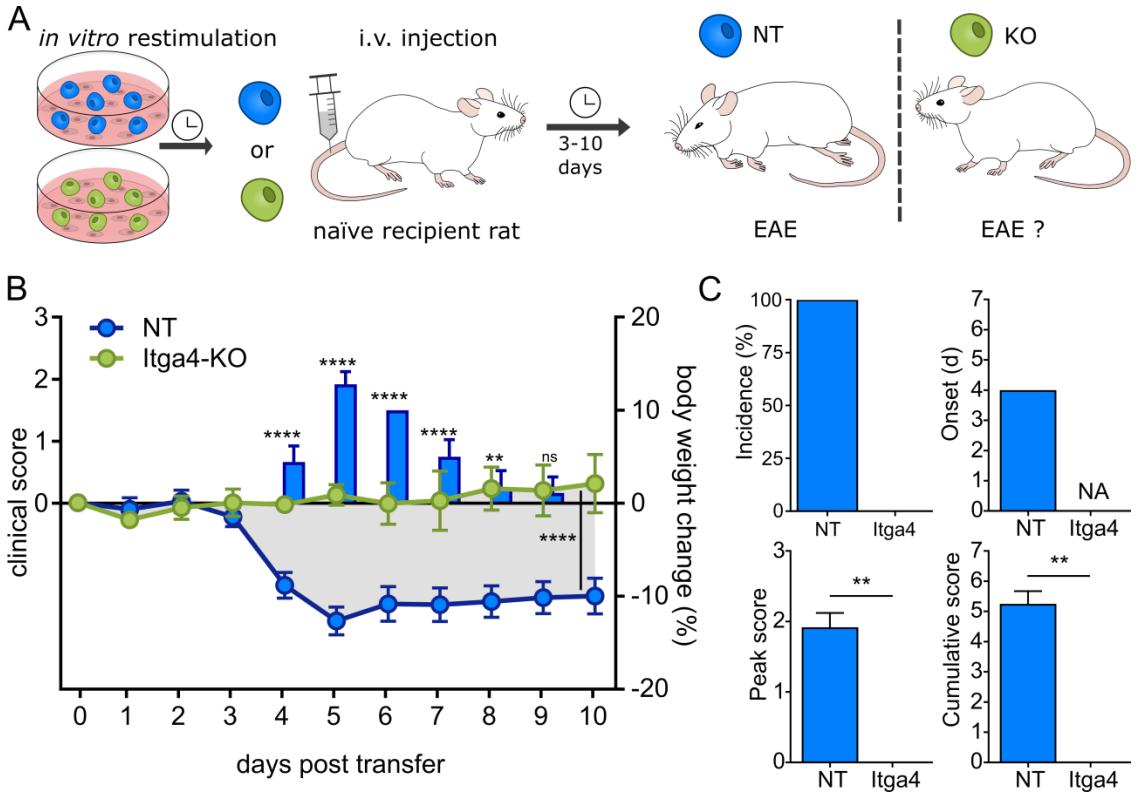

Figure 10 Clinical course of EAE induced by T_{MBP} Itga4-KO cells

A) Experimental design. T_{MBP} Itga4-KO and T_{MBP} NT cells were *in vitro* restimulated and were injected solely into rats. The EAE score and body weight was monitored daily. **B)** Clinical course of EAE measured by percentage of body weight change (lines) and EAE scores (bars) of injected animals. Repeated measures two-way ANOVA; days 0-10 disease score: $F = 424.5$, $P < 0.0001$, body weight change: $F = 107.8$, $P < 0.0001$; n = 6 (Itga4-KO); n = 6 (NT). Mean ± SD. **C)** Overview of additional EAE parameters: incidence of EAE (%), average onset (days post transfer) no data available (NA) in the Itga4-KO group since no animal developed disease, average EAE peak score and average EAE cumulative score. Following Sharpiro-Wilk normality test, Mann-Whitney test was performed. Mean ± SD.

4.3.2 The chaperon Hsp90b1 controls surface expression of integrins

Our screening revealed further adhesion-related genes that possibly affect T cell trafficking along with Itga4, so we continued by assessing the effects of knocking out the heat shock protein 90 beta family member 1 (Hsp90b1). It was reported to function as a master chaperone in the endoplasmic reticulum, where it is behind the correct folding of a variety of integrins (Staron et al., 2010). When characterizing the T_{MBP} Hsp90b1-KO cells *in vitro* we observed no difference in the cytokine profile in unstimulated and stimulated conditions (Figure 11 A, B, C) as well as in the activation status determined by the expression of CD4, TCR, CD25 and CD134 in comparison to T_{MBP} NT cells (Figure 11 D, E). However, the surface staining of integrins revealed a marked reduction of α4-integrin (CD49d), thereby arguing that the presence of Hsp90b1 is essential for the surface presentation of α4-integrin. Compared to

T_{MBP} NT cells there was a trend towards reduced surface presence of the α4-integrin binding partner β1-integrin (CD29), the LFA-1 components αL-integrin (CD11a) and β2-integrin (CD18) as well as α2-integrin (CD49b) yet it did not reach statistical significance (Figure 11 D, E).

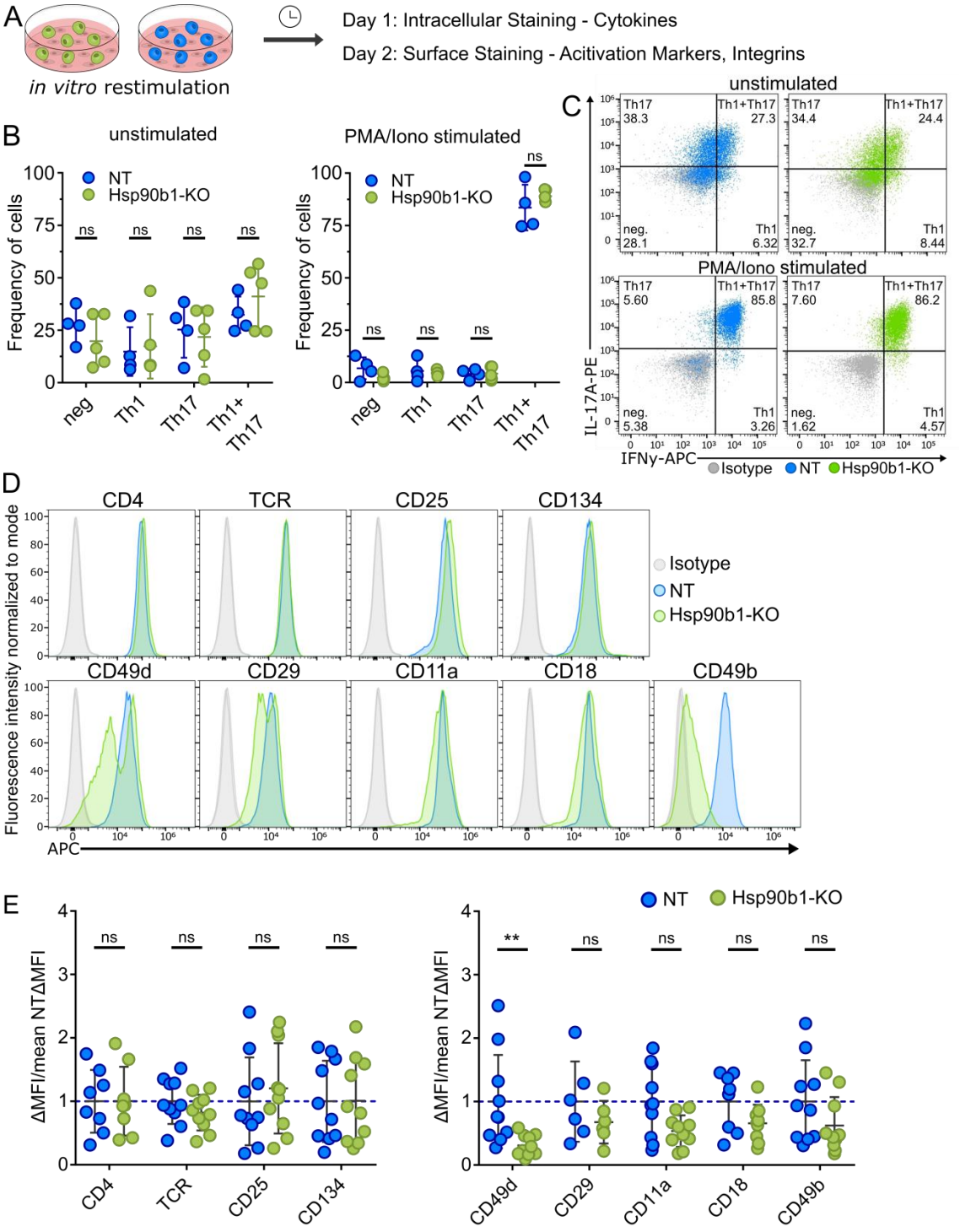

Figure 11 *In vitro* analysis of T_{MBP} Hsp90b1-KO cells

A) Experimental design. T_{MBP} Hsp90b1-KO and T_{MBP} NT cells were *in vitro* restimulated. After 24 h cells were stained for their produced cytokines and after 48 h activation markers or integrins were stained on the cell surface. **B)** Quantification of T cell subpopulation based on cytokine profile in flow cytometry

analysis. Two-way ANOVA with multiple comparisons with the two-stage linear step-up procedure of Benjamini, Krieger and Yekuteli. Unstimulated: $F < 0.0001$, P = ns, n = 4 (NT)/n=5 (Hsp90b1-KO); stimulated: $F < 0.0001$, P = ns, n = 4 (NT)/n=5 (Hsp90b1-KO). Mean ± SD. **C)** Representative flow cytometry plots showing intracellular staining of IL-17A or IFNy with or without stimulation and their classification into $IFNy^+$ Th1 cells, $IL\text{-}17A^+$ Th17 and $IFNy^+$ and $IL\text{-}17A^+$ Th1+Th17 cells. Cells were gated on lymphocytes > single cells > BFP^+ or GFP^+ > APC and PE values. **D)** Representative flow cytometry plots showing surface expression of various activation markers and integrins. Cells were gated on lymphocytes > single cells > BFP^+ or GFP^+. **E)** Quantification of the ΔMFI (MFI-MFI Isotype control) of the surface staining normalized to the mean ΔMFI of NT cells. MFI, two-way ANOVA with multiple comparisons with the two-stage linear step-up procedure of Benjamini, Krieger and Yekuteli. Activation markers: $F = 0.05017$, P = ns, CD4: n = 8, TCR/CD25/CD134: n = 10; integrins: $F = 17.17$, $P < 0.0001$, CD49d/CD11a/CD49b: n = 10, CD29: n = 6, CD18: n = 8 (NT)/n = 9 (Hsp90b1-KO). Mean ± SD.

To investigate the effect of Hsp90b1 KO on the migratory properties of T_{MBP} cells, we injected T_{MBP} Hsp90b1-KO cells together with T_{MBP} NT cells into rats and analyses their distribution in the different organs (Figure 12 A). Relative to the amount of T_{MBP} Hsp90b1-KO cells in the blood we observed decreased migration into meninges, parenchyma, and CSF as well as into the parathymic lymph nodes, while T_{MBP} Hsp90b1-KO cells seem to accumulate in the spleen (Figure 12 B, C). This resembles the results seen it the Itga4-KO, so it is not surprising to also see a reduction in the expression of α4-integrin (CD49d) and β1-integrin (CD29) in the T_{MBP} Hsp90b1-KO cells isolated from the spleen compared to control T_{MBP} NT cells. In difference to results of the Itag4-KO, also the expression levels of the LFA-1 dimer, CD11a and CD18 are significantly reduced, confirming the role of Hsp90b1 in chaperoning multiple integrins. The results also suggest that the downregulation of integrins seen in *in vitro* T cells is even more pronounced *in vivo*. This indicates that the T cells undergo structural changes *in vivo*, and that the impact of Hsp90b1's absence becomes apparent in these changes. The surface levels of the IL-2 receptor (CD25) were almost identical between T_{MBP} Hsp90b1-KO and T_{MBP} NT cells and the already low expression levels of CD134 were slightly further reduced in Hsp90b1, yet not significantly (Figure 12 D, E). Overall, the results suggest that the loss of Hsp90b1 results in a reduced expression of the VLA-4 and LFA-1 receptors on T_{MBP} cells that impedes their migration into the CNS.

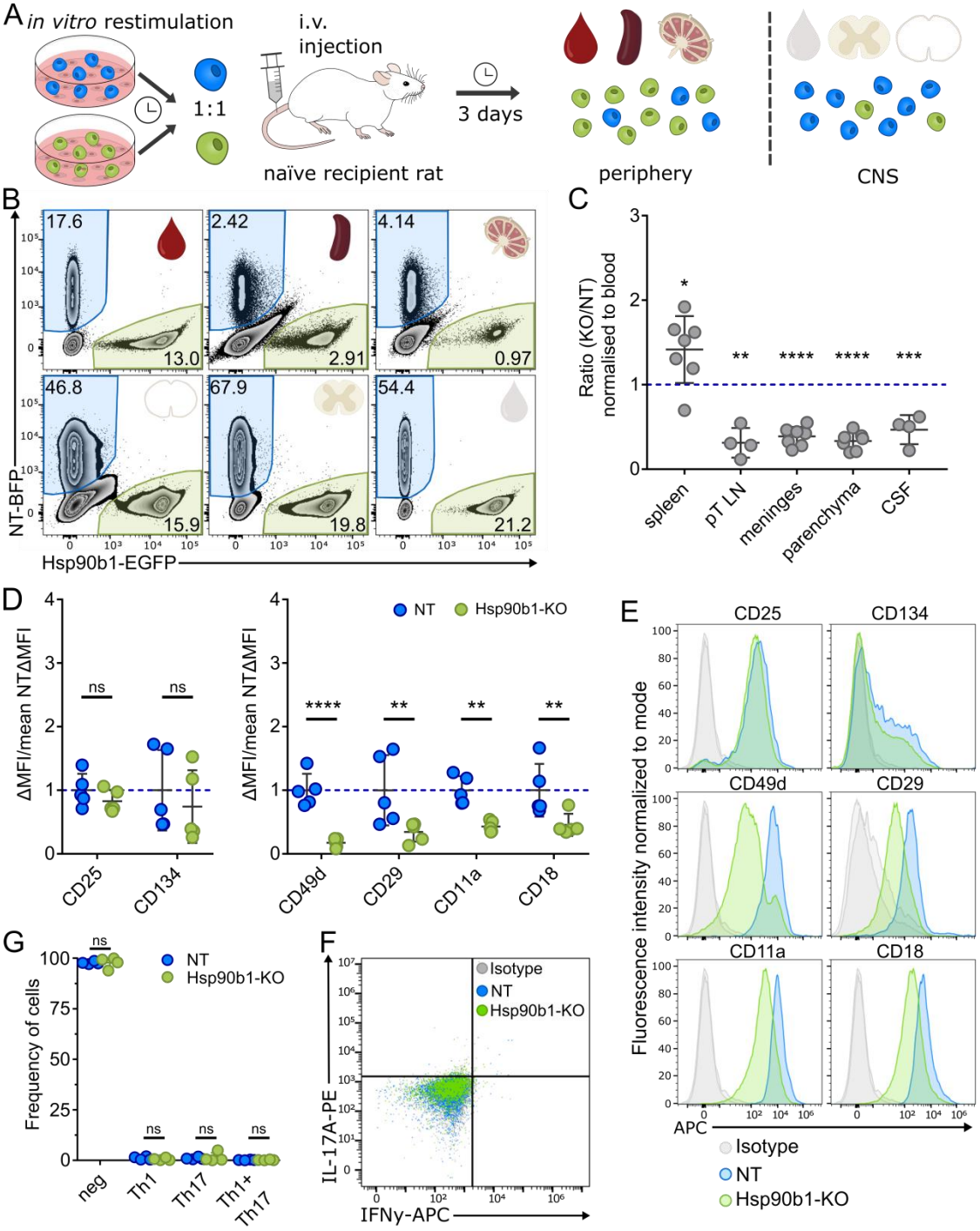

Figure 12 *In vivo* migration analysis following co-transfer of T_{MBP} Hsp90b1-KO cells

A) Experimental design. T_{MBP} Hsp90b1-KO and T_{MBP} NT cells were *in vitro* restimulated. After 48 h the fully restimulated T_{MBP} cells were mixed in a 1:1 ratio and injected into rats. With onset of disease on day three, rats were sacrificed and cells from peripheral organs (blood, spleen and pt LN) as well as CNS compartments (CSF, parenchyma, meninges) were collected. **B)** Representative flow cytometry plot with the distribution of T_{MBP} cells in different organs following co-transfer. BFP^+ T_{MBP} NT cells are highlighted in blue, $EGFP^+$ T_{MBP} Hsp90b1-KO in green. Gated on lymphocytes > single cells > BFP^+ or GFP^+. **C)** Migratory phenotype of T_{MBP} Hsp90b1-KO cells compared to T_{MBP} NT cells in different organs, shown as the ratio of KO cell number/ NT cell number divided by the KO/NT ratio in blood. A ratio of 1 indicates the migration behaviour of control T_{MBP} cells, a ratio below 1 indicates impaired migration and a ratio

above 1 enhanced migration towards an organ. One sample t-test against hypothetical mean = 1. n = 7 (spleen, meninges parenchyma), n = 4 (pT LN, CSF). Mean ± SD. **D)** Quantification of the ΔMFI (MFI-MFI Isotype control) of the surface staining normalized to the mean ΔMFI of T_{MBP} NT cells. MFI, two-way ANOVA with multiple comparisons with the two-stage linear step-up procedure of Benjamini, Krieger and Yekuteli. Activation markers: F = 1.113, P = ns, all stainings: n = 4; integrins: F = 51.13, P < 0.0001, all stainings: n = 5. Mean ± SD. **E)** Representative flow cytometry plots showing surface expression of activation markers and integrins of ex vivo splenic cells. Cells were gated on lymphocytes > single cells > BFP^+ or GFP^+. **F)** Quantification of T_{MBP} cell subpopulation based on the intracellular flow cytometry staining. Two-way ANOVA with multiple comparisons with the two-stage linear step-up procedure of Benjamini, Krieger and Yekuteli. F < 0.0001, P = ns, n = 4. Mean ± SD. **G)** Representative flow cytometry plots showing intracellular staining of IL-17A and IFNy of *ex vivo* splenic T_{MBP} Hsp90b1-KO and T_{MBP} NT cells.

Accordingly, when comparing rats that received a single transfer of T_{MBP} Hsp90b1-KO cells to those that received control T_{MBP} NT cells, notable differences in disease progression and associated symptoms were observed. The onset of disease symptoms in the T_{MBP} Hsp90b1-KO recipient rats was delayed, and they experienced only minor body weight loss compared to the control group (Figure 13 A, B). Not only was the incidence lower but also peak score and the cumulative score over the course of the EAE was significantly lower, confirming the impaired ability of T_{MBP} Hsp90b1-KO to migrate into the CNS and induce inflammation there (Figure 13 C).

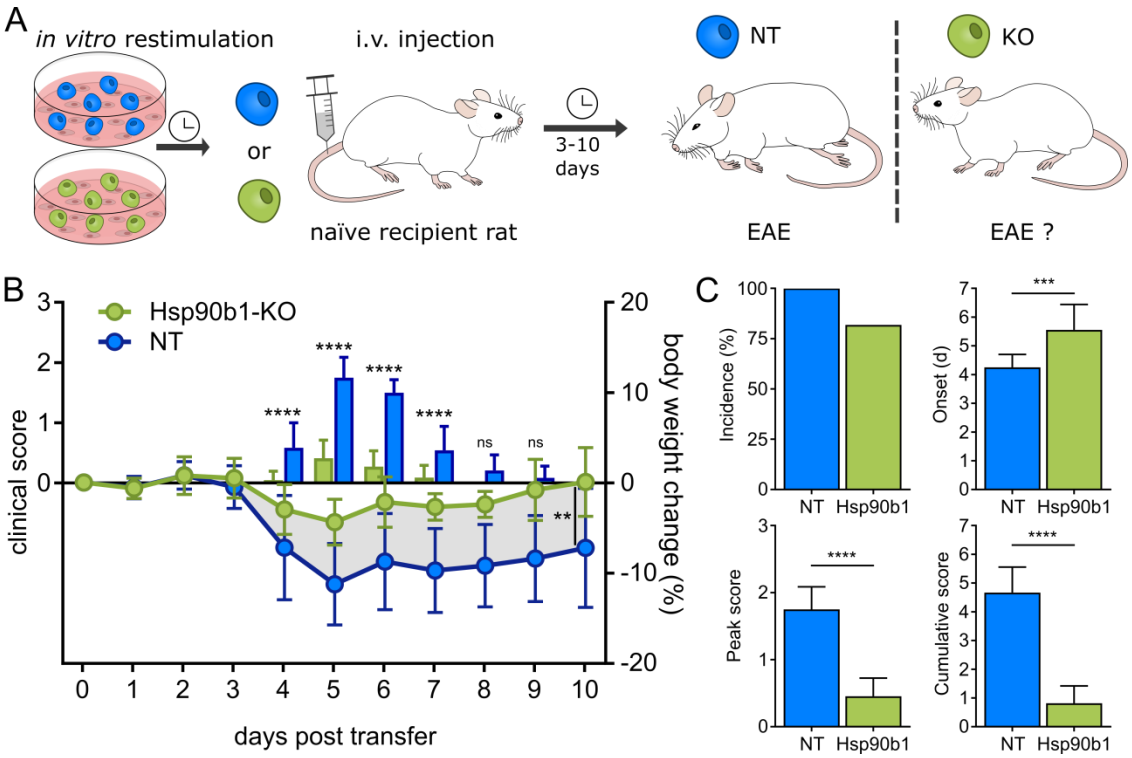

Figure 13 Clinical course induced by T_{MBP} Hsp90b1-KO cells

A) Experimental design. T_{MBP} Hsp90b1-KO and T_{MBP} NT cells were *in vitro* restimulated and were injected solely into rats. The EAE score and body weight was monitored daily. **B)** Clinical course of EAE measured

by percentage of body weight change (lines) and EAE scores (bars) of injected animals. Repeated measures two-way ANOVA; days 0-10 disease score: $F = 145.1$, $P < 0.0001$, body weight change: $F = 13.12$, $P = 0.0016$; $n = 11$ (Hsp90b1-KO); $n = 12$ (NT). Mean ± SD. **C)** Overview of additional EAE parameters: incidence of EAE (%), average onset (days post transfer), average EAE peak score and average EAE cumulative score. Following Sharpiro-Wilk normality test, Mann-Whitney test was performed. Mean ± SD.

4.3.3 The β1-integrin is essential for T_{MBP} cell trafficking into the CNS

In our CRISPR/Cas9 screening results Itgb1 only reached significance in the comparison blood to meninges, despite there being the same trend in the other comparisons. However, since the β1-integrin forms the VLA-4 receptor together with the α4-integrin and its surface expression was downregulated in the KO of the other essential adhesion regulators we decided to assess a KO here as well. In contrast to other candidate genes a surface antibody was available, and the cell population was sorted before experiments to enrich the KO efficiency close to 100 %. Characterization of the *in vitro* cells demonstrated a similar cytokine profile and activation status of T_{MBP} Itgb1-KO and T_{MBP} NT cells (Figure 14 B-E). The labelling of surface integrin expression not only confirmed the KO of the β1-integrin (CD29) but also revealed a marked reduction of the α2-integrin (CD49b) expression in comparison to T_{MBP} NT cells. This can be explained by the fact, that the α2-integrin can only bind to the β1 subunit to form the heterodimer VLA-2 (Adorno-Cruz and Liu, 2019). In addition, we observed a moderate downregulation of α4-integrin (CD49), although it did not reach significance, presumably also as a secondary effect to the downregulation of its binding partner, as there were no changes in the surface expression of αL-integrin (CD11a) and β2-integrin (CD18) in T_{MBP} Itgb1-KO cells (Figure 14 E, G).

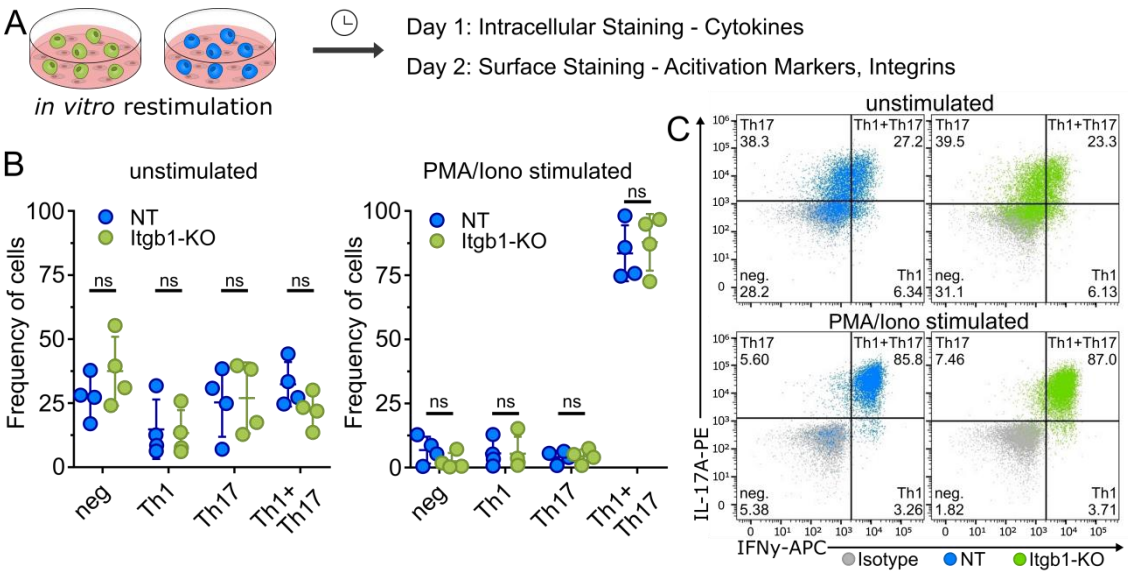

Figure continues on next page

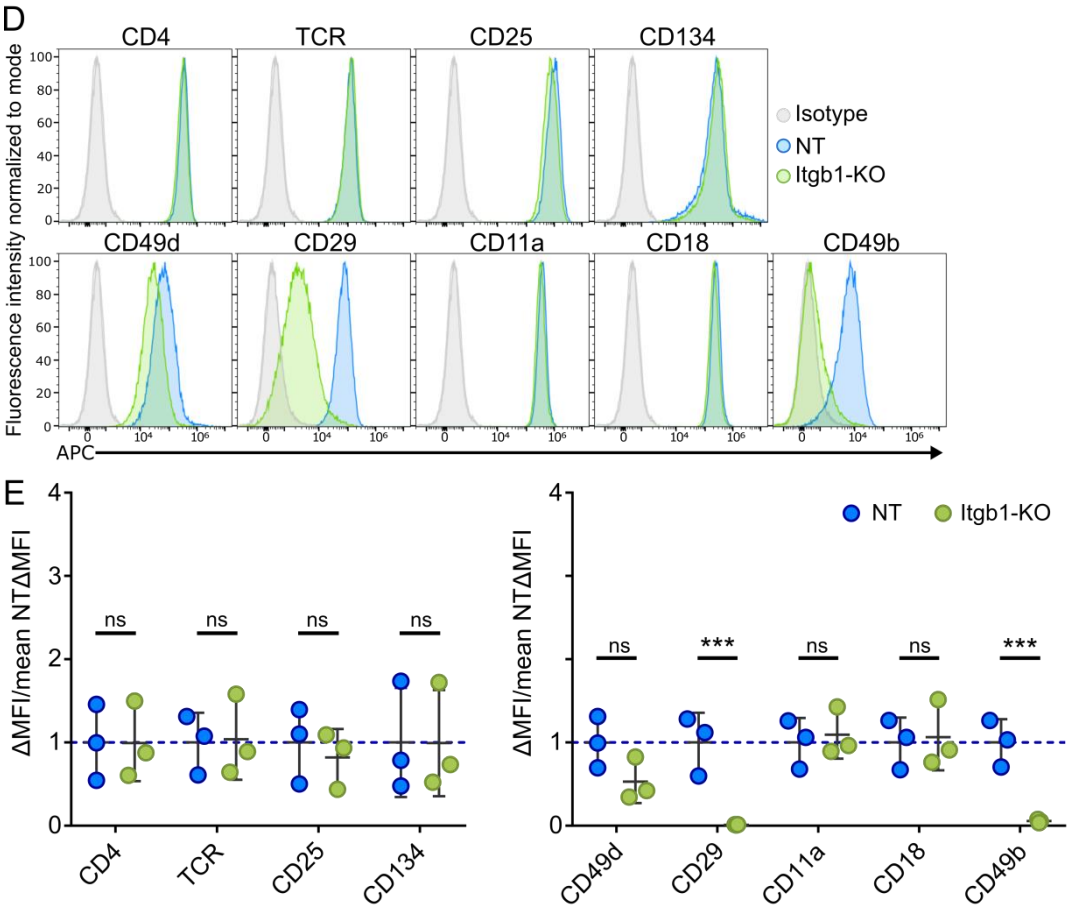

Figure 14 *In vitro* analysis of T_{MBP} Itgb1-KO cells

A) Experimental design. T_{MBP}-EGFP Itgb1-KO and T_{MBP}-BFP NT cells were *in vitro* restimulated. After 24 h cells were stained for their produced cytokines and after 48 h activation markers or integrins were stained on the cell surface. **B)** Quantification of T cell subpopulation based on cytokine profile in flow cytometry analysis. Two-way ANOVA with multiple comparisons with the two-stage linear step-up procedure of Benjamini, Krieger and Yekuteli. Unstimulated: $F < 0.0001$, P = ns, n = 4; stimulated: $F < 0.0001$, P = ns, n = 4. Mean ± SD. **C)** Representative flow cytometry plots showing intracellular staining of IL-17A or IFNy with or without stimulation and their classification into $IFNy^+$ Th1 cells, $IL\text{-}17A^+$ Th17 and $IFNy^+$ and $IL\text{-}17A^+$ Th1+Th17 cells. Cells were gated on lymphocytes > single cells > BFP^+ or GFP^+ > APC and PE values. **D)** Representative flow cytometry plots showing surface expression of various activation markers and integrins. Cells were gated on lymphocytes > single cells > BFP^+ or GFP^+. **E)** Quantification of the ΔMFI (MFI-MFI isotype control) of the surface staining normalized to the mean ΔMFI of NT cells. MFI, two-way ANOVA with multiple comparisons with the two-stage linear step-up procedure of Benjamini, Krieger and Yekuteli. Activation markers: $F = 0.03804$, P = ns, n = 3; integrins: $F = 19.16$, $P = 0.0003$, n = 3. Mean ± SD.

The co-transfer of T_{MBP} Itgb1-KO and T_{MBP} NT cells into rats and the following analysis of T_{MBP} cell distribution in the peripheral and CNS organs revealed a similar result to the other members of the adhesion module (Figure 15 A). In comparison to T_{MBP} NT cells the T_{MBP} Itgb1-KO appeared to exit the blood stream and accumulate in the spleen but were unable to migrate into the parathymic lymph nodes and more importantly into meninges and

parenchyma (Figure 15 B, C). The further analysis of the splenic cells showed no difference in the surface expression of the activation markers CD25 and CD134 (Figure 15 D, E). Interestingly, in the *ex vivo* cells the surface expression of the integrins changed compared to the results observed in the *in vitro* cells. While the β1-integrin (CD29) was still strongly downregulated its potential binding partner α4-integrin (CD49d) was now expressed at the same level as in T_{MBP} NT cells, likely because β1-integrin can be replaced by other ß-integrins such as ß7-integrin (Ley et al., 2007, Lin et al., 2019). In addition, the expression of β2-integrin (CD18) and αL-integrin (CD11a) was identical between KO and control cells (Figure 15 D, E). In line with the previous results the cells in the spleen did not produce cytokines in either of the groups (Figure 15 F, G).

Overall, considering our own experiments in combination with the well-established interactions described in literature we demonstrated the importance of the adhesion module that comprises of the α4-integrin (Itga4), its binding partner β1-integrin (Itgb1) and the integrin chaperone Hsp90b1 for T cell trafficking. Loss of these genes results in an impaired expression of the VLA-4 receptor, which is essential for the attachment of T cells to vascular endothelial cells, thereby affecting the ability of autoreactive T cells to transmigrate into the CNS.

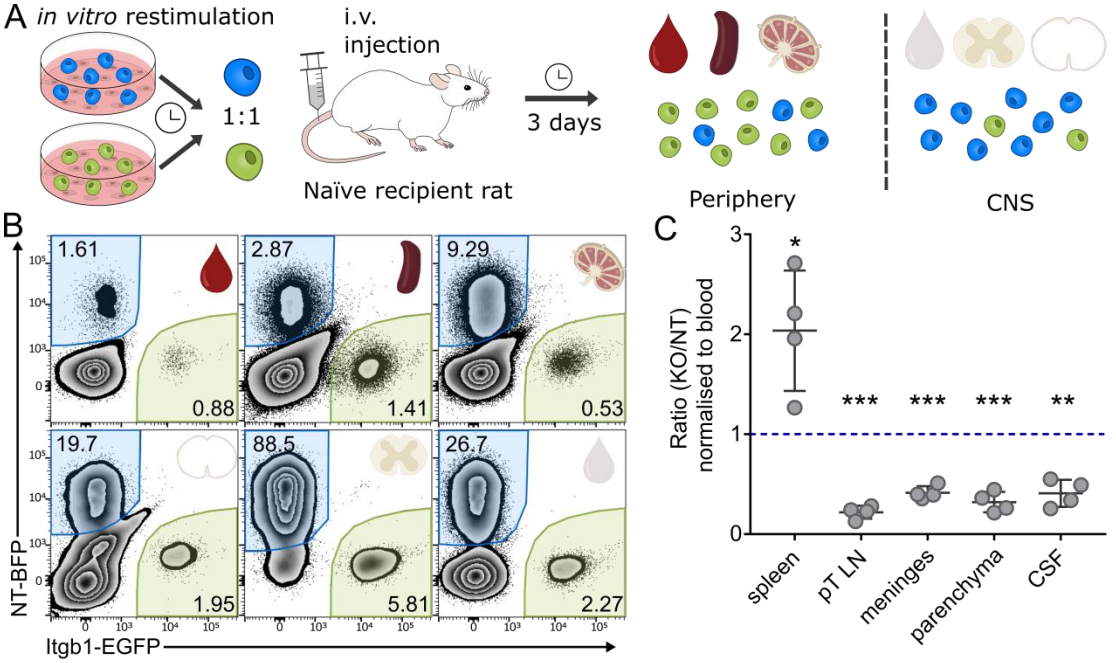

Figure continues on next page

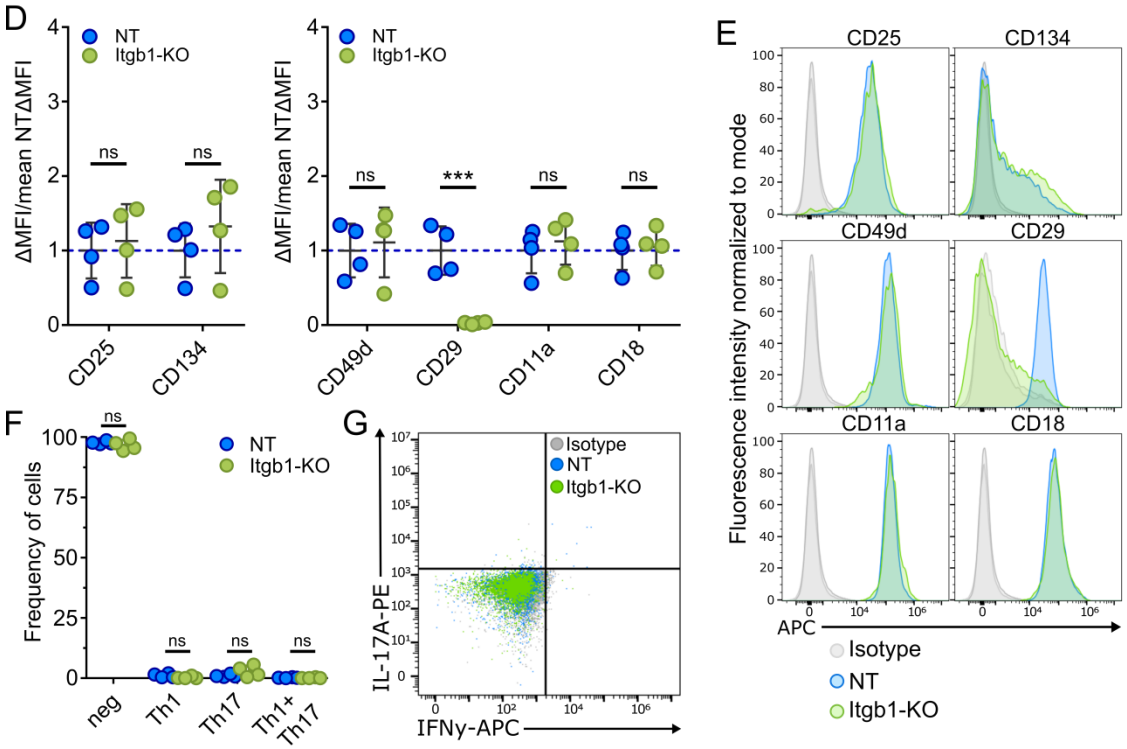

Figure 15 *In vivo* migration analysis following co-transfer of T_{MBP} Itgb1-KO cells

A) Experimental design. T_{MBP} Itgb1-KO and T_{MBP} NT cells were *in vitro* restimulated. After 48 h the fully restimulated T_{MBP} cells were mixed in a 1:1 ratio and injected into rats. With onset of disease on day three, rats were sacrificed and cells from peripheral organs (blood, spleen and pt LN) as well as CNS compartments (CSF, parenchyma, meninges) were collected. **B)** Representative flow cytometry plot with the distribution of T_{MBP} cells in different organs following co-transfer. BFP^+ T_{MBP} NT cells are highlighted in blue, $EGFP^+$ T_{MBP} Itgb1-KO in green. Gated on lymphocytes > single cells > BFP^+ or GFP^+. **C)** Migratory phenotype of T_{MBP} Itgb1-KO cells compared to T_{MBP} NT cells in different organs, shown as the ratio of KO cell number/ NT cell number divided by the KO/NT ratio in blood. A ratio of 1 indicates the migration behaviour of control T_{MBP} cells, a ratio below 1 indicates impaired migration and a ratio above 1 enhanced migration towards an organ. One sample t-test against hypothetical mean = 1. n = 4. Mean ± SD. **D)** Quantification of the ΔMFI (MFI-MFI Isotype control) of the surface staining normalized to the mean ΔMFI of T_{MBP} NT cells. MFI, two-way ANOVA with multiple comparisons with the two-stage linear step-up procedure of Benjamini, Krieger and Yekuteli. Activation markers: F = 0.905, P = ns, all stainings: n = 4; integrins: F = 2.441, P = 0.1313, all stainings: n = 4. Mean ± SD. **E)** Representative flow cytometry plots showing surface expression of activation markers and integrins of ex vivo splenic cells. Cells were gated on lymphocytes > single cells > BFP^+ or GFP^+. **F)** Quantification of T_{MBP} cell subpopulation based on the intracellular flow cytometry staining. Two-way ANOVA with multiple comparisons with the two-stage linear step-up procedure of Benjamini, Krieger and Yekuteli. F = 0, P = ns, n = 4. Mean ± SD. **G)** Representative flow cytometry plots showing intracellular staining of IL-17A and IFNγ of *ex vivo* splenic T_{MBP} Itgb1-KO and T_{MBP} NT cells.

4.4 Validation of the chemotactic module

4.4.1 Chemotaxis of T_{MBP} cells to the CNS is mediated by Cxcr3

Our CRISPR/Cas9 screening yielded an intriguing discovery concerning the chemokine receptor cluster, particularly with regards to *Cxcr3*, which emerged as the sole receptor ranking as a top hit. Cxcr3 is known for its involvement in regulating leukocyte trafficking through chemotactic migration in response to its corresponding chemokines CXCL9, CXCL10 and CXCL11 (Groom and Luster, 2011). Following the gene editing, we again addressed first whether the KO of Cxcr3 showed any effects on *in vitro* stimulated T_{MBP} cells (Figure 16 A). However, T_{MBP} Cxcr3-KO cells display no differences in their ability to produce cytokines, either in standard cell culture conditions or after stimulation with PMA/Ionomycin (Figure 16 B, C). Further, the activation profile defined by the expression of CD4, TCR as well as CD25 and CD134 is comparable between T_{MBP} Cxcr3-KO cells and T_{MBP} NT cells (Figure 16 E, F). Apart from a slight, yet insignificant trend in the upregulation of the α4-integrin (CD49d) there was no difference in the surface expression of the α2-integrin (CD49b), αL-integrin (CD11a), β1-integrin (CD29) or β2-integrin (CD18) (Figure 16 E, G).

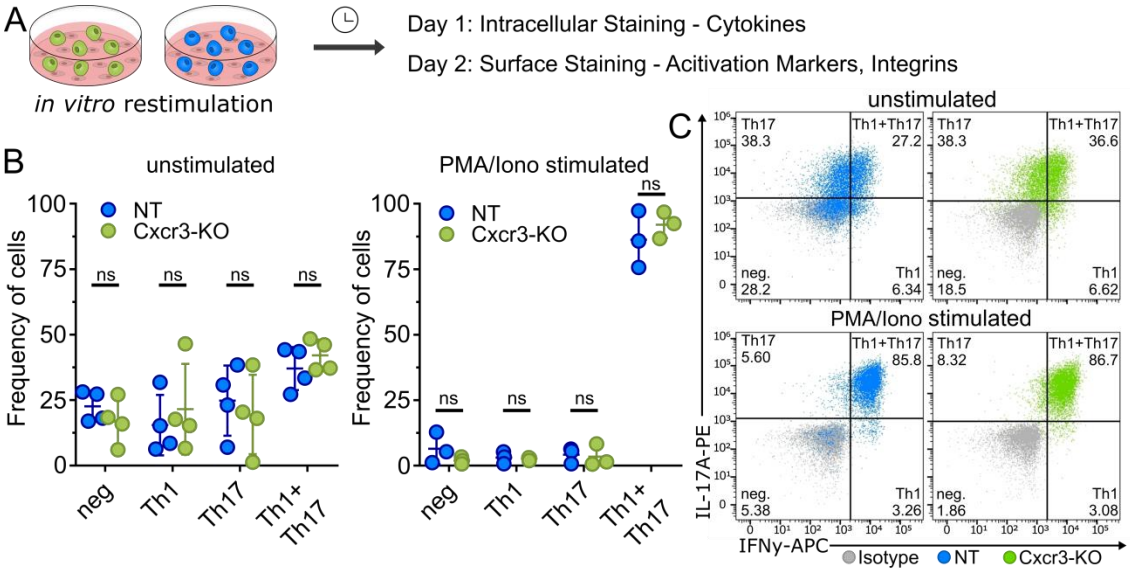

Figure continues on next page

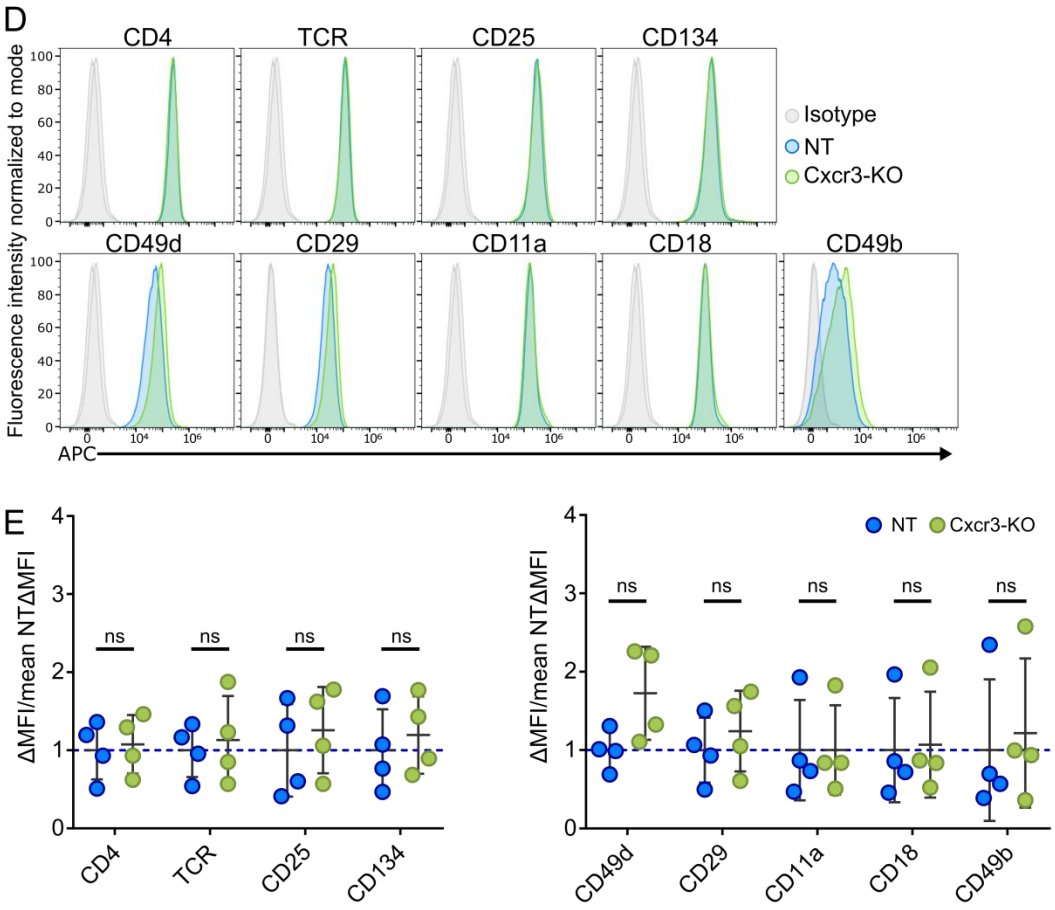

Figure 16 *In vitro* analysis of T_{MBP} Cxcr3-KO cells

A) Experimental design. T_{MBP} Cxcr3-KO and T_{MBP} NT cells were *in vitro* restimulated. After 24 h cells were stained for their produced cytokines and after 48 h activation markers or integrins were stained on the cell surface. **B)** Quantification of T cell subpopulation based on cytokine profile in flow cytometry analysis. Two-way ANOVA with multiple comparisons with the two-stage linear step-up procedure of Benjamini, Krieger and Yekuteli. Unstimulated: $F < 0.0001$, P = ns, n = 4; stimulated: $F < 0.0001$, P = ns, n = 3. Mean ± SD. **C)** Representative flow cytometry plots showing intracellular staining of IL-17A or IFNγ with or without stimulation and their classification into $IFN\gamma^+$ Th1 cells, $IL\text{-}17A^+$ Th17 and $IFN\gamma^+$ and $IL\text{-}17A^+$ Th1+Th17 cells. Cells were gated on lymphocytes > single cells > BFP^+ or GFP^+ > APC and PE values. **D)** Representative flow cytometry plots showing surface expression of various activation markers and integrins. Cells were gated on lymphocytes > single cells > BFP^+ or GFP^+. **E)** Quantification of the ΔMFI (MFI-MFI Isotype control) of the surface staining normalized to the mean ΔMFI of NT cells MFI, two-way ANOVA with multiple comparisons with the two-stage linear step-up procedure of Benjamini, Krieger and Yekuteli. Activation markers: $F = 0.09313$, P = ns, all stainings: n = 4; integrins: $F = 1.504$, P = ns, all stainings: n = 4. Mean ± SD.

To test the functional component of the Cxcr3 KO, we subjected the T_{MBP} cells to a transwell chemotactic assay. The transwell chamber consists of an upper and lower compartment separated by a porous membrane that enables for the passage of cells from the upper chamber to the lower chamber. This setup allowed us to assess the chemotactic response of the cells following the exposure to a certain chemokine. We compared the migration through a

transwell plate under three conditions: no chemokine present, the Cxcr3-ligand CXCL10 or the Cxcr3-unrelated CCL5 present in the medium (Figure 17 A). Comparing T_{MBP} Cxcr3-KO cells to T_{MBP} NT cells, we observed that a higher percentage of T_{MBP} Cxcr3-KO cells migrated to the lower well in the absence of any chemokine or in the presence of the unrelated CCL5. However, T_{MBP} Cxcr3-KO displayed an impaired chemotactic response specifically towards CXCL10 (Figure 17 B). These results provide compelling evidence supporting the notion that the DNA editing of the *Cxcr3* target gene led to a reduced expression of Cxcr3 on the T cells that ultimately resulted in an altered functional response in terms of chemotaxis.

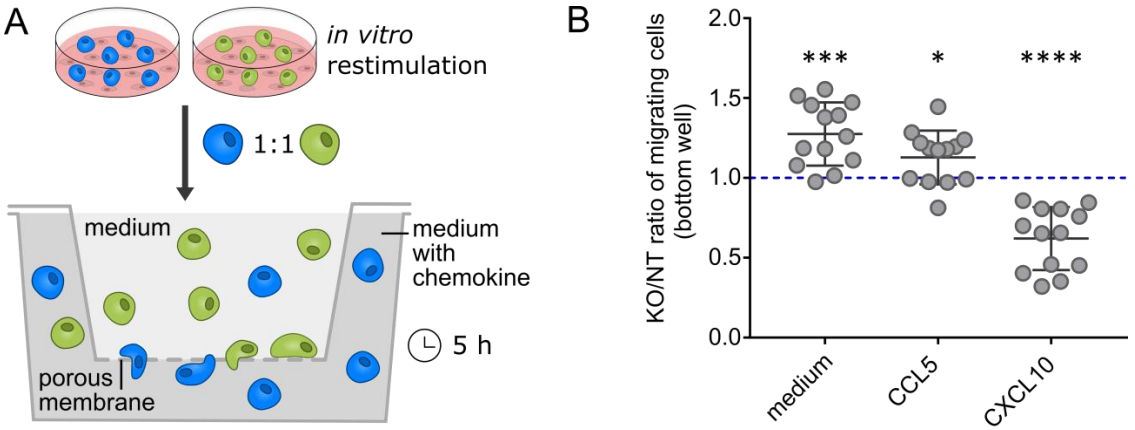

Figure 17 Altered response of T_{MBP} Cxcr3-KO cells in a transwell chemotactic assay

A) Experimental design. T_{MBP} Cxcr3-KO and T_{MBP}-BFP NT cells were *in vitro* restimulated. After 24 h - 48 h a mix with a 1:1 cell ratio was transferred into the upper well of a transwell, while the lower well was supplemented with or without CCL5 or CXCL10. After 5 h migrated cells in the lower part were counted by flow cytometry. **B)** Quantification of migrated cells displayed as ratio of KO cells to NT cells. A ratio of 1 indicates the migration behaviour of control T_{MBP} cells, a ratio below 1 indicates impaired migration and a ratio above 1 enhanced migration. One sample t-test against hypothetical mean = 1. n= 13. Mean ± SD.

To further test the migration behaviour of T_{MBP} Cxcr3-KO cells, they were co-transferred with T_{MBP} NT cells into rats and the cell distribution among the different organs was determined three days later (Figure 18 A). In comparison to blood, there was practically no difference in the migration towards the spleen, while the CNS compartment (meninges, parenchyma, and CSF) displayed a pronounced reduction in the ratio of T_{MBP} Cxcr3-KO to T_{MBP} NT cells (Figure 18 B, C). Although the representative flow cytometry plot shows about twice more T_{MBP} Cxcr3-KO than T_{MBP} NT cells in the CNS compartments, there were about five times more KO cells than control T_{MBP} cells in the blood, therefore we concluded that T_{MBP} Cxcr3-KO failed to migrate into the CNS. The differences in cell numbers likely occur as the proliferation and survival rate of the T cells after adoptive transfer is not identical among experiments even though we aimed to inject T cells in a 1:1 ratio. However, this is why we used the co-transfer model as it allowed

us to normalize the biological deviation by comparing the migration behaviour of KO and control NT T cells to different organs in the same animal. In addition, we stained the cells of the spleen for the expression of certain surface markers. In line with the results of the *in vitro* T cells, we did observe no differences between T_{MBP} Cxcr3-KO and T_{MBP} NT cells in any of the tested surface proteins. There was a trend in the markers of activation CD25 and CD134 to be slightly, yet insignificantly, reduced on the T_{MBP} Cxcr3-KO cells, but as those marker are anyways reduced once the T_{MBP} cells acquire their migratory phenotype, it is presumably biological negligible (Figure 18 D, E). In addition, there was no difference in the expression levels on the LFA-1 components αL-integrin (CD11a) and β2-integrin (CD18) as well as of the VLA-4 components α4-integrin (CD49d) and β1-integrin (CD29) (Figure 18 D, E). Moreover, the staining of the produced cytokines IFNγ and IL-17A showed no abnormal activation in neither of the two T_{MBP} cell types in the spleen (Figure 18 F, G).

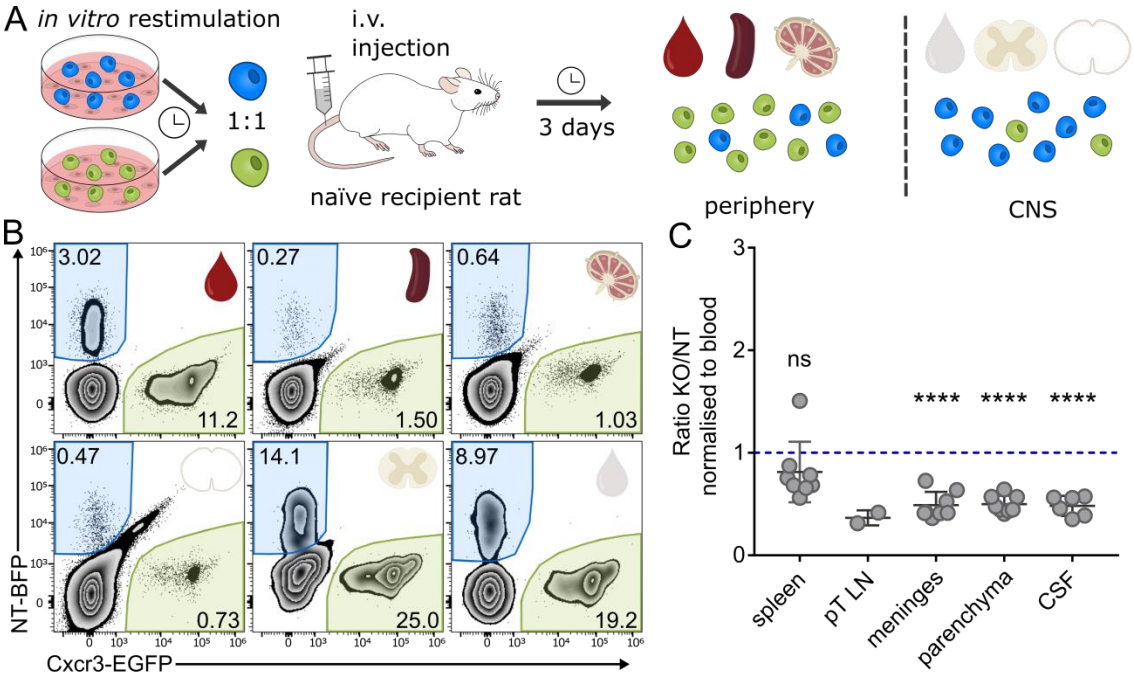

Figure continues on next page

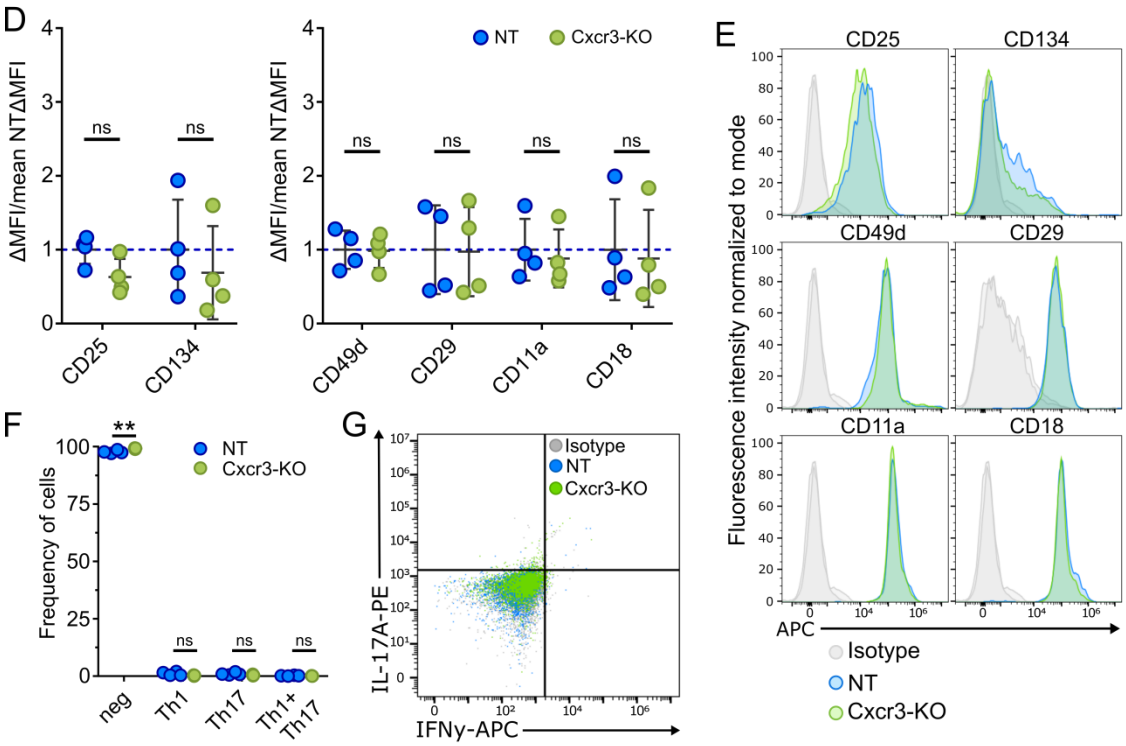

Figure 18 *In vivo* migration analysis following co-transfer of T_{MBP} Cxcr3-KO cells

A) Experimental design. T_{MBP} Cxcr3-KO and T_{MBP} NT cells were *in vitro* restimulated. After 48 h the fully restimulated T_{MBP} cells were mixed in a 1:1 ratio and injected into rats. With onset of disease on day three, rats were sacrificed and cells from peripheral organs (blood, spleen and pt LN) as well as CNS compartments (CSF, parenchyma, meninges) were collected. **B)** Representative flow cytometry plot with the distribution of T_{MBP} cells in different organs following co-transfer. BFP^+ T_{MBP} NT cells are highlighted in blue, $EGFP^+$ T_{MBP} Cxcr3-KO in green. Gated on lymphocytes > single cells > BFP^+ or GFP^+. **C)** Migratory phenotype of T_{MBP} Cxcr3-KO cells compared to T_{MBP} NT cells in different organs, shown as the ratio of KO cell number/ NT cell number divided by the KO/NT ratio in blood. A ratio of 1 indicates the migration behaviour of control T_{MBP} cells, a ratio below 1 indicates impaired migration and a ratio above 1 enhanced migration towards an organ. One sample t-test against hypothetical mean = 1. n = 8 (spleen, meninges parenchyma), n = 2 (pT LN), n = 6 (CSF). Mean ± SD. **D)** Quantification of the ΔMFI (MFI-MFI Isotype control) of the surface staining normalized to the mean ΔMFI of T_{MBP} NT cells. MFI, two-way ANOVA with multiple comparisons with the two-stage linear step-up procedure of Benjamini, Krieger and Yekuteli. Activation markers: F = 1.941, P = ns, all stainings: n = 4; integrins: F = 0.1481, P = ns, all stainings: n = 4. Mean ± SD. **E)** Representative flow cytometry plots showing surface expression of activation markers and integrins of ex vivo splenic cells. Cells were gated on lymphocytes > single cells > BFP^+ or GFP^+. **F)** Quantification of T_{MBP} cell subpopulation based on the intracellular flow cytometry staining. Two-way ANOVA with multiple comparisons with the two-stage linear step-up procedure of Benjamini, Krieger and Yekuteli. F < 0.0001, P = ns, n = 4. Mean ± SD. **G)** Representative flow cytometry plots showing intracellular staining of IL-17A and IFNγ of *ex vivo* splenic T_{MBP} Cxcr3-KO and T_{MBP} NT cells.

In the next step T_{MBP} Cxcr3-KO or T_{MBP} NT cells were individually injected into animals to assess their respective abilities to migrate to the CNS and induce EAE (Figure 19 A). Compared to the typical progression of EAE induced by T_{MBP} NT cells, the disease was ameliorated in the animals receiving T_{MBP} Cxcr3-KO cells. Those animals exhibited less body weight loss and milder clinical

symptoms throughout the course of the disease (Figure 19 B). Further the incidence of EAE was reduced by half in the Cxcr3-KO group. For those animals that did eventually show signs of disease, the onset was delayed by an average of one day, and both the peak and cumulative scores were substantially reduced (Figure 19 C).

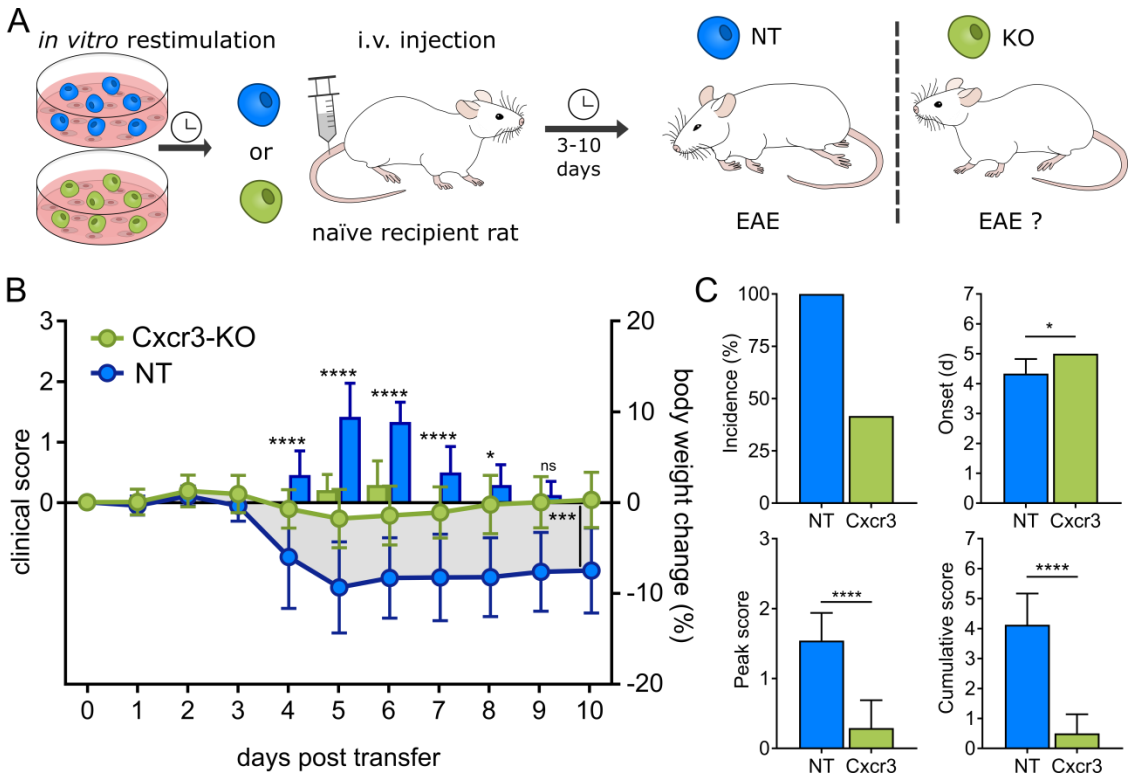

Figure 19 Clinical course induced by T_{MBP} Cxcr3-KO cells

A) Experimental design. T_{MBP} Cxcr3-KO and T_{MBP} NT cells were *in vitro* restimulated and were injected solely into rats. The EAE score and body weight was monitored daily. **B)** Clinical course of EAE measured by percentage of body weight change (lines) and EAE scores (bars) of injected animals. Repeated measures two-way ANOVA; days 0-10 disease score: $F = 104.7$, $P < 0.0001$, body weight change: $F = 20.51$, $P = 0.0002$; $n = 12$ (Cxcr3-KO); $n = 12$ (NT). Mean ± SD. **C)** Overview of additional EAE parameters: incidence of EAE (%), average onset (days post transfer), average EAE peak score and average EAE cumulative score. Following Sharpiro-Wilk normality test, Mann-Whitney test was performed. Mean ± SD. n = 12 (Cxcr3-KO); n = 12 (NT).

4.4.2 Gnai2 transduces Cxcr3 signals

Our analysis of the CRISPR/Cas9 screening results implied that, in addition to CXCR3, other key proteins might be involved in the chemotactic response of T cells into the CNS. Among those is the guanine nucleotide binding protein, alpha inhibiting 2 (Gnai2), which links chemoattractant receptors to downstream effectors thereby mediating cell migration induced by chemokines (Hwang et al., 2017). After knocking out the *Gnai2* gene, we again first checked the *in vitro* T cells for any differences compared to the T_{MBP} NT cells (Figure 20 A). However, the T_{MBP} Gnai2-KO cells displayed no difference in their ability to produce cytokines neither in an

unstimulated state nor following the stimulation with PMA/Ionomycin (Figure 20 B, C). Moreover, the analysis of the expression of surface molecules revealed comparable levels of activation markers as well as of integrins between T_{MBP} Gnai2-KO and T_{MBP} NT (Figure 20 D, E).

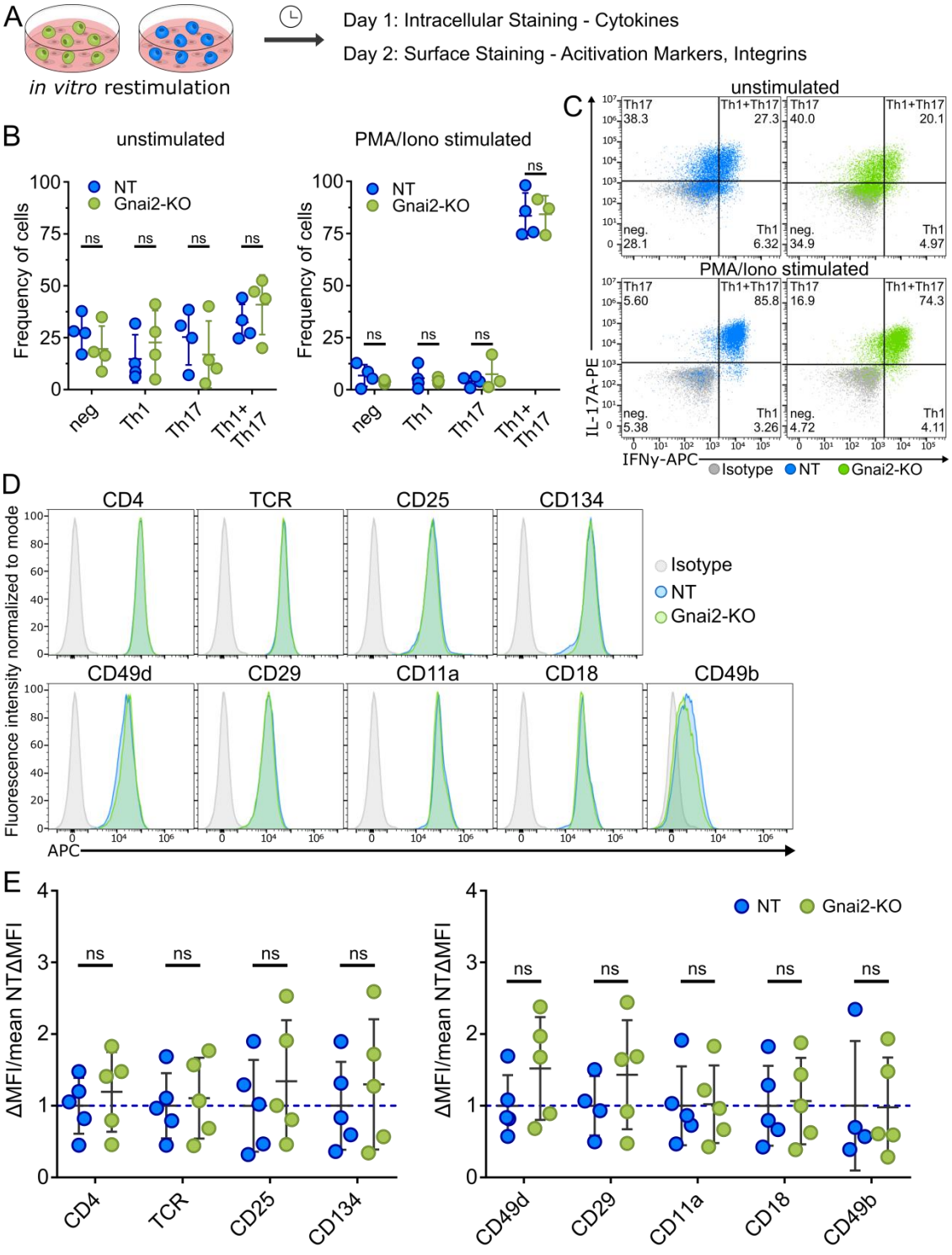

Figure 20 *In vitro* analysis of T_{MBP} Gnai2 KO cells

A) Experimental design. T_{MBP} Gnai2-KO and T_{MBP} NT cells were *in vitro* restimulated. After 24 h cells were stained for their produced cytokines and after 48 h activation markers or integrins were stained on the

cell surface. **B)** Quantification of T cell subpopulation based on cytokine profile in flow cytometry analysis. Two-way ANOVA with multiple comparisons with the two-stage linear step-up procedure of Benjamini, Krieger and Yekuteli. Unstimulated: F < 0.0001, P = ns, n = 4; stimulated: F < 0.0001, P = ns, n = 4 (NT)/n=3 (Gnai2-KO). Mean ± SD. **C)** Representative flow cytometry plots showing intracellular staining of IL-17A or IFNy with or without stimulation and their classification into $IFNy^+$ Th1 cells, $IL\text{-}17A^+$ Th17 and $IFNy^+$ and $IL\text{-}17A^+$ Th1+Th17 cells. Cells were gated on lymphocytes > single cells > BFP^+ or GFP^+ > APC and PE values. **D)** Representative flow cytometry plots showing surface expression of various activation markers and integrins. Cells were gated on lymphocytes > single cells > BFP^+ or GFP^+. **E)** Quantification of the ΔMFI (MFI-MFI Isotype control) of the surface staining normalized to the mean ΔMFI of NT cells. MFI, two-way ANOVA with multiple comparisons with the two-stage linear step-up procedure of Benjamini, Krieger and Yekuteli. Activation markers: F = 1.331, P = ns, all stainings: n = 8; integrins: F = 1.245, P = ns, CD49d/CD11a/CD18: n = 5, CD29/CD49b: n = 4 (NT)/n = 5 (Gnai2-KO). Mean ± SD.

Further we tested the response of T_{MBP} Gnai2-KO cells to certain chemokines *in vitro*. The T_{MBP} Gnai2-KO cells were tested in the same transwell chemotactic assay as the T_{MBP} Cxcr3-KO cells before (Figure 21 A). Interestingly, the observed results differed. While the T_{MBP} Cxcr3-KO cells showed a general higher migration than T_{MBP} NT cells and only a reduction in the CXCL10 condition, the T_{MBP} Gnai2-KO and T_{MBP} NT cells had a similar migration behaviour when no chemokine was present (Figure 21 B). In addition, the chemotactic response of T_{MBP} Gnai2-KO cells was reduced compared to T_{MBP} NT cells, when CCL5 or CXCL10 were present in the medium, suggesting a reduced ability of T_{MBP} Gnai2-KO cells to integrate signals from different receptors recognising one of those two cytokines (Figure 21 B).

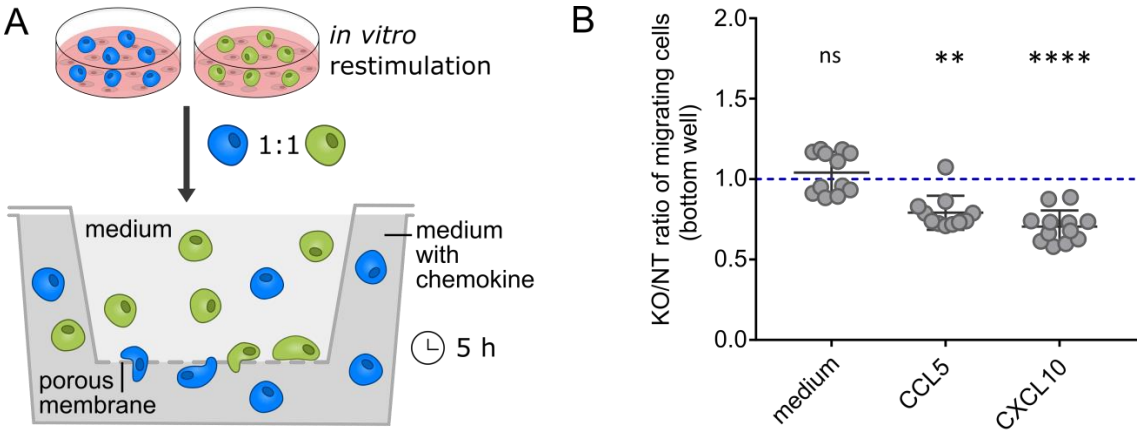

Figure 21 Altered response of T_{MBP} Gnai2-KO cells in a transwell chemotactic assay

A) Experimental design. T_{MBP} Gnai2-KO and T_{MBP}-BFP NT cells were *in vitro* restimulated. After 24 h - 48 h a mix with a 1:1 cell ratio was transferred into the upper well of a transwell, while the lower well was supplemented with or without CCL5 or CXCL10. After 5 h migrated cells in the lower part were counted by flow cytometry. **B)** Quantification of migrated cells displayed as ratio of KO cells to NT cells. A ratio of

1 indicates the migration behaviour of control T_{MBP} cells, a ratio below 1 indicates impaired migration and a ratio above 1 enhanced migration. One sample t-test against hypothetical mean = 1. n= 12. Mean ± SD.

To also asses the effect of the Gnai2 KO on the ability of T_{MBP} cell to migrate into the CNS, we co-transferred them together with T_{MBP} NT cells into rats and analysed their migration into the different organs (Figure 22 A). Similar to the T_{MBP} Cxcr3-KO cells, compared to blood the T_{MBP} Gnai2-KO cells migrated less to both peripheral organs (spleen and parathymic lymph nodes) and the CNS organs (meninges, parenchyma and CSF). A pronounced reduction was especially seen in the parenchyma (Figure 22 B, C). The characterization of the splenic cells, revealed further similarities to the T_{MBP} Cxcr3-KO cells. Again, there seemed to be a trend of mild reduction in the expression of surface CD25 and CD134, although not significant and likely biologically irrelevant. Moreover, the levels of labelled α4-integrin (CD49d) and β1-integrin (CD29) were comparable between T_{MBP} Gnai2-KO and T_{MBP} NT cells and also the αL-integrin (CD11a) and β2-integrin (CD18) were expressed at a similar level (Figure 22 D, E). In line with the observed results before neither T_{MBP} Gnai2-KO cells nor T_{MBP} NT cells produced cytokines in the spleen (Figure 22 F, G).

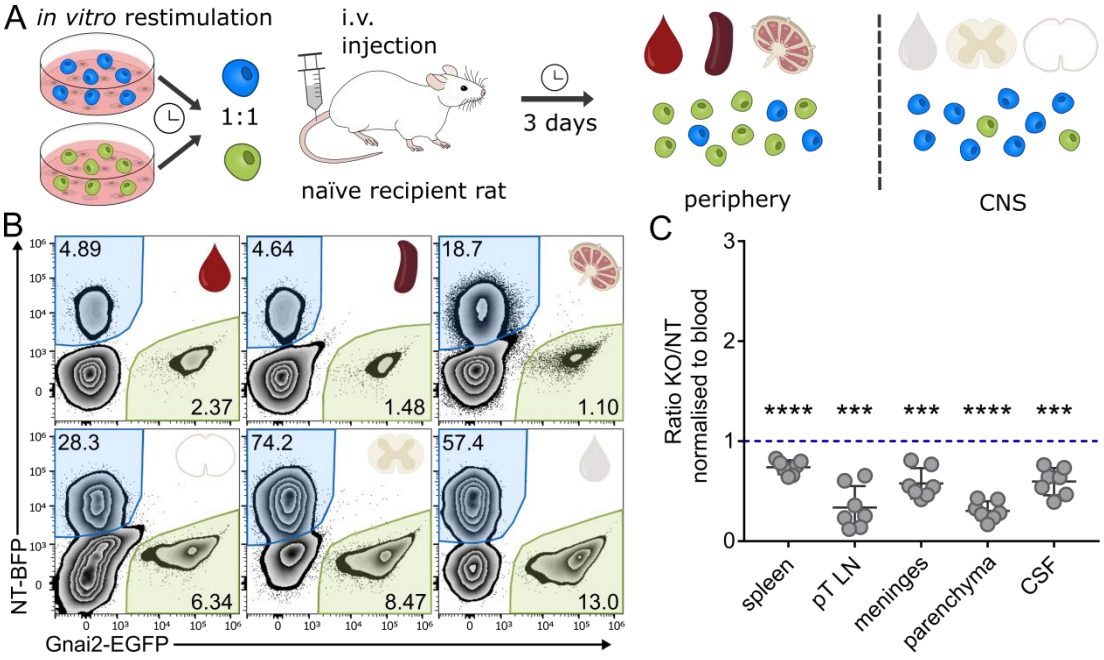

Figure continues on next page

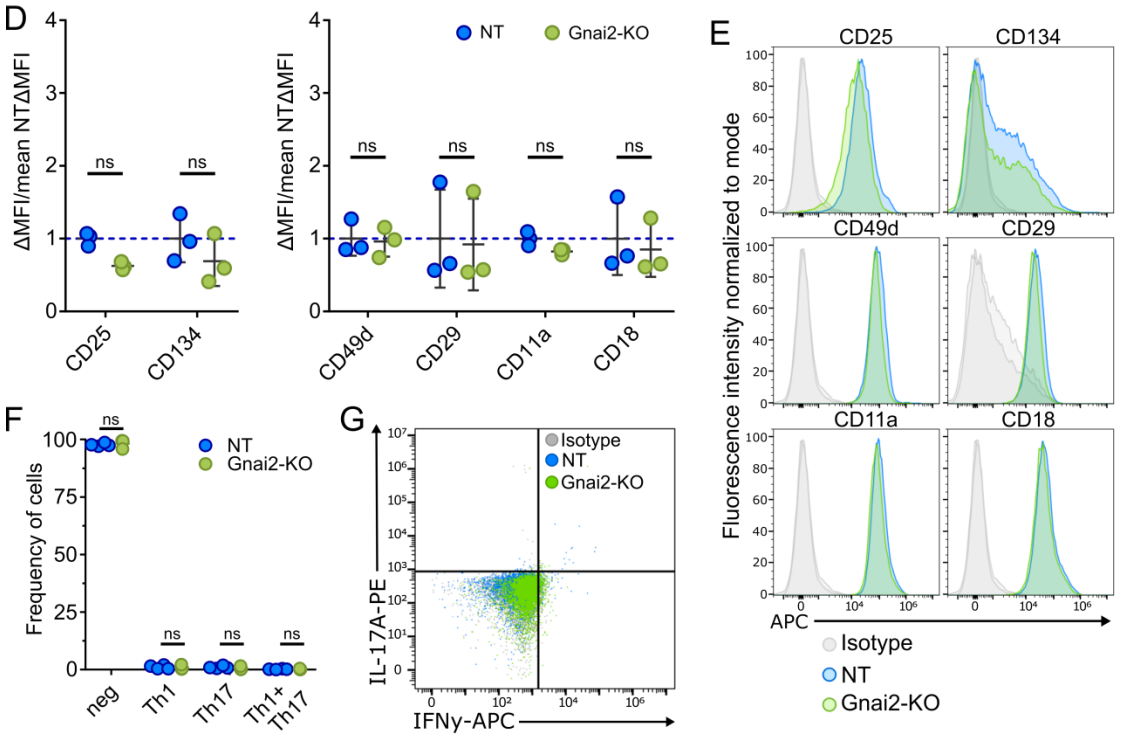

Figure 22 *In vivo* migration analysis following co-transfer of T_{MBP} Gnai2-KO cells

A) Experimental design. T_{MBP} Gnai2-KO and T_{MBP} NT cells were *in vitro* restimulated. After 48 h the fully restimulated T_{MBP} cells were mixed in a 1:1 ratio and injected into rats. With onset of disease on day three, rats were sacrificed and cells from peripheral organs (blood, spleen and pt LN) as well as CNS compartments (CSF, parenchyma, meninges) were collected. **B)** Representative flow cytometry plot with the distribution of T_{MBP} cells in different organs following co-transfer. BFP^+ T_{MBP} NT cells are highlighted in blue, $EGFP^+$ T_{MBP} Gnai2-KO in green. Gated on lymphocytes > single cells > BFP^+ or GFP^+. **C)** Migratory phenotype of T_{MBP} Gnai2-KO cells compared to T_{MBP} NT cells in different organs, shown as the ratio of KO cell number/ NT cell number divided by the KO/NT ratio in blood. A ratio of 1 indicates the migration behaviour of control T_{MBP} cells, a ratio below 1 indicates impaired migration and a ratio above 1 enhanced migration towards an organ. One sample t-test against hypothetical mean = 1. n = 7. Mean ± SD. **D)** Quantification of the ΔMFI (MFI-MFI Isotype control) of the surface staining normalized to the mean ΔMFI of T_{MBP} NT cells. MFI, two-way ANOVA with multiple comparisons with the two-stage linear step-up procedure of Benjamini, Krieger and Yekuteli. Activation markers: F = 6.018, P = 0.397, all stainings: n = 3; integrins: F = 0.4443, P = ns, all stainings: n = 3. Mean ± SD. **E)** Representative flow cytometry plots showing surface expression of activation markers and integrins of ex vivo splenic cells. Cells were gated on lymphocytes > single cells > BFP^+ or GFP^+. **F)** Quantification of T_{MBP} cell subpopulation based on the intracellular flow cytometry staining. Two-way ANOVA with multiple comparisons with the two-stage linear step-up procedure of Benjamini, Krieger and Yekuteli. F = 0.0002, P = ns, n = 4 (NT)/ n = 3 (Gnai2-KO). Mean ± SD. **G)** Representative flow cytometry plots showing intracellular staining of IL-17A and IFNγ of *ex vivo* splenic T_{MBP} Gnai2-KO and T_{MBP} NT cells.

4.4.3 Tbx21 is essential for Cxcr3 mediated signaling in T_{MBP} cells

Among the hits that possibly contribute to the chemotaxis of T cells was the transcription factor Tbx21/T-bet, which is known to control the expression of the Cxcr3 receptor (Beima et al., 2006, Lord et al., 2005). Since Tbx21 is also known to promote T helper cell commitment to

the Th1 lineage (Miller and Weinmann, 2010), it was important to first check for possible phenotypical changes in the T_{MBP} cells carrying a Tbx21 KO (Figure 23 A). Indeed, when we checked for the production of cytokines in the steady state we observed a shift from the IFNγ producing Th1 population, which ended up being less than 1 % of cells, towards the IL-17A producing Th17 population that was twice as big in T_{MBP} Tbx21-KO cells compared to T_{MBP} NT cells (Figure 23 B, C). Similar outcomes were observed upon stimulation with PMA/Ionomycin. While the majority of T_{MBP} NT cells shifted towards the double positive Th1+Th17 phenotype, a quarter of T_{MBP} Tbx21-KO cells remained in the Th17 only subpopulation (Figure 23 B, C). However, other activation markers like the surface expression of CD4, TCR, CD25 or CD134 showed no difference between T_{MBP} Tbx21-KO and T_{MBP} NT cells (Figure 23 D, E). Also, among the labelled surface integrins α4-integrin (CD49d), β1-integrin (CD29), αL-integrin (CD11a), β2-integrin (CD18), and α2-integrin (CD49b) we observed no differential expression (Figure 23 D, E).

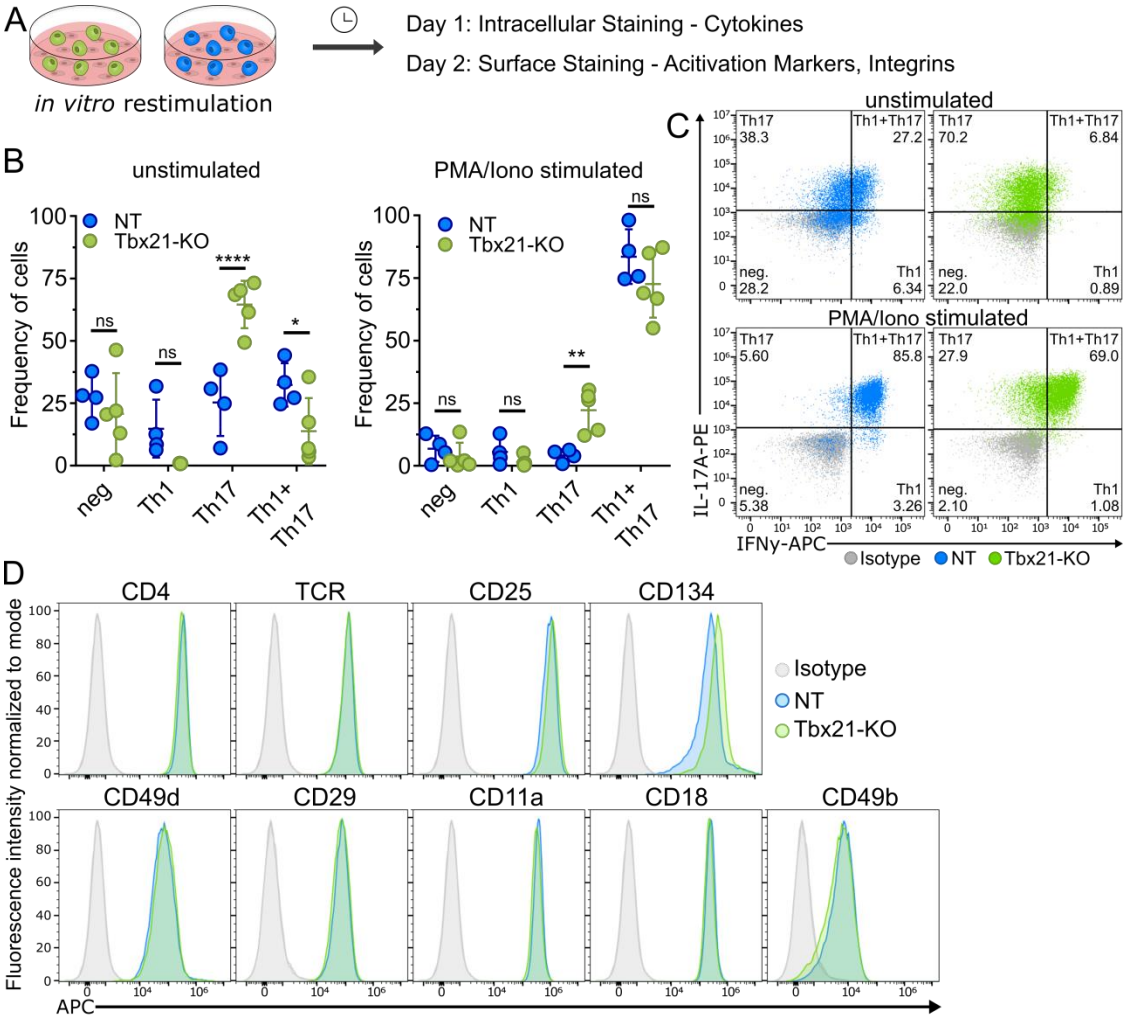

Figure continues on next page

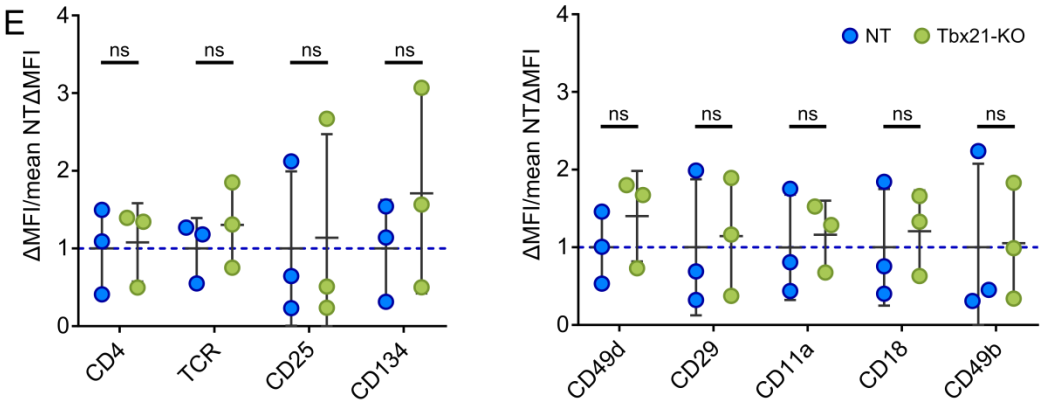

Figure 23 *In vitro* analysis of T_{MBP} Tbx21-KO cells

A) Experimental design. T_{MBP} Tbx21-KO and T_{MBP} NT cells were *in vitro* restimulated. After 24 h cells were stained for their produced cytokines and after 48 h activation markers or integrins were stained on the cell surface. **B)** Quantification of T cell subpopulation based on cytokine profile in flow cytometry analysis. Two-way ANOVA with multiple comparisons with the two-stage linear step-up procedure of Benjamini, Krieger and Yekuteli. Unstimulated: $F < 0.0001$, P = ns, n = 4 (NT)/n=5 (Tbx21-KO); stimulated: $F < 0.0001$, P = ns, n = 4 (NT)/n=5 (Tbx21-KO). Mean ± SD. **C)** Representative flow cytometry plots showing intracellular staining of IL-17A or IFNy with or without stimulation and their classification into $IFNy^+$ Th1 cells, $IL\text{-}17A^+$ Th17 and $IFNy^+$ and $IL\text{-}17A^+$ Th1+Th17 cells. Cells were gated on lymphocytes > single cells > BFP^+ or GFP^+ > APC and PE values. **D)** Representative flow cytometry plots showing surface expression of various activation markers and integrins. Cells were gated on lymphocytes > single cells > BFP^+ or GFP^+. **E)** Quantification of the ΔMFI (MFI-MFI Isotype control) of the surface staining normalized to the mean ΔMFI of NT cells. MFI, two-way ANOVA with multiple comparisons with the two-stage linear step-up procedure of Benjamini, Krieger and Yekuteli. Activation markers: $F = 0.7837$, P = ns, all stainings: n = 3; integrins: $F = 0.5499$, $P < 0.0001$, all stainings: n = 3. Mean ± SD.

Since Tbx21 is involved in CXCR3-mediated migration (Lord et al., 2005), we compared the migration of T_{MBP} Tbx21-KO and T_{MBP} NT cells in our transwell chemotaxis assay (Figure 24 A). We found that T_{MBP} Tbx21-KO showed a similar transmigration to T_{MBP} NT cells when no chemokine was present, but a reduced migration toward the chemokine CCL5 and an even more pronounced reduction in the chemotactic response towards the CXCR3 ligand CXCL10 (Figure 24 B). These results strongly resemble those observed in those of T_{MBP} Gnai2-KO cells. Furthermore, the effect on Cxcr3-mediated transmigration towards CXCL10 was even stronger in the T_{MBP} Tbx21-KO than in the T_{MBP} Cxcr3 cells, highlighting the importance of Tbx21 for Cxcr3-mediated chemokine signaling (Figure 24 B). Moreover, as the migration towards CCL5 is also reduced, likely other receptors or molecules involved in the signaling pathway are downregulated as well.

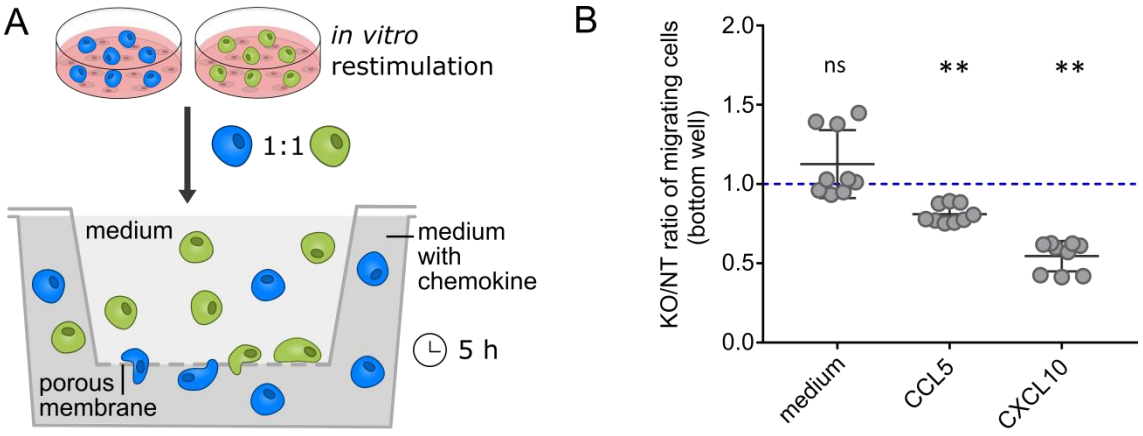

Figure 24 Altered response of T_{MBP} Tbx21-KO cells in a transwell chemotactic assay

A) Experimental design. T_{MBP} Tbx21-KO and T_{MBP}-BFP NT cells were *in vitro* restimulated. After 24 h - 48 h a mix with a 1:1 cell ratio was transferred into the upper well of a transwell, while the lower well was supplemented with or without CCL5 or CXCL10. After 5 h migrated cells in the lower part were counted by flow cytometry. **B)** Quantification of migrated cells displayed as ratio of KO cells to NT cells. A ratio of 1 indicates the migration behaviour of control T_{MBP} cells, a ratio below 1 indicates impaired migration and a ratio above 1 enhanced migration. One sample t-test against hypothetical mean = 1. n = 9. Mean ± SD.

In order to evaluate the impact of Tbx21 KO on the migratory capacity of T_{MBP} cells, we conducted co-transfer experiments with T_{MBP} NT cells in rats. Subsequently, we analysed the distribution and migration of these cells within the CNS and peripheral organs (Figure 25 A). Interestingly, there was no discernible difference in the migration patterns between T_{MBP} Tbx21-KO and T_{MBP} NT cells in the spleen and the parathymic lymph node (Figure 25 B). However, when examining the CNS compartments, a noteworthy finding emerged. Within the CNS, we observed a moderate decrease in migration of T_{MBP} Tbx21-KO cells specifically in the meninges, while a slightly more pronounced reduction was observed in the CSF. However, there was no significant difference in migration observed in the parenchyma between the T_{MBP} Tbx21-KO and T_{MBP} NT cells. This is particularly interesting as our CRISPR/Cas9 screening results predicted a reduced migration into the meninges and the parenchyma. In order to gain further insight, we conducted additional characterization of splenic cells by performing surface antigen staining. While T_{MBP} Tbx21-KO cells exhibited some upregulation of activation markers, the expression levels of surface CD25 and CD134 did not reach statistical significance in the individual comparisons (Figure 25 D, E). Furthermore, when examining the levels of α4-integrin (CD49d) and β1-integrin (CD29) labelling, there were no notable differences between T_{MBP} Tbx21-KO and T_{MBP} NT cells. Similarly, the expression of αL-integrin (CD11a) and β2-integrin (CD18) appeared to be comparable between these two groups (Figure 22 D, E). It is noteworthy that among the KO cells analysed in this study, T_{MBP} Tbx21-KO cells were the only

ones to exhibit an altered cytokine profile in the spleen, albeit the difference was relatively small. In comparison to T_{MBP} NT cells, the T_{MBP} Tbx21-KO cells demonstrated a slightly higher production of IL-17A, aligning with the previously observed *in vitro* results. (Figure 25 F, G).

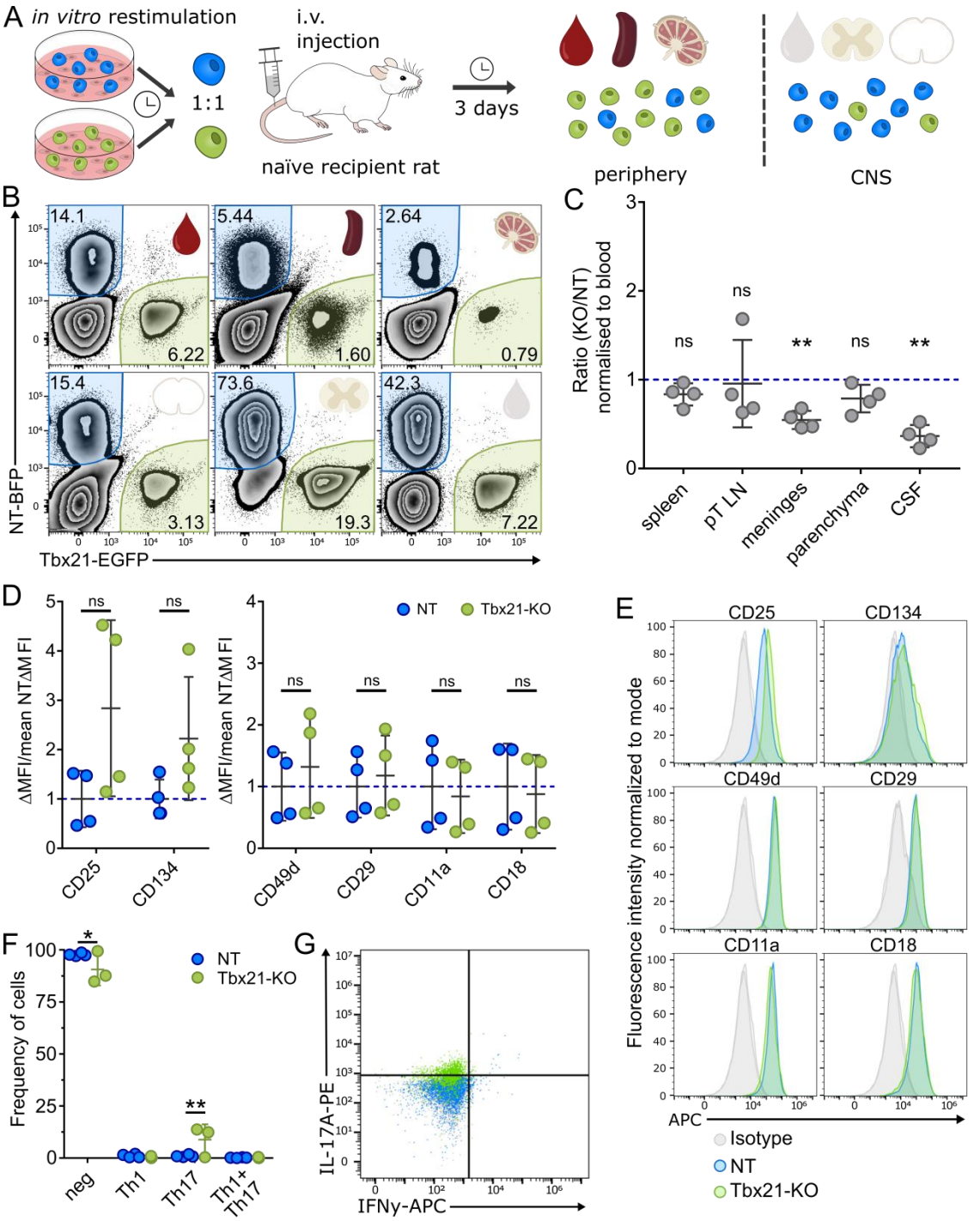

Figure 25 *In vivo* migration analysis following co-transfer of T_{MBP} Tbx21-KO cells

A) Experimental design. T_{MBP} Tbx21-KO and T_{MBP} NT cells were *in vitro* restimulated. After 48 h the fully restimulated T_{MBP} cells were mixed in a 1:1 ratio and injected into rats. With onset of disease on day three, rats were sacrificed and cells from peripheral organs (blood, spleen and pt LN) as well as CNS compartments (CSF, parenchyma, meninges) were collected. **B)** Representative flow cytometry plot with

the distribution of T_{MBP} cells in different organs following co-transfer. BFP^+ T_{MBP} NT cells are highlighted in blue, $EGFP^+$ T_{MBP} Tbx21-KO in green. Gated on lymphocytes > single cells > BFP^+ or GFP^+. **C)** Migratory phenotype of T_{MBP} Tbx21-KO cells compared to T_{MBP} NT cells in different organs, shown as the ratio of KO cell number/ NT cell number divided by the KO/NT ratio in blood. A ratio of 1 indicates the migration behaviour of control T_{MBP} cells, a ratio below 1 indicates impaired migration and a ratio above 1 enhanced migration towards an organ. One sample t-test against hypothetical mean = 1. n = 4. Mean ± SD. **D)** Quantification of the ΔMFI (MFI-MFI Isotype control) of the surface staining normalized to the mean ΔMFI of T_{MBP} NT cells. MFI, two-way ANOVA with multiple comparisons with the two-stage linear step-up procedure of Benjamini, Krieger and Yekuteli. Activation markers: F = 7.188, P = 0.02, all stainings: n = 4; integrins: F = 0.05737, P = ns, all stainings: n = 4. Mean ± SD. **E)** Representative flow cytometry plots showing surface expression of activation markers and integrins of ex vivo splenic cells. Cells were gated on lymphocytes > single cells > BFP^+ or GFP^+. **F)** Quantification of T_{MBP} cell subpopulation based on the intracellular flow cytometry staining. Two-way ANOVA with multiple comparisons with the two-stage linear step-up procedure of Benjamini, Krieger and Yekuteli. F < 0.0001, P = ns, n = 4 (NT)/ n = 3 (Tbx21-KO). Mean ± SD. **G)** Representative flow cytometry plots showing intracellular staining of IL-17A and IFNy of *ex vivo* splenic T_{MBP} Tbx21-KO and T_{MBP} NT cells.

4.4.4 CCR5 is dispensable for T_{MBP} cell migration into the CNS

Previous work implicated that the chemokine receptors CXCR3 and CCR5 play an essential role in the regulation of T cell trafficking into the CNS (Schläger et al., 2016). Although CCR5 has not appeared in the candidate list of our genome-wide CRISPR/Cas9 screening, we anyways decided to test the effects of knocking out CCR5 in our experimental setup (Figure 26 A). Like other components implicated in the chemotactic response, we observed no difference in the phenotype of T_{MBP} CCR5-KO cells *in vitro* compared to T_{MBP} NT cells. Both cell types had the same distribution of produced IFNy and IL-17A in the unstimulated as well as the PMA/Ionomycin stimulated condition (Figure 26 B, C). Furthermore, there was a similar expression of the surface markers CD4, TCR, CD25 and CD134 that indicate an identical activation status and also no difference in the expression of VLA-4 components α4-integrin (CD49d) and β1-integrin (CD29), LFA-1 subdomains αL-integrin (CD11a) and β2-integrin (CD18), as well as α2-integrin (CD49b) (Figure 26 D, E).

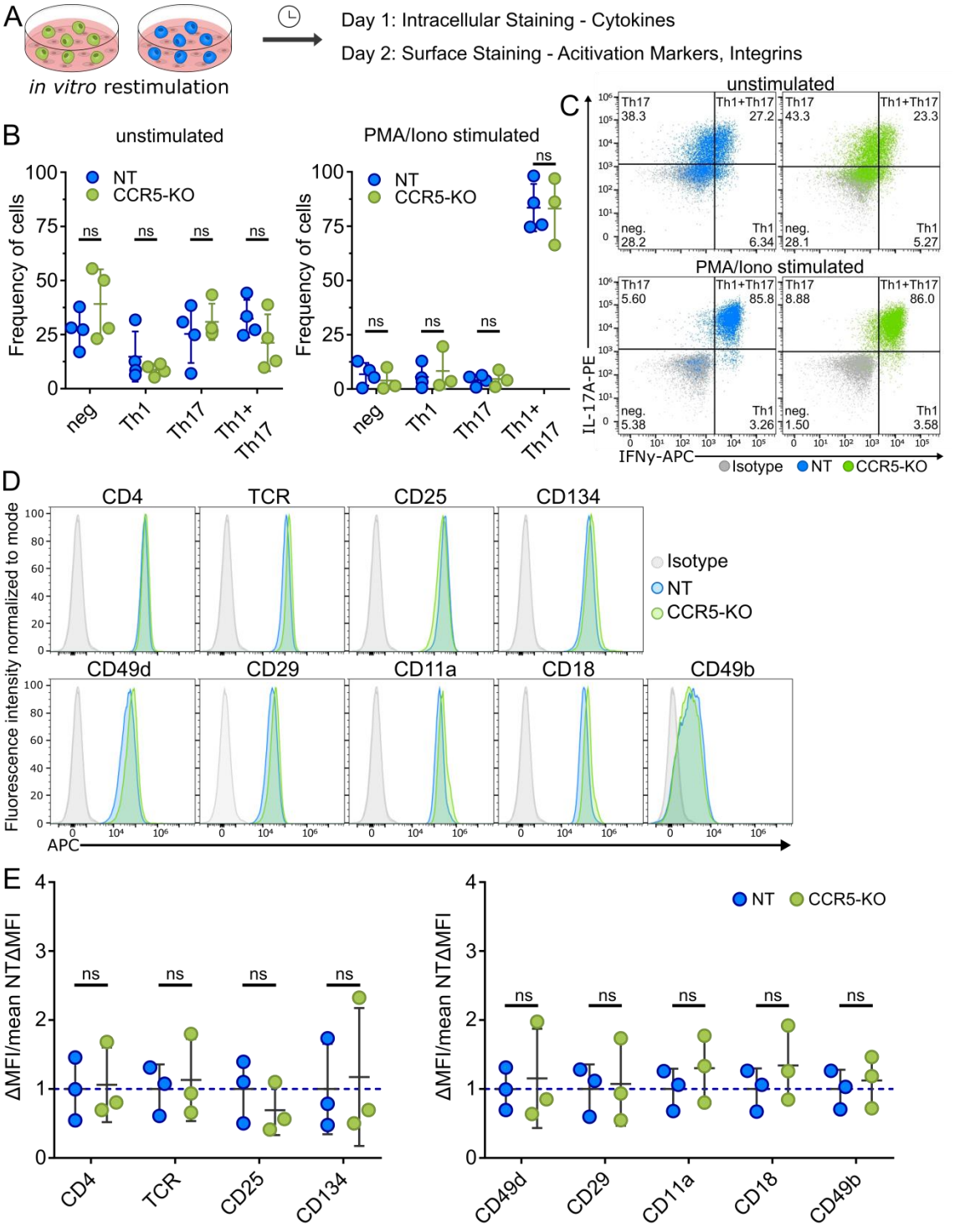

Figure 26 *In vitro* analysis of T_{MBP} CCR5-KO cells

A) Experimental design. T_{MBP} CCR5-KO and T_{MBP} NT cells were *in vitro* restimulated. After 24 h cells were stained for their produced cytokines and after 48 h activation markers or integrins were stained on the cell surface. **B)** Quantification of T cell subpopulation based on cytokine profile in flow cytometry analysis. Two-way ANOVA with multiple comparisons with the two-stage linear step-up procedure of Benjamini, Krieger and Yekuteli. Unstimulated: $F < 0.0001$, P = ns, n = 4; stimulated: $F < 0.0001$, P = ns, n = 4 (NT)/n=3 (CCR5-KO). Mean ± SD. **C)** Representative flow cytometry plots showing intracellular staining of IL-17A or IFNγ with or without stimulation and their classification into $IFN\gamma^+$ Th1 cells, $IL\text{-}17A^+$

Th17 and IFNy$^+$ and IL-17A$^+$ Th1+Th17 cells. Cells were gated on lymphocytes > single cells > BFP$^+$ or GFP$^+$ > APC and PE values. **D)** Representative flow cytometry plots showing surface expression of various activation markers and integrins. Cells were gated on lymphocytes > single cells > BFP$^+$ or GFP$^+$. **E)** Quantification of the ΔMFI (MFI-MFI Isotype control) of the surface staining normalized to the mean ΔMFI of NT cells. MFI, two-way ANOVA with multiple comparisons with the two-stage linear step-up procedure of Benjamini, Krieger and Yekuteli. Activation markers: F = 0.00386, P = ns, all stainings: n = 3; integrins: F = 1.466, P = ns, all stainings: n = 3. Mean ± SD.

To test the effect of the CCR5-KO on the CNS trafficking of T_{MBP} cells *in vivo*, we co-transferred them together with T_{MBP} NT cells into rats (Figure 27 A). When we assessed the distribution of the cells on the onset of disease three days after transfer, we observed a similar distribution of T_{MBP} CCR5-KO and T_{MBP} NT cells in almost all organs (Figure 27 B, C). Especially in the CNS organs meninges, parenchyma and CSF that are relevant in EAE, the CCR5 KO did not appear to have an effect on the migration of the T_{MBP} cells. While there was also no difference in the migration ratio of the spleen, there were less T_{MBP} CCR5-KO migrating into the parathymic lymph nodes. This suggests that KO of CCR5 seems to have an effect on T cell trafficking but is not involved in the T_{MBP} cell migration to the CNS in the aT-EAE of Lewis rats, thereby confirming the results of CRISPR/Cas9 screening. Further analysis of the cells from the spleen revealed no major differences in the surface expression of the two activation markers that usually become downregulated when the T_{MBP} cells acquire their migratory phenotype. While there was no difference in CD25 surface expression, CD134 seems to become less, but not significantly, downregulated in T_{MBP} CCR5-KO compared to T_{MBP} NT cells (Figure 27 D, E). Among the integrins α4-integrin (CD49d), β1-integrin (CD29), αL-integrin (CD11a) and β2-integrin (CD18) were similarly labelled on the surface. As expected, there was barely a detectable production of the cytokines IFNy and IL-17A in T_{MBP} CCR5-KO and T_{MBP} NT cells (Figure 27 F, G).

These results indicate that only a certain set of genes is implicated in the chemotactic response of T_{MBP} cells to migrate into the CNS. Based on our CRISPR/Cas9 screening and the following validation experiments we demonstrated that the chemotaxis module centres around the chemokine receptor CXCR3, its intracellular binding partner Gnai2 and its transcription factor Tbx21. All of them appear to be essential for the entry of autoreactive T_{MBP} cells to the CNS in our model.

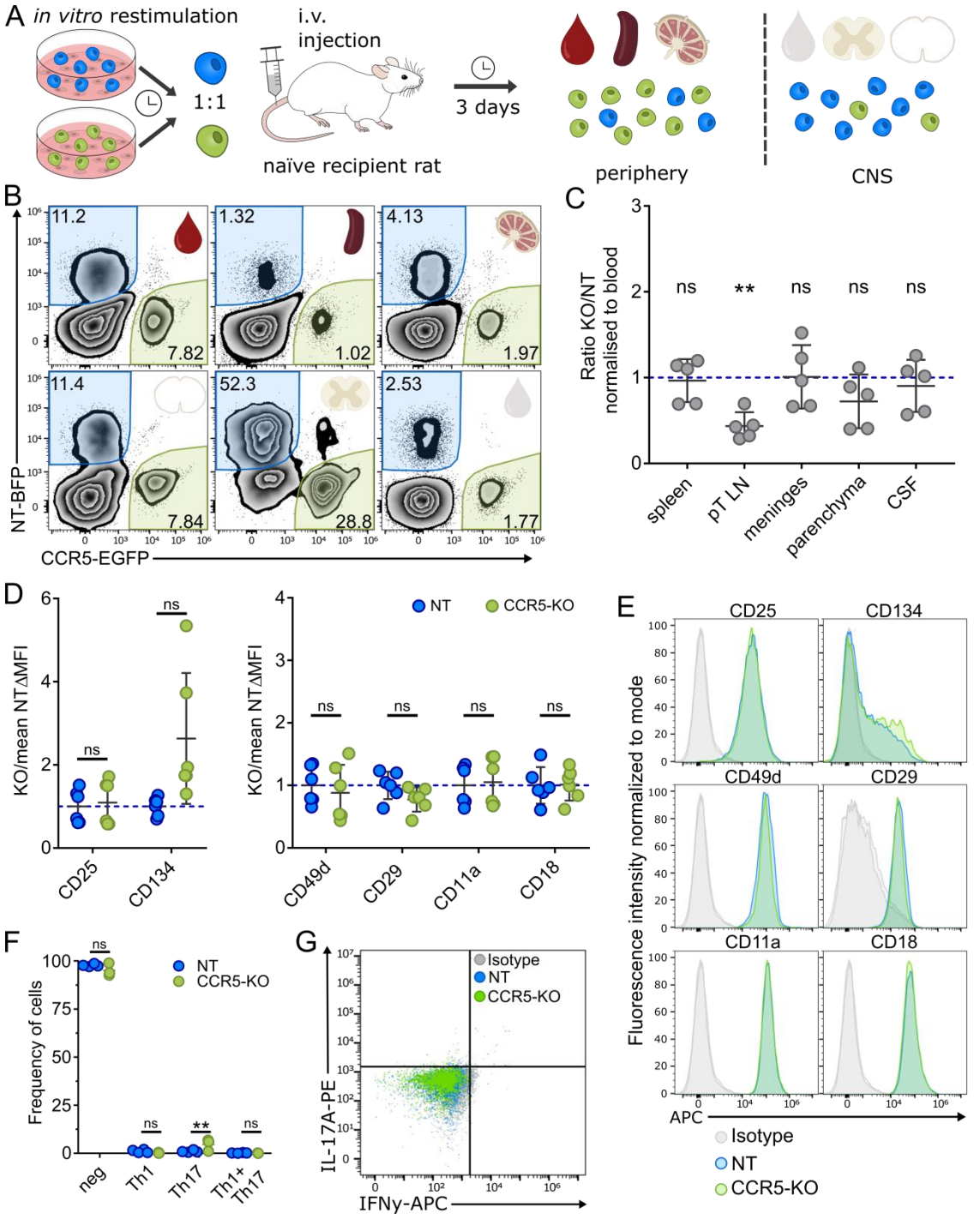

Figure 27 *In vivo* migration analysis following co-transfer of T_{MBP} CCR5-KO cells

A) Experimental design. T_{MBP} CCR5-KO and T_{MBP} NT cells were *in vitro* restimulated. After 48 h the fully restimulated T_{MBP} cells were mixed in a 1:1 ratio and injected into rats. With onset of disease on day three, rats were sacrificed and cells from peripheral organs (blood, spleen and pt LN) as well as CNS compartments (CSF, parenchyma, meninges) were collected. **B)** Representative flow cytometry plot with the distribution of T_{MBP} cells in different organs following co-transfer. BFP^+ T_{MBP} NT cells are highlighted in blue, $EGFP^+$ T_{MBP} CCR5-KO in green. Gated on lymphocytes > single cells > BFP^+ or GFP^+. **C)** Migratory phenotype of T_{MBP} CCR5-KO cells compared to T_{MBP} NT cells in different organs, shown as the ratio of KO cell number/ NT cell number divided by the KO/NT ratio in blood. A ratio of 1 indicates the migration behaviour of control T_{MBP} cells, a ratio below 1 indicates impaired migration and a ratio above 1

enhanced migration towards an organ. One sample t-test against hypothetical mean = 1. n = 5. Mean ± SD. **D)** Quantification of the ΔMFI (MFI-MFI Isotype control) of the surface staining normalized to the mean ΔMFI of T_{MBP} NT cells. MFI, two-way ANOVA with multiple comparisons with the two-stage linear step-up procedure of Benjamini, Krieger and Yekuteli. Activation markers: F = 0.5413, P = ns, all stainings: n = 6; integrins: F = 0.08018, P = ns, all stainings: n = 6. Mean ± SD. **E)** Representative flow cytometry plots showing surface expression of activation markers and integrins of ex vivo splenic cells. Cells were gated on lymphocytes > single cells > BFP^+ or GFP^+. **F)** Quantification of T_{MBP} cell subpopulation based on the intracellular flow cytometry staining. Two-way ANOVA with multiple comparisons with the two-stage linear step-up procedure of Benjamini, Krieger and Yekuteli. F < 0.0001, P = ns, n = 4 (NT)/ n = 3 (CCR5-KO). Mean ± SD. **G)** Representative flow cytometry plots showing intracellular staining of IL-17A and IFNy of *ex vivo* splenic T_{MBP} CCR5-KO and T_{MBP} NT cells.

4.5 Validation of the egress module

4.5.1 Grk2 is essential for T_{MBP} cell trafficking into the CNS

In our CRISPR/Cas9 screening, among the GPCR related proteins, the strongest candidate gene was the G protein coupled receptor kinase 2 (Grk2) as it reached significance in all four comparisons and had one of the strongest effect sizes of any regulator outside the adhesion module. Since Grk2 is a central signaling nod for multiple pathways, there was an array of potential mechanisms how KO of Grk2 can affect the transmigration process in T cells (Penela et al., 2019). To investigate any phenotypic changes associated with the Grk2 KO in T_{MBP} cells we conducted *in vitro* tests comparing them to T_{MBP} NT cells (Figure 28 A). Analysis of the cytokines produced by these cells revealed no differences in both the unstimulated and stimulated conditions (Figure 28 B, C). Additionally, we observed nearly identical expression levels of surface activation markers, including CD4, TCR, CD25, and CD134, as well as surface integrins such as α4-integrin (CD49d), β1-integrin (CD29), αL-integrin (CD11a), β2-integrin (CD18), and α2-integrin (CD49b) between the two cell types (Figure 28 D, E). These findings indicate that, at least at the examined phenotypic levels, T_{MBP} Grk2-KO cells did not exhibit substantial differences compared to T_{MBP} NT cells *in vitro*.

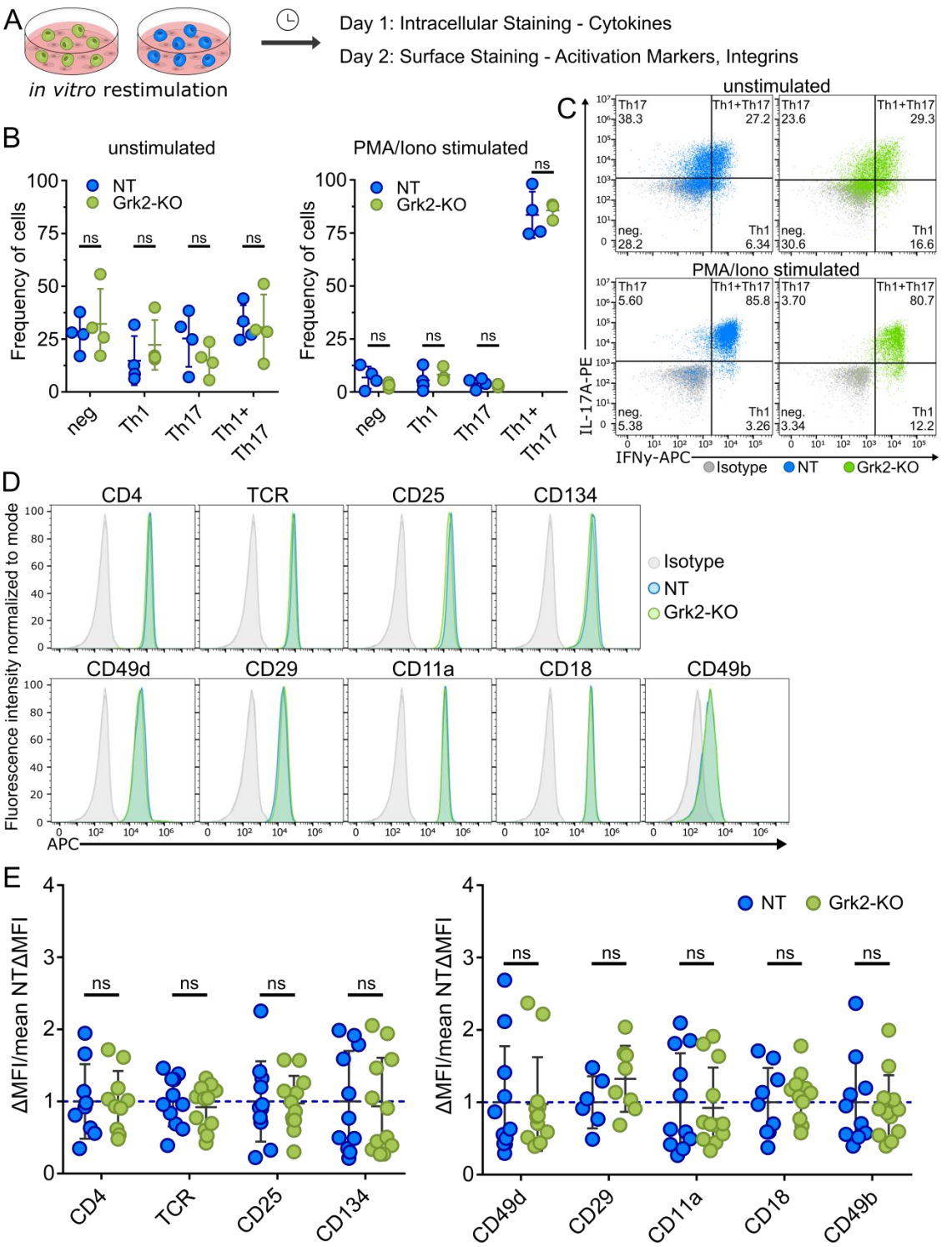

Figure 28 *In vitro* analysis of T_{MBP} Grk2-KO cells

A) Experimental design. T_{MBP} Grk2-KO and T_{MBP} NT cells were *in vitro* restimulated. After 24 h cells were stained for their produced cytokines and after 48 h activation markers or integrins were stained on the cell surface. **B)** Quantification of T cell subpopulation based on cytokine profile in flow cytometry analysis. Two-way ANOVA with multiple comparisons with the two-stage linear step-up procedure of Benjamini, Krieger and Yekuteli. Unstimulated: $F < 0.0001$, P = ns, n = 4; stimulated: $F < 0.0001$, P = ns, n = 4 (NT)/n=3 (Grk2-KO). Mean ± SD. **C)** Representative flow cytometry plots showing intracellular staining of IL-17A or IFNγ with or without stimulation and their classification into $IFN\gamma^+$ Th1 cells, $IL\text{-}17A^+$

Th17 and IFNy$^+$ and IL-17A$^+$ Th1+Th17 cells. Cells were gated on lymphocytes > single cells > BFP$^+$ or GFP$^+$ > APC and PE values. **D)** Representative flow cytometry plots showing surface expression of various activation markers and integrins. Cells were gated on lymphocytes > single cells > BFP$^+$ or GFP$^+$. **E)** Quantification of the ΔMFI (MFI-MFI Isotype control) of the surface staining normalized to the mean ΔMFI of NT cells. MFI, two-way ANOVA with multiple comparisons with the two-stage linear step-up procedure of Benjamini, Krieger and Yekuteli. Activation markers: F = 0.03834, P = ns, CD4: n = 9, TCR/CD25/CD134: n = 11; integrins: F = 0.2647, P = ns, CD49d/CD11a: n = 11, CD29: n = 6 (NT)/n = 7 (Grk2-KO), CD18: n = 9 (NT)/n = 10 (Grk2-KO), CD49b: n = 10 (NT)/n = 11 (Grk2-KO). Mean ± SD.

To investigate how the KO of Grk2 affects the migration of T cells we co-transferred them with T_{MBP} NT cells into rats to induce EAE (Figure 29 A). We assessed the distribution of EGFP expressing T_{MBP} Grk2-KO cells and BFP expressing T_{MBP} NT cells in each organ on the day of disease onset by flow cytometry (Figure 29 B). This analysis revealed a strong reduction in the capacity of T_{MBP} Grk2-KO cells to reach all three compartments of the CNS. Not only meninges, parenchyma and CSF showed a reduced ratio of T_{MBP} Grk2-KO to T_{MBP} NT cells, also less T_{MBP} Grk2-KO cells were detected in the parathymic lymph node (Figure 29 C). In contrast, the ratio in the spleen equals almost 1, indicating that there is no difference in the KO to NT T cell distribution compared to blood. When we further stained the cells in the spleen, we observed a significant downregulation of CD25 and a slight yet insignificant downregulation of CD134 on the surface of T_{MBP} Grk2-KO cells compared to T_{MBP} NT cells (Figure 29 D, E). Among the integrins, both of the subdomains of the VLA-4 receptor α4-integrin (CD49d) and β1-integrin (CD29) as well as the subdomains of the LFA-1 receptor αL-integrin (CD11a) and β2-integrin (CD18) were equally expressed on the surface of T_{MBP} Grk2-KO cells and T_{MBP} NT cells (Figure 29 D, E). As observed before neither T_{MBP} Grk2-KO cells nor T_{MBP} NT cells produced any of the tested cytokines in the spleen. (Figure 29 F, G).

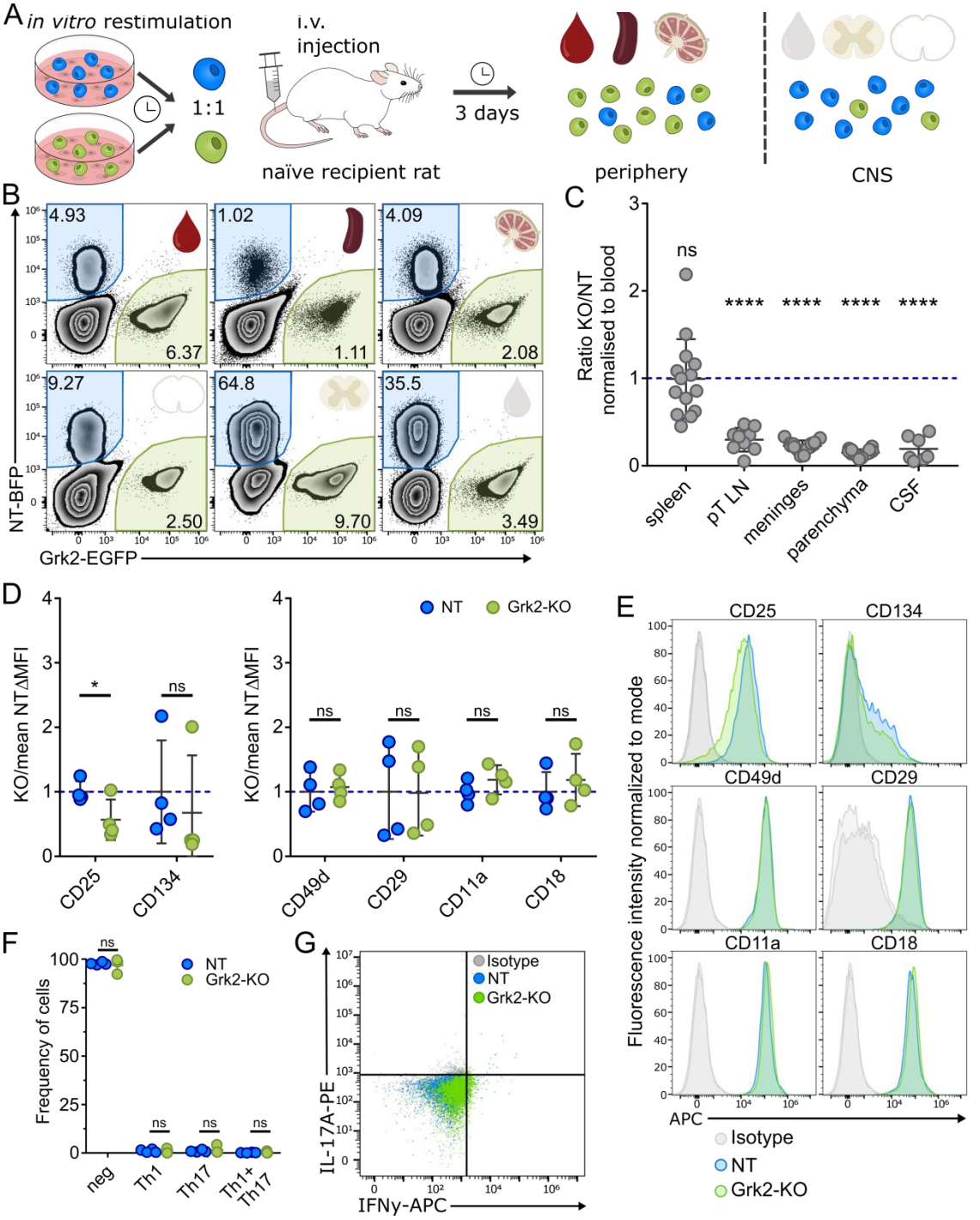

Figure 29 *In vivo* migration analysis following co-transfer of T_{MBP} Grk2-KO cells

A) Experimental design. T_{MBP} Grk2-KO and T_{MBP} NT cells were *in vitro* restimulated. After 48 h the fully restimulated T_{MBP} cells were mixed in a 1:1 ratio and injected into rats. With onset of disease on day three, rats were sacrificed and cells from peripheral organs (blood, spleen and pt LN) as well as CNS compartments (CSF, parenchyma, meninges) were collected. **B)** Representative flow cytometry plot with the distribution of T_{MBP} cells in different organs following co-transfer. BFP^+ T_{MBP} NT cells are highlighted in blue, $EGFP^+$ T_{MBP} Grk2-KO in green. Gated on lymphocytes > single cells > BFP^+ or GFP^+. **C)** Migratory phenotype of T_{MBP} Grk2-KO cells compared to T_{MBP} NT cells in different organs, shown as the ratio of KO cell number/ NT cell number divided by the KO/NT ratio in blood. A ratio of 1 indicates the migration behaviour of control T_{MBP} cells, a ratio below 1 indicates impaired migration and a ratio above 1

enhanced migration towards an organ. One sample t-test against hypothetical mean = 1. n = 14 (spleen, meninges parenchyma), n = 8 (pT LN), n = 9 (CSF). Mean ± SD. **D)** Quantification of the ΔMFI (MFI-MFI Isotype control) of the surface staining normalized to the mean ΔMFI of T_{MBP} NT cells. MFI, two-way ANOVA with multiple comparisons with the two-stage linear step-up procedure of Benjamini, Krieger and Yekuteli. Activation markers: F = 1.48, P = ns, all stainings: n = 4; integrins: F = 0.5042, P = ns, all stainings: n = 4. Mean ± SD. **E)** Representative flow cytometry plots showing surface expression of activation markers and integrins of ex vivo splenic cells. Cells were gated on lymphocytes > single cells > BFP^+ or GFP^+. **F)** Quantification of T_{MBP} cell subpopulation based on the intracellular flow cytometry staining. Two-way ANOVA with multiple comparisons with the two-stage linear step-up procedure of Benjamini, Krieger and Yekuteli. F < 0.0001, P = ns, n = 4 (NT)/ n = 3 (Grk2-KO). Mean ± SD. **G)** Representative flow cytometry plots showing intracellular staining of IL-17A and IFNγ of *ex vivo* splenic T_{MBP} Grk2-KO and T_{MBP} NT cells.

To test whether the observed difference in migration capacity of T cells also reflects in their ability to induce EAE T_{MBP} Grk2-KO cells or T_{MBP} NT cells were solely injected into rats (Figure 30 A). Throughout the course of disease, the animals that received the T_{MBP} Grk2-KO cells showed an ameliorated disease course and lost significantly less body weight (Figure 30 B). Although the incidence was slightly reduced, the onset of disease was significantly later and the peak score as well as the cumulative score were markedly reduced in the Grk2-KO group compared to rats that received T_{MBP} NT cells (Figure 30 C).

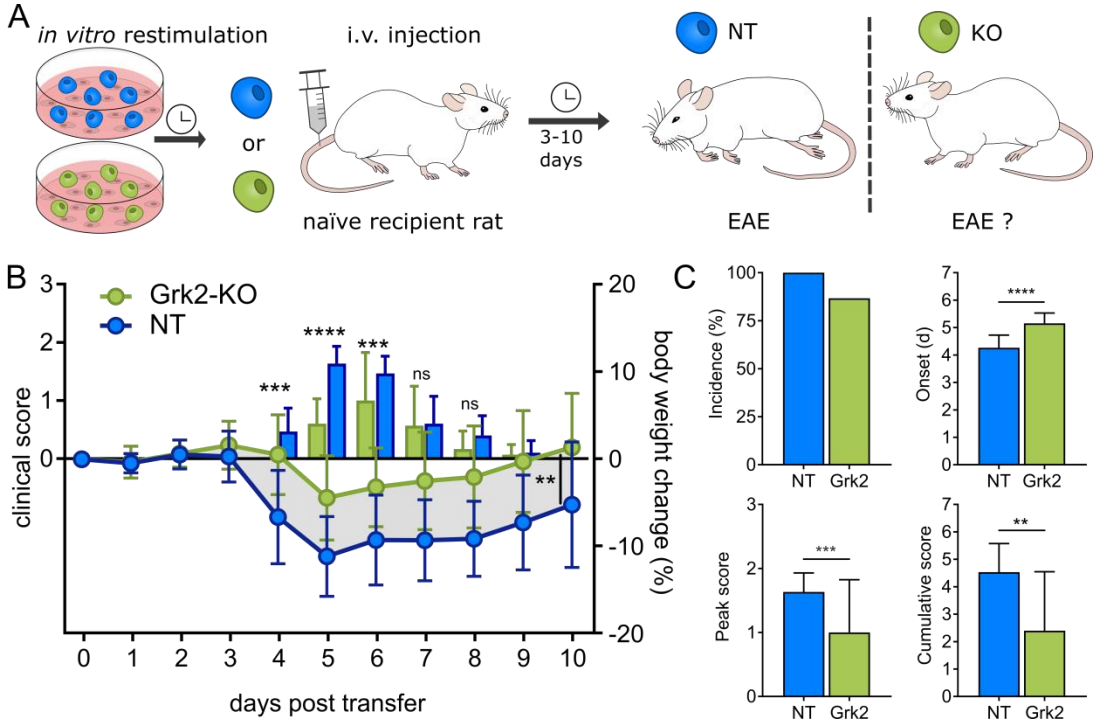

Figure 30 Clinical course induced by T_{MBP} Grk2-KO cells

A) Experimental design. T_{MBP} Grk2-KO and T_{MBP} NT cells were *in vitro* restimulated and were injected solely into rats. The EAE score and body weight was monitored daily. **B)** Clinical course of EAE measured by percentage of body weight change (lines) and EAE scores (bars) of injected animals. Repeated measures two-way ANOVA; days 0-10 disease score: F = 12.3, P = 0.0014, body weight change: F = 12.03,

P = 0.0017; n = 15 (Grk2-KO); n = 15 (NT). Mean ± SD. **C)** Overview of additional EAE parameters: incidence of EAE (%), average onset (days post transfer), average EAE peak score and average EAE cumulative score. Following Sharpiro-Wilk normality test, Mann-Whitney test was performed. Mean ± SD.

Our next goal was to determine which stage of the transmigration process into the CNS was affected by the absence of Grk2, so we utilized intravital 2-photon imaging to examine the leptomeninges of the rat spinal cord two to three days after co-transfer of EGFP expressing T_{MBP} Grk2-KO cells and BFP expressing control T_{MBP} NT cells (Figure 31 A). While circulating cells in the blood stream cannot be visualized through imaging due to their high speeds, T cells that have tethered themselves and are actively moving within blood vessels can be observed using microscopy. We tracked the number, location, and motility of the labelled T_{MBP} cells crawling in the meningeal vessels and in the surrounding tissue once they exited the blood vessel (Figure 31 B). While the numbers of intraluminal T_{MBP} Grk2-KO and T_{MBP} NT cells are comparable, we detected significantly less T_{MBP} Grk2-KO that have extravasated from the vessels than T_{MBP} NT cells (Figure 31 C). Moreover, with the comparison of the cell ratios inside and outside the blood vessel it becomes obvious that T_{MBP} Grk2-KO fail to exit the vasculature (Figure 31 C). The analysis of additional migration parameters demonstrated that T_{MBP} Grk2-KO cells exhibited a noticeably slower crawling speed alongside the vessels compared to the control T_{MBP} NT cells. However, it is important to note that the mean difference of 1.5 µm/min between the two groups was relatively small when considering the overall range and variability of crawling speeds. This suggests that the observed difference, while statistically significant, may not had a substantial impact on the overall migratory behaviour of the cells. Therefore, in terms of their biological implications, this small difference in crawling speed could be considered negligible. Furthermore, the similarity in crawling distance between both cell types indicated that they likely encountered a similar number of potential exit sites (Figure 31 D). This similarity suggests that despite the disparity in crawling speed, both cell types had comparable opportunities to reach potential exit sites for the diapedesis process.

Overall, the imaging results revealed that T_{MBP} Grk2-KO cells are able to attach to the blood vessel wall and successfully crawl along it yet fail to accomplish transendothelial migration. Together with our observations that T_{MBP} Grk2-KO cells had only minor alterations in the surface expression of activation markers and integrins this suggests that the loss of Grk2 alters the responsiveness of T cells to signals that determine their diapedesis.

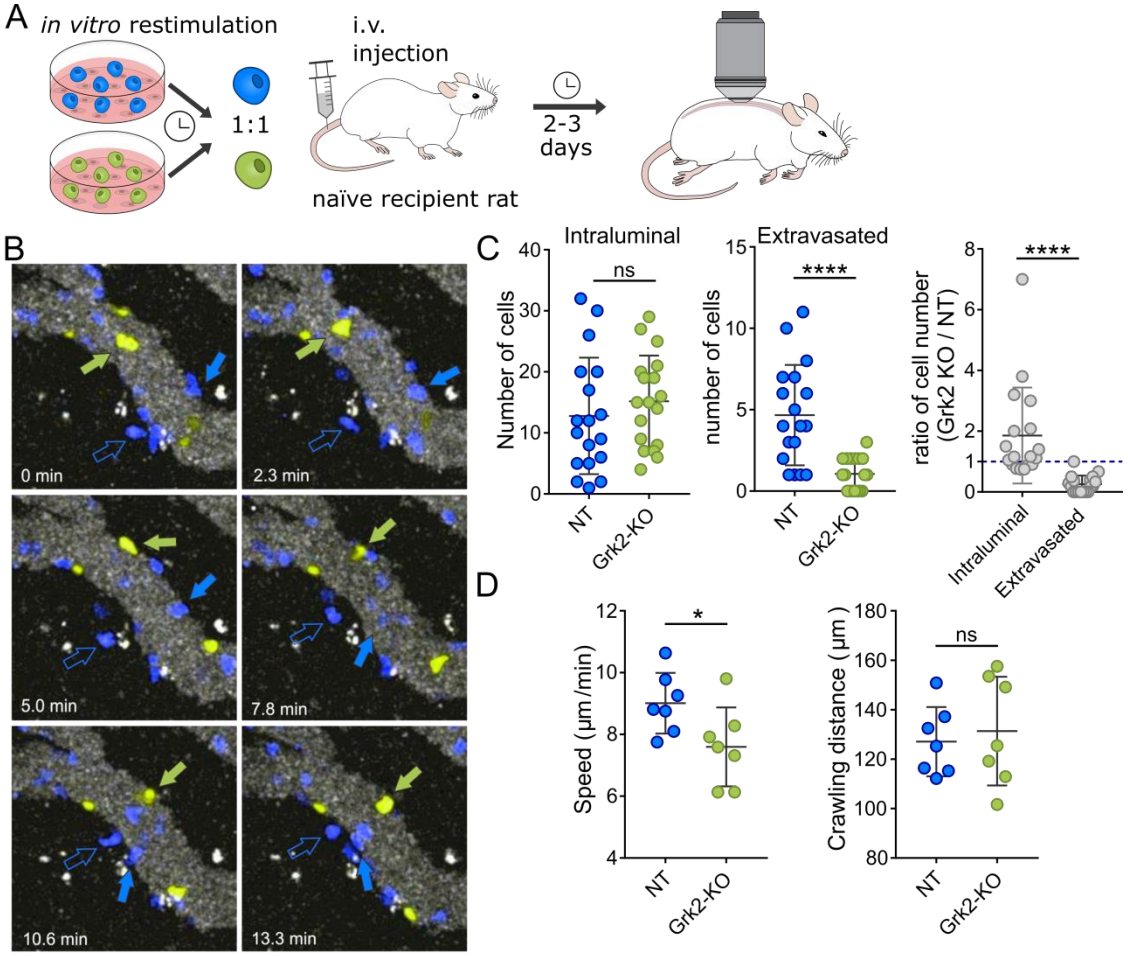

Figure 31 Leptomeningeal imaging following co-transfer of T_{MBP} Grk2-KO cells

A) Experimental design. T_{MBP} Grk2-KO and T_{MBP} NT cells were *in vitro* restimulated and were injected in a 1:1 mix into rats. After two to three days intravital 2-photon imaging was performed. **B)** Time-lapse images tracking T_{MBP} cells along the meningeal vasculature (white). Blue indicates BFP^+ T_{MBP} NT cells, green indicates $EGFP^+$ T_{MBP} Grk2-KO cells, filled arrows point to cells inside the blood vessel lumen, empty arrows point to extravasated cells. **C)** Absolute numbers of intraluminal or extravasted T_{MBP} cells in the leptomeningal vasculature and the ratio of KO/control cells derived from the previous two panels. n = 3 animals, 6-8 images per animal. Following Sharpiro-Wilk normality test either paired parametric t-test or Wilcoxon matched-pairs signed rank test was performed. Mean ± SD. **D)** Analysis of T cell movement parameters in the lumen of blood vessels: speed (left) and crawling distance (right). Data summarized per movie, n = 3 animals, 2-3 movies per animal, 15-76 cells per condition per movie. Following Sharpiro-Wilk normality test either paired parametric t-test was performed. Mean ± SD. Modified from (Kendirli et al., 2023).

4.5.2 Grk2 controls T_{MBP} cell attraction to the blood via S1PR1

The results of the intravital microscopy are reminiscent of those observed in a study that investigated the impact of Grk2-KO on the desensitization of the Sphingosine-1-phosphate receptor 1 (S1PR1) in T and B cells (Arnon et al., 2011). Signaling over the S1PR1 receptor by its ligand Sphingosine-1-phosphate (S1P) induces the T cells egress from lymphatic organs to the blood; later T cells exit the blood stream against the S1P gradient. To do so the S1PR1 receptor

must be internalized, which might be transacted by Grk2. Therefore, we hypothesised that this mechanism might also mediate the altered T cell trafficking into the CNS in our model. Since altered migration in the study was restored in S1P-deficient mice (Arnon et al., 2011), we established additional T_{MBP} S1PR1-KO and double deficient T_{MBP} Grk2-S1PR1-KO cells and tested those in our co-transfer setup (Figure 32 A). While the T_{MBP} Grk2-KO cells showed a drastic reduction in their capability to migrate from the blood into the meninges and parenchyma, this was not the case for T_{MBP} S1PR1-KO and T_{MBP} Grk2-S1PR1-KO cells. The T_{MBP} S1PR1-KO migrated in the same ratio as T_{MBP} NT cells from the blood to the CNS and the additional deletion of S1PR1 in Grk2 deficient T_{MBP} cells restored the trafficking deficits of the single knocked out Grk2 T_{MBP} cells (Figure 32 B). Interestingly, when we assessed the distribution of cells in the other organs, we observed a drastic accumulation of T_{MBP} cells that lacked S1PR1 in the spleen and the parathymic lymph nodes (Figure 32 C). This is particularly interesting since the opposite was observed in T_{MBP} Grk2-KO cells (Figure 29 C).

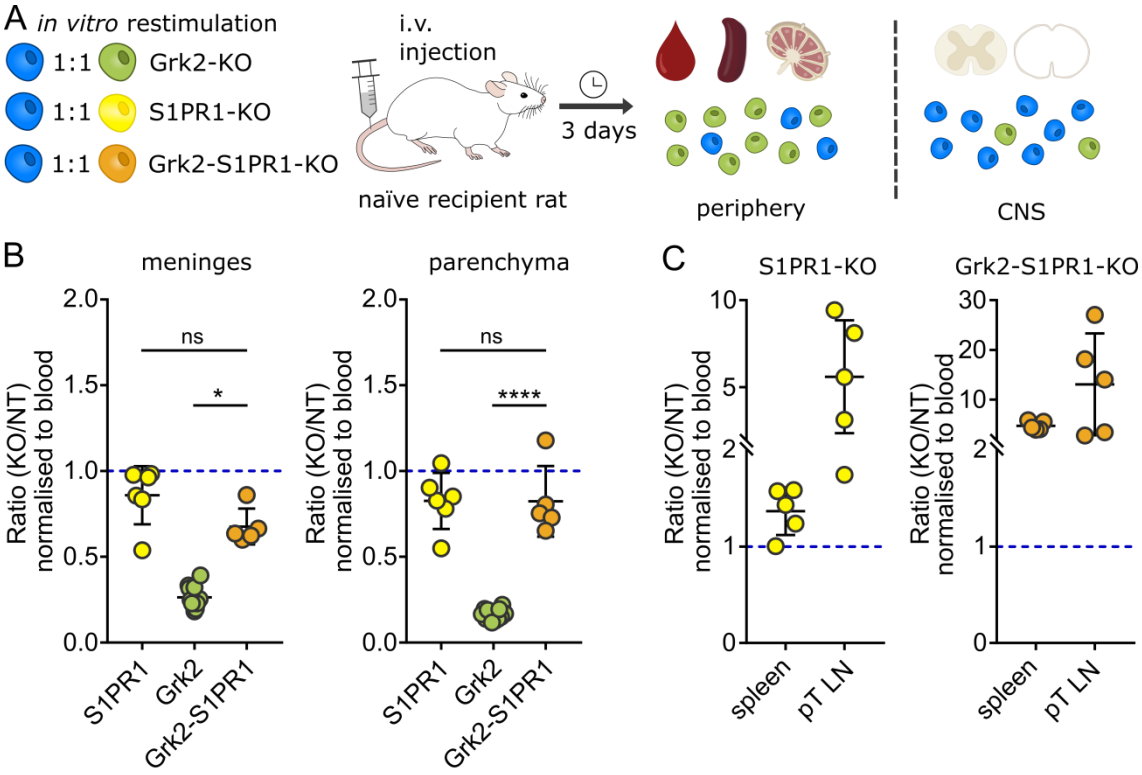

Figure 32 *In vivo* migration analysis following co-transfer of T_{MBP} Grk2-S1PR1-KO cells

A) Experimental design. T_{MBP} Grk2-S1PR1-KO and T_{MBP} NT cells were *in vitro* restimulated. After 48 h the fully restimulated T_{MBP} cells were mixed in a 1:1 ratio and injected into rats. With onset of disease on day three, rats were sacrificed and cells from peripheral organs (blood, spleen and pt LN) as well as CNS compartments (parenchyma, meninges) were collected. **B)** Migratory phenotype of KO cells compared to control, shown as the ratio of KO to control in meninges (left panel) or parenchyma (right panel) divided by the KO/control ratio in blood. n = 6 (S1PR1-KO), n = 12 (Grk2-KO) same data as in panel b; n = 5 (Grk2/S1PR1-KO). Following Sharpio Kruskal-Wallis test (Kruskal-Wallis = 17.01, P = 0.0002) with

Dunn's multiple comparison test for meninges, and ordinary one way ANOVA (F = 75.6, P < 0.0001) with Turkey's multiple comparison test for parenchyma. **C)** Migratory phenotype of T_{MBP} Grk2-S1PR1-KO cells compared to T_{MBP} NT cells in different organs, shown as the ratio of KO cell number/ NT cell number divided by the KO/NT ratio in blood. A ratio of 1 indicates the migration behaviour of control T_{MBP} cells, a ratio below 1 indicates impaired migration and a ratio above 1 enhanced migration towards an organ. One sample t-test against hypothetical mean = 1. Mean ± SD.

In addition, S1PR1 agonists are already used in the treatment of MS and achieve reduced lesion formation and disease progression (Brinkmann et al., 2010). It is assumed that the disrupted S1P signal transmission detains the cells from egressing into the blood stream but sequesters them in the lymphatic organs, which strongly resembles what we observed in our S1PR1-deficient T_{MBP} cells (Sanford, 2014).

Taken together, we propose an "egress module" that regulates T cell trafficking from the blood to the CNS by controlling the expression of S1PR1 on the surface of T cells. Previous studies have already established that the deletion of S1PR1 can disrupt this process; accordingly we observed an accumulation of S1PR1-deficient T_{MBP} cells in the spleen and the parathymic lymph nodes. However, our findings demonstrate that the Grk2/S1PR1-axis also plays a significant role in facilitating extravasation at the BBB and subsequent entry into the CNS. The KO of Grk2 likely results in an impaired internalization of S1PR1, preventing adequate desensitization of the receptors. Consequently, Grk2-deficient T cells continue to receive attractive signals from the CNS, compelling them to adhere and crawl along the vascular endothelium of the leptomeninges. Despite their interaction with the endothelium, these cells are unable to overcome their strong affinity to the high levels of S1P in the blood, preventing their transmigration into the CNS. These observations suggest that the Grk2 deficiency interferes with the proper regulation of S1PR1, resulting in a failure of T cells to complete the diapedesis process required for CNS entry. This highlights the importance of the Grk2/S1PR1-axis in orchestrating T cell migration across the BBB and its contribution to the overall trafficking of T cells from the blood to the CNS.

4.6 Validation of the ubiquitination module

4.6.1 Loss of Arih1 leads to accumulation of T_{MBP} cells in lymphatic organs

In our CRISPR/Cas9 screening, we identified genes that exhibited a strong effect size in only one of the two comparisons involving the CNS compartment and peripheral organs. Two candidate genes, namely Arih1 and Ube2l3, demonstrated a substantial fold change when comparing the spleen with the two CNS compartments, while their impact was only minimally reduced in the comparisons with the blood. Interestingly, these candidates also displayed

significant enrichment specifically in the comparison between the spleen and blood, further adding to their intriguing nature (Supplementary Figure 1). One of those specific candidates was Arih1, an E3 ubiquitin-protein ligase that catalyses the ubiquitination of target proteins. As in the previous modules we first checked whether any phenotypical changes can be already observed at *in vitro* stimulated cells (Figure 33 A). There was no difference between T_{MBP} Arih1-KO cells and T_{MBP} NT cells in production of the cytokines IFNγ an IL-17A in the unstimulated or stimulated condition (Figure 33 B, C). In addition, the expression of the surface markers that determine activation CD4, TCR, CD25 and CD134 was similar between KO and NT T cells (Figure 33 D, E). Also, among the labelled surface integrins α4-integrin (CD49d), β1-integrin (CD29), αL-integrin (CD11a), β2-integrin (CD18), and α2-integrin (CD49b) we observed comparable expression levels (Figure 33 D, E). Therefore, we concluded that T_{MBP} Arih1-KO cells have an unchanged activation and adhesion potential despite their KO.

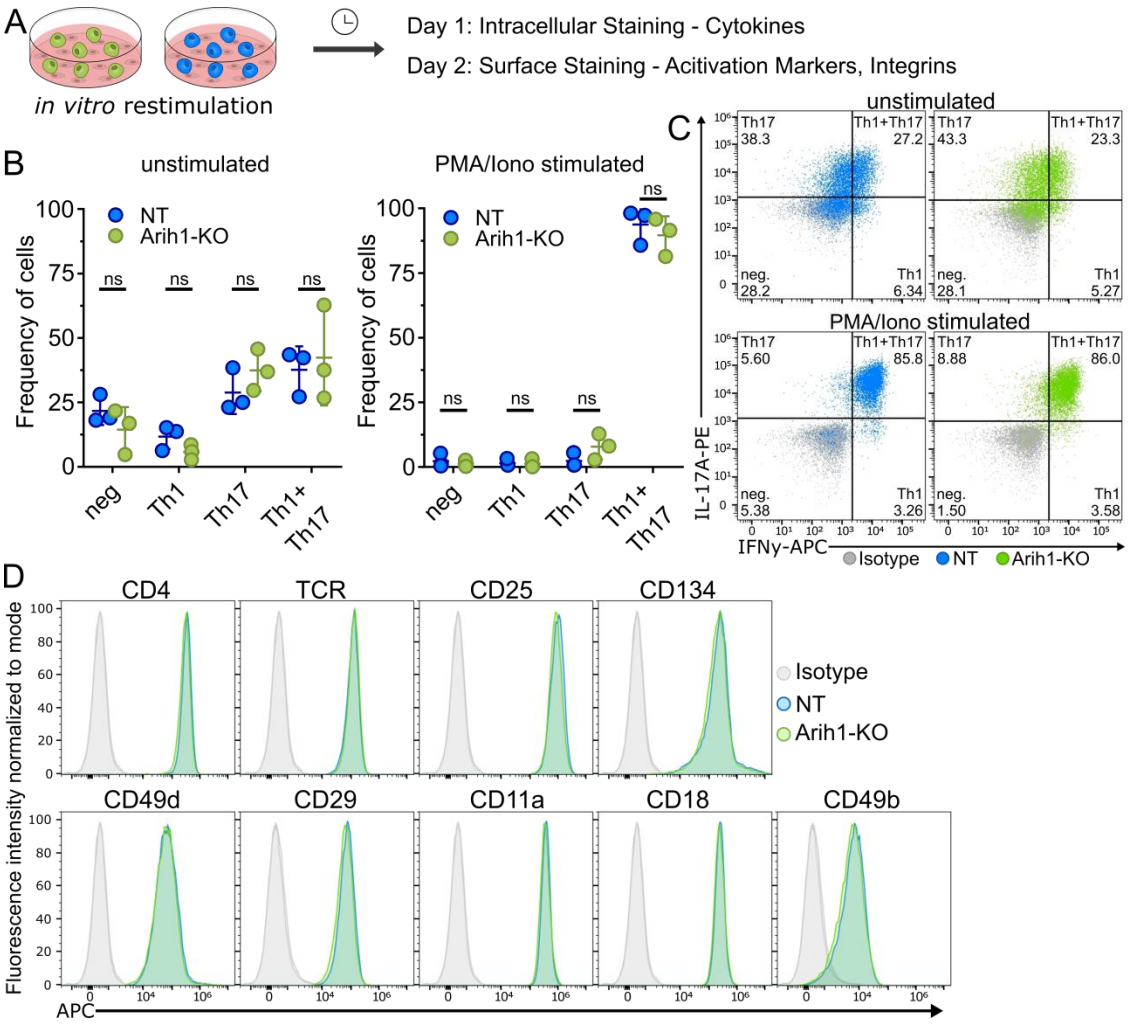

Figure continues on next page

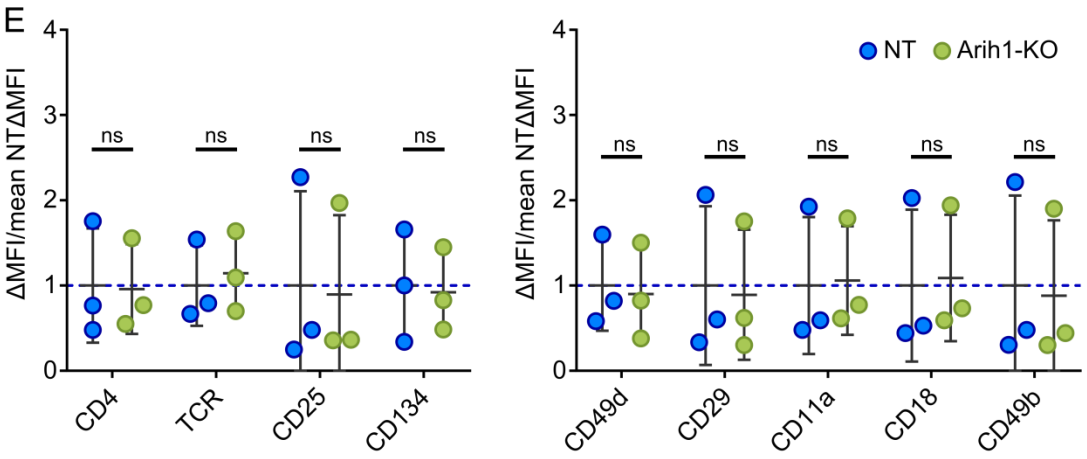

Figure 33 *In vitro* analysis of T_{MBP} Arih1-KO cells

A) Experimental design. T_{MBP} Arih1-KO and T_{MBP} NT cells were *in vitro* restimulated. After 24 h cells were stained for their produced cytokines and after 48 h activation markers or integrins were stained on the cell surface. **B)** Quantification of T cell subpopulation based on cytokine profile in flow cytometry analysis. Two-way ANOVA with multiple comparisons with the two-stage linear step-up procedure of Benjamini, Krieger and Yekuteli. Unstimulated: $F < 0.0001$, P = ns, n = 3; stimulated: $F < 0.0001$, P = ns, n = 3. Mean ± SD. **C)** Representative flow cytometry plots showing intracellular staining of IL-17A or IFNγ with or without stimulation and their classification into $IFN\gamma^+$ Th1 cells, $IL\text{-}17A^+$ Th17 and $IFN\gamma^+$ and $IL\text{-}17A^+$ Th1+Th17 cells. Cells were gated on lymphocytes > single cells > BFP^+ or GFP^+ > APC and PE values. **D)** Representative flow cytometry plots showing surface expression of various activation markers and integrins. Cells were gated on lymphocytes > single cells > BFP^+ or GFP^+. **E)** Quantification of the ΔMFI (MFI-MFI Isotype control) of the surface staining normalized to the mean ΔMFI of NT cells. MFI, two-way ANOVA with multiple comparisons with the two-stage linear step-up procedure of Benjamini, Krieger and Yekuteli. Activation markers: $F = 0.004791$, P = ns, all stainings: n = 3; integrins: $F = 0.01473$, P = ns, all stainings: n = 3. Mean ± SD.

To address their migration capacity *in vivo*, we co-transferred the T_{MBP} Arih1-KO cells together with T_{MBP} NT cells into rats and analysed the distribution of cells three days later (Figure 34 A). The flow cytometry analysis revealed reduced migration of the T_{MBP} Arih1-KO cells into all three compartments of the CNS (Figure 34 B). Interestingly, there was a substantial increase in the ratio of T_{MBP} Arih1-KO to T_{MBP} NT cells in the spleen and especially in the parathymic lymph nodes compared to the blood, suggesting that the T_{MBP} Arih1-KO cells exit the blood stream and remain in the secondary lymphatic organs (Figure 34 C). When we further stained the cells of the spleen for surface activation markers and integrins, we observed a significant difference in the expression of CD134, which was downregulated in T_{MBP} Arih1-KO cells, but not in the levels of CD25 (Figure 34 D, E). Among the integrins, the surface expression of both subunits of the VLA-4 receptor α4-integrin (CD49d) and β1-integrin (CD29) were significantly reduced, while the expression of components of the LFA-1 receptor αL-integrin (CD11a) and β2-integrin (CD18) remained similar between T_{MBP} Arih1-KO and T_{MBP} NT cells (Figure 34 D, E). As observed before neither of the T_{MBP} cells produced cytokines in the spleen (Figure 34 F, G).

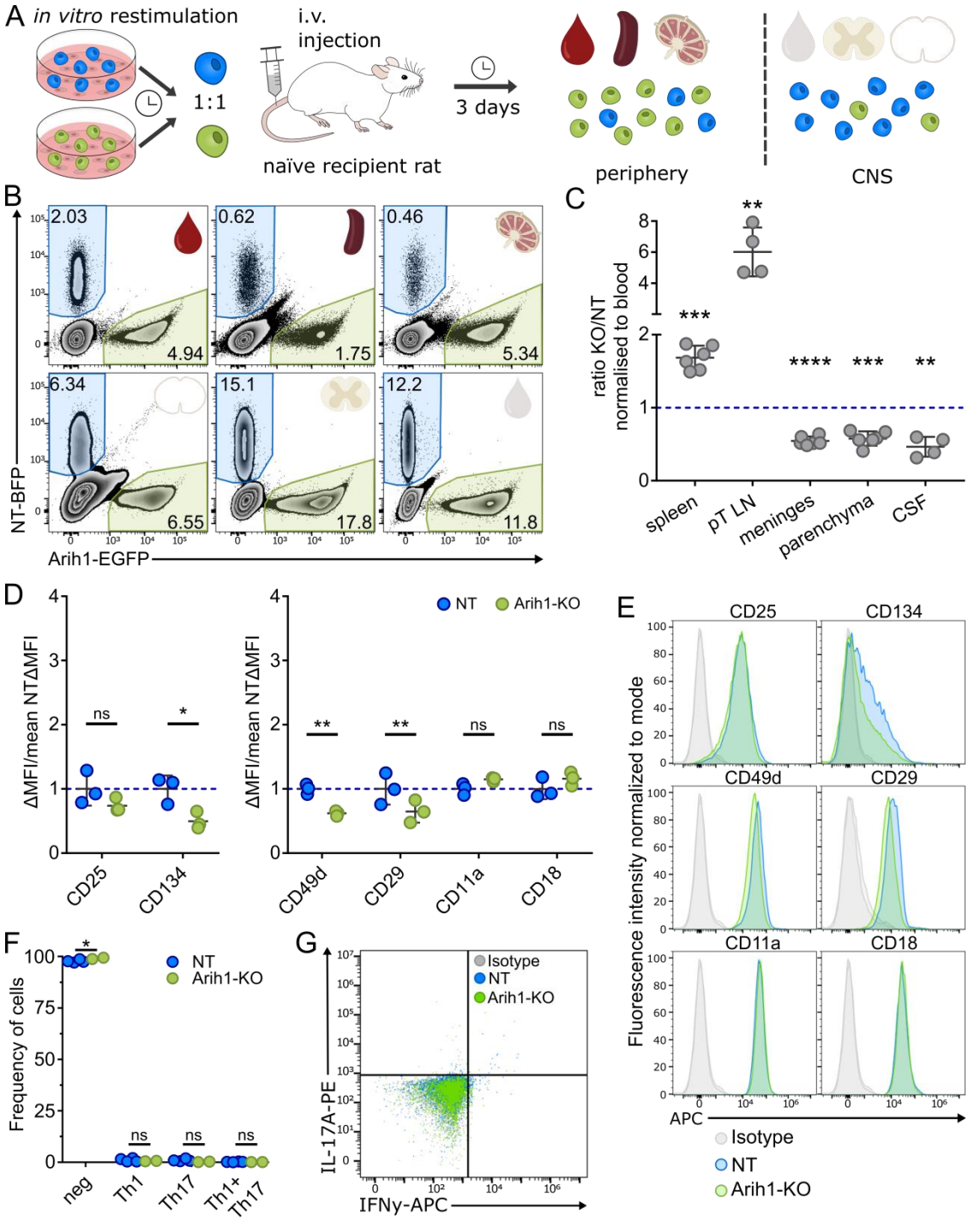

Figure 34 *In vivo* migration analysis following co-transfer of T_{MBP} Arih1-KO cells

A) Experimental design. T_{MBP} Arih1-KO and T_{MBP} NT cells were *in vitro* restimulated. After 48 h the fully restimulated T_{MBP} cells were mixed in a 1:1 ratio and injected into rats. With onset of disease on day three, rats were sacrificed and cells from peripheral organs (blood, spleen and pt LN) as well as CNS compartments (CSF, parenchyma, meninges) were collected. **B)** Representative flow cytometry plot with the distribution of T_{MBP} cells in different organs following co-transfer. BFP^+ T_{MBP} NT cells are highlighted in blue, $EGFP^+$ T_{MBP} Arih1-KO in green. Gated on lymphocytes > single cells > BFP^+ or GFP^+. **C)** Migratory phenotype of T_{MBP} Arih1-KO cells compared to T_{MBP} NT cells in different organs, shown as the ratio of KO cell number/ NT cell number divided by the KO/NT ratio in blood. A ratio of 1 indicates the migration behaviour of control T_{MBP} cells, a ratio below 1 indicates impaired migration and a ratio above 1

enhanced migration towards an organ. One sample t-test against hypothetical mean = 1. n = 6 (spleen, meninges parenchyma), n = 4 (pT LN, CSF). Mean ± SD. **D)** Quantification of the ΔMFI (MFI-MFI Isotype control) of the surface staining normalized to the mean ΔMFI of T_{MBP} NT cells. MFI, two-way ANOVA with multiple comparisons with the two-stage linear step-up procedure of Benjamini, Krieger and Yekuteli. Activation markers: F = 12.42, P = 0.0078, all stainings: n = 3; integrins: F = 3.755, P = 0.0705, all stainings: n = 3. Mean ± SD. **E)** Representative flow cytometry plots showing surface expression of activation markers and integrins of ex vivo splenic cells. Cells were gated on lymphocytes > single cells > BFP^+ or GFP^+. **F)** Quantification of T_{MBP} cell subpopulation based on the intracellular flow cytometry staining. Two-way ANOVA with multiple comparisons with the two-stage linear step-up procedure of Benjamini, Krieger and Yekuteli. F = 0.0002, P = ns, n = 4 (NT)/ n = 2 (Arih1-KO). Mean ± SD. **G)** Representative flow cytometry plots showing intracellular staining of IL-17A and IFNγ of *ex vivo* splenic T_{MBP} Arih1-KO and T_{MBP} NT cells.

Further we induced EAE in rats by i.v. injection of either T_{MBP} Arih1-KO or T_{MBP} NT cells (Figure 35 A). Compared to the typical disease course of the rats that received the NT cells, the rats that had received the T_{MBP} Arih1-KO cells showed a strongly ameliorated disease course with reduced clinical score and less body weight loss (Figure 35 B). Moreover, the incidence in the KO group was only around 25 % and first clinical signs appeared significantly later (Figure 35 C). Also, the peak score and the cumulate score were drastically reduced, suggesting that loss of Arih1 has a large effect on the capability of autoreactive T cells to migrate into the CNS and induce disease (Figure 35 C).

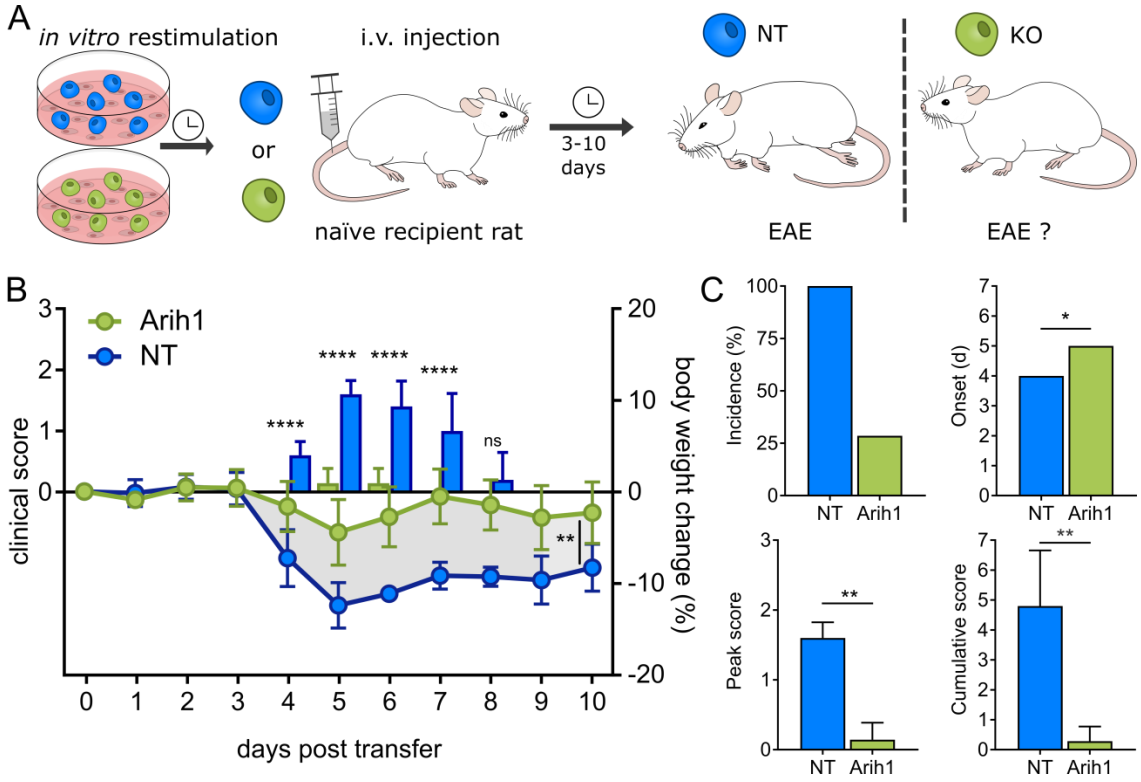

Figure 35 Clinical course induced by T_{MBP} Arih1-KO cells

A) Experimental design. T_{MBP} Arih1-KO and T_{MBP} NT cells were *in vitro* restimulated and were injected solely into rats. The EAE score and body weight was monitored daily. **B)** Clinical course of EAE measured

by percentage of body weight change (lines) and EAE scores (bars) of injected animals. Repeated measures two-way ANOVA; days 0-10 disease score: $F = 39.03$, $P < 0.0001$, body weight change: $F = 20.15$, $P = 0.0012$; n = 7 (Arih1-KO); n = 5 (NT). Mean ± SD. **C)** Overview of additional EAE parameters: incidence of EAE (%), average onset (days post transfer), average EAE peak score and average EAE cumulative score. Following Sharpiro-Wilk normality test, Mann-Whitney test was performed. Mean ± SD.

4.6.2 T_{MBP} cells lacking Ube2l3 migrate into the spleen but not the CNS

In addition to Arih1, our CRISPR/Cas9 screening also revealed Ube2l3 as a potential candidate in the comparison of spleen to the CNS compartments and additionally in the comparison of spleen to blood (Supplementary Figure 1). This is of particular interest, since Ube2l3 is a E2 ubiquitin-conjugating enzyme that was already described to interact with Arih1 to ubiquitinate proteins (Wenzel et al., 2011). Following the KO of Ube2l3 we first checked the cells for phenotypical changes *in vitro* (Figure 36 A). We observed a consistent pattern in the production of the cytokines IFNy and/or IL-17A in T_{MBP} Ube2l3-KO and T_{MBP} NT cells. This pattern remained evident both in the unstimulated condition and after the addition of PMA/Ionomycin to stimulate the cells (Figure 36 B, C). Furthermore, the surface staining of activation markers including CD4, TCR, CD25 and CD134 showed no difference between the two cell types (Figure 36 D, E). Also, the surface expression of the integrins α4-integrin (CD49d), β1-integrin (CD29), αL-integrin (CD11a), β2-integrin (CD18), and α2-integrin (CD49b) was similar between T_{MBP} Ube2l3-KO and T_{MBP} NT cells (Figure 36 D, E).

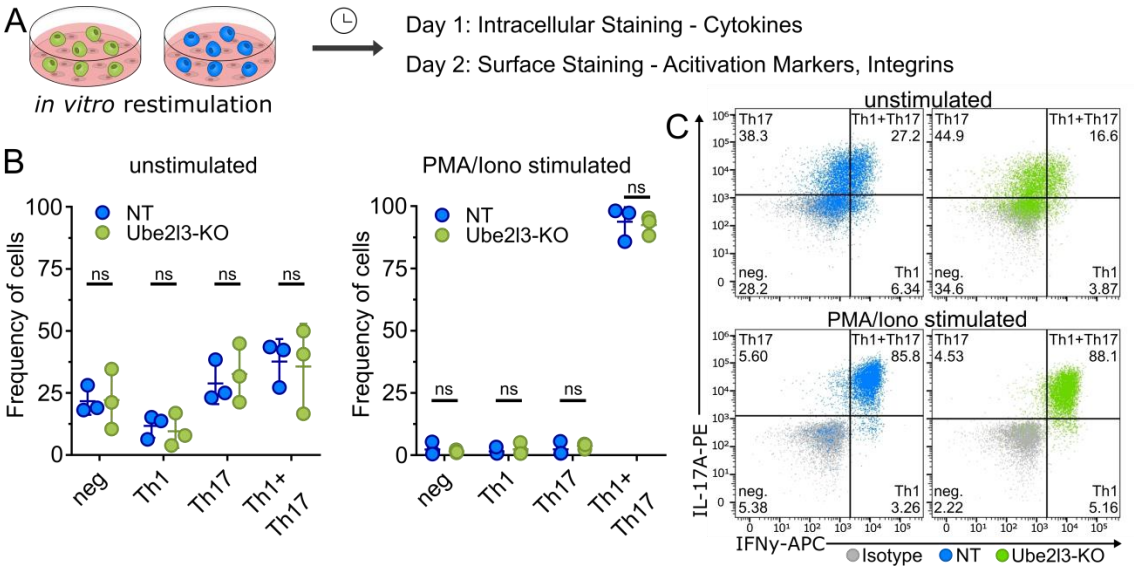

Figure continues on next page

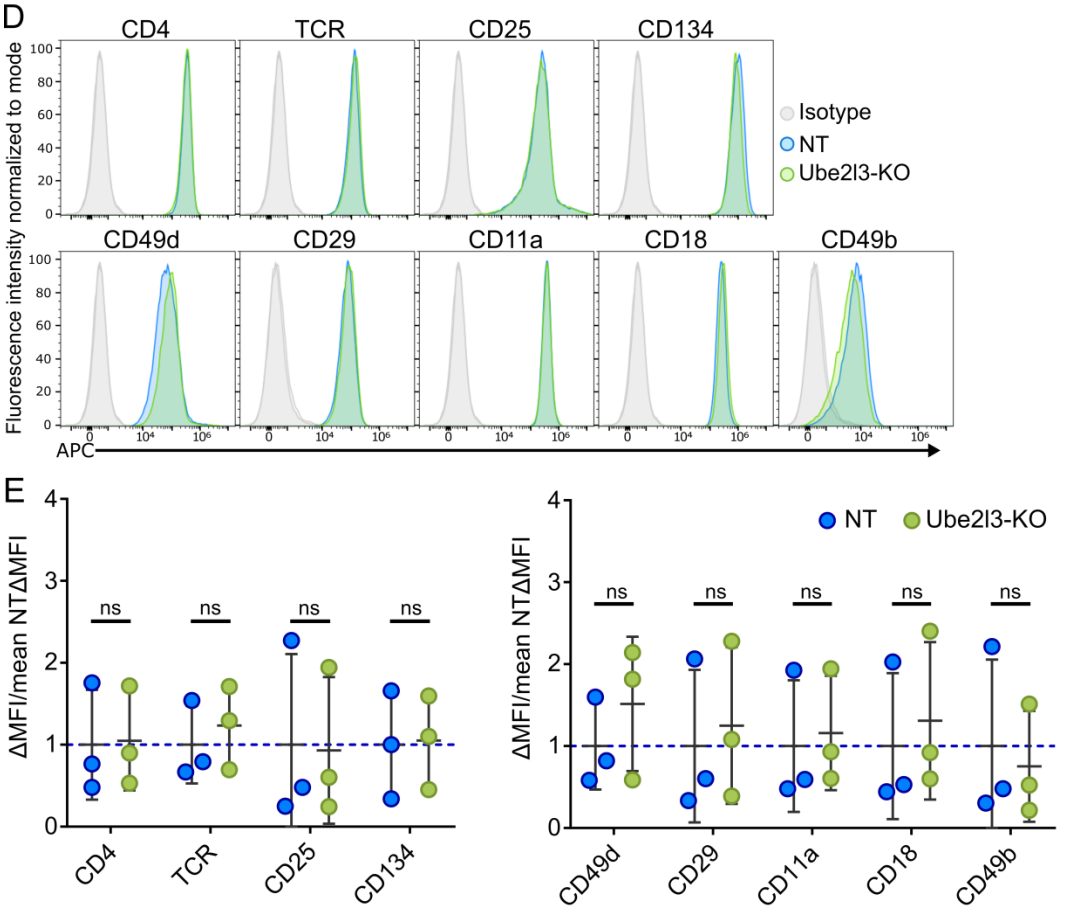

Figure 36 *In vitro* analysis of T_{MBP} Ube2l3-KO cells

A) Experimental design. T_{MBP} Ube2l3-KO and T_{MBP} NT cells were *in vitro* restimulated. After 24 h cells were stained for their produced cytokines and after 48 h activation markers or integrins were stained on the cell surface. **B)** Quantification of T cell subpopulation based on cytokine profile in flow cytometry analysis. Two-way ANOVA with multiple comparisons with the two-stage linear step-up procedure of Benjamini, Krieger and Yekuteli. Unstimulated: F < 0.0001, P = ns, n = 3; stimulated: F = 0.0001, P = ns, n = 3. Mean ± SD. **C)** Representative flow cytometry plots showing intracellular staining of IL-17A or IFNy with or without stimulation and their classification into $IFNy^+$ Th1 cells, $IL\text{-}17A^+$ Th17 and $IFNy^+$ and $IL\text{-}17A^+$ Th1+Th17 cells. Cells were gated on lymphocytes > single cells > BFP^+ or GFP^+ > APC and PE values. **D)** Representative flow cytometry plots showing surface expression of various activation markers and integrins. Cells were gated on lymphocytes > single cells > BFP^+ or GFP^+. **E)** Quantification of the ΔMFI (MFI-MFI Isotype control) of the surface staining normalized to the mean ΔMFI of NT cells. MFI, two-way ANOVA with multiple comparisons with the two-stage linear step-up procedure of Benjamini, Krieger and Yekuteli. Activation markers: F = 0.05086, P = ns, all stainings: n = 3; integrins: F = 0.4075, P = ns, all stainings: n = 3. Mean ± SD.

When we assessed the distribution of T_{MBP} cells in the peripheral and CNS tissues on day three, after the co-transferred of T_{MBP} Ube2l3-KO and T_{MBP} NT cells, the observed results resembled those of the T_{MBP} Arih1-KO cells (Figure 37 A-C). There was a moderate, yet clear reduction in the migration to meninges, parenchyma, and CSF while there was remarked increase in the migration of T_{MBP} Ube2l3-KO cells towards the spleen. Unfortunately, due to the instability of

distribution in the parathymic lymph nodes, conclusive observations could not be drawn. Nevertheless, these findings indicate a strong preference of T_{MBP} Ube2l3-KO cells to exit the bloodstream and accumulate in the spleen (Figure 37 C). Notably, upon staining the spleen cells to evaluate their surface activation and adhesion markers, intriguing variations were observed between T_{MBP} Ube2l3-KO and T_{MBP} NT cells, exhibiting striking similarities to the alterations observed in T_{MBP} Arih1-KO cells. While the levels of CD25 were comparable between the two groups, there was slight trend in T_{MBP} Ube2l3-KO to a reduction of CD134 (Figure 37 D, E). Moreover, the surface expression of the VLA-4 subdomains α4-integrin (CD49d) and β1-integrin (CD29) was mildly reduced in T_{MBP} Ube2l3-KO cells, while the same cells showed an modest increase in the expression of LFA-2 subdomains αL-integrin (CD11a) and β2-integrin (CD18) that potentially could be a compensatory mechanism, although this was not observed in the T_{MBP} Itga4-KO (Figure 9 D, E). As observed previously neither T_{MBP} Ube2l3-KO nor T_{MBP} NT cells showed a production of the cytokines IFNy and IL-17A in the spleen (Figure 37 F, G).

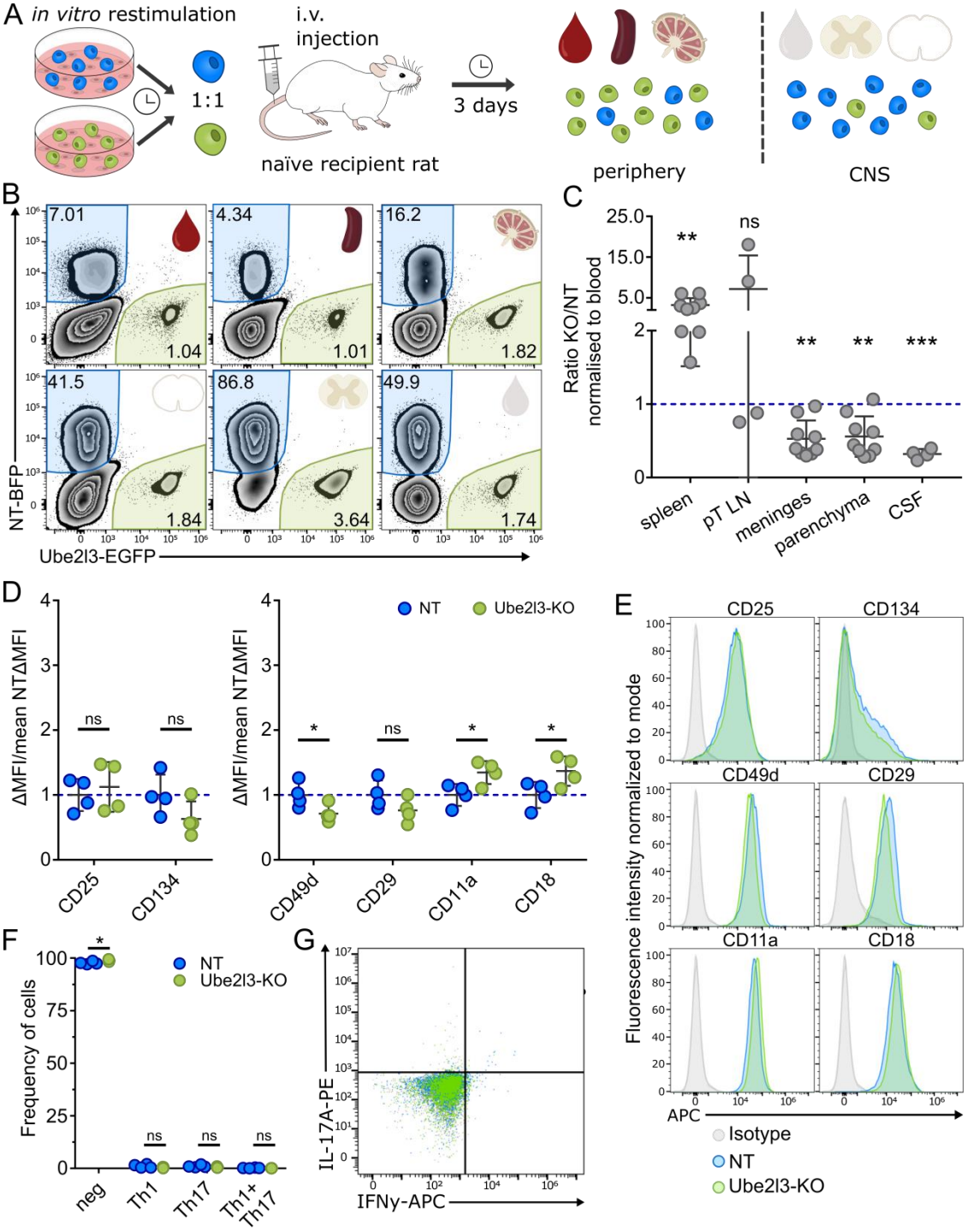

Figure 37 *In vivo* migration analysis following co-transfer of T_{MBP} Ube2l3-KO cells

A) Experimental design. T_{MBP} Ube2l3-KO and T_{MBP} NT cells were *in vitro* restimulated. After 48 h the fully restimulated T_{MBP} cells were mixed in a 1:1 ratio and injected into rats. With onset of disease on day three, rats were sacrificed and cells from peripheral organs (blood, spleen and pt LN) as well as CNS compartments (CSF, parenchyma, meninges) were collected. **B)** Representative flow cytometry plot with the distribution of T_{MBP} cells in different organs following co-transfer. BFP^+ T_{MBP} NT cells are highlighted in blue, $EGFP^+$ T_{MBP} Ube2l3-KO in green. Gated on lymphocytes > single cells > BFP^+ or GFP^+. **C)** Migratory phenotype of T_{MBP} Ube2l3-KO cells compared to T_{MBP} NT cells in different organs, shown as the ratio of KO cell number/ NT cell number divided by the KO/NT ratio in blood. A ratio of 1 indicates the migration

behaviour of control T_{MBP} cells, a ratio below 1 indicates impaired migration and a ratio above 1 enhanced migration towards an organ. One sample t-test against hypothetical mean = 1. n = 9 (spleen, meninges parenchyma), n = 4 (pT LN, CSF). Mean ± SD. **D)** Quantification of the ΔMFI (MFI-MFI Isotype control) of the surface staining normalized to the mean ΔMFI of T_{MBP} NT cells. MFI, two-way ANOVA with multiple comparisons with the two-stage linear step-up procedure of Benjamini, Krieger and Yekuteli. Activation markers: F = 0.6326, P = ns, all stainings: n = 4; integrins: F = 0.4966, P = ns, all stainings: n = 4. Mean ± SD. **E)** Representative flow cytometry plots showing surface expression of activation markers and integrins of ex vivo splenic cells. Cells were gated on lymphocytes > single cells > BFP^+ or GFP^+. **F)** Quantification of T_{MBP} cell subpopulation based on the intracellular flow cytometry staining. Two-way ANOVA with multiple comparisons with the two-stage linear step-up procedure of Benjamini, Krieger and Yekuteli. F = 0.0003, P = ns, n = 4 (NT)/ n = 3 (Ube2l3-KO). Mean ± SD. **G)** Representative flow cytometry plots showing intracellular staining of IL-17A and IFNγ of *ex vivo* splenic T_{MBP} Ube2l3-KO and T_{MBP} NT cells.

We adoptively transferred either T_{MBP} Ube2l3-KO or T_{MBP} NT cells into rats to induce EAE (Figure 38 A). In line with the previous results, we observed a milder disease course with reduced clinical score and body weight loss in the rats that received T_{MBP} Ube2l3-KO compared to those that obtained the control T_{MBP} NT cells (Figure 38 B). The incidence was drastically reduced, but there was no difference in the onset of clinical signs in rats that develop EAE (Figure 38 C). Furthermore, the peak score as well as the cumulative score was substantial reduced in rats that received T_{MBP} Ube2l3-KO cells (Figure 38 C).

Overall, the strong resemblance between the results of Arih1 KO and Ube2l3 KO together with their already described interaction argues that these two proteins operate in a coordinated ubiquitination module and that the target of the ubiquitination likely modulates the altered migration of the T_{MBP} cells. Our findings demonstrate that the deficiency of either of these genes causes T cells to depart from the blood stream and instead accumulate in secondary lymphatic organs. Consequently, this impedes their migration into the CNS. These findings highlight the importance of the Arih1-Ube2l3 ubiquitination module and their influence on the migratory behaviour of T_{MBP} cells.

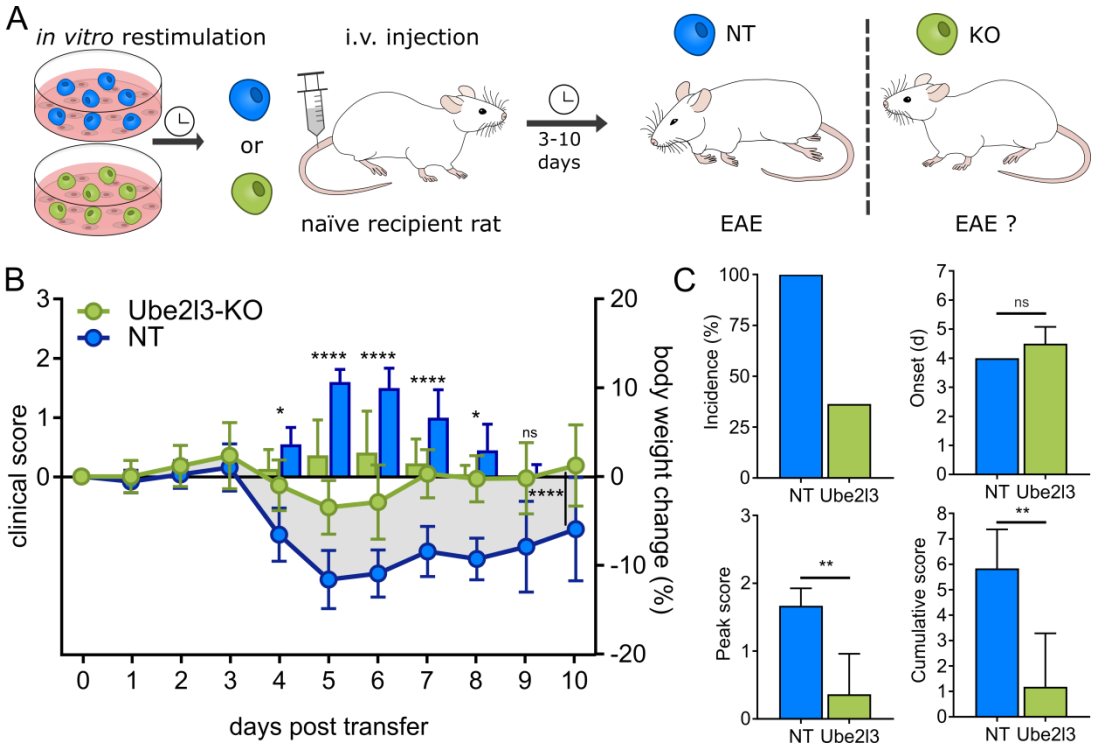

Figure 38 Clinical course induced by T_{MBP} Ube2l3-KO cells

A) Experimental design. T_{MBP} Ube2l3-KO and T_{MBP} NT cells were *in vitro* restimulated and were injected solely into rats. The EAE score and body weight was monitored daily. **B)** Clinical course of EAE measured by percentage of body weight change (lines) and EAE scores (bars) of injected animals. Repeated measures two-way ANOVA; days 0-10 disease score: $F = 4.948$, $P < 0.0001$, body weight change: $F = 8.042$, $P < 0.0001$; $n = 11$ (Ube2l3-KO); $n = 9$ (NT). Mean ± SD. **C)** Overview of additional EAE parameters: incidence of EAE (%), average onset (days post transfer), average EAE peak score and average EAE cumulative score. Following Sharpiro-Wilk normality test, Mann-Whitney test was performed. Mean ± SD.

4.7 KO of Ets1 enhances migration of T_{MBP} cells into the CNS

Our validation of candidate genes mainly focussed on genes whose loss limits the migration of T_{MBP} cells into the spinal cord meninges and parenchyma, since those might be drug-able targets in the treatment of CNS autoimmune disorders like MS. However, our CRISPR/Cas9 screening also detected negative regulators of T cell migration that - when knocked out - enhance the T_{MBP} cells trafficking into the CNS. Among those migration regulators, the transcription factor Ets1 was the top ranked candidate. As it is implicated in the differentiation, survival, and proliferation of lymphoid cells (Russell and Garrett-Sinha, 2010), we first tested T_{MBP} Ets1-KO *in vitro* to assess the effects of the gene KO on activation and cytokine production (Figure 39 A). However, we observed no difference in the capability of T_{MBP} Ets1-KO cells to produce IFNγ or IL-17A neither in their non-stimulated state nor following the stimulation with

PMA/Ionomycin compared to control T_{MBP} NT cells (Figure 39 B, C). Interestingly, we also observed no difference in the surface expression of activation markers. The labels of surface CD4, TCR, CD25 and CD134 were also similar to those of the T_{MBP} NT cells (Figure 39 D, E). Likewise, we observed comparable surface expression levels of the adhesion molecules, the components of the VLA-4 receptor α4-integrin (CD49d) and β1-integrin (CD29), the subdomains of the LFA-1 receptor αL-integrin (CD11a), β2-integrin (CD18), and α2-integrin (CD49b) were all similarly detected in T_{MBP} Ets1-KO cells and T_{MBP} NT cells (Figure 39 D, E). On a side note, we repeatedly observed reduced cell numbers of T_{MBP} Ets1-KO compared to all other T_{MBP} cells at the end of each restimulation cycle that correlated with the KO efficiency, likely due to increased cell death.

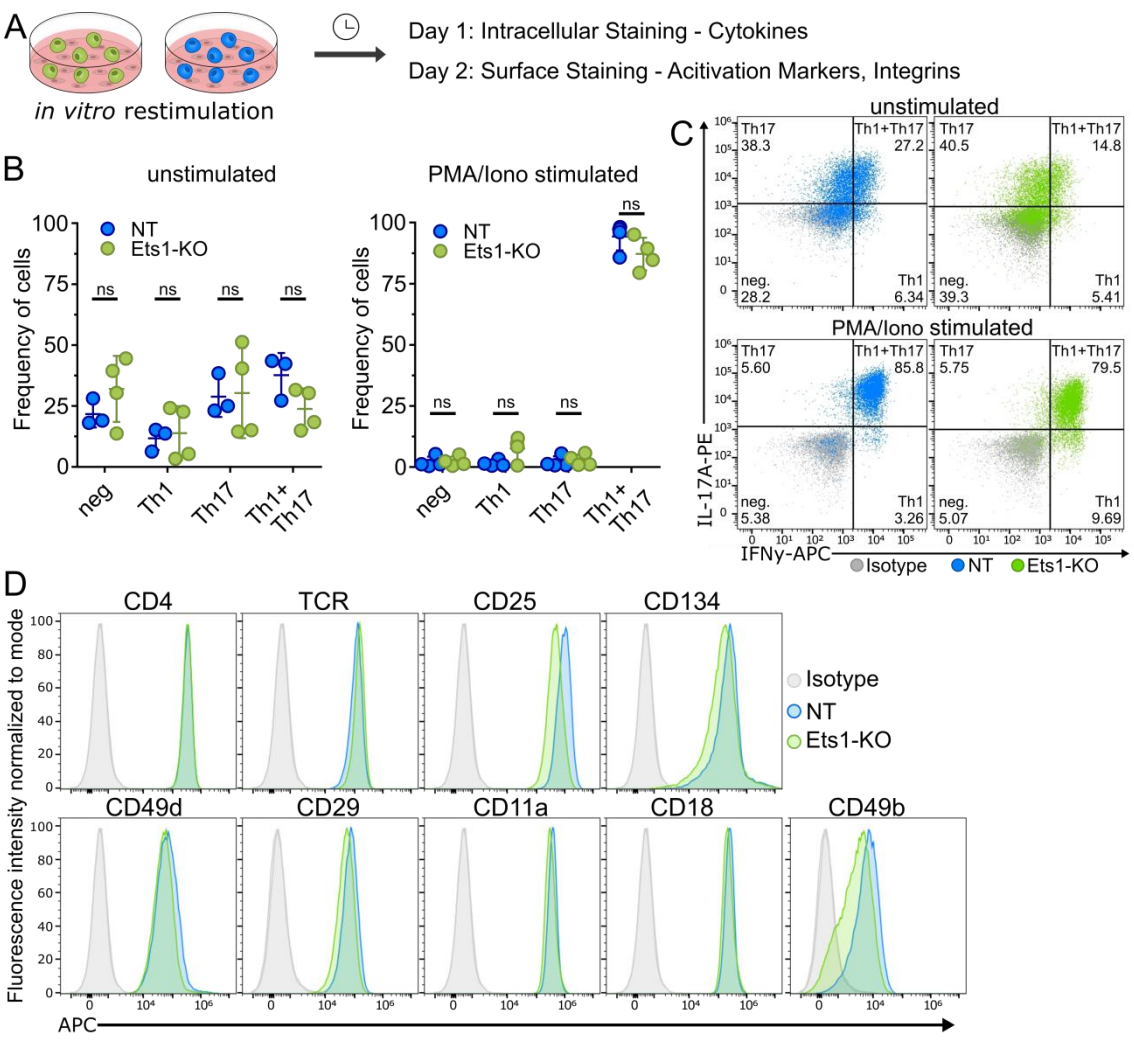

Figure continues on next page

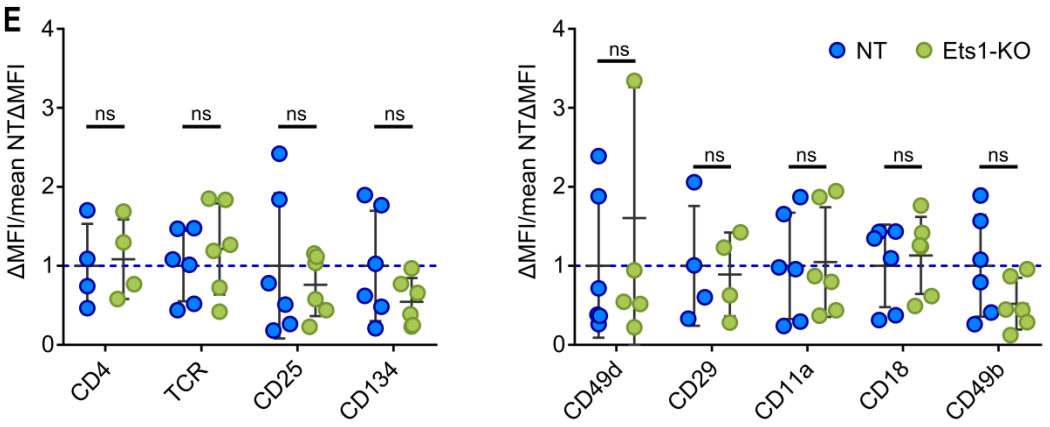

Figure 39 *In vitro* analysis of T_{MBP} Ets1-KO cells

A) Experimental design. T_{MBP} Ets1-KO and T_{MBP} NT cells were *in vitro* restimulated. After 24 h cells were stained for their produced cytokines and after 48 h activation markers or integrins were stained on the cell surface. **B)** Quantification of T cell subpopulation based on cytokine profile in flow cytometry analysis. Two-way ANOVA with multiple comparisons with the two-stage linear step-up procedure of Benjamini, Krieger and Yekuteli. Unstimulated: F < 0.0001, P = ns, n = 3 (NT)/n = 4 (Ets1-KO); stimulated: F < 0.0001, P = ns, n = 4. Mean ± SD. **C)** Representative flow cytometry plots showing intracellular staining of IL-17A or IFNy with or without stimulation and their classification into $IFNy^+$ Th1 cells, $IL\text{-}17A^+$ Th17 and $IFNy^+$ and $IL\text{-}17A^+$ Th1+Th17 cells. Cells were gated on lymphocytes > single cells > BFP^+ or GFP^+ > APC and PE values. **D)** Representative flow cytometry plots showing surface expression of various activation markers and integrins. Cells were gated on lymphocytes > single cells > BFP^+ or GFP^+. **E)** Quantification of the ΔMFI (MFI-MFI Isotype control) of the surface staining normalized to the mean ΔMFI of NT cells. MFI, two-way ANOVA with multiple comparisons with the two-stage linear step-up procedure of Benjamini, Krieger and Yekuteli. Activation markers: F = 0.3116, P = ns, CD4: n = 4, TCR/CD25/CD134: n = 6; integrins: F = 0.03323, P = ns, CD49d/CD11a/CD18/CD49b: n = 6, CD29: n = 4. Mean ± SD.

As with previous KOs we co-transferred the T_{MBP} Ets1-KO together with T_{MBP} NT into rats and examined the distribution of cells in the different organs on the day of disease onset (Figure 40 A, B). We observed a significant increase in the ratio of KO to control cells in all the CNS organs and especially in meninges and parenchyma (Figure 40 C). While the ratio in the parathymic lymph nodes decreased significantly, there was no difference in the T cell trafficking between Ets1-KO and NT cells in the spleen. This confirms that our CRISPR/Cas9 screening is also sufficient to detect genes that likely inhibit T cell trafficking when present, but if lost facilitate the migration of autoreactive T cells into the CNS. The additional staining of splenic cells revealed some changes in the expression of surface markers. While the activation marker CD25 and was slightly but significantly downregulated on T_{MBP} Ets1-KO cells, there was no change in the expression of CD134 between Ets1-KO and NT T_{MBP} cells (Figure 40 D, E). Among the surface integrins the expression of the VLA-4 subdomains α4-integrin (CD49d) and β1-integrin (CD29) was reduced in T_{MBP} Ets1-KO cells, while the same cells showed an increase in the expression of LFA-1 subdomains αL-integrin (CD11a) and β2-integrin (CD18) compared to

T_{MBP} NT cells (Figure 40 D, E). The additional staining of cytokines in T_{MBP} cells of the spleen showed again no difference in the overall very low production of IFNy and IL-17A (Figure 40 F, G).

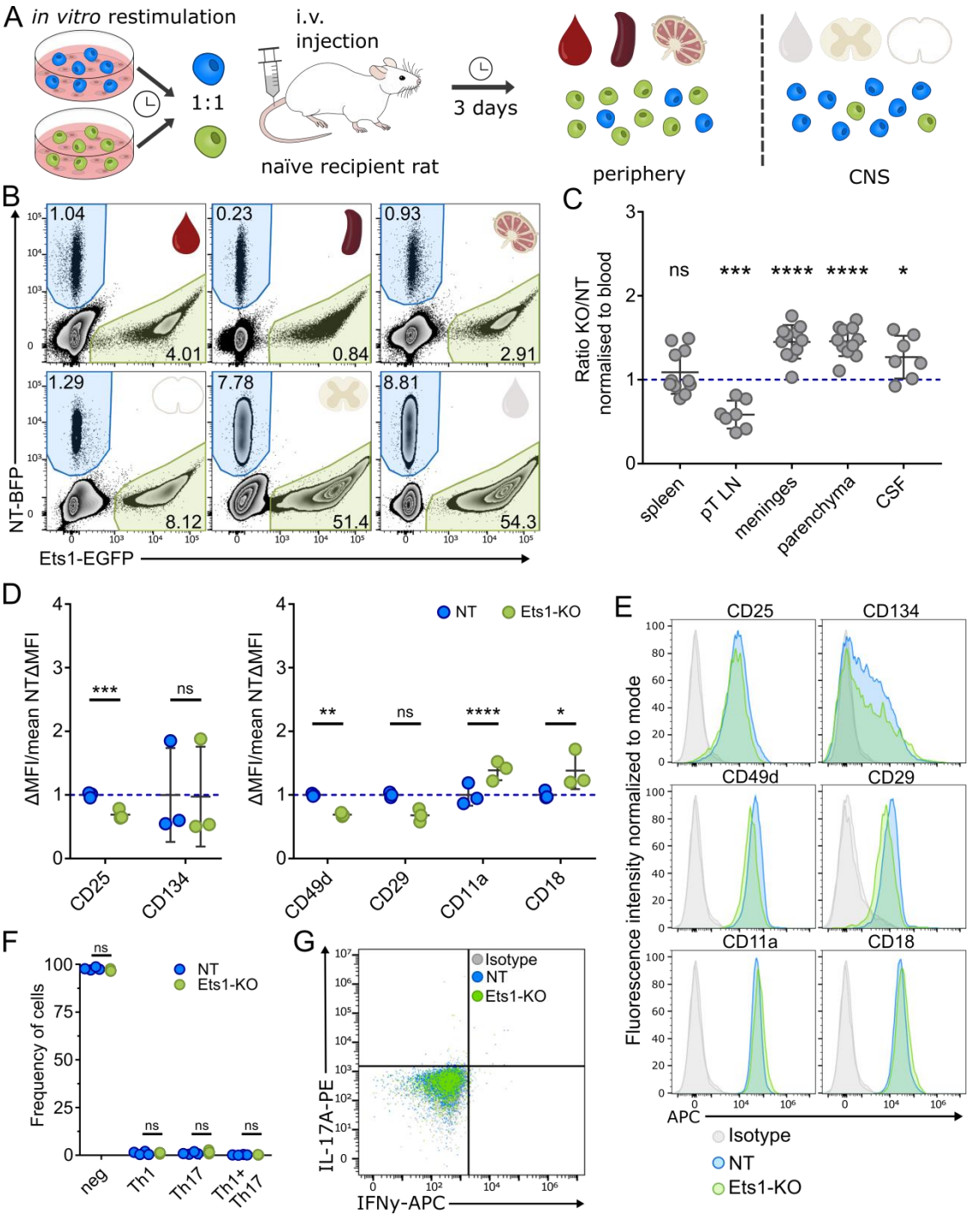

Figure 40 *In vivo* migration analysis following co-transfer of T_{MBP} Ets1-KO cells

A) Experimental design. T_{MBP} Ets1-KO and T_{MBP} NT cells were *in vitro* restimulated. After 48 h the fully restimulated T_{MBP} cells were mixed in a 1:1 ratio and injected into rats. With onset of disease on day three, rats were sacrificed and cells from peripheral organs (blood, spleen and pt LN) as well as CNS compartments (CSF, parenchyma, meninges) were collected. **B)** Representative flow cytometry plot with

the distribution of T_{MBP} cells in different organs following co-transfer. BFP^+ T_{MBP} NT cells are highlighted in blue, $EGFP^+$ T_{MBP} Ets1-KO in green. Gated on lymphocytes > single cells > BFP^+ or GFP^+. **C)** Migratory phenotype of T_{MBP} Ets1-KO cells compared to T_{MBP} NT cells in different organs, shown as the ratio of KO cell number/ NT cell number divided by the KO/NT ratio in blood. A ratio of 1 indicates the migration behaviour of control T_{MBP} cells, a ratio below 1 indicates impaired migration and a ratio above 1 enhanced migration towards an organ. One sample t-test against hypothetical mean = 1. n = 11 (spleen, meninges parenchyma), n = 7 (pT LN, CSF). Mean ± SD. **D)** Quantification of the ΔMFI (MFI-MFI Isotype control) of the surface staining normalized to the mean ΔMFI of T_{MBP} NT cells. MFI, two-way ANOVA with multiple comparisons with the two-stage linear step-up procedure of Benjamini, Krieger and Yekuteli. Activation markers: F = 16, P = 0.0039, all stainings: n = 3; integrins: F = 3.871, P = ns, all stainings: n = 3. Mean ± SD. **E)** Representative flow cytometry plots showing surface expression of activation markers and integrins of ex vivo splenic cells. Cells were gated on lymphocytes > single cells > BFP^+ or GFP^+. **F)** Quantification of T_{MBP} cell subpopulation based on the intracellular flow cytometry staining. Two-way ANOVA with multiple comparisons with the two-stage linear step-up procedure of Benjamini, Krieger and Yekuteli. F = 0.0005, P = ns, n = 4 (NT)/ n = 3 (Ets1-KO). Mean ± SD. **G)** Representative flow cytometry plots showing intracellular staining of IL-17A and IFNγ of *ex vivo* splenic T_{MBP} Ets1-KO and T_{MBP} NT cells.

5 DISCUSSION

5.1 Opportunities and constraints of the CRISPR/Cas9 screening

The infiltration of autoreactive $CD4^+$ T cells from the peripheral organs into the CNS is the initial critical step in the formation of MS lesions. In this context, the migration of T cells across the BBB is a complex and tightly regulated process that involves a series of molecular interactions between T cells and blood vessel endothelial cells (Engelhardt and Ransohoff, 2012). CRISPR/Cas9 screenings are a powerful technique that allows for rapid and efficient identification of genes that play critical roles in various biological processes by disrupting their function (Hsu et al., 2015). To identify the key molecules that regulate T cell migration into the CNS, we conducted a genome-wide CRISPR/Cas9 screening *in vivo*, taking advantage of the benefits of studying gene function in the complex environment of a living organism and on the onset of disease (Kendirli et al., 2023). We first initiated an unbiased whole-genome screening with lenient criteria to ensure that we identified all potential genes that could affect CNS migration (Figure 5). Next, we subjected those genes to a more rigorous validation screening to narrow it down to the genes that were "essential regulators" of CNS migration (Figure 6).

Although our CRISPR/Cas9 screening is a valuable tool for identifying potential regulators of T cell migration *in vivo*, it has its limitations. It is important to note that the screening may not been able to capture the full dynamic of gene regulation and interactions over time, since the screening is performed at a single time point and the CNS microenvironment may affect T cell migration and alter the function of certain molecules. Moreover, CRISPR/Cas9 screenings, like all CRISPR/Cas9 experiments, are affected by off-target effects, which can make it difficult to distinguish between on-target and off-target effects that can potentially result in inaccurate results (Ran et al., 2013). In addition, CRISPR/Cas9 screenings are unable to detect functionally important but molecularly redundant regulatory mechanisms, so they were likely not identified by the screening approach used in our study. Another limitation is the possibility of missing molecules that only regulate the trafficking of a smaller subset of the studied cell population, since all samples were analysed in a bulk. However, those restrictions are inherent to the technology and unavoidable to some extent. To address the limitation of false negative results due to inefficient CRISPR editing, we utilized multiple sgRNAs per gene, which helped to reduce the probability of missing essential regulators of CNS migration. Nevertheless, variations in the fold change could arise from the intrinsic variation of the sgRNA efficiency, and as such, further confirmation of the KO efficiency is necessary to determine the relative importance of the hits identified in our screening (Bock et al., 2022). Finally, false positive results may arise if a gene regulates a functional property such as T cell activation that is

required for subsequent CNS migration, but does not have a direct influence on migration. To address this issue, we performed additional analyses to assess potential effects on T cell adhesion, activation, and differentiation for candidate genes. In order to investigate potential effects on T cell adhesion and activation, we conducted a thorough analysis of adhesion molecules such as the α4-integrin and the β1-integrin, which together form the VLA-4 heterodimer, as well as components of the LFA-1 receptor αL-integrin and β2-integrin, and the α2-integrin. Additionally, we studied the expression of activation-dependent molecules like CD25 and CD134 in both T_{MBP} cells cultured *in vitro* and those isolated from the spleen. Since T_{MBP} cells in general downregulate activation markers in the spleen to acquire their migratory phenotype, the minor differences in the activation profile observed in some of the candidate genes are negligibly (Flügel et al., 2001). To assess potential effects on the differentiation of T cell subsets we studied the expression of the hallmark cytokines IFNγ and IL-17A. We found that overall no substantial alterations in the expression of adhesion, activation, or differentiation molecules were observed in T cells deficient for any of the essential regulators we studied; if it was not directly linked to the gene KO itself. Therefore, our results suggest that the essential regulators we identified were not false positives due to their involvement in T cell activation processes, but that they are likely to play a role in the regulation of T cell migration.

Our study has revealed several important insights into the molecular mechanisms underlying T cell migration into the CNS. Firstly, it was found that only a small number of molecules are essential for this process, and that these molecules naturally cluster into four functional modules (Kendirli et al., 2023). The first module centers around the adhesion molecule α4-integrin (Itga4), which has previously been implicated in T cell migration (Yednock et al., 1992). The second module involves the chemokine receptor Cxcr3, which is known to be important for T cell migration in general (Groom and Luster, 2011). The third module involves the Grk2-S1PR1 axis, which is involved in regulating T cell trafficking. While the role of S1PR1 in T cell egress from lymph nodes to the blood is already well-established (Schwab and Cyster, 2007), we have also demonstrated its significance in the trafficking of T cells from the blood to the CNS. The fourth module is focused on the ubiquitination by Arih1 and Ube2l3 via a yet unknown mechanism. The central functional hubs identified in our genome-wide screen, namely blocking α4-integrin and interfering with the S1PR1 receptor, align with two major clinical strategies employed to limit CNS infiltration of T cells in MS patients. These findings suggest that our screening has identified important targets with potential therapeutic implications. While some of the molecules identified in our analysis have been previously implicated in T cell migration, our study is the first to provide an unbiased analysis of all non-

redundant targets among transcriptional regulators, chaperones, binding partners, and intracellular signaling pathways (Kendirli et al., 2023). These findings represent a significant advancement in this research area, as to our knowledge, there has been no previous study in the literature that has investigated T cell trafficking in an *in vivo* environment at a genome-wide scale in EAE.

5.2 Adhesion molecules and their importance in T cell migration

The extravasation of T cells involves a series of steps, including initial tethering and rolling of T cells on the endothelium, firm adhesion, crawling, and transmigration across the endothelial barrier. These steps are mediated by a variety of adhesion molecules, chemokines, and signaling pathways that are tightly regulated (Engelhardt and Ransohoff, 2012). This includes P-selectin glycoprotein ligand-1 (PSGL-1), which facilitates the initial rolling of T cells in brain vessels through its interaction with endothelial ligands E- and P-selectin during EAE, but is not essential for the successful entry of T cells into the CNS and initiation of EAE (Sathiyanadan et al., 2014). Also, our CRISPR/Cas9 screening did not identify PSGL-1 as crucial regulator, suggesting that other mechanisms like integrin-mediated adhesion and crawling may compensate for the tethering and rolling steps, making the interaction of P/E selectins dispensable for T cell transmigration. Integrins are a family of cell surface adhesion receptors that play a crucial role in cell migration and adhesion, including T cell migration into the CNS during EAE (Rossi et al., 2011). They are composed of α and β subunits and exist in various combinations, with each combination having a unique ligand specificity and signaling properties (Anderson et al., 2014). Itga4, a α4-integrin molecule in the VLA-4 complex, plays a crucial role in T cell migration during EAE (Yednock et al., 1992). It is required for encephalitogenic T cell adhesion to its endothelial ligand VCAM-1, which is expressed on the surface of endothelial cells in the CNS vasculature. VCAM-1 is upregulated in the CNS during EAE, and its interaction with VLA-4 on T cells is a critical step in T cell migration across the BBB (Steffen et al., 1994). Our CRISPR/Cas9 screening identified *Itgα4* as a top hit, and subsequent validation experiments confirmed its efficacy in preventing T cell migration into the CNS and their subsequent inability to induce EAE (Figure 9, Figure 10). This finding aligns with the efficacy of Natalizumab, an FDA-approved drug that targets VLA-4 to prevent T cell infiltration into the CNS, and has been demonstrated to decrease disease activity in MS patients (Polman et al., 2006). Despite its success, Natalizumab has been linked to serious side effects such as progressive multifocal leukoencephalopathy (PML), an opportunistic brain infection that can be fatal (Cortese et al., 2021). Therefore, it is crucial to develop alternative therapies that

specifically target the migration of autoreactive T cells while preserving the CNS immunosurveillance function.

During CRISPR/Cas9 screening, the *Itgb1* gene encoding for β1-integrin, which is the other subunit of VLA-4, showed a relatively minor fold change (Figure 6). However, in validation experiments where a 100 % knockout was achieved through sorting, a significant reduction in T cell migration into the CNS was observed (Figure 15). It is worth noting that α4-integrin surface expression was not affected, most likely due to the replacement of β1-integrin by other β integrins such as β7-integrin, which can interact with Mucosal vascular addressin cell adhesion molecule 1 (MAdCAM-1) to mediate adhesion (Ley et al., 2007, Lin et al., 2019). However, although binding to other β integrins may result in a normal level of α4-integrin surface expression, their interaction seems to be inferior compared to the VLA-4 receptor, which would explain the observed decrease in the numbers of Itgb1-deficient T cells in the CNS. Interestingly, while the surface staining of Itgb1-deficient T cells revealed no alteration in the surface expression of its VLA-4 partner α4-integrin, we observed a marked reduction in α2-integrin (Itga2) expression. The α2-integrin exclusively forms heterodimers with β1-integrin, generating the α2β1 receptor (VLA-2) that acts as a receptor for collagen and laminin (Emsley et al., 2000). In contrast, β1-integrin can form a heterodimer with at least 12 different α subunits (Adorno-Cruz and Liu, 2019). In a study conducted on SJL/J mice immunized with PLP peptide to induce EAE, the administration of VLA-2 antibody during the induction phase did not affect disease onset, clinical scores, and weight loss when compared to control-treated mice. However, in the same study treatment with VLA-2 antibody immediately after disease onset led to a significant reduction in clinical signs and CNS inflammation of EAE (Tsunoda et al., 2007). This indicates that VLA-2 is not essential in the initial phase of T cell migration to the CNS, although it is important to note that this study was conducted in an active EAE model targeting a different peptide. Nonetheless, since the *Itgα2* gene was not identified as a crucial factor in our CRISPR/Cas9 screen, it suggests that VLA-2 also plays a non-essential role in T cell migration in our aT-EAE model. Also previous unpublished data from our lab showed that injection of anti-α2-integrin antibodies has no protective effect on aT-EAE. The reason for this could be that the loss of VLA-2 can be easily compensated by other integrin receptors like VLA-4, which is the preferred receptor for T cell trafficking. Overall, our study has demonstrated that the presences of the VLA-4 components are critical for T cell transmigration into the CNS. Although α4-integrin and β1-integrin are both necessary to form the VLA-4 receptor, our results suggest that the loss of α4-integrin has a more pronounced effect on T cell migration than the loss of β1-integrin. Likely compensatory mechanisms involving other integrins partially account for the observed effects of β1-integrin KO (DeNucci et al., 2010). It is

noteworthy that our CRISPR/Cas9 screening did not identify any other integrins that exhibited a migration deficient phenotype.

Integrin activation is regulated by various mechanisms, including changes in the conformation of integrin molecules, the binding of intracellular and extracellular ligands, and the activity of intracellular signaling pathways. The process of integrin activation involves a switch from a low-affinity to a high-affinity state, which is necessary for the interaction of integrins with their ligands on the extracellular matrix or cell surface (Calderwood, 2004). One key mechanism of integrin activation is the binding of intracellular proteins, such as kindlins and talins, to the cytoplasmic tails of integrin molecules. These proteins induce conformational changes in integrins that promote their activation and binding to extracellular ligands (Chen et al., 2019). During our CRISPR/Cas9 screening, we identified *Fermt3* (Kindlin-3) and *Tln1* (Talin-1) as intracellular proteins that are involved in T cell migration (Figure 6). Specifically, *Tln1* was identified as a candidate with a milder fold change compared to *Fermt3*, suggesting that it has a less pronounced effect on T cell migration. However, it should be noted that the variations in the fold change observed could arise from the intrinsic variation of sgRNA efficiency, which may lead to false interpretations. Thus, it is crucial to further confirm the KO efficiency to determine the relative importance of *Tln1* and *Fermt3* in integrin activation and CNS transmigration. A study has shown that Kindlin-3 plays a regulatory role in VLA-4 and LFA-1 mediated T cell arrest and adhesion, consistent with our own findings (Moretti et al., 2013). The study also found that T cells lacking Kindlin-3 were unable to induce adoptive transfer EAE, but were still able to induce active EAE effectively. This inconsistency may be attributed to variations in the levels of integrin ligands expressed on endothelial cells during EAE induction.

Moreover, a study has reported that fever enhances T cell trafficking through the activation and signaling of α4-integrin induced by two isoforms of heat shock protein 90 Hsp90aa1 and Hsp90ab1 (Lin et al., 2019). Although *Hsp90aa1* or *Hsp90ab1* were not identified as essential in our CRISPR/Cas9 screening, we observed a migration-deficient phenotype in T cells lacking the Hsp90 paralogue *Hsp90b1*. The master chaperone Hsp90b1, which resides in the endoplasmic reticulum, was among the top essential candidates in our CRISPR/Cas9 screening. It has been postulated that Hsp90b1 is essential for chaperoning the majority of α-subunits and β-subunits of integrins, thereby being critical for the cell surface expression of 14 of 17 integrin pairs in hematopoietic cells of mice (Staron et al., 2010). Notably, the *in vitro* surface staining of integrins in T_{MBP} Hsp90b1-KO cells revealed a significant reduction only in the expression of α4-integrin, whereas the expression levels of β1-integrin and LFA-1 components αL-integrin and β2-integrin as well as α2-integrin showed a noticeable decrease, but the difference was not statistically significant (Figure 11). In contrast, the results obtained from *ex vivo* cells

isolated from the spleen indicated a lowered surface expression of all tested integrins in the Hsp90b1 deficient group, which could be attributed to the reorganization of integrins once T cells acquire a migratory phenotype (Figure 12). In summary, the presence of Hsp90b1 is crucial for the surface presentation of integrins, including VLA-4 and LFA-1. The reduced expression of these receptors on T_{MBP} cells inhibits their migration into the CNS, consequently reducing the onset and severity of EAE (Figure 13).

Apart from VLA-4, also the interaction of LFA-1 interaction with ICAM-1 plays a role in T cell adhesion (Ley et al., 2007). However, our screening did not reveal a migration deficient phenotype of the LFA-1 subunits αL-integrin and β2-integrin. This is consistent with the findings from the same rat aT-EAE model, where anti-LFA-1 treatment did not block the migration of T_{MBP} cells into the CNS and had no protective or therapeutic effect on the development of EAE (Bartholomäus et al., 2009). In the same setting anti-VLA-4 treatment prevented cells from crossing the BBB, suggesting that in this aT-EAE model only the VLA-4 - VCAM-1 interaction is indispensable for T cell trafficking onto the CNS. In a general sense, the involvement of distinct integrins and receptors in T cell trafficking appears to be dependent on various factors, including the subtype of T cell, the used EAE model, and the specific target tissue for migration. Blocking α4 integrins has differential effects on the trafficking of Th1 and Th17 cells into the CNS during EAE, as Itga4 deletion reduces the homing of Th1 cells but has minimal impact on Th17 cell migration (Glatigny et al., 2011). Th1 cells require α4-integrin expression to infiltrate the CNS, while Th17 cells can only infiltrate the brain, not the spinal cord, without α4-integrin expression, but depend on LFA-1 for infiltration (Rothhammer et al., 2011). In contrast another study reported that blockage of LFA-1 only affected Th1 but not Th17 and that the α4β7 integrin is the key molecule in Th17 cell trafficking (Rossi et al., 2023). This highlights how different integrins are important for different subpopulations varying between models. Additionally, similar to Th17 cells Tregs can enter the CNS independently of α4-integrin, but their entry is LFA-1-dependent in the absence of α4-integrin (Glatigny et al., 2015). However, it is important to note that the experiments in these studies were conducted in mice, whereas our study utilized an aT-EAE model in Lewis rats. It is worth mentioning that Lewis rats do not exhibit as distinct a Th1/Th17 subdivision of T cell subsets as observed in mice. This is evident in our cytokine staining experiments (with the exception of the Tbx21-KO), where unstimulated rat T cells mainly produce IL-17A alone or in combination with IFNy. Furthermore, upon stimulation, they consistently produce both cytokines. A compelling avenue for future research would be to examine how distinct T cell subpopulations behave and differ in their migration patterns, thereby elucidating the mechanisms underlying autoimmune migration.

Numerous adhesion molecules have been reported to participate in T cell migration and EAE, such as Ninjurin 1 (Odoardi et al., 2012), the melanoma cell adhesion molecule (MCAM) (Larochelle et al., 2012), the transmembrane glycoprotein CD6 (Cayrol et al., 2008, Freitas et al., 2019), and the dual immunoglobulin domain containing cell adhesion molecule (DICAM) (Charabati et al., 2022). However, none appeared as an essential regulator in our screening (Kendirli et al., 2023). This raises intriguing questions regarding the functional redundancy of these mediators in our aT-EAE model. Alternatively, it is possible that these adhesion molecules are only required for a specific subpopulation of $CD4^+$ T cells that were not targeted in our screening, as some of those molecules were reported to be primarily implicated in Th17 migration. Further investigations are necessary to elucidate the specific functions and potential interactions of these adhesion molecules in T cell migration and whether they are implicated in EAE pathogenesis. In summary, our study emphasizes the significance of a set of molecules that work together to regulate cellular adhesiveness, which we call the adhesion module. This module revolves around the α4-integrin (Itga4), which forms the VLA-4 receptor together with the less significant β1-integrin (Itgb1). Additionally, the chaperone Hsp90b1, essential for integrin folding, and the intracellular binding partners of integrins Kindlin-3 (Fermt3) and Talin-1 (Tln1) play a crucial role in T cell migration into the CNS.

5.3 The significance of chemotaxis in T cell trafficking

Chemokines and their corresponding receptors are critical for leukocyte migration into tissues and play an essential role in the induction of directed cell movement, activation of integrin-mediated binding and subsequent involvement in inflammatory responses (Hughes and Nibbs, 2018). Our CRISPR/Cas9 screening approach identified *Cxcr3* as one of the top hits, and the only hit among chemokine receptors. Cxcr3 is primarily expressed on $CD4^+$ and $CD8^+$ T cells and responds to its corresponding chemokines CXCL9, CXCL10, and CXCL11 (Groom and Luster, 2011). Although CXCL10 has been shown to promote the activity and recruitment of effector T cells at inflammatory sites, the role of Cxcr3 depending on the bound ligand in neuroinflammation is complex and controversial (Karin, 2020). Nevertheless, $CXCR3^+$ T cells were observed to be increased in the peripheral blood of progressive MS patients compared to healthy controls (Balashov et al., 1999), and anti-Cxcr3 treatment in Lewis rats inhibited T-cell migration into the CNS during EAE and prevented the development of adoptively transferred, but not actively induced disease (Sporici and Issekutz, 2010, Schläger et al., 2016). The findings are consistent with our observed migration impairments of Cxcr3-deficient T cells into the CNS, and with the results of the validation study which indicate no noteworthy impact on T cell activation, adhesion, and differentiation (Figure 18). However, T_{MBP} Cxcr3-KO cells have a

deficiency in the ability to migrate in response to CXCL10 (Figure 17), resulting in reduced incidence and severity of EAE (Figure 19).

Chemokine receptors are part of the GPCR superfamily and activate intracellular G-proteins, which trigger downstream signaling pathways that regulate the processes of cell migration and differentiation. One important member of the Gαi protein family, Gnai2, is involved in chemoattractant receptor signaling (Hwang et al., 2017). In our CRISPR/Cas9 screening, we identified Gnai2 among the essential regulators in the group of GPCRs. Our subsequent validation studies demonstrated that the lack of Gnai2 result in impaired cell migration, as it affects the ability of cells to respond to the chemokines CXCL10 and CCL5 (Figure 21, Figure 22). These findings are consistent with previously published data, which revealed that Gnai2 is necessary for T cell responses to three Cxcr3 ligands, specifically CXCL9, CXCL10 and absence of Gnai2 leads to profound defects in chemokine-induced chemotaxis, and homing (Thompson et al., 2007, Hwang et al., 2007).

Tbx21, or T-bet, is a transcription factor that is of utmost importance in the development and function of Th1 cells. It functions as a master regulator of Th1 differentiation and is required for the proper activation of Th1 genes, including those that encode the hallmark Th1 cytokine, IFNγ (Szabo et al., 2000). Our CRISPR/Cas9 screening also identified it as one of the essential regulators in T cell migration among the group of transcription factors. Our analysis of *in vitro* T_{MBP} Tbx21-KO cells showed a significant decrease in the production of IFNγ in both unstimulated and stimulated conditions, indicating the impact of our knockout, while there was no change observed in the expression of surface activation markers and adhesion molecules (Figure 23). The analysis of the *in vivo* migration assay revealed a decrease in the migration of T_{MBP} cells deficient in Tbx21 to the meninges and CSF, but not into the parenchyma (Figure 25). This finding is of particular interest as it contrasts with the predictions made by our CRISPR/Cas9 screening, which suggested a reduced migration into both the meninges and the parenchyma. The underlying reason for this discrepancy remains elusive, possibly due to the limitations of CRISPR/Cas9 screenings discussed earlier. Nonetheless, this difference underscores the importance of further validating the screening results. Another intriguing observation is that T_{MBP} cells lacking Tbx21 appear to bypass migration through the leptomeninges and instead directly migrate into the parenchyma, possibly utilizing intra-parenchymal blood vessels. However, additional experiments are necessary to provide support for this hypothesis. Previous research has suggested that Tbx21 controls the binding of $CD4^+$ T cells to P-selectin, and the absence of Tbx21 abolishes the selective migration of T cells *in vivo* (Lord et al., 2005). However, as discussed above binding to selectins does not appear to be essential for T cell transmigration into the CNS in our model. Intriguingly, it was shown that

Tbx21 is also required for the expression of the chemokine receptor Cxcr3 in $CD4^+$ T cells (Beima et al., 2006, Lord et al., 2005), and that Tbx21 deficiency in $CD8^+$ T cells leads to decreased RNA levels of CCR5 (Prier et al., 2019). Likewise, we observed impaired migration of T cells lacking Tbx21 towards the chemokines CCL5 and CXCL10, implying that the migration deficient phenotype of T_{MBP} Tbx21-KO in our CRISPR/Cas9 screening is linked to the decreased expression of Cxcr3 and the resulting altered chemotactic response (Figure 24).

Chemokine receptors are a key component of the T cell recruitment process and apart from Cxcr3 also CCR5 has also been suggested to play a role in MS an EAE. A study suggested the involvement of CCR5 in the migration of T cells to the CNS, as evidenced by the increased number of $CCR5^+$ T cells in the peripheral blood of progressive MS patients (Balashov et al., 1999). In addition, CCR5 knockout led to a reduction in the severity of active EAE in C57BL/6 mice (Gu et al., 2016), and interference with CCR5 chemokine signaling in Lewis rats led to the release of T_{MBP} cells from the leptomeninges, thereby preventing their entry into the CNS (Schläger et al., 2016). However, conflicting results have been reported, as another study demonstrated that CCR5 blockade does not affect leukocyte trafficking in chronic-relapsing EAE in C57BL/6 mice (Matsui et al., 2002). In our CRISPR/Cas9 screening, despite previous suggestions of CCR5 playing a role in T cell migration into the CNS, we did not identify it as an essential regulator in our study. Nonetheless, we decided to investigate its role further. Consistent with the screening results, depletion of CCR5 did not affect the migration of T_{MBP} cells to the spinal cord meninges or parenchyma (Figure 27). Hence, we can draw two conclusions. Firstly, our screening accurately excluded CCR5 as an essential candidate. Secondly, CCR5 appears to be dispensable for T cell transmigration into the CNS, probably because other chemokine receptors compensate for its function or it is only necessary for the migration of a specific subpopulation.

Therefore, our CRISPR/Cas9 screening and subsequent validation experiments led us to conclude that the efficient migration of T cells into the CNS relies on the chemotaxis module, which includes the chemokine receptor Cxcr3, its intracellular G protein Gnai2, and its transcription factor Tbx21. Our findings suggest that these components play a crucial role in facilitating T cell migration into the CNS.

5.4 The S1P-S1PR1 axis regulates T cell egress dynamics

One of the top essential regulators identified through our CRISPR/Cas9 screening was Grk2, which captivated our interest as a potential new candidate for T cell transmigration into the CNS. Grk2 is best known for its capability to recognize and phosphorylate agonist-activated GPCRs, which promotes β-arrestin recruitment and functional uncoupling from heterotrimeric

G proteins, resulting in receptor desensitization (Penela et al., 2019). Additionally, β-arrestin binding targets phosphorylated receptors for clathrin-mediated endocytosis, which ultimately results in either their recycling back to the plasma membrane or their degradation (Reiter and Lefkowitz, 2006, Tian et al., 2014). Grk2 not only regulates receptor activity but also interacts with various signaling molecules, which can affect downstream activity or initiate alternative signal transduction pathways independently of receptor phosphorylation. For example, it can modulate cell signaling by interacting with Gαq and Gβγ subunits (Evron et al., 2012). In addition, emerging evidence suggests that Grk2 phosphorylates various non-GPCR substrates and has a complex network of functional interactions with proteins including diverse receptors, molecular switches, structural proteins, scaffolding molecules, and kinases (Penela et al., 2019). As a result of these interactions and regulatory mechanisms, Grk2 as a key integrative signaling node, is capable of modulating numerous biological processes such as cell growth, proliferation, cell motility, and chemotaxis (Cheng et al., 2021). Grk2 is expressed at high levels in cells of the immune system (Chuang et al., 1992). Notably, alterations in the expression and activity of Grk2 have been reported in various inflammatory conditions in both humans and animals, indicating a potential role of this kinase in immune regulation. Reduced expression levels of Grk2 were found in peripheral blood mononuclear cells from MS and rheumatoid arthritis patients (Giorelli et al., 2004, Lombardi et al., 1999). However, it was reported that T cells obtained from MS patients during remission exhibit even lower levels of Grk2 expression (Vroon et al., 2005). Interestingly, during EAE the expression of Grk2 protein in spleen cells of Dark Agouti rats is decreased (Vroon et al., 2003). Additionally, $Grk2^{+/-}$ mice, which express only 50% of the Grk2 protein, were found to have an earlier onset of EAE but did not develop relapses (Vroon et al., 2005). These cells also exhibited increased responsiveness to the chemokines CCL3, CCL4, and CCL5 (Vroon et al., 2004). These studies suggest that a reduction in Grk2 leads to an increased chemotactic response and thus presumably to an enhanced migration of T cells into the CNS. However, in our CRISPR/Cas9 screening and subsequent validation experiments, we clearly observed a reduction of T cell trafficking (Figure 29), leading to an alleviated EAE course (Figure 30).

Our intravital microscopy of T_{MBP} Grk2-KO cell migration in the leptomeninges revealed that T_{MBP} Grk2-KO cells are able to attach to the blood vessel wall and successfully crawl along it in a similar manner to NT T_{MBP} cells (Figure 31). However, T_{MBP} cells deficient in Grk2 failed to accomplish transendothelial migration and as a result their number of extravasated T cells across the endothelial barrier was markedly reduced. These observations are analogous to those from a previous study, which examined the effect of Grk2 knockout on the desensitization of S1PR1 in T and B cells (Arnon et al., 2011). Based on these findings, we

hypothesize that the migration deficient phenotype of T_{MBP} Grk2-KO cells is linked to the S1PR1-S1P axis. The receptor S1PR1 and its ligand S1P have emerged over the past decade as a central mediator of lymphocyte egress from lymph nodes. S1P is a signaling molecule that that is abundant in the blood originating from erythrocytes (Pappu et al., 2007), and in the lymph where it is produced by lymphatic endothelial cells (Pham et al., 2010). Naive T cells increase their expression of S1PR1, exit the thymus, and migrate towards the blood following the S1P gradient. Once in the blood, lymphocytes downregulate S1PR1 after binding of S1P, but upregulate them again upon entering secondary lymphoid organs (Schwab and Cyster, 2007). Studies in mice with hematopoietic cells deficient in S1PR1 have demonstrated that mature T cells are unable to exit the thymus (Matloubian et al., 2004). Additionally, it has been observed that T cells lacking Grk2-mediated constitutive S1PR1 signaling exhibit a defect in entering lymph nodes (Arnon et al., 2011), underscoring the critical role of this pathway in T cell egress. In our migration experiments we also observed a strong reduction of the T_{MBP} Grk2-KO cells migration into the CNS organs (meninges, parenchyma, and CNS), but also into the parathymic lymph nodes indicating a similar mode of action (Figure 29). Arnon et al. demonstrated that the migration of T cells from the bloodstream to the lymph nodes is reduced in the absence of Grk2, but this effect is reversed in S1P-deficient mice (Arnon et al., 2011). Additionally, Grk2 deficient B cells treated with an S1PR1 antagonist displayed a partial restoration of their ability to migrate to lymph nodes and splenic follicles (Hwang et al., 2019). Based on this, we established additional T_{MBP} S1PR1-KO and double deficient T_{MBP} Grk2-S1PR1-KO cells and evaluated them in our co-transfer setup (Figure 32). We found that the trafficking deficits into the CNS of Grk2-deficient T_{MBP} cells were ameliorated by additional deletion of S1PR1, suggesting that S1PR1 indeed mediates the altered T cell trafficking. Interestingly, we also observed a drastic accumulation of T_{MBP} cells that lacked S1PR1 in the spleen and parathymic lymph nodes, which strongly resembles what is observed when S1PR1 agonists are used in the treatment of MS to detain cells from egressing into the blood stream but sequester them in the lymphatic organs (Sanford, 2014). Fingolimod (FTY720), an FDA-approved medication, functions as an antagonist by inducing internalization and degradation of the receptors, thereby decreasing the S1P-S1PR1-dependent egress of lymphocytes from lymph nodes and reducing the recirculation of autoaggressive T cells through the lymph and blood to the CNS (Brinkmann et al., 2010). Drawing on the literature and our own experimental findings, we postulate that the migratory deficiency observed in Grk2-deficient T cells is likely due to the absence of desensitization and internalization of S1PR1. This results in prolonged retention of the cells in the bloodstream and an inability to overcome the S1P gradient in the blood, thereby impeding their migration into the CNS.

Our CRISPR/Cas9 screening in T_{MBP} cells not only allowed us to compare peripheral organs to CNS organs to identify essential regulators of transmigration across the BBB, but also enabled us to analyse each comparison individually to identify hits that affect the distribution within the peripheral and central compartments. As expected, S1PR1 was identified as a compartment-specific hit that regulates T cell entry and egress from blood to the spleen, as T_{MBP} S1PR1-KO cells were unable to exit the spleen (Supplementary Figure 1). Interestingly, the transcription factor Klf2, which is known to regulate S1PR1 expression (Bai et al., 2007), was significantly depleted in comparisons of CNS tissues with the spleen but not with the blood, suggesting a potential link between its migration-deficient phenotype and S1PR1 (Figure 6).

Further hits of the CRISPR/Cas9 screening that were only significantly depleted in comparisons of CNS tissues with the spleen but not with the blood were Arih1 and Ube2l3. Notably, those two were the top hits in the comparison of spleen to blood and T cells deficient of those genes were even more enriched in the spleen than T cells with a S1PR1 KO (Supplementary Figure 1). Arih1 is an E3 ubiquitin-protein ligase and Ube2l3 is an E2 ubiquitin-conjugating enzyme. Both have been described to interacts together to catalyse the ubiquitination of target proteins (Wenzel et al., 2011). The similar outcomes of our CRISPR/Cas9 screening and the subsequent migration studies suggest that both genes work in collaboration through a common mechanism that is essential for spleen egress of encephalitogenic T cells in our model (Figure 34, Figure 37). Currently, not much is known about Arih1, also known as Human Homolog of Drosophila Ariadne (HHARI). It has been implicated in tumour immunity (Wang et al., 2020, Howley et al., 2022), genotoxic stress (von Stechow et al., 2015) and antiviral immunity and autoimmunity (Xiong et al., 2022). Ube2l3 also known as UbcH7 is widely expressed by lymphocytes (Cui et al., 2013). Genome-wide association studies have found that genetic variants in the Ube2l3 region are associated with several autoimmune diseases, including systemic lupus erythematosus (Wang et al., 2012), rheumatoid arthritis (Orozco et al., 2011), and Crohn's disease (Fransen et al., 2010). Further it is believed to be implicated in in several signaling pathways, including NF-κB, as well as autophagy and DSB repair (Zhang et al., 2022). Studies suggest that Ube2l3 can influence the pathogenesis of inflammatory and autoimmune diseases by enhancing NF-κB activation (Fu et al., 2014, Lewis et al., 2015). However, the role of Arih1 and Ube2l3 in T cell egress has not been elucidated yet. Although a mild downregulation of the VLA-4 receptor was observed in both candidates, this does not appear to be the sole cause of their increased migratory capacity (Figure 34, Figure 37). This is evidenced by the fact that Ets1-KO cells, which exhibit a comparable level of VLA-4 downregulation, displayed enhanced migration (Figure 40). Therefore, it seems likely that other factors are involved in mediating this phenotype. Given their selective enrichment in

lymphoid organs, it is tempting to speculate that Arih1 and Ube2l3 may collaborate in a mechanism that is relevant to the regulation of S1PR1, especially since it has been suggested that ubiquitination of S1PR1 triggers its rapid and quantitative degradation and Arih1 was predicted to be an E3 ligase in this process (Oo et al., 2007, Li et al., 2017). However, additional investigations are needed to determine whether a connection exists between Arih1/Ube2l3 and the modulation of S1PR1.

5.5 Transcription factor involvement in T cell transmigration

In our CRISPR/Cas9 screening, several transcription factors were identified as regulators of T cell migration, including *Cbfb* (Figure 6). It is a non-DNA binding subunit that essential for the transcriptional activity of the three DNA binding CBFα units, also known as Runx proteins and deleting *Cbfb* leads to the complete loss of Runx function (Rudra et al., 2009, Speck, 2001). The Runx-Cbfb heterodimer is involved in definitive haematopoiesis, thymic T cell development (Taniuchi et al., 2002), and differentiation and function of peripheral T cells (Djuretic et al., 2007, Komine et al., 2003). It is particularly recognized for its role in maintaining a constant and elevated level of FoxP3 expression, which is a key determinant of the Treg cell lineage stability (Rudra et al., 2009, Kitoh et al., 2009). Like *Cbfb*, the transcription factor *Foxo1* is implicated in T cell homeostasis and was also identified in our CRISPR/Cas9 screening as essential regulator (Newton et al., 2018, Ouyang et al., 2009). The impaired migration phenotype of T cells lacking *Cbfb* and *Foxo1* function may be due to the importance of both proteins in T cell differentiation and development and therefore may be attributed to disrupted T cell function. Nonetheless, it is important to acknowledge that the CRISPR/Cas9 DNA perturbations were performed in already differentiated antigen-activated $CD4^+$ T cells. *Foxo1* has been demonstrated to play a role in promoting the expression of Klf2 and L-selectin in human T cells (Fabre et al., 2008). Furthermore, in mice, it is required for the expression of the transcription factor Klf2, the adhesion molecule L-selectin, and the chemokine receptor CCR7 (Kerdiles et al., 2009, Gubbels Bupp et al., 2009, Ouyang et al., 2009). Given Klf2's connection to the S1P-S1PR1 axis, it is plausible that all three molecules may operate together in a shared mechanism. However, further investigation is required to determine whether these transcription factors have a novel function in T cells that are already differentiated or if they act through established pathways.

Furthermore, we observed that the absence of the transcription factor Blimp-1, which is encoded by the *Prdm1* gene locus, led to a reduction in T cell trafficking into the CNS during our CRISPR/Cas9 screening. As a transcriptional repressor, BLIMP-1 plays a critical role in the regulation of T cell differentiation, homeostasis, and activation and is present in both $CD4^+$ and

$CD8^+$ T cells (Martins et al., 2006, Kallies et al., 2009, Rutishauser et al., 2009, Fu et al., 2017). In T-cell biology, BLIMP-1 is a transcription factor that can function as an activator or a repressor depending on the cellular context. It has been shown to have a critical role in regulating the fate of multiple T-cell lineages. BLIMP-1 can inhibit Th1 differentiation, suppress T follicular helper cell differentiation, and maintain Treg cell function, among other functions (Cimmino et al., 2008, Johnston et al., 2009, Cretney et al., 2011). Moreover, it plays a part in regulating the activity of IL-17 producing Th17 cells (Lin et al., 2013, Salehi et al., 2012). The impact of BLIMP-1 has been evaluated in animal EAE models with inconsistent outcomes; one study demonstrated that T cell-specific BLIMP-1 deficiency worsened EAE by increasing encephalitogenic Th1 and Th17 cells in the CNS (Lin et al., 2014), whereas another study found that peripheral deletion of Blimp-1 led to decreased Th17 activation and EAE severity (Jain et al., 2016). In the same study Blimp-1 has been identified as a crucial transcription factor that activates the Th17 inflammatory program by inducing the expression of GM-CSF and IFNγ in response to IL-23 (Jain et al., 2016). The observed discrepancies in the role of BLIMP-1 in EAE could potentially be attributed to variations in the mouse models employed. Nevertheless, this emphasizes the intricate nature of this transcription factor and underscores the need for additional investigations to elucidate its function in the context of the observed migration deficient phenotype in our aT-EAE model.

In our CRISPR/Cas9 screening, the primary objective was to identify positive regulators that enhance T cell transmigration in the CNS, as they could be potential therapeutic targets for MS treatment. However, the identification of negative regulators that impede T cell migration under normal conditions is also of interest, as they could be potentially augmented in a MS therapy or utilized as a therapeutic approach for other diseases where an increased immune response is desired, such as brain cancers. One interesting observation is that there are fewer negative regulators that show a clear effect on T cell migration compared to positive regulators. This might be because autoreactive, encephalitogenic T_{MBP} cells, being antigen-specific and activated, are already predisposed to migrate to the CNS, making it harder to detect further increases in migration. We identified the Ets1 transcription factor as the top hit among the positive regulators, as its knock out led to a stronger migration phenotype in all tissue comparisons (Figure 6). *Ets1* has been identified as a susceptibility locus for various autoimmune diseases, such as systemic lupus erythematosus, rheumatoid arthritis, and atopic dermatitis, through genome-wide association studies (Sullivan et al., 2000, Yang et al., 2010, Paternoster et al., 2015). Additionally, in patients with inflammatory bowel disease, Ets1 was found to be highly expressed in $CD4^+$ T cells (He et al., 2022). Ets1 expression is particularly high in lymphoid cells and has a major influence on the differentiation, survival and

proliferation of T helper cell subsets (Russell and Garrett-Sinha, 2010). Research has shown that T cells lacking Ets1 exhibit defects in activation and survival, as well as reduced ability to produce Th1 and Th2 cytokines (Muthusamy et al., 1995, Russell and Garrett-Sinha, 2010). Ets1-KO mice exhibit a reduction in Treg cell population, and the remaining Treg cells have decreased suppressive activity *in vitro* (Mouly et al., 2010). Although $CD4^+$ T cells lacking Ets1 expression have been shown to upregulate the expression of IL-17 and other Th17-specific genes when differentiated into the Th17 pathway (Moisan et al., 2007), we did not observe a shift in the production of IL-17 or IFNy in our T_{MBP} Ets1-KO cells (Figure 39). Notably, Ets1 was found to have interactions with other transcription factors that were identified in our screening. For example, it has been shown to interfere with the activity of the transcription factor Blimp-1 in B cells (John et al., 2008). In addition, it was shown that Ets1 is required for Tbx21 to promote interferon-gamma production, which is essential for Th1 inflammatory responses (Grenningloh et al., 2005). Although Ets1 has been implicated in various immune functions, the underlying mechanism by which Ets1 regulates the migration of T cells remains largely unknown. Our study revealed that Ets1-deficient T_{MBP} cells exhibit an enhanced migration phenotype into the CNS (Figure 40). Nonetheless, further investigations are warranted to decipher the precise molecular mechanism by which Ets1 regulates the migration of T cells into the CNS in the context of aT-EAE.

While the only gene that reached significance in all four tissue comparisons was *Ets1*, we also found genes that showed an enhanced migration phenotype in only part of the comparisons. Little is known about the majority of these genes, and none of them have been previously associated with promoting T cell migration. Among those was the tyrosin kinase Jak3, which absence was shown to have a defect in very early T-cell development as well as impaired chemokine-induced migration (Soldevila et al., 2004, Baird et al., 2000), Further it was shown that Jak3-deficient T lymphocytes have intrinsic defects in CCR7-mediated homing to peripheral lymphoid organs (García-Zepeda et al., 2007). How this reconciles with our observed phenotype of increased migration in Jak3-deficient T cells will require further research. Additional candidates that emerged from our CRISPR/Cas9 screening were relatively understudied, such as the *ZFP407* gene that encodes for Zinc finger protein 407, which has only been described in the context of glucose homeostasis (Buchner et al., 2015). Additionally, *Adgre4* that encodes for the GPCR EMR4, is thought to play a role in immunity related to cell adhesion and migration due to the fact that it is almost exclusively expressed on leukocytes (Kwakkenbos et al., 2004). Nevertheless, the precise mechanism by which this protein operates in these processes remains obscure. Another hit was the formyl peptide receptor 3 (FPR3), which is a member of the formyl peptide chemoattractant receptor family belonging to

the GPCR. It is known to be involved in inflammation and antibacterial host and was further identified as a critical gene in the pathogenesis of the autoimmune disease cutaneous lupus erythematosus (Gao et al., 2022). Unlike other formyl peptide receptors that have been linked to leukocyte trafficking and immune responses, FPR3's role in these processes is not well characterized (Chen et al., 2017). Therefore, subsequent investigations are required to uncover the molecular mechanisms driving these gene effects.

6 CONCLUSION

In this work, we performed an *in vivo* unbiased genome-wide CRISPR/Cas9 KO screening in activated encephalitogenic $CD4^+$ T_{MBP} cells using an adoptive-transfer EAE model in Lewis rats. Through this approach, we identified essential positive and negative regulators of T cell transmigration across the BBB into the CNS.

To gain a deeper understanding of the role of the identified candidates in regulating T cell migration, our second objective was to validate them by generating single KO T_{MBP} cells and investigate their mechanism of action. Through a combination of *in vitro* and *in vivo* techniques, including surface protein and cytokine stainings, chemotactic and migration assays as well as intravital two-photon microscopy experiments, we grouped the identified hits into modules related to adhesion, chemotaxis, egress, and ubiquitination.

As expected, some of the molecules identified in our screening were already known to be involved in T cell migration and some are even used in MS therapy already. This highlights the applicability of our screening approach and suggests that additional discovered molecules may also have clinical relevance. In this work we have elucidated the mechanism of action of Grk2, which operates through the S1PR1 axis but disrupts the T cell migration process at a distinct stage compared to S1PR1 KO. Additionally, we could underscore the importance of Cxcr3 mediated signaling and discover completely unknown genes that have the potential to limit T cell migration, such as Arih1 and Ube2l3. Unravelling their mechanisms of action is one of our next objectives.

Overall, this comprehensive characterization of distinct molecular modules sheds light on the intricate regulatory mechanisms underlying T cell migration in the context of EAE. These findings contribute to a deeper understanding of the pathogenesis of autoimmune diseases and may hold potential for the development of novel therapeutic strategies.

REFERENCES

ADORNO-CRUZ, V. & LIU, H. 2019. Regulation and functions of integrin α2 in cell adhesion and disease. *Genes Dis,* 6**,** 16-24.

AFGAN, E., BAKER, D., BATUT, B., VAN DEN BEEK, M., BOUVIER, D., CECH, M., CHILTON, J., CLEMENTS, D., CORAOR, N., GRÜNING, B. A., GUERLER, A., HILLMAN-JACKSON, J., HILTEMANN, S., JALILI, V., RASCHE, H., SORANZO, N., GOECKS, J., TAYLOR, J., NEKRUTENKO, A. & BLANKENBERG, D. 2018. The Galaxy platform for accessible, reproducible and collaborative biomedical analyses: 2018 update. *Nucleic Acids Res,* 46**,** W537-w544.

AGGARWAL, S., GHILARDI, N., XIE, M. H., DE SAUVAGE, F. J. & GURNEY, A. L. 2003. Interleukin-23 promotes a distinct CD4 T cell activation state characterized by the production of interleukin-17. *J Biol Chem,* 278**,** 1910-4.

AI, W., LI, H., SONG, N., LI, L. & CHEN, H. 2013. Optimal method to stimulate cytokine production and its use in immunotoxicity assessment. *Int J Environ Res Public Health,* 10**,** 3834-42.

ANDERSON, L. R., OWENS, T. W. & NAYLOR, M. J. 2014. Structural and mechanical functions of integrins. *Biophys Rev,* 6**,** 203-213.

ARDLEY, H. C., TAN, N. G. S., ROSE, S. A., MARKHAM, A. F. & ROBINSON, P. A. 2001. Features of the Parkin/Ariadne-like Ubiquitin Ligase, HHARI, That Regulate Its Interaction with the Ubiquitin-conjugating Enzyme, UbcH7 *. *Journal of Biological Chemistry,* 276**,** 19640-19647.

ARNON, T. I., XU, Y., LO, C., PHAM, T., AN, J., COUGHLIN, S., DORN, G. W. & CYSTER, J. G. 2011. GRK2-dependent S1PR1 desensitization is required for lymphocytes to overcome their attraction to blood. *Science,* 333**,** 1898-903.

ATTFIELD, K. E., JENSEN, L. T., KAUFMANN, M., FRIESE, M. A. & FUGGER, L. 2022. The immunology of multiple sclerosis. *Nat Rev Immunol*.

BACH, J.-F. 2002. The Effect of Infections on Susceptibility to Autoimmune and Allergic Diseases. *New England Journal of Medicine,* 347**,** 911-920.

BAECHER-ALLAN, C., KASKOW, B. J. & WEINER, H. L. 2018. Multiple Sclerosis: Mechanisms and Immunotherapy. *Neuron,* 97**,** 742-768.

BAI, A., HU, H., YEUNG, M. & CHEN, J. 2007. Kruppel-like factor 2 controls T cell trafficking by activating L-selectin (CD62L) and sphingosine-1-phosphate receptor 1 transcription. *J Immunol,* 178**,** 7632-9.

BAIRD, A. M., LUCAS, J. A. & BERG, L. J. 2000. A profound deficiency in thymic progenitor cells in mice lacking Jak3. *J Immunol,* 165**,** 3680-8.

BALASHOV, K. E., ROTTMAN, J. B., WEINER, H. L. & HANCOCK, W. W. 1999. CCR5+ and CXCR3+ T cells are increased in multiple sclerosis and their ligands MIP-1α and IP-10 are expressed in demyelinating brain lesions. *Proceedings of the National Academy of Sciences,* 96**,** 6873-6878.

BARANZINI, S. E., MUDGE, J., VAN VELKINBURGH, J. C., KHANKHANIAN, P., KHREBTUKOVA, I., MILLER, N. A., ZHANG, L., FARMER, A. D., BELL, C. J., KIM, R. W., MAY, G. D., WOODWARD, J. E., CAILLIER, S. J., MCELROY, J. P., GOMEZ, R., PANDO, M. J., CLENDENEN, L. E., GANUSOVA, E. E., SCHILKEY, F. D., RAMARAJ, T., KHAN, O. A., HUNTLEY, J. J., LUO, S., KWOK, P.-Y., WU, T. D., SCHROTH, G. P., OKSENBERG, J. R., HAUSER, S. L. & KINGSMORE, S. F. 2010. Genome, epigenome and RNA sequences of monozygotic twins discordant for multiple sclerosis. *Nature,* 464**,** 1351-1356.

BARCELLOS, L. F., OKSENBERG, J. R., BEGOVICH, A. B., MARTIN, E. R., SCHMIDT, S., VITTINGHOFF, E., GOODIN, D. S., PELLETIER, D., LINCOLN, R. R., BUCHER, P., SWERDLIN, A., PERICAK-VANCE, M. A., HAINES, J. L. & HAUSER, S. L. 2003. HLA-DR2 dose effect on susceptibility to multiple sclerosis and influence on disease course. *Am J Hum Genet,* 72**,** 710-6.

BARRANGOU, R., FREMAUX, C., DEVEAU, H., RICHARDS, M., BOYAVAL, P., MOINEAU, S., ROMERO, D. A. & HORVATH, P. 2007. CRISPR Provides Acquired Resistance Against Viruses in Prokaryotes. *Science,* 315**,** 1709-1712.

BARTHOLOMÄUS, I., KAWAKAMI, N., ODOARDI, F., SCHLÄGER, C., MILJKOVIC, D., ELLWART, J. W., KLINKERT, W. E., FLÜGEL-KOCH, C., ISSEKUTZ, T. B., WEKERLE, H. & FLÜGEL, A. 2009. Effector T cell interactions with meningeal vascular structures in nascent autoimmune CNS lesions. *Nature,* 462**,** 94-8.

BATOULIS, H., RECKS, M. S., ADDICKS, K. & KUERTEN, S. 2011. Experimental autoimmune encephalomyelitis – achievements and prospective advances. *APMIS,* 119**,** 819-830.

BECHER, B., DURELL, B. G. & NOELLE, R. J. 2002. Experimental autoimmune encephalitis and inflammation in the absence of interleukin-12. *J Clin Invest,* 110**,** 493-7.

BEIMA, K. M., MIAZGOWICZ, M. M., LEWIS, M. D., YAN, P. S., HUANG, T. H. & WEINMANN, A. S. 2006. T-bet binding to newly identified target gene promoters is cell type-independent but results in variable context-dependent functional effects. *J Biol Chem,* 281**,** 11992-2000.

BEN-NUN, A., KAUSHANSKY, N., KAWAKAMI, N., KRISHNAMOORTHY, G., BERER, K., LIBLAU, R., HOHLFELD, R. & WEKERLE, H. 2014. From classic to spontaneous and humanized models of multiple sclerosis: impact on understanding pathogenesis and drug development. *J Autoimmun,* 54**,** 33-50.

BEN-NUN, A., WEKERLE, H. & COHEN, I. R. 1981. The rapid isolation of clonable antigen-specific T lymphocyte lines capable of mediating autoimmune encephalomyelitis. *Eur J Immunol,* 11**,** 195-9.

BERER, K., GERDES, L. A., CEKANAVICIUTE, E., JIA, X., XIAO, L., XIA, Z., LIU, C., KLOTZ, L., STAUFFER, U., BARANZINI, S. E., KÜMPFEL, T., HOHLFELD, R., KRISHNAMOORTHY, G. & WEKERLE, H. 2017. Gut microbiota from multiple sclerosis patients enables spontaneous autoimmune encephalomyelitis in mice. *Proceedings of the National Academy of Sciences,* 114**,** 10719-10724.

BETTELLI , E., PAGANY , M., WEINER , H. L., LININGTON , C., SOBEL , R. A. & KUCHROO , V. K. 2003. Myelin Oligodendrocyte Glycoprotein–specific T Cell Receptor Transgenic Mice Develop Spontaneous Autoimmune Optic Neuritis. *Journal of Experimental Medicine,* 197**,** 1073-1081.

BILLIAU, A., HEREMANS, H., VANDEKERCKHOVE, F., DIJKMANS, R., SOBIS, H., MEULEPAS, E. & CARTON, H. 1988. Enhancement of experimental allergic encephalomyelitis in mice by antibodies against IFN-gamma. *J Immunol,* 140**,** 1506-10.

BJORNEVIK, K., CORTESE, M., HEALY, B. C., KUHLE, J., MINA, M. J., LENG, Y., ELLEDGE, S. J., NIEBUHR, D. W., SCHER, A. I., MUNGER, K. L. & ASCHERIO, A. 2022. Longitudinal analysis reveals high prevalence of Epstein-Barr virus associated with multiple sclerosis. *Science,* 375**,** 296-301.

BOCK, C., DATLINGER, P., CHARDON, F., COELHO, M. A., DONG, M. B., LAWSON, K. A., LU, T., MAROC, L., NORMAN, T. M., SONG, B., STANLEY, G., CHEN, S., GARNETT, M., LI, W., MOFFAT, J., QI, L. S., SHAPIRO, R. S., SHENDURE, J., WEISSMAN, J. S. & ZHUANG, X. 2022. High-content CRISPR screening. *Nature Reviews Methods Primers,* 2**,** 8.

BRESLOW, D. K., HOOGENDOORN, S., KOPP, A. R., MORGENS, D. W., VU, B. K., KENNEDY, M. C., HAN, K., LI, A., HESS, G. T., BASSIK, M. C., CHEN, J. K. & NACHURY, M. V. 2018. A CRISPR-based screen for Hedgehog signaling provides insights into ciliary function and ciliopathies. *Nat Genet,* 50**,** 460-471.

BRINKMANN, V., BILLICH, A., BAUMRUKER, T., HEINING, P., SCHMOUDER, R., FRANCIS, G., ARADHYE, S. & BURTIN, P. 2010. Fingolimod (FTY720): discovery and development of an oral drug to treat multiple sclerosis. *Nat Rev Drug Discov,* 9**,** 883-97.

BRUCKLACHER-WALDERT, V., STUERNER, K., KOLSTER, M., WOLTHAUSEN, J. & TOLOSA, E. 2009. Phenotypical and functional characterization of T helper 17 cells in multiple sclerosis. *Brain,* 132**,** 3329-41.

BUCHNER, D. A., CHARRIER, A., SRINIVASAN, E., WANG, L., PAULSEN, M. T., LJUNGMAN, M., BRIDGES, D. & SALTIEL, A. R. 2015. Zinc finger protein 407 (ZFP407) regulates insulin-stimulated glucose uptake and glucose transporter 4 (Glut4) mRNA. *J Biol Chem,* 290**,** 6376-86.

BURNS, J., ROSENZWEIG, A., ZWEIMAN, B. & LISAK, R. P. 1983. Isolation of myelin basic protein-reactive T-cell lines from normal human blood. *Cell Immunol,* 81**,** 435-40.

BUTIUC-KEUL, A., FARKAS, A., CARPA, R. & IORDACHE, D. 2022. CRISPR-Cas System: The Powerful Modulator of Accessory Genomes in Prokaryotes. *Microbial Physiology,* 32**,** 2-17.

CALDERWOOD, D. A. 2004. Integrin activation. *Journal of Cell Science,* 117**,** 657-666.

CAMPBELL, B., VOGEL, P. J., FISHER, E. & LORENZ, R. 1973. Myelin basic protein administration in multiple sclerosis. *Arch Neurol,* 29**,** 10-5.

CAYROL, R., WOSIK, K., BERARD, J. L., DODELET-DEVILLERS, A., IFERGAN, I., KEBIR, H., HAQQANI, A. S., KREYMBORG, K., KRUG, S., MOUMDJIAN, R., BOUTHILLIER, A., BECHER, B., ARBOUR, N., DAVID, S., STANIMIROVIC, D. & PRAT, A. 2008. Activated leukocyte cell adhesion molecule promotes leukocyte trafficking into the central nervous system. *Nat Immunol,* 9**,** 137-45.

CHAN, Y. T., LU, Y., WU, J., ZHANG, C., TAN, H. Y., BIAN, Z. X., WANG, N. & FENG, Y. 2022. CRISPR-Cas9 library screening approach for anti-cancer drug discovery: overview and perspectives. *Theranostics,* 12**,** 3329-3344.

CHANG, H. H. Y., PANNUNZIO, N. R., ADACHI, N. & LIEBER, M. R. 2017. Non-homologous DNA end joining and alternative pathways to double-strand break repair. *Nature Reviews Molecular Cell Biology,* 18**,** 495-506.

CHARABATI, M., GRASMUCK, C., GHANNAM, S., BOURBONNIÈRE, L., FOURNIER, A. P., LÉCUYER, M. A., TASTET, O., KEBIR, H., RÉBILLARD, R. M., HOORNAERT, C., GOWING, E., LAROUCHE, S., FORTIN, O., PITTET, C., FILALI-MOUHIM, A., LAHAV, B., MOUMDJIAN, R., BOUTHILLIER, A., GIRARD, M., DUQUETTE, P., CAYROL, R., PEELEN, E., QUINTANA, F. J., ANTEL, J. P., FLÜGEL, A., LAROCHELLE, C., ARBOUR, N., ZANDEE, S. & PRAT, A. 2022. DICAM promotes T(H)17 lymphocyte trafficking across the blood-brain barrier during autoimmune neuroinflammation. *Sci Transl Med,* 14.

CHEN, C., MANSO, A. M. & ROSS, R. S. 2019. Talin and Kindlin as Integrin-Activating Proteins: Focus on the Heart. *Pediatr Cardiol,* 40**,** 1401-1409.

CHEN, K., BAO, Z., GONG, W., TANG, P., YOSHIMURA, T. & WANG, J. M. 2017. Regulation of inflammation by members of the formyl-peptide receptor family. *Journal of Autoimmunity,* 85**,** 64-77.

CHEN, Z., ARAI, E., KHAN, O., ZHANG, Z., NGIOW, S. F., HE, Y., HUANG, H., MANNE, S., CAO, Z., BAXTER, A. E., CAI, Z., FREILICH, E., ALI, M. A., GILES, J. R., WU, J. E., GREENPLATE, A. R., HAKEEM, M. A., CHEN, Q., KURACHI, M., NZINGHA, K., EKSHYYAN, V., MATHEW, D., WEN, Z., SPECK, N. A., BATTLE, A., BERGER, S. L., WHERRY, E. J. & SHI, J. 2021. In vivo CD8(+) T cell CRISPR screening reveals control by Fli1 in infection and cancer. *Cell,* 184**,** 1262-1280.

CHENG, J., LUCAS, P. C. & MCALLISTER-LUCAS, L. M. 2021. Canonical and Non-Canonical Roles of GRK2 in Lymphocytes. *Cells,* 10.

CHUANG, T. T., SALLESE, M., AMBROSINI, G., PARRUTI, G. & DE BLASI, A. 1992. High expression of beta-adrenergic receptor kinase in human peripheral blood leukocytes. Isoproterenol and platelet activating factor can induce kinase translocation. *J Biol Chem,* 267**,** 6886-92.

CIMMINO, L., MARTINS, G. A., LIAO, J., MAGNUSDOTTIR, E., GRUNIG, G., PEREZ, R. K. & CALAME, K. L. 2008. Blimp-1 Attenuates Th1 Differentiation by Repression of ifng, tbx21, and bcl6 Gene Expression. *The Journal of Immunology,* 181**,** 2338-2347.

COMPSTON, A. & COLES, A. 2008. Multiple sclerosis. *The Lancet,* 372**,** 1502-1517.

CONANT, D., HSIAU, T., ROSSI, N., OKI, J., MAURES, T., WAITE, K., YANG, J., JOSHI, S., KELSO, R., HOLDEN, K., ENZMANN, B. L. & STONER, R. 2022. Inference of CRISPR Edits from Sanger Trace Data. *Crispr j,* 5**,** 123-130.

CONG, L., RAN, F. A., COX, D., LIN, S., BARRETTO, R., HABIB, N., HSU, P. D., WU, X., JIANG, W., MARRAFFINI, L. A. & ZHANG, F. 2013. Multiplex Genome Engineering Using CRISPR/Cas Systems. *Science,* 339**,** 819-823.

CONSTANTIN, G., MAJEED, M., GIAGULLI, C., PICCIO, L., KIM, J. Y., BUTCHER, E. C. & LAUDANNA, C. 2000. Chemokines Trigger Immediate β2 Integrin Affinity and Mobility Changes: Differential Regulation and Roles in Lymphocyte Arrest under Flow. *Immunity,* 13**,** 759-769.

CORTESE, I., REICH, D. S. & NATH, A. 2021. Progressive multifocal leukoencephalopathy and the spectrum of JC virus-related disease. *Nature Reviews Neurology,* 17**,** 37-51.

CRETNEY, E., XIN, A., SHI, W., MINNICH, M., MASSON, F., MIASARI, M., BELZ, G. T., SMYTH, G. K., BUSSLINGER, M., NUTT, S. L. & KALLIES, A. 2011. The transcription factors Blimp-1 and IRF4 jointly control the differentiation and function of effector regulatory T cells. *Nature Immunology,* 12**,** 304-311.

CROXFORD, A. L., KURSCHUS, F. C. & WAISMAN, A. 2011. Mouse models for multiple sclerosis: Historical facts and future implications. *Biochimica et Biophysica Acta (BBA) - Molecular Basis of Disease,* 1812**,** 177-183.

CUI, Y., SHENG, Y. & ZHANG, X. 2013. Genetic susceptibility to SLE: Recent progress from GWAS. *Journal of Autoimmunity,* 41**,** 25-33.

DELTCHEVA, E., CHYLINSKI, K., SHARMA, C. M., GONZALES, K., CHAO, Y., PIRZADA, Z. A., ECKERT, M. R., VOGEL, J. & CHARPENTIER, E. 2011. CRISPR RNA maturation by trans-encoded small RNA and host factor RNase III. *Nature,* 471**,** 602-7.

DENDROU, C. A., FUGGER, L. & FRIESE, M. A. 2015. Immunopathology of multiple sclerosis. *Nat Rev Immunol,* 15**,** 545-58.

DENIC, A., WOOTLA, B. & RODRIGUEZ, M. 2013. CD8+ T cells in multiple sclerosis. *Expert Opin Ther Targets,* 17**,** 1053-66.

DENUCCI, C. C., PAGÁN, A. J., MITCHELL, J. S. & SHIMIZU, Y. 2010. Control of alpha4beta7 integrin expression and CD4 T cell homing by the beta1 integrin subunit. *J Immunol,* 184**,** 2458-67.

DETTKE, M., SCHEIDT, P., PRANGE, H. & KIRCHNER, H. 1997. Correlation Between Interferon Production and Clinical Disease Activity in Patients with Multiple Sclerosis. *Journal of Clinical Immunology,* 17**,** 293-300.

DJURETIC, I. M., LEVANON, D., NEGREANU, V., GRONER, Y., RAO, A. & ANSEL, K. M. 2007. Transcription factors T-bet and Runx3 cooperate to activate Ifng and silence Il4 in T helper type 1 cells. *Nature Immunology,* 8**,** 145-153.

EMSLEY, J., KNIGHT, C. G., FARNDALE, R. W., BARNES, M. J. & LIDDINGTON, R. C. 2000. Structural Basis of Collagen Recognition by Integrin α2β1. *Cell,* 101**,** 47-56.

ENGELHARDT, B. & RANSOHOFF, R. M. 2012. Capture, crawl, cross: the T cell code to breach the blood-brain barriers. *Trends Immunol,* 33**,** 579-89.

EVRON, T., DAIGLE, T. L. & CARON, M. G. 2012. GRK2: multiple roles beyond G protein-coupled receptor desensitization. *Trends in Pharmacological Sciences,* 33**,** 154-164.

FABRE, S., CARRETTE, F., CHEN, J., LANG, V., SEMICHON, M., DENOYELLE, C., LAZAR, V., CAGNARD, N., DUBART-KUPPERSCHMITT, A., MANGENEY, M., FRUMAN, D. A. & BISMUTH, G. 2008. FOXO1 regulates L-Selectin and a network of human T cell homing molecules downstream of phosphatidylinositol 3-kinase. *J Immunol,* 181**,** 2980-9.

FLÜGEL, A., BERKOWICZ, T., RITTER, T., LABEUR, M., JENNE, D. E., LI, Z., ELLWART, J. W., WILLEM, M., LASSMANN, H. & WEKERLE, H. 2001. Migratory activity and functional changes of green fluorescent effector cells before and during experimental autoimmune encephalomyelitis. *Immunity,* 14**,** 547-60.

FLÜGEL, A., ODOARDI, F., NOSOV, M. & KAWAKAMI, N. 2007. Autoaggressive effector T cells in the course of experimental autoimmune encephalomyelitis visualized in the light of two-photon microscopy. *J Neuroimmunol,* 191**,** 86-97.

FLÜGEL, A., WILLEM, M., BERKOWICZ, T. & WEKERLE, H. 1999. Gene transfer into CD4+ T lymphocytes: Green fluorescent protein-engineered, encephalitogenic T cells illuminate brain autoimmune responses. *Nature Medicine,* 5**,** 843-847.

FRANSEN, K., VISSCHEDIJK, M. C., VAN SOMMEREN, S., FU, J. Y., FRANKE, L., FESTEN, E. A., STOKKERS, P. C., VAN BODEGRAVEN, A. A., CRUSIUS, J. B., HOMMES, D. W., ZANEN, P., DE JONG, D. J., WIJMENGA, C., VAN DIEMEN, C. C. & WEERSMA, R. K. 2010. Analysis of SNPs with an effect on gene expression identifies UBE2L3 and BCL3 as potential new risk genes for Crohn's disease. *Hum Mol Genet,* 19**,** 3482-8.

FREITAS, R. F., BASTO, A., ALMEIDA, S. C. P., SANTOS, R. F., GONÇALVES, C. M., CORRIA-OSORIO, J., CARVALHO, T., CARMO, A. M., OLIVEIRA, V. G., LEON, K. & GRACA, L. 2019. Modulation of CD4 T cell function via CD6-targeting. *EBioMedicine,* 47**,** 427-435.

FREUND, J. & MCDERMOTT, K. 1942. Sensitization to Horse Serum by Means of Adjuvants. *Proceedings of the Society for Experimental Biology and Medicine,* 49**,** 548-553.

FREUND, J., STERN, E. R. & PISANI, T. M. 1947. Isoallergic encephalomyelitis and radiculitis in guinea pigs after one injection of brain and Mycobacteria in water-in-oil emulsion. *J Immunol,* 57**,** 179-94.

FU, B., LI, S., WANG, L., BERMAN, M. A. & DORF, M. E. 2014. The ubiquitin conjugating enzyme UBE2L3 regulates TNFα-induced linear ubiquitination. *Cell Res,* 24**,** 376-9.

FU, S. H., YEH, L. T., CHU, C. C., YEN, B. L. & SYTWU, H. K. 2017. New insights into Blimp-1 in T lymphocytes: a divergent regulator of cell destiny and effector function. *J Biomed Sci,* 24**,** 49.

GAO, Z.-Y., SU, L.-C., WU, Q.-C., SHENG, J.-E., WANG, Y.-L., DAI, Y.-F., CHEN, A.-P., HE, S.-S., HUANG, X. & YAN, G.-Q. 2022. Bioinformatics analyses of gene expression profile identify key genes and functional pathways involved in cutaneous lupus erythematosus. *Clinical Rheumatology,* 41**,** 437-452.

GARCÍA-ZEPEDA, E. A., LICONA-LIMÓN, I., JIMÉNEZ-SÓLOMON, M. F. & SOLDEVILA, G. 2007. Janus kinase 3-deficient T lymphocytes have an intrinsic defect in CCR7-mediated homing to peripheral lymphoid organs. *Immunology,* 122**,** 247-60.

GARG, N. & SMITH, T. W. 2015. An update on immunopathogenesis, diagnosis, and treatment of multiple sclerosis. *Brain Behav,* 5**,** e00362.

GIORELLI, M., LIVREA, P. & TROJANO, M. 2004. Post-receptorial mechanisms underlie functional disregulation of beta2-adrenergic receptors in lymphocytes from Multiple Sclerosis patients. *J Neuroimmunol,* 155**,** 143-9.

GIUNTI, D., BORSELLINO, G., BENELLI, R., MARCHESE, M., CAPELLO, E., VALLE, M. T., PEDEMONTE, E., NOONAN, D., ALBINI, A., BERNARDI, G., MANCARDI, G. L., BATTISTINI, L. & UCCELLI, A. 2003. Phenotypic and functional analysis of T cells homing into the CSF of subjects with inflammatory diseases of the CNS. *Journal of Leukocyte Biology,* 73**,** 584-590.

GLATIGNY, S., DUHEN, R., ARBELAEZ, C., KUMARI, S. & BETTELLI, E. 2015. Integrin alpha L controls the homing of regulatory T cells during CNS autoimmunity in the absence of integrin alpha 4. *Sci Rep,* 5**,** 7834.

GLATIGNY, S., DUHEN, R., OUKKA, M. & BETTELLI, E. 2011. Cutting Edge: Loss of α4 Integrin Expression Differentially Affects the Homing of Th1 and Th17 Cells. *The Journal of Immunology,* 187**,** 6176-6179.

GOLD, R., LININGTON, C. & LASSMANN, H. 2006. Understanding pathogenesis and therapy of multiple sclerosis via animal models: 70 years of merits and culprits in experimental autoimmune encephalomyelitis research. *Brain,* 129**,** 1953-71.

GONDEK, D. C., LU, L.-F., QUEZADA, S. A., SAKAGUCHI, S. & NOELLE, R. J. 2005. Cutting Edge: Contact-Mediated Suppression by CD4+CD25+ Regulatory Cells Involves a Granzyme B-

Dependent, Perforin-Independent Mechanism1. *The Journal of Immunology,* 174**,** 1783-1786.

GOVERMAN, J. 2009. Autoimmune T cell responses in the central nervous system. *Nat Rev Immunol,* 9**,** 393-407.

GRENNINGLOH, R., KANG, B. Y. & HO, I. C. 2005. Ets-1, a functional cofactor of T-bet, is essential for Th1 inflammatory responses. *J Exp Med,* 201**,** 615-26.

GREVET, J. D., LAN, X., HAMAGAMI, N., EDWARDS, C. R., SANKARANARAYANAN, L., JI, X., BHARDWAJ, S. K., FACE, C. J., POSOCCO, D. F., ABDULMALIK, O., KELLER, C. A., GIARDINE, B., SIDOLI, S., GARCIA, B. A., CHOU, S. T., LIEBHABER, S. A., HARDISON, R. C., SHI, J. & BLOBEL, G. A. 2018. Domain-focused CRISPR screen identifies HRI as a fetal hemoglobin regulator in human erythroid cells. *Science,* 361**,** 285-290.

GROOM, J. R. & LUSTER, A. D. 2011. CXCR3 in T cell function. *Experimental Cell Research,* 317**,** 620-631.

GU, S. M., PARK, M. H., YUN, H. M., HAN, S. B., OH, K. W., SON, D. J., YUN, J. S. & HONG, J. T. 2016. CCR5 knockout suppresses experimental autoimmune encephalomyelitis in C57BL/6 mice. *Oncotarget,* 7**,** 15382-93.

GUBBELS BUPP, M. R., EDWARDS, B., GUO, C., WEI, D., CHEN, G., WONG, B., MASTELLER, E. & PENG, S. L. 2009. T cells require Foxo1 to populate the peripheral lymphoid organs. *European Journal of Immunology,* 39**,** 2991-2999.

HAEUSSLER, M. & CONCORDET, J. P. 2016. Genome Editing with CRISPR-Cas9: Can It Get Any Better? *J Genet Genomics,* 43**,** 239-50.

HAFLER, D. A., COMPSTON, A., SAWCER, S., LANDER, E. S., DALY, M. J., DE JAGER, P. L., DE BAKKER, P. I., GABRIEL, S. B., MIREL, D. B., IVINSON, A. J., PERICAK-VANCE, M. A., GREGORY, S. G., RIOUX, J. D., MCCAULEY, J. L., HAINES, J. L., BARCELLOS, L. F., CREE, B., OKSENBERG, J. R. & HAUSER, S. L. 2007. Risk alleles for multiple sclerosis identified by a genomewide study. *N Engl J Med,* 357**,** 851-62.

HART, T., TONG, A. H. Y., CHAN, K., VAN LEEUWEN, J., SEETHARAMAN, A., AREGGER, M., CHANDRASHEKHAR, M., HUSTEDT, N., SETH, S., NOONAN, A., HABSID, A., SIZOVA, O., NEDYALKOVA, L., CLIMIE, R., TWORZYANSKI, L., LAWSON, K., SARTORI, M. A., ALIBEH, S., TIEU, D., MASUD, S., MERO, P., WEISS, A., BROWN, K. R., USAJ, M., BILLMANN, M., RAHMAN, M., CONSTANZO, M., MYERS, C. L., ANDREWS, B. J., BOONE, C., DUROCHER, D. & MOFFAT, J. 2017. Evaluation and Design of Genome-Wide CRISPR/SpCas9 Knockout Screens. *G3 (Bethesda),* 7**,** 2719-2727.

HAVRDOVÁ, E., BELOVA, A., GOLOBORODKO, A., TISSERANT, A., WRIGHT, A., WALLSTROEM, E., GARREN, H., MAGUIRE, R. P. & JOHNS, D. R. 2016. Activity of secukinumab, an anti-IL-17A antibody, on brain lesions in RRMS: results from a randomized, proof-of-concept study. *J Neurol,* 263**,** 1287-95.

HE, Q., GAO, H., CHANG, Y.-L., WU, X., LIN, R., LI, G., LIN, J., LU, H., CHEN, H., LI, Z., CONG, Y., YAO, J. & LIU, Z. 2022. ETS-1 facilitates Th1 cell-mediated mucosal inflammation in inflammatory bowel diseases through upregulating CIRBP. *Journal of Autoimmunity,* 132**,** 102872.

HÖFTBERGER, R., ABOUL-ENEIN, F., BRUECK, W., LUCCHINETTI, C., RODRIGUEZ, M., SCHMIDBAUER, M., JELLINGER, K. & LASSMANN, H. 2004. Expression of major histocompatibility complex class I molecules on the different cell types in multiple sclerosis lesions. *Brain Pathol,* 14**,** 43-50.

HOWLEY, B. V., MOHANTY, B., DALTON, A., GRELET, S., KARAM, J., DINCMAN, T. & HOWE, P. H. 2022. The ubiquitin E3 ligase ARIH1 regulates hnRNP E1 protein stability, EMT and breast cancer progression. *Oncogene,* 41**,** 1679-1690.

HSU, P. D., LANDER, E. S. & ZHANG, F. Development and Applications of CRISPR-Cas 9 for Genome Engineering. 2015.

HUBER, M., HEINK, S., PAGENSTECHER, A., REINHARD, K., RITTER, J., VISEKRUNA, A., GURALNIK, A., BOLLIG, N., JELTSCH, K., HEINEMANN, C., WITTMANN, E., BUCH, T., PRAZERES DA COSTA, O., BRÜSTLE, A., BRENNER, D., MAK, T. W., MITTRÜCKER, H. W., TACKENBERG,

B., KAMRADT, T. & LOHOFF, M. 2013. IL-17A secretion by CD8+ T cells supports Th17-mediated autoimmune encephalomyelitis. *J Clin Invest,* 123**,** 247-60.

HUGHES, C. E. & NIBBS, R. J. B. 2018. A guide to chemokines and their receptors. *Febs j,* 285**,** 2944-2971.

HWANG, I.-Y., PARK, C. & KEHRL, J. H. 2007. Impaired Trafficking of Gnai2+/− and Gnai2−/− T Lymphocytes: Implications for T Cell Movement within Lymph Nodes. *The Journal of Immunology,* 179**,** 439-448.

HWANG, I. Y., HARRISON, K., PARK, C. & KEHRL, J. H. 2017. Loss of Gα(i) proteins impairs thymocyte development, disrupts T-cell trafficking, and leads to an expanded population of splenic CD4+ PD-1+ CXCR5+/- T-cells. *Sci Rep,* 7**,** 4156.

HWANG, I. Y., PARK, C., HARRISON, K. & KEHRL, J. H. 2019. Biased S1PR1 Signaling in B Cells Subverts Responses to Homeostatic Chemokines, Severely Disorganizing Lymphoid Organ Architecture. *J Immunol,* 203**,** 2401-2414.

JÄGER, A., DARDALHON, V. R., SOBEL, R. A., BETTELLI, E. & KUCHROO, V. K. 2009. Th1, Th17, and Th9 Effector Cells Induce Experimental Autoimmune Encephalomyelitis with Different Pathological Phenotypes1. *The Journal of Immunology,* 183**,** 7169-7177.

JAIN, R., CHEN, Y., KANNO, Y., JOYCE-SHAIKH, B., VAHEDI, G., HIRAHARA, K., BLUMENSCHEIN, WENDY M., SUKUMAR, S., HAINES, CHRISTOPHER J., SADEKOVA, S., MCCLANAHAN, TERRILL K., MCGEACHY, MANDY J., O'SHEA, J. J. & CUA, DANIEL J. 2016. Interleukin-23-Induced Transcription Factor Blimp-1 Promotes Pathogenicity of T Helper 17 Cells. *Immunity,* 44**,** 131-142.

JANGI, S., GANDHI, R., COX, L. M., LI, N., VON GLEHN, F., YAN, R., PATEL, B., MAZZOLA, M. A., LIU, S., GLANZ, B. L., COOK, S., TANKOU, S., STUART, F., MELO, K., NEJAD, P., SMITH, K., TOPÇUOLU, B. D., HOLDEN, J., KIVISÄKK, P., CHITNIS, T., DE JAGER, P. L., QUINTANA, F. J., GERBER, G. K., BRY, L. & WEINER, H. L. 2016. Alterations of the human gut microbiome in multiple sclerosis. *Nature Communications,* 7**,** 12015.

JIANG, F. & DOUDNA, J. A. 2017. CRISPR-Cas9 Structures and Mechanisms. *Annu Rev Biophys,* 46**,** 505-529.

JINEK, M., CHYLINSKI, K., FONFARA, I., HAUER, M., DOUDNA, J. A. & CHARPENTIER, E. 2012. A programmable dual RNA-guided DNA endonuclease in adaptive bacterial immunity. *Science,* 337**,** 816-821.

JOHN, S. A., CLEMENTS, J. L., RUSSELL, L. M. & GARRETT-SINHA, L. A. 2008. Ets-1 Regulates Plasma Cell Differentiation by Interfering with the Activity of the Transcription Factor Blimp-1 *Journal of Biological Chemistry,* 283**,** 951-962.

JOHNSTON, R. J., POHOLEK, A. C., DITORO, D., YUSUF, I., ETO, D., BARNETT, B., DENT, A. L., CRAFT, J. & CROTTY, S. 2009. Bcl6 and Blimp-1 Are Reciprocal and Antagonistic Regulators of T Follicular Helper Cell Differentiation. *Science,* 325**,** 1006-1010.

JOUNG, J., KONERMANN, S., GOOTENBERG, J. S., ABUDAYYEH, O. O., PLATT, R. J., BRIGHAM, M. D., SANJANA, N. E. & ZHANG, F. 2017. Genome-scale CRISPR-Cas9 knockout and transcriptional activation screening. *Nat Protoc,* 12**,** 828-863.

KABAT, E. A., WOLF, A. & BEZER, A. E. 1947. The rapid production of acute disseminated encephalomyelitis in rhesus monkeys by injection of heterologous and homologous brain tissue with adjuvants. *Journal of Experimental Medicine,* 85**,** 117-130.

KABAT, E. A., WOLF, A., BEZER, A. E. & MURRAY, J. P. 1951. Studies on acute disseminated encephalomyelitis produced experimentally in rhesus monkeys. *Journal of Experimental Medicine,* 93**,** 615-633.

KALLIES, A., XIN, A., BELZ, G. T. & NUTT, S. L. 2009. Blimp-1 Transcription Factor Is Required for the Differentiation of Effector CD8+ T Cells and Memory Responses. *Immunity,* 31**,** 283-295.

KARIN, N. 2020. CXCR3 Ligands in Cancer and Autoimmunity, Chemoattraction of Effector T Cells, and Beyond. *Frontiers in Immunology,* 11.

KASKOW, B. J. & BAECHER-ALLAN, C. 2018. Effector T Cells in Multiple Sclerosis. *Cold Spring Harb Perspect Med,* 8.

KAWAKAMI, N., BARTHOLOMÄUS, I., PESIC, M. & MUES, M. 2012. An autoimmunity odyssey: how autoreactive T cells infiltrate into the CNS. *Immunol Rev,* 248**,** 140-55.

KAWAKAMI , N., LASSMANN , S., LI , Z., ODOARDI , F., RITTER , T., ZIEMSSEN , T., KLINKERT , W. E. F., ELLWART , J. W., BRADL , M., KRIVACIC , K., LASSMANN , H., RANSOHOFF , R. M., VOLK , H.-D., WEKERLE , H., LININGTON , C. & FLÜGEL , A. 2004. The Activation Status of Neuroantigen-specific T Cells in the Target Organ Determines the Clinical Outcome of Autoimmune Encephalomyelitis. *Journal of Experimental Medicine,* 199**,** 185-197.

KEBIR, H., IFERGAN, I., ALVAREZ, J. I., BERNARD, M., POIRIER, J., ARBOUR, N., DUQUETTE, P. & PRAT, A. 2009. Preferential recruitment of interferon-gamma-expressing TH17 cells in multiple sclerosis. *Ann Neurol,* 66**,** 390-402.

KEBIR, H., KREYMBORG, K., IFERGAN, I., DODELET-DEVILLERS, A., CAYROL, R., BERNARD, M., GIULIANI, F., ARBOUR, N., BECHER, B. & PRAT, A. 2007. Human TH17 lymphocytes promote blood-brain barrier disruption and central nervous system inflammation. *Nat Med,* 13**,** 1173-5.

KENDIRLI, A., DE LA ROSA, C., LÄMMLE, K. F., EGLSEER, K., BAUER, I. J., KAVAKA, V., WINKLMEIER, S., ZHUO, L., WICHMANN, C., GERDES, L. A., KÜMPFEL, T., DORNMAIR, K., BELTRÁN, E., KERSCHENSTEINER, M. & KAWAKAMI, N. 2023. A genome-wide in vivo CRISPR screen identifies essential regulators of T cell migration to the CNS in a multiple sclerosis model. *Nature Neuroscience,* 26**,** 1713-1725.

KERDILES, Y. M., BEISNER, D. R., TINOCO, R., DEJEAN, A. S., CASTRILLON, D. H., DEPINHO, R. A. & HEDRICK, S. M. 2009. Foxo1 links homing and survival of naive T cells by regulating L-selectin, CCR7 and interleukin 7 receptor. *Nat Immunol,* 10**,** 176-84.

KITOH, A., ONO, M., NAOE, Y., OHKURA, N., YAMAGUCHI, T., YAGUCHI, H., KITABAYASHI, I., TSUKADA, T., NOMURA, T., MIYACHI, Y., TANIUCHI, I. & SAKAGUCHI, S. 2009. Indispensable Role of the Runx1-Cbfβ Transcription Complex for In Vivo-Suppressive Function of FoxP3+ Regulatory T Cells. *Immunity,* 31**,** 609-620.

KIVISÄKK, P., IMITOLA, J., RASMUSSEN, S., ELYAMAN, W., ZHU, B., RANSOHOFF, R. M. & KHOURY, S. J. 2009. Localizing central nervous system immune surveillance: meningeal antigen-presenting cells activate T cells during experimental autoimmune encephalomyelitis. *Ann Neurol,* 65**,** 457-69.

KOCH-HENRIKSEN, N. & SØRENSEN, P. S. 2010. The changing demographic pattern of multiple sclerosis epidemiology. *The Lancet Neurology,* 9**,** 520-532.

KOIKE-YUSA, H., LI, Y., TAN, E. P., VELASCO-HERRERA MDEL, C. & YUSA, K. 2014. Genome-wide recessive genetic screening in mammalian cells with a lentiviral CRISPR-guide RNA library. *Nat Biotechnol,* 32**,** 267-73.

KOMINE , O., HAYASHI , K., NATSUME , W., WATANABE , T., SEKI , Y., SEKI , N., YAGI , R., SUKZUKI , W., TAMAUCHI , H., HOZUMI , K., HABU , S., KUBO , M. & SATAKE , M. 2003. The Runx1 Transcription Factor Inhibits the Differentiation of Naive CD4+ T Cells into the Th2 Lineage by Repressing GATA3 Expression. *Journal of Experimental Medicine,* 198**,** 51-61.

KORITSCHONER, R. & SCHWEINBURG, F. 1925. Induktion von Paralyse und Rückenmarksentzündung durch Immunisierung von Kaninchen mit menschlichem Rückenmarksgewebe. *Z Immunitätsf Exp Therapie,* 42**,** 217-83.

KRISHNAMOORTHY, G., LASSMANN, H., WEKERLE, H. & HOLZ, A. 2006. Spontaneous opticospinal encephalomyelitis in a double-transgenic mouse model of autoimmune T cell/B cell cooperation. *The Journal of Clinical Investigation,* 116**,** 2385-2392.

KROENKE , M. A., CARLSON , T. J., ANDJELKOVIC , A. V. & SEGAL , B. M. 2008. IL-12– and IL-23–modulated T cells induce distinct types of EAE based on histology, CNS chemokine profile, and response to cytokine inhibition. *Journal of Experimental Medicine,* 205**,** 1535-1541.

KUCHROO, V. K., MARTIN, C. A., GREER, J. M., JU, S. T., SOBEL, R. A. & DORF, M. E. 1993. Cytokines and adhesion molecules contribute to the ability of myelin proteolipid

protein-specific T cell clones to mediate experimental allergic encephalomyelitis. *J Immunol,* 151**,** 4371-82.

KUHLMANN, T., LINGFELD, G., BITSCH, A., SCHUCHARDT, J. & BRÜCK, W. 2002. Acute axonal damage in multiple sclerosis is most extensive in early disease stages and decreases over time. *Brain,* 125**,** 2202-12.

KURI, A., JACOBS, B. M., VICKARYOUS, N., PAKPOOR, J., MIDDELDORP, J., GIOVANNONI, G. & DOBSON, R. 2020. Epidemiology of Epstein-Barr virus infection and infectious mononucleosis in the United Kingdom. *BMC Public Health,* 20**,** 912.

KWAKKENBOS, M. J., KOP, E. N., STACEY, M., MATMATI, M., GORDON, S., LIN, H.-H. & HAMANN, J. 2004. The EGF-TM7 family: a postgenomic view. *Immunogenetics,* 55**,** 655-666.

LAROCHELLE, C., CAYROL, R., KEBIR, H., ALVAREZ, J. I., LÉCUYER, M. A., IFERGAN, I., VIEL, É., BOURBONNIÈRE, L., BEAUSEIGLE, D., TEROUZ, S., HACHEHOUCHE, L., GENDRON, S., POIRIER, J., JOBIN, C., DUQUETTE, P., FLANAGAN, K., YEDNOCK, T., ARBOUR, N. & PRAT, A. 2012. Melanoma cell adhesion molecule identifies encephalitogenic T lymphocytes and promotes their recruitment to the central nervous system. *Brain,* 135**,** 2906-24.

LASSMANN, H., BRUNNER, C., BRADL, M. & LININGTON, C. 1988. Experimental allergic encephalomyelitis: the balance between encephalitogenic T lymphocytes and demyelinating antibodies determines size and structure of demyelinated lesions. *Acta Neuropathologica,* 75**,** 566-576.

LEWIS, M. J., VYSE, S., SHIELDS, A. M., BOELTZ, S., GORDON, P. A., SPECTOR, T. D., LEHNER, P. J., WALCZAK, H. & VYSE, T. J. 2015. UBE2L3 polymorphism amplifies NF-κB activation and promotes plasma cell development, linking linear ubiquitination to multiple autoimmune diseases. *Am J Hum Genet,* 96**,** 221-34.

LEY, K., LAUDANNA, C., CYBULSKY, M. I. & NOURSHARGH, S. 2007. Getting to the site of inflammation: the leukocyte adhesion cascade updated. *Nat Rev Immunol,* 7**,** 678-89.

LI, Q. V., DIXON, G., VERMA, N., ROSEN, B. P., GORDILLO, M., LUO, R., XU, C., WANG, Q., SOH, C. L., YANG, D., CRESPO, M., SHUKLA, A., XIANG, Q., DÜNDAR, F., ZUMBO, P., WITKIN, M., KOCHE, R., BETEL, D., CHEN, S., MASSAGUÉ, J., GARIPPA, R., EVANS, T., BEER, M. A. & HUANGFU, D. 2019. Genome-scale screens identify JNK-JUN signaling as a barrier for pluripotency exit and endoderm differentiation. *Nat Genet,* 51**,** 999-1010.

LI, W., XU, H., XIAO, T., CONG, L., LOVE, M. I., ZHANG, F., IRIZARRY, R. A., LIU, J. S., BROWN, M. & LIU, X. S. 2014. MAGeCK enables robust identification of essential genes from genome-scale CRISPR/Cas9 knockout screens. *Genome Biology,* 15**,** 554.

LI, Y., XIE, P., LU, L., WANG, J., DIAO, L., LIU, Z., GUO, F., HE, Y., LIU, Y., HUANG, Q., LIANG, H., LI, D. & HE, F. 2017. An integrated bioinformatics platform for investigating the human E3 ubiquitin ligase-substrate interaction network. *Nature Communications,* 8**,** 347.

LILL, C. M. 2014. Recent advances and future challenges in the genetics of multiple sclerosis. *Front Neurol,* 5**,** 130.

LIN, C., ZHANG, Y., ZHANG, K., ZHENG, Y., LU, L., CHANG, H., YANG, H., YANG, Y., WAN, Y., WANG, S., YUAN, M., YAN, Z., ZHANG, R., HE, Y., GE, G., WU, D. & CHEN, J. 2019. Fever Promotes T Lymphocyte Trafficking via a Thermal Sensory Pathway Involving Heat Shock Protein 90 and α4 Integrins. *Immunity,* 50**,** 137-151.e6.

LIN, M.-H., YEH, L.-T., CHEN, S.-J., CHIOU, H.-Y. C., CHU, C.-C., YEN, L. B., LIN, K.-I., CHANG, D.-M. & SYTWU, H.-K. 2014. T cell-specific BLIMP-1 deficiency exacerbates experimental autoimmune encephalomyelitis in nonobese diabetic mice by increasing Th1 and Th17 cells. *Clinical Immunology,* 151**,** 101-113.

LIN, M. H., CHOU, F. C., YEH, L. T., FU, S. H., CHIOU, H. Y. C., LIN, K. I., CHANG, D. M. & SYTWU, H. K. 2013. B lymphocyte-induced maturation protein 1 (BLIMP-1) attenuates autoimmune diabetes in NOD mice by suppressing Th1 and Th17 cells. *Diabetologia,* 56**,** 136-146.

LIPTON, M. M. & FREUND, J. 1952. Encephalomyelitis in the Rat Following Intracutaneous Injection of Central Nervous System Tissue with Adjuvant. *Proceedings of the Society for Experimental Biology and Medicine,* 81**,** 260-261.

LITZENBURGER, T., FÄSSLER, R., BAUER, J., LASSMANN, H., LININGTON, C., WEKERLE, H. & IGLESIAS, A. 1998. B Lymphocytes Producing Demyelinating Autoantibodies: Development and Function in Gene-targeted Transgenic Mice. *Journal of Experimental Medicine,* 188**,** 169-180.

LOMBARDI, M. S., KAVELAARS, A., SCHEDLOWSKI, M., BIJLSMA, J. W., OKIHARA, K. L., VAN DE POL, M., OCHSMANN, S., PAWLAK, C., SCHMIDT, R. E. & HEIJNEN, C. J. 1999. Decreased expression and activity of G-protein-coupled receptor kinases in peripheral blood mononuclear cells of patients with rheumatoid arthritis. *Faseb j,* 13**,** 715-25.

LOPES, R., SPROUFFSKE, K., SHENG, C., UIJTTEWAAL, E. C. H., WESDORP, A. E., DAHINDEN, J., WENGERT, S., DIAZ-MIYAR, J., YILDIZ, U., BLEU, M., APFEL, V., MERMET-MEILLON, F., KRESE, R., EDER, M., OLSEN, A. V., HOPPE, P., KNEHR, J., CARBONE, W., CUTTAT, R., WALDT, A., ALTORFER, M., NAUMANN, U., WEISCHENFELDT, J., DEWECK, A., KAUFFMANN, A., ROMA, G., SCHÜBELER, D. & GALLI, G. G. 2021. Systematic dissection of transcriptional regulatory networks by genome-scale and single-cell CRISPR screens. *Sci Adv,* 7.

LORD, G. M., RAO, R. M., CHOE, H., SULLIVAN, B. M., LICHTMAN, A. H., LUSCINSKAS, F. W. & GLIMCHER, L. H. 2005. T-bet is required for optimal proinflammatory CD4+ T-cell trafficking. *Blood,* 106**,** 3432-3439.

LOVETT-RACKE, A. E., TROTTER, J. L., LAUBER, J., PERRIN, P. J., JUNE, C. H. & RACKE, M. K. 1998. Decreased dependence of myelin basic protein-reactive T cells on CD28-mediated costimulation in multiple sclerosis patients. A marker of activated/memory T cells. *J Clin Invest,* 101**,** 725-30.

LUCAS, R. M., BYRNE, S. N., CORREALE, J., ILSCHNER, S. & HART, P. H. 2015. Ultraviolet radiation, vitamin D and multiple sclerosis. *Neurodegener Dis Manag,* 5**,** 413-24.

MALI, P., YANG, L., ESVELT, K. M., AACH, J., GUELL, M., DICARLO, J. E., NORVILLE, J. E. & CHURCH, G. M. 2013. RNA-Guided Human Genome Engineering via Cas9. *Science,* 339**,** 823-826.

MAPUNDA, J. A., TIBAR, H., REGRAGUI, W. & ENGELHARDT, B. 2022. How Does the Immune System Enter the Brain? *Frontiers in Immunology,* 13.

MARCHETTI, L. & ENGELHARDT, B. 2020. Immune cell trafficking across the blood-brain barrier in the absence and presence of neuroinflammation. *Vasc Biol,* 2**,** H1-h18.

MARTINS, G. A., CIMMINO, L., SHAPIRO-SHELEF, M., SZABOLCS, M., HERRON, A., MAGNUSDOTTIR, E. & CALAME, K. 2006. Transcriptional repressor Blimp-1 regulates T cell homeostasis and function. *Nature Immunology,* 7**,** 457-465.

MATLOUBIAN, M., LO, C. G., CINAMON, G., LESNESKI, M. J., XU, Y., BRINKMANN, V., ALLENDE, M. L., PROIA, R. L. & CYSTER, J. G. 2004. Lymphocyte egress from thymus and peripheral lymphoid organs is dependent on S1P receptor 1. *Nature,* 427**,** 355-60.

MATSUI, M., WEAVER, J., PROUDFOOT, A. E. I., WUJEK, J. R., WEI, T., RICHER, E., TRAPP, B. D., RAO, A. & RANSOHOFF, R. M. 2002. Treatment of experimental autoimmune encephalomyelitis with the chemokine receptor antagonist Met-RANTES. *Journal of Neuroimmunology,* 128**,** 16-22.

MILLER, D., BARKHOF, F., MONTALBAN, X., THOMPSON, A. & FILIPPI, M. 2005. Clinically isolated syndromes suggestive of multiple sclerosis, part I: natural history, pathogenesis, diagnosis, and prognosis. *The Lancet Neurology,* 4**,** 281-288.

MILLER, D. H. & LEARY, S. M. 2007. Primary-progressive multiple sclerosis. *The Lancet Neurology,* 6**,** 903-912.

MILLER, S. A. & WEINMANN, A. S. 2010. Molecular mechanisms by which T-bet regulates T-helper cell commitment. *Immunol Rev,* 238**,** 233-46.

MOISAN, J., GRENNINGLOH, R., BETTELLI, E., OUKKA, M. & HO, I.-C. 2007. Ets-1 is a negative regulator of Th17 differentiation (35.34). *The Journal of Immunology,* 178**,** S8-S8.

MOKHTARIAN, F., MCFARLIN, D. E. & RAINE, C. S. 1984. Adoptive transfer of myelin basic protein-sensitized T cells produces chronic relapsing demyelinating disease in mice. *Nature,* 309**,** 356-8.

MORETTI, F. A., MOSER, M., LYCK, R., ABADIER, M., RUPPERT, R., ENGELHARDT, B. & FÄSSLER, R. 2013. Kindlin-3 regulates integrin activation and adhesion reinforcement of effector T cells. *Proc Natl Acad Sci U S A,* 110**,** 17005-10.

MORGAN , I. M. 1947. ALLERGIC ENCEPHALOMYELITIS IN MONKEYS IN RESPONSE TO INJECTION OF NORMAL MONKEY NERVOUS TISSUE. *Journal of Experimental Medicine,* 85**,** 131-140.

MOSER, M., LEGATE, K. R., ZENT, R. & FÄSSLER, R. 2009. The Tail of Integrins, Talin, and Kindlins. *Science,* 324**,** 895-899.

MOULY, E., CHEMIN, K., NGUYEN, H. V., CHOPIN, M., MESNARD, L., LEITE-DE-MORAES, M., BURLEN-DEFRANOUX, O., BANDEIRA, A. & BORIES, J. C. 2010. The Ets-1 transcription factor controls the development and function of natural regulatory T cells. *J Exp Med,* 207**,** 2113-25.

MUES, M., BARTHOLOMÄUS, I., THESTRUP, T., GRIESBECK, O., WEKERLE, H., KAWAKAMI, N. & KRISHNAMOORTHY, G. 2013. Real-time in vivo analysis of T cell activation in the central nervous system using a genetically encoded calcium indicator. *Nat Med,* 19**,** 778-83.

MUTHUSAMY, N., BARTON, K. & LEIDEN, J. M. 1995. Defective activation and survival of T cells lacking the Ets-1 transcription factor. *Nature,* 377**,** 639-42.

NEWTON, R. H., SHRESTHA, S., SULLIVAN, J. M., YATES, K. B., COMPEER, E. B., RON-HAREL, N., BLAZAR, B. R., BENSINGER, S. J., HAINING, W. N., DUSTIN, M. L., CAMPBELL, D. J., CHI, H. & TURKA, L. A. 2018. Maintenance of CD4 T cell fitness through regulation of Foxo1. *Nat Immunol,* 19**,** 838-848.

ODOARDI, F., SIE, C., STREYL, K., ULAGANATHAN, V. K., SCHLÄGER, C., LODYGIN, D., HECKELSMILLER, K., NIETFELD, W., ELLWART, J., KLINKERT, W. E., LOTTAZ, C., NOSOV, M., BRINKMANN, V., SPANG, R., LEHRACH, H., VINGRON, M., WEKERLE, H., FLÜGEL-KOCH, C. & FLÜGEL, A. 2012. T cells become licensed in the lung to enter the central nervous system. *Nature,* 488**,** 675-9.

OLITSKY, P. K. & YAGER, R. H. 1949. Experimental disseminated encephalomyelitis in white mice. *J Exp Med,* 90**,** 213-24.

OLSSON, T., BARCELLOS, L. F. & ALFREDSSON, L. 2017. Interactions between genetic, lifestyle and environmental risk factors for multiple sclerosis. *Nature Reviews Neurology,* 13**,** 25-36.

OO, M. L., THANGADA, S., WU, M.-T., LIU, C. H., MACDONALD, T. L., LYNCH, K. R., LIN, C.-Y. & HLA, T. 2007. Immunosuppressive and Anti-angiogenic Sphingosine 1-Phosphate Receptor-1 Agonists Induce Ubiquitinylation and Proteasomal Degradation of the Receptor. *Journal of Biological Chemistry,* 282**,** 9082-9089.

OROZCO, G., EYRE, S., HINKS, A., BOWES, J., MORGAN, A. W., WILSON, A. G., WORDSWORTH, P., STEER, S., HOCKING, L., THOMSON, W., WORTHINGTON, J. & BARTON, A. 2011. Study of the common genetic background for rheumatoid arthritis and systemic lupus erythematosus. *Ann Rheum Dis,* 70**,** 463-8.

OUYANG, W., BECKETT, O., FLAVELL, R. A. & LI, M. O. 2009. An Essential Role of the Forkhead-Box Transcription Factor Foxo1 in Control of T Cell Homeostasis and Tolerance. *Immunity,* 30**,** 358-371.

PANDIYAN, P., ZHENG, L., ISHIHARA, S., REED, J. & LENARDO, M. J. 2007. CD4+CD25+Foxp3+ regulatory T cells induce cytokine deprivation–mediated apoptosis of effector CD4+ T cells. *Nature Immunology,* 8**,** 1353-1362.

PANITCH, H. S., HIRSCH, R. L., HALEY, A. S. & JOHNSON, K. P. 1987. Exacerbations of multiple sclerosis in patients treated with gamma interferon. *Lancet,* 1**,** 893-5.

PAPPU, R., SCHWAB, S. R., CORNELISSEN, I., PEREIRA, J. P., REGARD, J. B., XU, Y., CAMERER, E., ZHENG, Y. W., HUANG, Y., CYSTER, J. G. & COUGHLIN, S. R. 2007. Promotion of

lymphocyte egress into blood and lymph by distinct sources of sphingosine-1-phosphate. *Science,* 316**,** 295-8.

PATERNOSTER, L., STANDL, M., WAAGE, J., BAURECHT, H., HOTZE, M., STRACHAN, D. P., CURTIN, J. A., BØNNELYKKE, K., TIAN, C., TAKAHASHI, A., ESPARZA-GORDILLO, J., ALVES, A. C., THYSSEN, J. P., DEN DEKKER, H. T., FERREIRA, M. A., ALTMAIER, E., SLEIMAN, P. M., XIAO, F. L., GONZALEZ, J. R., MARENHOLZ, I., KALB, B., YANES, M. P., XU, C. J., CARSTENSEN, L., GROEN-BLOKHUIS, M. M., VENTURINI, C., PENNELL, C. E., BARTON, S. J., LEVIN, A. M., CURJURIC, I., BUSTAMANTE, M., KREINER-MØLLER, E., LOCKETT, G. A., BACELIS, J., BUNYAVANICH, S., MYERS, R. A., MATANOVIC, A., KUMAR, A., TUNG, J. Y., HIROTA, T., KUBO, M., MCARDLE, W. L., HENDERSON, A. J., KEMP, J. P., ZHENG, J., SMITH, G. D., RÜSCHENDORF, F., BAUERFEIND, A., LEE-KIRSCH, M. A., ARNOLD, A., HOMUTH, G., SCHMIDT, C. O., MANGOLD, E., CICHON, S., KEIL, T., RODRÍGUEZ, E., PETERS, A., FRANKE, A., LIEB, W., NOVAK, N., FÖLSTER-HOLST, R., HORIKOSHI, M., PEKKANEN, J., SEBERT, S., HUSEMOEN, L. L., GRARUP, N., DE JONGSTE, J. C., RIVADENEIRA, F., HOFMAN, A., JADDOE, V. W., PASMANS, S. G., ELBERT, N. J., UITTERLINDEN, A. G., MARKS, G. B., THOMPSON, P. J., MATHESON, M. C., ROBERTSON, C. F., RIED, J. S., LI, J., ZUO, X. B., ZHENG, X. D., YIN, X. Y., SUN, L. D., MCALEER, M. A., O'REGAN, G. M., FAHY, C. M., CAMPBELL, L. E., MACEK, M., KUREK, M., HU, D., ENG, C., POSTMA, D. S., FEENSTRA, B., GELLER, F., HOTTENGA, J. J., MIDDELDORP, C. M., HYSI, P., BATAILLE, V., SPECTOR, T., TIESLER, C. M., et al. 2015. Multi-ancestry genome-wide association study of 21,000 cases and 95,000 controls identifies new risk loci for atopic dermatitis. *Nat Genet,* 47**,** 1449-1456.

PATERSON , P. Y. 1960. Transfer of allergic encephalomyelitis in rats my means of lymph cells *Journal of Experimental Medicine,* 111**,** 119-136.

PENELA, P., RIBAS, C., SÁNCHEZ-MADRID, F. & MAYOR, F., JR. 2019. G protein-coupled receptor kinase 2 (GRK2) as a multifunctional signaling hub. *Cell Mol Life Sci,* 76**,** 4423-4446.

PETEREIT, H. F., RICHTER, N., PUKROP, R. & BAMBORSCHKE, S. 2000. Interferon gamma production in blood lymphocytes correlates with disability score in multiple sclerosis patients. *Multiple Sclerosis Journal,* 6**,** 19-23.

PHAM, T. H., BALUK, P., XU, Y., GRIGOROVA, I., BANKOVICH, A. J., PAPPU, R., COUGHLIN, S. R., MCDONALD, D. M., SCHWAB, S. R. & CYSTER, J. G. 2010. Lymphatic endothelial cell sphingosine kinase activity is required for lymphocyte egress and lymphatic patterning. *J Exp Med,* 207**,** 17-27.

PICCIO, L., ROSSI, B., SCARPINI, E., LAUDANNA, C., GIAGULLI, C., ISSEKUTZ, A. C., VESTWEBER, D., BUTCHER, E. C. & CONSTANTIN, G. 2002. Molecular mechanisms involved in lymphocyte recruitment in inflamed brain microvessels: critical roles for P-selectin glycoprotein ligand-1 and heterotrimeric G(i)-linked receptors. *J Immunol,* 168**,** 1940-9.

PÖLLINGER, B., KRISHNAMOORTHY, G., BERER, K., LASSMANN, H., BÖSL, M. R., DUNN, R., DOMINGUES, H. S., HOLZ, A., KURSCHUS, F. C. & WEKERLE, H. 2009. Spontaneous relapsing-remitting EAE in the SJL/J mouse: MOG-reactive transgenic T cells recruit endogenous MOG-specific B cells. *Journal of Experimental Medicine,* 206**,** 1303-1316.

POLMAN, C. H., O'CONNOR, P. W., HAVRDOVA, E., HUTCHINSON, M., KAPPOS, L., MILLER, D. H., PHILLIPS, J. T., LUBLIN, F. D., GIOVANNONI, G., WAJGT, A., TOAL, M., LYNN, F., PANZARA, M. A. & SANDROCK, A. W. 2006. A Randomized, Placebo-Controlled Trial of Natalizumab for Relapsing Multiple Sclerosis. *New England Journal of Medicine,* 354**,** 899-910.

PONSONBY, A. L., LUCAS, R. M., VAN DER MEI, I. A., DEAR, K., VALERY, P. C., PENDER, M. P., TAYLOR, B. V., KILPATRICK, T. J., COULTHARD, A., CHAPMAN, C., WILLIAMS, D., MCMICHAEL, A. J. & DWYER, T. 2012. Offspring number, pregnancy, and risk of a first clinical demyelinating event: the AusImmune Study. *Neurology,* 78**,** 867-74.

PRIER, J. E., LI, J., GEARING, L. J., OLSHANSKY, M., SNG, X. Y. X., HERTZOG, P. J. & TURNER, S. J. 2019. Early T-BET Expression Ensures an Appropriate CD8+ Lineage–Specific

Transcriptional Landscape after Influenza A Virus Infection. *The Journal of Immunology,* 203**,** 1044-1054.

PROCACCINI, C., DE ROSA, V., PUCINO, V., FORMISANO, L. & MATARESE, G. 2015. Animal models of Multiple Sclerosis. *European Journal of Pharmacology,* 759**,** 182-191.

QU, N., XU, M., MIZOGUCHI, I., FURUSAWA, J., KANEKO, K., WATANABE, K., MIZUGUCHI, J., ITOH, M., KAWAKAMI, Y. & YOSHIMOTO, T. 2013. Pivotal roles of T-helper 17-related cytokines, IL-17, IL-22, and IL-23, in inflammatory diseases. *Clin Dev Immunol,* 2013**,** 968549.

R CORE TEAM 2021. R: A language and environment for statistical computing.

RAINE, C. S. 1994. The Dale E. McFarlin Memorial Lecture: the immunology of the multiple sclerosis lesion. *Ann Neurol,* 36 Suppl**,** S61-72.

RAN, F. A., HSU, P. D., WRIGHT, J., AGARWALA, V., SCOTT, D. A. & ZHANG, F. 2013. Genome engineering using the CRISPR-Cas9 system. *Nature Protocols,* 8**,** 2281-2308.

RANSOHOFF, R. M., KIVISÄKK, P. & KIDD, G. 2003. Three or more routes for leukocyte migration into the central nervous system. *Nature Reviews Immunology,* 3**,** 569-581.

REICH, D. S., LUCCHINETTI, C. F. & CALABRESI, P. A. 2018. Multiple Sclerosis. *N Engl J Med,* 378**,** 169-180.

REITER, E. & LEFKOWITZ, R. J. 2006. GRKs and β-arrestins: roles in receptor silencing, trafficking and signaling. *Trends in Endocrinology & Metabolism,* 17**,** 159-165.

RIVERS, T. M., SPRUNT , D. H. & BERRY , G. P. 1933. Observations on attempts to produce acute disseminated encephalomyelitis in monkeys. *Journal of Experimental Medicine,* 58**,** 39-53.

ROBINSON, A. P., HARP, C. T., NORONHA, A. & MILLER, S. D. 2014. The experimental autoimmune encephalomyelitis (EAE) model of MS: utility for understanding disease pathophysiology and treatment. *Handb Clin Neurol,* 122**,** 173-89.

ROSSI, B., ANGIARI, S., ZENARO, E., BUDUI, S. L. & CONSTANTIN, G. 2011. Vascular inflammation in central nervous system diseases: adhesion receptors controlling leukocyte–endothelial interactions. *Journal of Leukocyte Biology,* 89**,** 539-556.

ROSSI, B., DUSI, S., ANGELINI, G., BANI, A., LOPEZ, N., DELLA BIANCA, V., PIETRONIGRO, E. C., ZENARO, E., ZOCCO, C. & CONSTANTIN, G. 2023. Alpha4 beta7 integrin controls Th17 cell trafficking in the spinal cord leptomeninges during experimental autoimmune encephalomyelitis. *Front Immunol,* 14**,** 1071553.

ROTHHAMMER, V., HEINK, S., PETERMANN, F., SRIVASTAVA, R., CLAUSSEN, M. C., HEMMER, B. & KORN, T. 2011. Th17 lymphocytes traffic to the central nervous system independently of α4 integrin expression during EAE. *Journal of Experimental Medicine,* 208**,** 2465-2476.

RUDRA, D., EGAWA, T., CHONG, M. M. W., TREUTING, P., LITTMAN, D. R. & RUDENSKY, A. Y. 2009. Runx-CBFβ complexes control expression of the transcription factor Foxp3 in regulatory T cells. *Nature Immunology,* 10**,** 1170-1177.

RUIZ, F., VIGNE, S. & POT, C. 2019. Resolution of inflammation during multiple sclerosis. *Semin Immunopathol,* 41**,** 711-726.

RUSSELL, L. & GARRETT-SINHA, L. A. 2010. Transcription factor Ets-1 in cytokine and chemokine gene regulation. *Cytokine,* 51**,** 217-226.

RUTISHAUSER, R. L., MARTINS, G. A., KALACHIKOV, S., CHANDELE, A., PARISH, I. A., MEFFRE, E., JACOB, J., CALAME, K. & KAECH, S. M. 2009. Transcriptional Repressor Blimp-1 Promotes CD8+ T Cell Terminal Differentiation and Represses the Acquisition of Central Memory T Cell Properties. *Immunity,* 31**,** 296-308.

SAKAGUCHI, S., MIKAMI, N., WING, J. B., TANAKA, A., ICHIYAMA, K. & OHKURA, N. 2020. Regulatory T Cells and Human Disease. *Annual Review of Immunology,* 38**,** 541-566.

SALEHI, S., BANKOTI, R., BENEVIDES, L., WILLEN, J., COUSE, M., SILVA, J. S., DHALL, D., MEFFRE, E., TARGAN, S. & MARTINS, G. A. 2012. B Lymphocyte–Induced Maturation Protein-1 Contributes to Intestinal Mucosa Homeostasis by Limiting the Number of IL-17–Producing CD4+ T Cells. *The Journal of Immunology,* 189**,** 5682-5693.

SANFORD, M. 2014. Fingolimod: A Review of Its Use in Relapsing-Remitting Multiple Sclerosis. *Drugs,* 74**,** 1411-1433.

SASTRE-GARRIGA, J., TINTORÉ, M., NOS, C., TUR, C., RÍO, J., TÉLLEZ, N., CASTILLÓ, J., HORGA, A., PERKAL, H., COMABELLA, M., ROVIRA, A. & MONTALBAN, X. 2010. Clinical features of CIS of the brainstem/cerebellum of the kind seen in MS. *J Neurol,* 257**,** 742-6.

SATHIYANADAN, K., COISNE, C., ENZMANN, G., DEUTSCH, U. & ENGELHARDT, B. 2014. PSGL-1 and E/P-selectins are essential for T-cell rolling in inflamed CNS microvessels but dispensable for initiation of EAE. *Eur J Immunol,* 44**,** 2287-94.

SAWCER, S., FRANKLIN, R. J. M. & BAN, M. 2014. Multiple sclerosis genetics. *The Lancet Neurology,* 13**,** 700-709.

SCHLÄGER, C., KÖRNER, H., KRUEGER, M., VIDOLI, S., HABERL, M., MIELKE, D., BRYLLA, E., ISSEKUTZ, T., CABAÑAS, C., NELSON, P. J., ZIEMSSEN, T., ROHDE, V., BECHMANN, I., LODYGIN, D., ODOARDI, F. & FLÜGEL, A. 2016. Effector T-cell trafficking between the leptomeninges and the cerebrospinal fluid. *Nature,* 530**,** 349-353.

SCHMIED, M., BREITSCHOPF, H., GOLD, R., ZISCHLER, H., ROTHE, G., WEKERLE, H. & LASSMANN, H. 1993. Apoptosis of T lymphocytes in experimental autoimmune encephalomyelitis. Evidence for programmed cell death as a mechanism to control inflammation in the brain. *Am J Pathol,* 143**,** 446-52.

SCHOLZ, C., PATTON, K. T., ANDERSON, D. E., FREEMAN, G. J. & HAFLER, D. A. 1998. Expansion of autoreactive T cells in multiple sclerosis is independent of exogenous B7 costimulation. *J Immunol,* 160**,** 1532-8.

SCHWAB, S. R. & CYSTER, J. G. 2007. Finding a way out: lymphocyte egress from lymphoid organs. *Nature Immunology,* 8**,** 1295-1301.

SEBZDA, E., ZOU, Z., LEE, J. S., WANG, T. & KAHN, M. L. 2008. Transcription factor KLF2 regulates the migration of naive T cells by restricting chemokine receptor expression patterns. *Nat Immunol,* 9**,** 292-300.

SEGAL, B. M., CONSTANTINESCU, C. S., RAYCHAUDHURI, A., KIM, L., FIDELUS-GORT, R. & KASPER, L. H. 2008. Repeated subcutaneous injections of IL12/23 p40 neutralising antibody, ustekinumab, in patients with relapsing-remitting multiple sclerosis: a phase II, double-blind, placebo-controlled, randomised, dose-ranging study. *Lancet Neurol,* 7**,** 796-804.

SEGAL, B. M., DWYER, B. K. & SHEVACH, E. M. 1998. An interleukin (IL)-10/IL-12 immunoregulatory circuit controls susceptibility to autoimmune disease. *J Exp Med,* 187**,** 537-46.

SHALEM, O., SANJANA, N. E., HARTENIAN, E., SHI, X., SCOTT, D. A., MIKKELSON, T., HECKL, D., EBERT, B. L., ROOT, D. E., DOENCH, J. G. & ZHANG, F. 2014. Genome-scale CRISPR-Cas9 knockout screening in human cells. *Science,* 343**,** 84-87.

SHEFFER, M., LOWRY, E., BEELEN, N., BORAH, M., AMARA, S. N., MADER, C. C., ROTH, J. A., TSHERNIAK, A., FREEMAN, S. S., DASHEVSKY, O., GANDOLFI, S., BENDER, S., BRYAN, J. G., ZHU, C., WANG, L., TARIQ, I., KAMATH, G. M., SIMOES, R. M., DHIMOLEA, E., YU, C., HU, Y., DUFVA, O., GIANNAKIS, M., SYRGKANIS, V., FRAENKEL, E., GOLUB, T., ROMEE, R., MUSTJOKI, S., CULHANE, A. C., WIETEN, L. & MITSIADES, C. S. 2021. Genome-scale screens identify factors regulating tumor cell responses to natural killer cells. *Nat Genet,* 53**,** 1196-1206.

SHI, J., WANG, E., MILAZZO, J. P., WANG, Z., KINNEY, J. B. & VAKOC, C. R. 2015. Discovery of cancer drug targets by CRISPR-Cas9 screening of protein domains. *Nat Biotechnol,* 33**,** 661-7.

SHIFRUT, E., CARNEVALE, J., TOBIN, V., ROTH, T. L., WOO, J. M., BUI, C. T., LI, P. J., DIOLAITI, M. E., ASHWORTH, A. & MARSON, A. 2018. Genome-wide CRISPR Screens in Primary Human T Cells Reveal Key Regulators of Immune Function. *Cell,* 175**,** 1958-1971.e15.

SIMPSON, S., BLIZZARD, L., OTAHAL, P., VAN DER MEI, I. & TAYLOR, B. 2011. Latitude is significantly associated with the prevalence of multiple sclerosis: a meta-analysis. *Journal of Neurology, Neurosurgery & Psychiatry,* 82**,** 1132.

SOLDEVILA, G., LICONA, I., SALGADO, A., RAMÍREZ, M., CHÁVEZ, R. & GARCÍA-ZEPEDA, E. 2004. Impaired chemokine-induced migration during T-cell development in the absence of Jak 3. *Immunology,* 112**,** 191-200.

SPECK, N. A. 2001. Core binding factor and its role in normal hematopoietic development. *Current Opinion in Hematology,* 8.

SPORICI, R. & ISSEKUTZ, T. B. 2010. CXCR3 blockade inhibits T-cell migration into the CNS during EAE and prevents development of adoptively transferred, but not actively induced, disease. *European Journal of Immunology,* 40**,** 2751-2761.

STARON, M., YANG, Y., LIU, B., LI, J., SHEN, Y., ZÚÑIGA-PFLÜCKER, J. C., AGUILA, H. L., GOLDSCHNEIDER, I. & LI, Z. 2010. gp96, an endoplasmic reticulum master chaperone for integrins and Toll-like receptors, selectively regulates early T and B lymphopoiesis. *Blood,* 115**,** 2380-2390.

STEFFEN, B. J., BUTCHER, E. C. & ENGELHARDT, B. 1994. Evidence for involvement of ICAM-1 and VCAM-1 in lymphocyte interaction with endothelium in experimental autoimmune encephalomyelitis in the central nervous system in the SJL/J mouse. *Am J Pathol,* 145**,** 189-201.

STROMNES, I. M. & GOVERMAN, J. M. 2006. Active induction of experimental allergic encephalomyelitis. *Nat Protoc,* 1**,** 1810-9.

SULLIVAN, K. E., PILIERO, L. M., DHARIA, T., GOLDMAN, D. & PETRI, M. A. 2000. 3' polymorphisms of ETS1 are associated with different clinical phenotypes in SLE. *Human Mutation,* 16**,** 49-53.

SUTRA DEL GALY, A., MENEGATTI, S., FUENTEALBA, J., LUCIBELLO, F., PERRIN, L., HELFT, J., DARBOIS, A., SAITAKIS, M., TOSELLO, J., ROOKHUIZEN, D., DELOGER, M., GESTRAUD, P., SOCIÉ, G., AMIGORENA, S., LANTZ, O. & MENGER, L. 2021. In vivo genome-wide CRISPR screens identify SOCS1 as intrinsic checkpoint of CD4(+) T(H)1 cell response. *Sci Immunol,* 6**,** eabe8219.

SZABO, S. J., KIM, S. T., COSTA, G. L., ZHANG, X., FATHMAN, C. G. & GLIMCHER, L. H. 2000. A Novel Transcription Factor, T-bet, Directs Th1 Lineage Commitment. *Cell,* 100**,** 655-669.

TAKADA, Y., YE, X. & SIMON, S. 2007. The integrins. *Genome Biol,* 8**,** 215.

TANIUCHI, I., OSATO, M., EGAWA, T., SUNSHINE, M. J., BAE, S.-C., KOMORI, T., ITO, Y. & LITTMAN, D. R. 2002. Differential Requirements for Runx Proteins in CD4 Repression and Epigenetic Silencing during T Lymphocyte Development. *Cell,* 111**,** 621-633.

TESTONI, M., CHUNG, E. Y. L., PRIEBE, V. & BERTONI, F. 2015. The transcription factor ETS1 in lymphomas: friend or foe? *Leukemia & Lymphoma,* 56**,** 1975-1980.

THOMPSON, A. J., BARANZINI, S. E., GEURTS, J., HEMMER, B. & CICCARELLI, O. 2018. Multiple sclerosis. *The Lancet,* 391**,** 1622-1636.

THOMPSON, B. D., JIN, Y., WU, K. H., COLVIN, R. A., LUSTER, A. D., BIRNBAUMER, L. & WU, M. X. 2007. Inhibition of Gαi2 Activation by Gαi3 in CXCR3-mediated Signaling*. *Journal of Biological Chemistry,* 282**,** 9547-9555.

TIAN, X., KANG, D. S. & BENOVIC, J. L. 2014. β-arrestins and G protein-coupled receptor trafficking. *Handb Exp Pharmacol,* 219**,** 173-86.

TRAUGOTT, U., REINHERZ, E. L. & RAINE, C. S. 1983. Multiple sclerosis: distribution of T cell subsets within active chronic lesions. *Science,* 219**,** 308-10.

TSUNODA, I., TERRY, E. J., MARBLE, B. J., LAZARIDES, E., WOODS, C. & FUJINAMI, R. S. 2007. Modulation of experimental autoimmune encephalomyelitis by VLA-2 blockade. *Brain Pathol,* 17**,** 45-55.

TULADHAR, R., YEU, Y., TYLER PIAZZA, J., TAN, Z., RENE CLEMENCEAU, J., WU, X., BARRETT, Q., HERBERT, J., MATHEWS, D. H., KIM, J., HYUN HWANG, T. & LUM, L. 2019. CRISPR-Cas9-based mutagenesis frequently provokes on-target mRNA misregulation. *Nature Communications,* 10**,** 4056.

TZARTOS, J. S., FRIESE, M. A., CRANER, M. J., PALACE, J., NEWCOMBE, J., ESIRI, M. M. & FUGGER, L. 2008. Interleukin-17 production in central nervous system-infiltrating T

cells and glial cells is associated with active disease in multiple sclerosis. *Am J Pathol,* 172**,** 146-55.

VENKEN, K., HELLINGS, N., BROEKMANS, T., HENSEN, K., RUMMENS, J. L. & STINISSEN, P. 2008. Natural naive CD4+CD25+CD127low regulatory T cell (Treg) development and function are disturbed in multiple sclerosis patients: recovery of memory Treg homeostasis during disease progression. *J Immunol,* 180**,** 6411-20.

VON STECHOW, L., TYPAS, D., CARRERAS PUIGVERT, J., OORT, L., SIDDAPPA, R., PINES, A., VRIELING, H., VAN DE WATER, B., MULLENDERS, L. H. & DANEN, E. H. 2015. The E3 ubiquitin ligase ARIH1 protects against genotoxic stress by initiating a 4EHP-mediated mRNA translation arrest. *Mol Cell Biol,* 35**,** 1254-68.

VOORTHUIS, J. A., UITDEHAAG, B. M., DE GROOT, C. J., GOEDE, P. H., VAN DER MEIDE, P. H. & DIJKSTRA, C. D. 1990. Suppression of experimental allergic encephalomyelitis by intraventricular administration of interferon-gamma in Lewis rats. *Clin Exp Immunol,* 81**,** 183-8.

VROON, A., HEIJNEN, C. J., LOMBARDI, M. S., COBELENS, P. M., MAYOR, F., JR., CARON, M. G. & KAVELAARS, A. 2004. Reduced GRK2 level in T cells potentiates chemotaxis and signaling in response to CCL4. *J Leukoc Biol,* 75**,** 901-9.

VROON, A., KAVELAARS, A., LIMMROTH, V., LOMBARDI, M. S., GOEBEL, M. U., VAN DAM, A.-M., CARON, M. G., SCHEDLOWSKI, M. & HEIJNEN, C. J. 2005. G Protein-Coupled Receptor Kinase 2 in Multiple Sclerosis and Experimental Autoimmune Encephalomyelitis. *The Journal of Immunology,* 174**,** 4400-4406.

VROON, A., LOMBARDI, M. S., KAVELAARS, A. & HEIJNEN, C. J. 2003. Changes in the G-protein-coupled receptor desensitization machinery during relapsing–progressive experimental allergic encephalomyelitis. *Journal of Neuroimmunology,* 137**,** 79-86.

WALTON, C., KING, R., RECHTMAN, L., KAYE, W., LERAY, E., MARRIE, R. A., ROBERTSON, N., LA ROCCA, N., UITDEHAAG, B., VAN DER MEI, I., WALLIN, M., HELME, A., ANGOOD NAPIER, C., RIJKE, N. & BANEKE, P. 2020. Rising prevalence of multiple sclerosis worldwide: Insights from the Atlas of MS, third edition. *Mult Scler,* 26**,** 1816-1821.

WANG, P., DAI, X., JIANG, W., LI, Y. & WEI, W. 2020. RBR E3 ubiquitin ligases in tumorigenesis. *Semin Cancer Biol,* 67**,** 131-144.

WANG, S., ADRIANTO, I., WILEY, G. B., LESSARD, C. J., KELLY, J. A., ADLER, A. J., GLENN, S. B., WILLIAMS, A. H., ZIEGLER, J. T., COMEAU, M. E., MARION, M. C., WAKELAND, B. E., LIANG, C., KAUFMAN, K. M., GUTHRIDGE, J. M., ALARCÓN-RIQUELME, M. E., ALARCÓN, G. S., ANAYA, J. M., BAE, S. C., KIM, J. H., JOO, Y. B., BOACKLE, S. A., BROWN, E. E., PETRI, M. A., RAMSEY-GOLDMAN, R., REVEILLE, J. D., VILÁ, L. M., CRISWELL, L. A., EDBERG, J. C., FREEDMAN, B. I., GILKESON, G. S., JACOB, C. O., JAMES, J. A., KAMEN, D. L., KIMBERLY, R. P., MARTIN, J., MERRILL, J. T., NIEWOLD, T. B., PONS-ESTEL, B. A., SCOFIELD, R. H., STEVENS, A. M., TSAO, B. P., VYSE, T. J., LANGEFELD, C. D., HARLEY, J. B., WAKELAND, E. K., MOSER, K. L., MONTGOMERY, C. G. & GAFFNEY, P. M. 2012. A functional haplotype of UBE2L3 confers risk for systemic lupus erythematosus. *Genes Immun,* 13**,** 380-7.

WANG, T., WEI, J. J., SABATINI, D. M. & LANDER, E. S. 2014. Genetic screens in human cells using the CRISPR-Cas9 system. *Science,* 343**,** 80-4.

WARDELL, C. M., MACDONALD, K. N., LEVINGS, M. K. & COOK, L. 2021. Cross talk between human regulatory T cells and antigen-presenting cells: Lessons for clinical applications. *European Journal of Immunology,* 51**,** 27-38.

WEKERLE, H., FLÜGEL, A., FUGGER, L., SCHETT, G. & SERREZE, D. 2012. Autoimmunity's next top models. *Nature Medicine,* 18**,** 66-70.

WEKERLE, H., KOJIMA, K., LANNES-VIEIRA, J., LASSMANN, H. & LININGTON, C. 1994. Animal models. *Ann Neurol,* 36 Suppl**,** S47-53.

WENZEL, D. M., LISSOUNOV, A., BRZOVIC, P. S. & KLEVIT, R. E. 2011. UBCH7 reactivity profile reveals parkin and HHARI to be RING/HECT hybrids. *Nature,* 474**,** 105-8.

WICKHAM, H., AVERICK, M., BRYAN, J., CHANG, W., MCGOWAN, L., FRANÇOIS, R., GROLEMUND, G., HAYES, A., HENRY, L., HESTER, J., KUHN, M., PEDERSEN, T., MILLER, E., BACHE, S., MÜLLER, K., OOMS, J., ROBINSON, D., SEIDEL, D., SPINU, V. & YUTANI, H. 2019. Welcome to the Tidyverse. *Journal of Open Source Software,* 4**,** 1686.

XIONG, T.-C., WEI, M.-C., LI, F.-X., SHI, M., GAN, H., TANG, Z., DONG, H.-P., LIUYU, T., GAO, P., ZHONG, B., ZHANG, Z.-D. & LIN, D. 2022. The E3 ubiquitin ligase ARIH1 promotes antiviral immunity and autoimmunity by inducing mono-ISGylation and oligomerization of cGAS. *Nature Communications,* 13**,** 5973.

XUE, C. & GREENE, E. C. 2021. DNA Repair Pathway Choices in CRISPR-Cas9-Mediated Genome Editing. *Trends Genet,* 37**,** 639-656.

YANG, L., ANDERSON, D. E., BAECHER-ALLAN, C., HASTINGS, W. D., BETTELLI, E., OUKKA, M., KUCHROO, V. K. & HAFLER, D. A. 2008. IL-21 and TGF-beta are required for differentiation of human T(H)17 cells. *Nature,* 454**,** 350-2.

YANG, W., SHEN, N., YE, D.-Q., LIU, Q., ZHANG, Y., QIAN, X.-X., HIRANKARN, N., YING, D., PAN, H.-F., MOK, C. C., CHAN, T. M., WONG, R. W. S., LEE, K. W., MOK, M. Y., WONG, S. N., LEUNG, A. M. H., LI, X.-P., AVIHINGSANON, Y., WONG, C.-M., LEE, T. L., HO, M. H. K., LEE, P. P. W., CHANG, Y. K., LI, P. H., LI, R.-J., ZHANG, L., WONG, W. H. S., NG, I. O. L., LAU, C. S., SHAM, P. C., LAU, Y. L. & ASIAN LUPUS GENETICS, C. 2010. Genome-Wide Association Study in Asian Populations Identifies Variants in ETS1 and WDFY4 Associated with Systemic Lupus Erythematosus. *PLOS Genetics,* 6**,** e1000841.

YEDNOCK, T. A., CANNON, C., FRITZ, L. C., SANCHEZ-MADRID, F., STEINMAN, L. & KARIN, N. 1992. Prevention of experimental autoimmune encephalomyelitis by antibodies against alpha 4 beta 1 integrin. *Nature,* 356**,** 63-6.

ZANG, Y. C., LI, S., RIVERA, V. M., HONG, J., ROBINSON, R. R., BREITBACH, W. T., KILLIAN, J. & ZHANG, J. Z. 2004. Increased CD8+ cytotoxic T cell responses to myelin basic protein in multiple sclerosis. *J Immunol,* 172**,** 5120-7.

ZHANG, X., HUO, C., LIU, Y., SU, R., ZHAO, Y. & LI, Y. 2022. Mechanism and Disease Association With a Ubiquitin Conjugating E2 Enzyme: UBE2L3. *Front Immunol,* 13**,** 793610.

ZHAO, L., CANNONS, J. L., ANDERSON, S., KIRBY, M., XU, L., CASTILLA, L. H., SCHWARTZBERG, P. L., BOSSELUT, R. & LIU, P. P. 2007. CBFB-MYH11 hinders early T-cell development and induces massive cell death in the thymus. *Blood,* 109**,** 3432-40.

ZHOU, Y., ZHU, S., CAI, C., YUAN, P., LI, C., HUANG, Y. & WEI, W. 2014. High-throughput screening of a CRISPR/Cas9 library for functional genomics in human cells. *Nature,* 509**,** 487-491.

SUPPLEMENT

Table 5 INDEL frequency of KO genes

Target gene	INDEL % by ICE (Synthego)
Arih1	N.A. reduced protein counts were detected in proteomics analysis (data not shown)
CCR5	Clone 1: 88 %
Cxcr3	Clone 1: 77 %
Ets1	Clone 1: 85 %
	Clone 2: 51 %
	Clone 3: 58 %
	Clone 4: 86 %
Grk2	Clone 1: 98 %
	Clone 2: 82 %
Grk2-S1PR1	Clone 1: 94 % (S1PR1) & 98 % (Grk2)
Hsp90b1	Clone 1: 74 %
	Clone 2: 89 %
Itga4	Clone 1: 98 %
	Clone 2: 97 %
Itgb1	T_{MBP} Itgb1-KO cells were enriched by sorting based on protein surface expression from around 60 % KO to almost 100 % KO
S1PR1	Clone 1: 93 %
Tbx21	Clone 1: 86 %
Ube2l3	Clone 1: 93 %
	Clone 2: 96 %

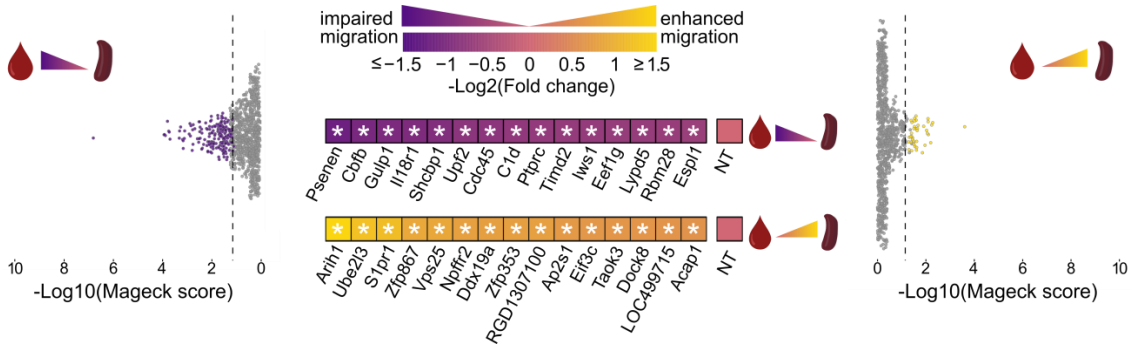

Supplementary Figure 1 Compartment specific T cell migration

Results of the validation screening depicting the top-ranking genes whose KO showed impaired (left) or enhanced (right) migration of T_{MBP} cells to the spleen compared to blood. In the middle log2(Fold Change) heatmaps showing on the top panel positive regulators of T_{MBP} cell entry to the spleen from the blood (KO impairs migration, purple) and the lower panel negative regulators of spleen migration (KO enhances migration, yellow) Stars indicate, for all heatmaps, p-value < 0.05, absolute log2(Fold Change) > 3 standard deviations of the log2(Fold Changes) of the controls and ≥ 3 "neg/pos|goodsgrna". Modified from (Kendirli et al., 2023).

CONTRIBUTIONS

PD. Dr. Naoto Kawakami (NK) established the T_{MBP} Cas9-EGFP cells and Dr. Arek Kendirli (AK) sorted these cells. Both optimised the experimental setup prior to the results presented in this thesis. The genome-wide and the validation CRISPR/Cas9 screening was a joint effort together with NK, AK and Clara de la Rosa del Val (CRV). CRV performed all the bioinformatics analyses and created the resulting graphical representation. Single KO validation experiments were supported by NK. The *in vivo* two-photon imaging experiment was supported and performed by NK and Dr. Isabel Bauer.

Due to the joint effort, part of this work has been previously presented in Dr. Arek Kendirli's dissertation:

Kendirli A. *In vivo CRISPR screens to dissect regulatory genes controlling T cell transmigration and macrophage polarization in animal models of Multiple Sclerosis.*
Fakultät für Medizin, Technische Universität München. **2022**. (not yet public available)

Part of the data presented in this thesis was uploaded to bioRxiv as:

Kendirli A.*, de la Rosa C.*, **Lämmle K. F.***, Eglseer K., Bauer I. J., Kavaka V., Winklmeier S., Wichmann C., Gerdes L. A., Kümpfel T., Dornmair K., Beltrán E., Kerschensteiner M.‡, Kawakami N. **Equal contribution ‡ Co-senior authors*
Identification of essential modules regulating T cell migration to the central nervous system in multiple sclerosis. bioRxiv, 2022.06.17.496548

and published as:

Kendirli A.*, de la Rosa C.*, **Lämmle K. F.***, Eglseer K., Bauer I. J., Kavaka V., Winklmeier S., Zhuo L., Wichmann C., Gerdes L. A., Kümpfel T., Dornmair K., Beltrán E., Kerschensteiner M.‡, Kawakami N.‡ **Equal contribution ‡ Co-senior authors*
Identification of essential modules regulating T cell migration to the central nervous system in multiple sclerosis. **Nature Neuroscience 26**, 1713–1725 (2023).

ACKNOWLEDGEMENTS

First, I want to express my deepest appreciation and gratitude to my supervisor, PD Dr. Naoto Kawakami, for his invaluable guidance and continuous encouragement throughout the journey of my PhD thesis. Throughout this research journey, he played a pivotal role in not only providing valuable insights and expertise but also actively assisting with the experimental aspects of this study. Beyond his academic proficiency, he created a welcoming environment within our research group. His approachability, open-mindedness, and genuine interest in our well-being have created a supportive atmosphere for academic and personal growth. I am truly grateful for the privilege of working with such an exceptional supervisor.

Besides, I would like to extend my sincere gratitude to Prof. Dr. Martin Kerschensteiner for his vast knowledge and exceptional scientific input that has been invaluable in shaping the direction and quality of this research.

I am deeply thankful to my two colleagues, Dr. Arek Kendirli and Clara de la Rosa del Val, without whom the completion of this work would not have been possible. Our collaboration in sharing the experimental workload and engaging in profound scientific discussions has been invaluable and Clara's expertise and dedication in bioinformatical data analysis were instrumental in the successful completion of this research project.

I am truly appreciative of all the current and former colleagues of the AG Kawakami. Bella, Lian, Zola and Tobias: Thank you for stimulating discussions, intellectual exchanges, the collaborative spirit, and the fun events within and outside the lab.

Furthermore, I would like to thank my colleagues at the institute of clinical neuroimmunology and the staff of the core facilities at the BMC for their assistance, resources, and the friendly and supportive research environment they have provided.

I am immensely grateful for the remarkable friendships that developed among my colleagues during our time in the lab. Alina, Bella, Cate, Lian, Michelle, Miriam and Ramona: even though we may no longer be working side by side, I cherish the memories we created together and I am grateful for the ongoing support and laughter that has enriched our lives. These friendships are truly treasured, and I look forward to the many more adventures and shared moments that lie ahead.

Lastly, I want to express my heartfelt gratitude to my non-lab friends, and especially my dear family - Ute, Rainer and Hanna - for their unwavering support, understanding, and encouragement throughout this challenging academic journey. Their belief in my abilities and their unconditional support has been a constant source of motivation.

AFFIDAVIT

Eidesstattliche Versicherung

Lämmle, Katrin Franziska

Name, Vorname

Ich erkläre hiermit an Eides statt, dass ich die vorliegende Dissertation mit dem Titel:

Discovery and Validation of Essential Modules of T cell Migration into the Central Nervous System in a Genome-wide CRISPR/Cas9 Screening in Experimental Autoimmune Encephalomyelitis

selbständig verfasst, mich außer der angegebenen keiner weiteren Hilfsmittel bedient und alle Erkenntnisse, die aus dem Schrifttum ganz oder annähernd übernommen sind, als solche kenntlich gemacht und nach ihrer Herkunft unter Bezeichnung der Fundstelle einzeln nachgewiesen habe.

Ich erkläre des Weiteren, dass die hier vorgelegte Dissertation nicht in gleicher oder in ähnlicher Form bei einer anderen Stelle zur Erlangung eines akademischen Grades eingereicht wurde.

Martinsried, 18. Dezember 2023
Ort, Datum

Katrin Lämmle
Unterschrift Doktorandin bzw. Doktorand